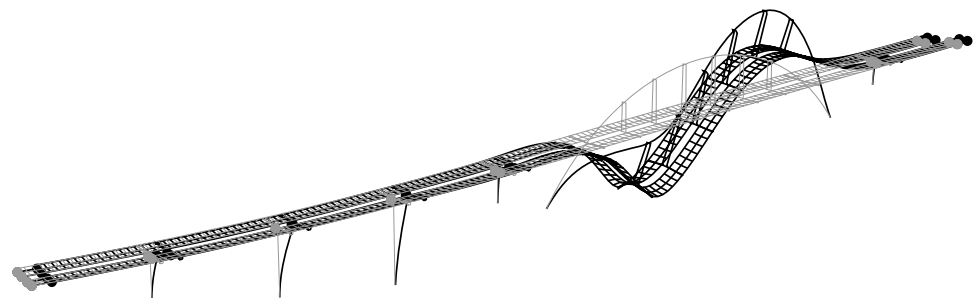
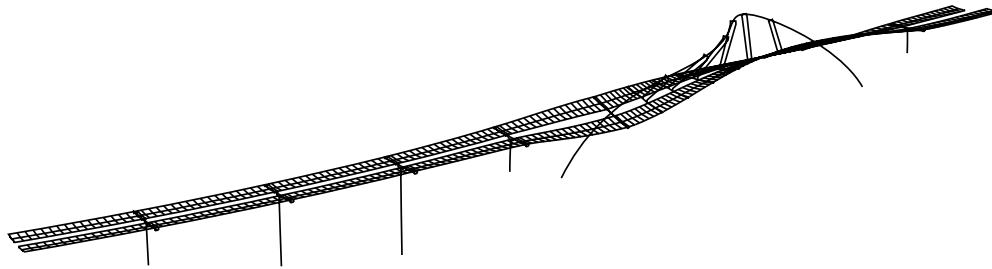


CHALMERS



Finite Element Model Updating of the New Svinesund Bridge

Manual Model Refinement with Non-Linear Optimization

Master's Thesis in the International Master's Programme Structural Engineering

FREDRIK JONSSON

DAVID JOHNSON

Department of Civil and Environmental Engineering

Division of Structural Engineering

Concrete Structures

CHALMERS UNIVERSITY OF TECHNOLOGY

Göteborg, Sweden 2007

Master's Thesis 2007:130

MASTER'S THESIS 2007:130

Finite Element Model Updating of the New Svinesund Bridge

Manual Model Refinement with Non-Linear Optimization

Master's Thesis in the *International Master's Program Structural Engineering*

FREDRIK JONSSON

DAVID JOHNSON

Department of Civil and Environmental Engineering
Division of Structural Engineering
Concrete Structures

CHALMERS UNIVERSITY OF TECHNOLOGY

Göteborg, Sweden 2007

Finite Element Model Updating of the New Svinesund Bridge
Manual Model Refinement with Non-Linear Optimization
Master's Thesis in the *International Master's Program Structural Engineering*
FREDRIK JONSSON
DAVID JOHNSON

© FREDRIK JONSSON, DAVID JOHNSON, 2007

Master's Thesis 2007:130
Department of Civil and Environmental Engineering
Division of Structural Engineering
Concrete Structures
Chalmers University of Technology
SE-412 96 Göteborg
Sweden
Telephone: + 46 (0)31-772 1000

Cover:

Top: Theoretical eigenmode 4, 2nd transversal mode of the arch with optimized FE model.

Bottom: Simulated bridge deflection for static load case E (scale factor = 1500) with optimized FE model.

Chalmers Reproservice / Department of Civil and Environmental Engineering
Göteborg, Sweden 2007

Finite Element Model Updating of the New Svinesund Bridge
Manual Model Refinement with Non-Linear Optimization
Master's Thesis in the *International Master's Program Structural Engineering*

FREDRIK JONSSON

DAVID JOHNSON

Department of Civil and Environmental Engineering

Division of Structural Engineering

Concrete Structures

Chalmers University of Technology

ABSTRACT

In order to improve understanding of the structural behaviour and to verify the design of the New Svinesund Bridge, the Swedish and Norwegian road administrations (Vägverket and Statens Vegvesen) initiated an extensive monitoring project. Monitoring was used to understand the real behaviour of the bridge. The collected data were then used as a case study to improve assessment and maintenance of bridges by finite element analysis (FEA) and finite element (FE) model updating in a research project supported by Vägverket and Banverket. The monitoring project has extensively studied the New Svinesund Bridge from construction phase through the first years of the service life. The Royal Institute of Technology (KTH) is responsible for instrumentation, analysis and documentation of the monitoring project. Results obtained by KTH from the New Svinesund Bridge monitoring project were used by Chalmers University, division of Structural Engineering, Concrete Structures, as a case study for a research project to improve bridge assessment and maintenance of bridges through FEA.

In order to obtain an FE model of the New Svinesund Bridge capable of accurate static and dynamic response prediction, an existing model of the bridge was modified using FE model updating. The updating was made through manual model refinement and non-linear optimization with statistical considerations. Uncertain structural parameters of interest included the stiffness of sections of the arch, stiffness and mass of the bridge deck, connection stiffness between the arch and the bridge deck, bearing restraint at the connection between the piers and the bridge deck and the degree of fixture of the arch foundation. A proof of concept test study was conducted using an FE model of a beam with spring supports. The physical meaning of numerical results were analysed in accordance with practical engineering judgement.

The initial FE model was manually refined to more accurately represent the stiffness profile in the arch, to include the masses of non-structural elements including the asphalt layer and railings and to more realistically model the bearings. Measured strains, deflections and forces from a static load test and measured eigenfrequencies from ambient vibration testing were then used to update the FE model using least non-linear optimization. The updated FE model was capable of more accurately reproducing the measured responses. Guidelines for FE model updating for structural design verification and assessment were developed based on the results obtained from the study.

Key words:

Svinesund bridge, FE model updating, optimization, structural dynamics

Uppdatering av finit element modell av den nya Svinesundsbron
Manuel modellförbättring och icke linjär optimering
Examensarbete inom *International Master's Program Structural Engineering*
FREDRIK JONSSON
DAVID JOHNSON
Institutionen för bygg- och miljöteknik
Avdelningen för Konstruktionsteknik
Betongbyggnad
Chalmers tekniska högskola

SAMMANFATTNING

I syfte att verifiera konstruktionen och öka förståelsen för verkningssättet hos den nya Svinesundsbron, initierade Vägverket tillsammans med Statens Vegvesen (motsvarigheten till Vägverket till i Norge) ett omfattande övervakningsprojekt. Kungliga Tekniska Högskolan (KTH) ansvarade för instrumentering, analys av mätdata och dokumentation av projektet. Övervakningsprojektet fortgår under bronns första bruksår. De av KTH insamlade mätdata användes sedan till en fallstudie vid Chalmers Tekniska Högskola för att förbättra utvärdering och underhåll av broar med hjälp av uppdatering av strukturmodeller, modellerade med finit element metod (FEM), ett forskningsprojekt stöttat av Vägverket och Banverket.

För att erhålla en FE-modell för den nya Svinesundbron som är kapabel att på ett noggrant sätt förutspå verkningssättet för bron, både dynamiskt och statiskt, modifierades en befintlig FE-modell genom modelluppdatering. Uppdateringen utfördes genom manuell FE-modell förbättring och minimering med hjälp av icke linjär optimering. Tekniken med uppdatering av FE-modeller är att använda olika optimeringsmetoder för att kalibrera osäkra strukturparametrar i modellen för att kunna reproducera experimentella mätdata. De osäkra strukturparametrarna som studerats är, styvhet i bågen, styvheten för kopplingen mellan bågen och farbanorna, massan för farbanorna, tvångskrafter i farbanornas upplag och bågens inspänningsstyvhet.

Konceptet provades genom att genomföra FE-modelluppdatering på en fritt upplagd balk med fjädrar som upplag i båda ändarna. Detta utfördes med olika typer av optimeringsmetoder, däribland minsta kvadratmetoden och en icke-gradientbaserad metod, Nelder-Mead simplex metod. För förhindra att resultaten av uppdateringen skulle sakna fysisk relevans utfördes validering och utvärdering av dem med hjälp av ingenjörsmässiga bedömningar och överslagberäkningar.

Ursprungsmodellen förfinades först manuellt, för att mer noggrant representera styvhetens variation i bågen, för att ta hänsyn till massan av vägbeläggningen och räckan genom masselement och för att mer realistiskt modellera farbanornas rörelser vid upplagen. Vid modelluppdatering användes icke-linjär- och minstakvadrat-optimering. Den uppmätta strukturrespons som användes vid modelluppdateringen var, töjningar, förskjutningar, kraft i hängstag och egenfrekvenser. Den uppdaterade

FE-modellen reproducerade den uppmätta responsen bättre än den ursprungliga FE-modellen.

Nyckelord:

Svinesundsbron, FEM, strukturmodell, optimering, strukturdynamik

Contents

ABSTRACT	II
SAMMANFATTNING	IV
CONTENTS	VI
PREFACE	X
NOTATIONS	XI
1 INTRODUCTION	1
1.1 Description of the New Svinesund Bridge	1
1.2 Instrumentation of the bridge	3
1.3 Finite element modelling of the bridge	3
1.4 Aim and objectives	3
1.5 Scope of study	3
1.6 Limitations	4
2 THEORY	6
2.1 Finite element method	6
2.1.1 FE overview	6
2.1.2 FEM applications	6
2.1.3 FE general concepts	13
2.2 Optimization	17
2.2.1 Optimization overview	17
2.2.2 Optimization general mathematical formulation	17
2.2.3 Optimization – classical least squares estimate	19
2.2.4 Optimization – Nelder-Mead simplex method	21
2.3 Statistics	21
2.4 Finite element model updating	25
2.4.1 FE model updating overview	25
2.4.2 FE model updating conceptual framework	26
2.4.3 Least squares FE model updating techniques	27
2.4.4 FE model with Nelder-Mead simplex method	33
3 FE MODEL UPDATING OF A SIMPLE BEAM	35
3.1 Problem description	35
3.2 Numerical modelling	37
3.2.1 Analytical formulas: MATLAB	37
3.2.2 FE modelling: MATLAB	37
3.2.3 FE modelling: ABAQUS	37
3.2.4 FE model verification	39
3.3 FE model updating procedure	40

3.3.1	Least squares FE model updating techniques	40
3.3.2	Simple beam results: least squares FE model updating techniques	40
3.3.3	FE model updating with Nelder-Mead simplex method	44
3.4	Simple beam FE model updating results	45
3.5	Noisy measurements	49
3.6	Conclusions	55
4	FE MODELLING AND EXPERIMENTAL TESTING OF THE NEW SVINESUND BRIDGE	57
4.1	FE modelling	57
4.1.1	FE model description	57
4.1.2	Boundary conditions and internal constraints	58
4.2	New Svinesund Bridge response	59
4.2.1	Permanent sensors	59
4.2.2	Static load tests	60
4.2.3	Experimentally measured response	60
5	FE MODEL MANUAL REFINEMENT OF THE NEW SVINESUND BRIDGE THROUGH STRUCTURAL CALCULATIONS	67
5.1	Structural parameter investigation	67
5.1.1	Increase of arch section stiffness	67
5.1.2	Asphalt mass	70
5.1.3	Asphalt dynamic stiffness	73
5.1.4	Arch-carriageway connection stiffness	80
5.1.5	Static friction in bearings	81
5.2	FE model evolution	83
5.2.1	Model 0: initial model	83
5.2.2	Model 1: boundary condition study	84
5.2.3	Model 2 to Model 7	89
6	FE MODEL MANUAL REFINEMENT OF THE NEW SVINESUND BRIDGE THROUGH PARAMETER SENSITIVITY ANALYSIS	92
6.1	Statistics for measurements	92
6.2	Objective function formulation for the New Svinesund bridge	94
6.2.1	Standard deviation objective function	94
6.2.2	Variance objective function	96
6.2.3	Error objective function	97
6.2.4	Uncertainty objective function	98
6.3	Parameter sensitivity study	99
6.3.1	Concrete stiffness	100
6.3.2	Carriageway steel elastic modulus	103
6.3.3	Asphalt mass	106
6.3.4	Asphalt stiffness	107
6.3.5	Arch-carriageway connection stiffness	109
6.3.6	Arch foundation stiffness	110

6.3.7	Bearing static friction	111
6.3.8	Carriageway longitudinal stiffeners	112
6.3.9	Parameter sensitivity study results	114
6.4	Revised FE model	115
6.4.1	Eigenfrequencies	115
6.4.2	Strains	117
6.4.3	Displacements	118
6.4.4	Hanger loads	118
7	FE MODEL UPDATING OF THE NEW SVINESUND BRIDGE	119
7.1	Calculations	119
7.2	Results	119
7.2.1	Frequency optimization	119
7.2.2	Strain optimization	122
7.2.3	Displacement optimization	124
7.2.4	Hanger load optimization	126
7.2.5	FE model optimization	127
7.3	Results summary	131
8	CONCLUSIONS	132
8.1	Discussion of FE model updating of the New Svinesund Bridge	132
8.2	Recommendations for further FE model updating for the New Svinesund Bridge	133
8.3	FE model updating for improved structural assessment	134
8.3.1	Design	137
8.3.2	Service life	138
9	REFERENCES	140
	APPENDIX A. SIMPLE BEAM FE MODEL VERIFICATION	142
	APPENDIX B. MATLAB SUBROUTINE: EIGENFREQUENCY VERIFICATION OF SIMPLE BEAM	146
	APPENDIX C. MATLAB SUBROUTINE: BEAM RESPONSE	147
	APPENDIX D. FE MODEL UPDATING OF SIMPLE BEAM	148
	D.1 Simple beam results: classical FE updating techniques	148
	D.2 Simple beam results: FE updating with ABAQUS and MATLAB optimization toolbox	156
	APPENDIX E. NEW SVINESUND BRIDGE BEARING FRICTION STUDY	157
	APPENDIX F. MODEL EVOLUTION	166
	F.1 Eigenfrequencies	166
	F.2 Strains	167
	F.3 Displacements	182

F.4	Hanger loads	201
APPENDIX G. FE UPDATING RESULTS FOR THE NEW SVINESUND BRIDGE		203
G.1	Model 7 optimized for frequencies	203
G.2	Model 7 optimized for strains	204
G.3	Model 7 optimized for displacements	209
G.4	Model 7 optimized for hanger loads	211
G.5	Model 7 optimized for entire response	211
G.6	Model 7 optimized for entire response with regularization	212
G.7	FE model updating results summary	213
APPENDIX H. SUBROUTINES FOR FE MODEL UPDATING FOR THE NEW SVINESUND BRIDGE		215
H.1	MATLAB CODE – zSB	215
H.2	MATLAB CODE – SBphi \hat{h}	217
H.3	MATLAB CODE – SBphi	220
H.4	MATLAB CODE – SBobj	221
H.5	User subroutine – SBfreq	225
H.6	User subroutine – SBstat	227

Preface

This master's thesis was carried out at Chalmers University of Technology, Department of Civil and Environmental Engineering, Division of Structural Engineering, Concrete Structures between August 2007 and December 2007.

The main purpose of the master's thesis was to utilize measured data from ambient vibration frequency measurements and static load tests to perform finite element model updating for the New Svinesund Bridge.

Ph.D. Mario Plos at Concrete Structures, Chalmers University of Technology was the examiner and Hendrik Schlune, Ph.D. student at Concrete Structures, Chalmers University of Technology was the supervisor for the master's thesis.

We would like to thank and acknowledge Ph.D. Mario Plos for assistance, guidance and support, especially regarding finite element analysis. For his support and assistance throughout the project, we would like to thank and acknowledge Hendrik Schlune. For the experimentally measured data, we would like to thank Raid Karoumi and Mahir Ülker-Kaustell from The Royal Institute of Technology (KTH). For structural drawings and related information, we would like to thank the Swedish Road Administration (Vägverket). We would also like to express our gratitude to Professor Thomas Abrahamsson and Ph.D. Håkan Johansson for valuable advice and discussions.

To our opposition group, Kaspar Lasn and Oscar Jaramillo de Leon, we would like to express our appreciation for their constructive criticism throughout the project.

Finally, we would like to thank our families and our friends in Sweden and the United States for their love and constant support throughout the project.

Göteborg December 2007

David Johnson and Fredrik Jonsson

Notations

Roman upper case letters

A_c	Area of concrete
A_{Asph}	Area of asphalt
COV	Covariance
\mathbf{D}	Correlation matrix parameter estimate and noise
$E\{ \}$	Expected value operator
E_{cm}	Mean modulus of elasticity of concrete
E_{eq}	Equivalent modulus of elasticity of the arch
$F_{hang,FEM}$	Calculated force in the hangers
$F_{hang,measured}$	Measured force in the hangers
G_c	Shear modulus of concrete
$I11_{eq}$	The equivalent bending inertia of the carriageway about transverse axis
$I22_{eq}$	The equivalent bending inertia of the carriageway about vertical axis
J_{Asph}	Torsional inertia of the asphalt layer
J_{eq}	The equivalent torsional inertia of the carriageway
J_{a-carr}	The torsional inertia in the connections arch/carriageway
K_{a-carr}	The rotational stiffness in spring element in the connections arch/carriageway
$T_{asphalt,mean}$	The mean temperature in the asphalt layer
\mathbf{V}	Variance matrix
\mathbf{W}_{zz}	Weighting matrix

Roman lower case letters

\mathbf{e}	Error vector
f_{cm}	Mean compressive strength of concrete
f_i	Eigenfrequency , $i = 1, 2 \dots n$
u	Displacement
\mathbf{z}	Response vector
\mathbf{z}_{FEM}	Calculated response vector
\mathbf{z}_M	Measured response vector

Greek letters

ε	Strain
$\boldsymbol{\theta}$	Updating parameter vector
$\boldsymbol{\theta}_0$	Initial value, updating parameter

Φ	Normalized updating parameter vector
Π	Objective function in general
$\sigma_{\Phi}^{\Phi} \Pi$	Standard deviation regularization term for updating parameters
$\sigma^z \Pi$	Standard deviation objective function for response
$\sigma^f \Pi$	Standard deviation objective function for frequency, \mathbf{f}
$\sigma^{\epsilon} \Pi$	Standard deviation objective function for strain, ϵ
$\sigma^u \Pi$	Standard deviation objective function for displacement, \mathbf{u}
$\rho_{Railings}$	Equivalent density of the railings
$\rho_{Drainage}$	Equivalent density of the drainage
$\rho_{walkways}$	Equivalent density of the walkways
$\rho_{asphalt}$	Density of the asphalt
σ	In statistical context, the standard deviation
σ_{ϕ}	Deviation of update parameter
σ_z	Deviation of response

1 Introduction

The New Svinesund Bridge is a connection between Sweden and Norway with huge symbolic value as a “borderless partnership” between the two countries. The design of the single arch with a suspended deck was the victor of an international design competition, chosen because the design harmonized aesthetic and environmental demands with technological capability and economics.

Due to the uniqueness and intrinsic value of the bridge, it has been carefully studied through an extensive long-term monitoring program. The monitoring program has been developed in collaboration with the Swedish National Road Administration (Vägverket), the Royal Institute of Technology (KTH), the Norwegian Geotechnical Institute (NGI), and the Norwegian Public Roads Administration (Statens vegvesen). KTH gathered static and dynamic data for the New Svinesund Bridge during the construction and operation phases, additional information regarding the monitoring project may be found in James and Karoumi (2003) and Ülker-Kaustell, Karoumi (2006) and Karoumi and Andersson (2007).

Chalmers University of Technology initiated a research project concerning bridge assessment and maintenance based on finite element (FE) analysis and field measurements, for which the New Svinesund Bridge is used as a case study. Results from the monitoring project are used in this thesis to update the FE model. The updated FE model developed in this project is intended to be used by Chalmers, KTH and Vägverket for further analysis and assessment during the service state of the bridge.

1.1 Description of the New Svinesund Bridge

The New Svinesund Bridge was constructed between 2002 and 2005 as an essential link in the Scandinavian transportation infrastructure and is now in operational phase with an expected service life of at least 120 years according to Vägverket (2004). The bridge consists of 8 spans for a total of 704 m with a main span of 247 m and was the world’s largest single-arch bridge at the time of completion, see Figure 1.1. The large, slender arch of the main span crosses the Ide fjord at Svinesund, providing a crucial link for the European route E6 between Sweden and Norway. The arch consists of a hollow rectangular box section of reinforced concrete that tapers in both directions from the abutment to the arch crown, thereby reducing the cross-section. The bridge superstructure is composed of two steel box girders, one for each direction of traffic. The steel bridge deck is monolithically attached to the arch at approximately half its height with transversally oriented prestressing tendons, thus assuring full interaction between the arch and bridge superstructure and providing lateral stability to the slender arch. In order to prevent uplifting of the bridge superstructure from the piers, prestressing tendons secure the cross-members of the bridge superstructure to the pier, see Figure 1.2. At the top of each pier is a spherical bearing, designed to allow translation and/or rotation according to the design. Construction was completed in February 2004 and the bridge was opened in June 2005. Detailed information regarding the bridge geometry, structural system and construction may be found in

James and Karoumi (2003), or in the web sites www.vv.se/svinesund or www.byv.kth.se/svinesund.

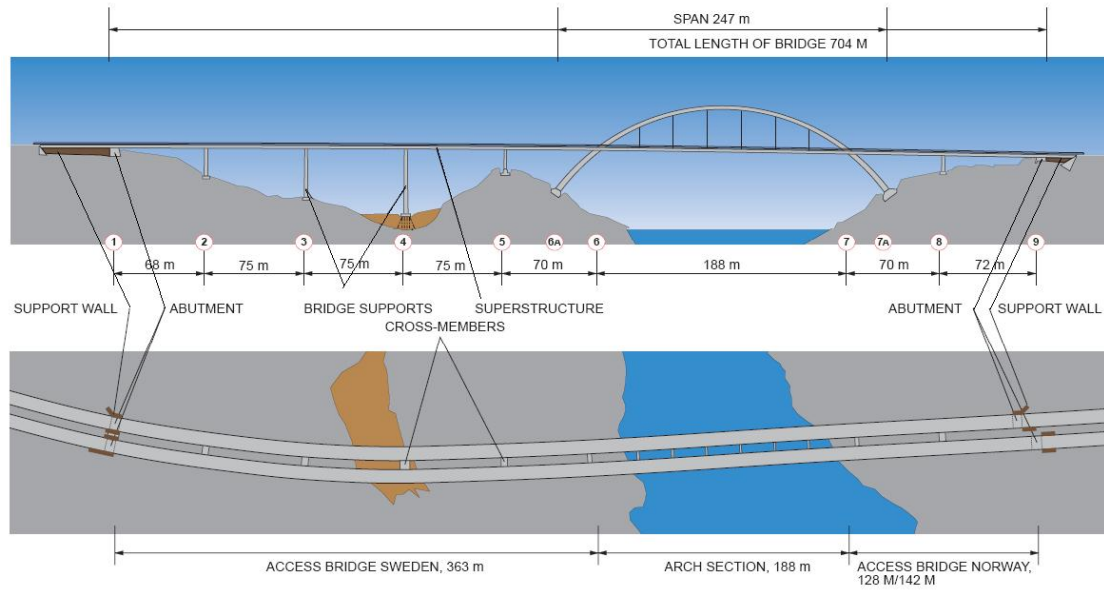


Figure 1.1 Layout sketch of the New Svinesund Bridge showing numbered supports and span lengths (From www.vv.se/svinesund)



Figure 1.2 Section of bridge deck superstructure (From www.vv.se/svinesund)

1.2 Instrumentation of the bridge

Structural monitoring of the New Svinesund Bridge is accomplished using sensors installed during construction. Data acquisition systems at the base of the arch on each side of the bridge record data. The permanent bridge instrumentation system is capable of measuring strain, acceleration, temperature, and wind speed and direction. The measured data from the sensors is remotely accessible from KTH via an asymmetric digital subscriber line (ADSL).

Static and dynamic load tests were conducted 18-19 May 2005, before the bridge opening in June 2005, to verify the predicted structural behaviour of the bridge. In addition to the permanently installed instrumentation, displacement measurements of the arch and carriageway were conducted by FB Engineering during the static load testing. Hanger load forces due to dead weight were also measured.

1.3 Finite element modelling of the bridge

The FE model presented in this report is based on the original FE model produced by the bridge contractor, Bilfinger Berger (2004), which was used for global structural analysis of the bridge. The original FE model created for bridge design was converted to the FE program ABAQUS by Plos and Movaffaghi (2004) for further analysis as part of the operational monitoring project. Continued development of the FE model of the New Svinesund Bridge by FE model updating allows for accurate structural static and dynamic analysis and assessment during the service life of the bridge.

1.4 Aim and objectives

The aim of this study was to use the FE updating procedure for calibration of the FE model that is to be used for analysis of static and dynamic response. The FE model and ABAQUS input files were obtained for the model created by Plos and Movaffaghi (2004) to ensure consistency of work. Both static and dynamic target responses were used for FE model updating and to provide verification of the updated model. The updated FE model may be used for assessment of the global structural behaviour of the bridge during its service life and as a starting point for non-linear analysis including ultimate limit state capacity.

1.5 Scope of study

The FE model ABAQUS input files created by Plos and Movaffaghi (2004) were utilized and a structured FE model updating procedure was developed. Refinement of the original model was first implemented manually and changes were made according to a parametric study of the uncertain structural parameters of the bridge. The FE updating procedure of the refined FE model was accomplished using MATLAB while ABAQUS performed FE calculations. The FE model updating procedure was tested

with a simple model of a beam with translational and rotational spring supports. This simple model verified the updating procedures before the FE model updating methodology was applied to the New Svinesund Bridge FE model. Results from FE model updating were verified by engineering judgement and comparison with results from previous analyses.

In order to verify the FE model used during design to predict ultimate load carrying capacity, load tests for the New Svinesund Bridge were conducted in the service state. FE model updating is useful when the uncertainty of the FE model used in design is unacceptable due to deviation between the FE results and measurements. If the FE model cannot accurately predict the response in the service state, it should not be trusted for ultimate limit state capacity calculations and thus the ultimate load carrying capacity of the bridge is uncertain. In such a case, FE model updating is useful for model calibration. If the updated FE model is capable of accurately reproducing the experimental measurements, it may be used to verify the ultimate limit state capacity of the bridge and thus to verify the ultimate load-bearing capacity.

1.6 Limitations

Intrinsic limitations exist in numerical modelling of existing structures. Material properties, structural behaviour and model geometry are idealized and discretized using finite elements whose behaviour are governed by known analytical differential equations. At each step in modelling, approximations are therefore introduced. For FE model updating, the chosen FE model must be able to accurately model the bridge while minimizing model complexity and thus reducing computational time. Although highly detailed FE models with non-linear material constitutive relationships and higher-order elements are capable of modelling in great detail, the high degree of complexity of the model and the non-linear behaviour requires robust iterative solution methods which drastically increase computational time, making such models impractical for FE model updating.

Furthermore, uncertainties exist in the physical structural parameters (e.g. concrete stiffness, boundary conditions, etc.) of the bridge. Quality control during construction can minimize uncertainty, but deviations from the design model are expected and accounted for during the design process. Experimental measurements of the bridge response should account for uncertainty of the structural parameters as well as the uncertainty of the sensors and the measurement system. Environmental parameters including wind and temperature variations produce measurement noise and bias which contribute to experimental uncertainty.

Engineering judgement and statistical methods should be used when evaluating the results of an FE model. An engineer must consider the ability of the numerical model to represent the actual physical behaviour of the bridge with regard to previously discussed limitations. Due to the use of linear material constitutive relations, the developed FE model should only be used directly for serviceability limit state (SLS) analysis. The updated FE model of the New Svinesund Bridge obtained by this analysis is a sort of “footprint” that can be utilized for further research. If the developed FE model is modified to include the non-linear behaviour of reinforced concrete and steel, the modified model can be used to verify structural integrity for

ultimate limit state (ULS) load combinations and even to predict a failure mechanism in failure modelling. One should exercise caution when modelling different loading cases or using non-linear constitutive models (e.g. failure modelling) and scrutinize results carefully. Boundary conditions should be carefully studied and all results should be evaluated with regard to engineering judgement.

2 Theory

2.1 Finite element method

2.1.1 FE overview

The finite element method, FEM, is an extremely useful engineering tool for numerically approximating physical systems that are too complex for an analytical solution or are governed by behaviour that is too complicated for classical analytical solution methods. Specifically, FEM is used in engineering to find an approximate solution to partial differential equations and integral equations. Finite element analysis (FEA) refers to numerical analysis of physical phenomena by dividing the region of interest into smaller pieces, *finite elements*. Over the finite elements, physical parameters are considered to be constant, vary linearly or vary according to a polynomial depending on the analysis method. Linear approximation is a common approximation and generates useful results for most applications. Complex physical problems governed by differential equations may be simplified using finite elements with linear elastic behaviour modelled with gradients calculated by the finite difference method for the non-linear problem near the values of interest. Matrix algebra is then used to solve the linear approximation systematically.

Global equilibrium of the system with compatibility and constitutive relations for each element must be maintained in order to solve a given system. The value of each parameter of interest for a specific element is approximated and depends on the element size and approximation technique. Simple models with large elements are quickly computed, but overly approximated systems intrinsically contain numerical errors that render the FE model useless for physical interpretation of results. Complex models with fine resolution (small elements, fine mesh) can yield more realistic results at the cost of increased computational time. An optimal model yields accurate, physically realistic results with minimal computational time.

Each degree of freedom (such as x , y , or z translation or rotation of a node) added to the model increases the number of necessary computations, so models should be simplified whenever possible. Large, slender objects such as plates or beams may be approximated according to plane stress, plane strain or beam theory, thus reducing the total degrees of freedom in the model and thus the required computations. Convergence analysis can be implemented by evaluating a target response with an increasingly fine finite element mesh (decreasing element size) or by refining some other model parameter. If the results deviate instead of converge, an intrinsic problem with the finite element model likely exists and the results of the numerical analysis should not be trusted.

2.1.2 FEM applications

FEM has been extensively utilized in structural and mechanical engineering and many FEA programs exist for the civil, aeronautical and automotive industries. Applications include structural, fluid flow, dynamic mechanical and electrostatic analysis. In structural analysis, the applications of FEM and FEA are virtually limitless and many

analysis types and element types exist for solving special problems while new methodologies, programs and element types are constantly being developed.

Generally, FEA requires three steps: pre-processing, FE calculations and post-processing. Many commercial FE software packages include graphical user interfaces for each of these steps and many are compatible at each step.

Pre-processing is the step where the FE model is built and the material properties, loads and boundary conditions are defined. This crucial step realizes the FE model and modelling parameters as to best represent the behaviour of the object of interest. Many commercial FE programs utilize an inbuilt CAD-type (Computer Aided Drafting) interface to build the model geometry in 1, 2 or 3 dimensions. Sometimes the model is imported from CAD files, IGES (Initial Graphics Exchange Specification) files, blueprints or text input files. Material properties for individual elements, as well as global environment parameters (e.g. gravity) are assigned to best represent reality. After the geometry is defined, element types are chosen and the model is transformed into a system of discrete elements by meshing. Commercial FE programs offer a choice between automatic meshing and user-defined meshing. The resulting discrete system is composed of *finite elements*. Boundary conditions must be carefully chosen as to provide constraints. Typical boundary conditions for structural analysis include constrained translation and rotation at foundations while typical internal constraints resist translation and rotation in connections between structural members. These constraints either allow no translation or rotation (fully-fixed DOF) or apply a load proportional to the node translation or rotation (linear-elastic spring at DOF). Finally, load cases are defined for the analysis; options include static, dynamic and frequency analysis.

The analysis step, which performs FE calculations, solves the equation system defined in the pre-processor. Model geometry, element types, material models, internal constraints and boundary conditions are all taken into consideration by the FE solver.

FE post-processing utilizes the results of the FE calculations for output, visualization and further analysis. At this point, FE results may be compared to measured values, hand calculations or other analyses for FE model verification. The verified model may then be used to predict behaviour resulting from various loads and conditions. The FE model updating procedure compares the structural response and eigenvalues predicted by the FE model with field or laboratory measurements, and then updates uncertain FE modelling parameters to obtain a better correlation and to minimize modelling error.

2.1.2.1 Modeling

In the FE pre-processing stage, the model is defined. Most structural FE models are use Cartesian coordinates (rectangular x,y,z coordinate system) in 2D or 3D modeling space. For a general node in 3D, there are six degrees of freedom (DOF): x,y,z translation (DOF: 1-3 in ABAQUS) and x,y,z rotation (DOF: 4-6 in ABAQUS).

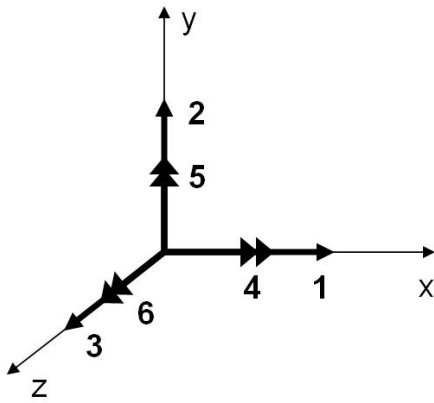


Figure 2.1 ABAQUS degrees of freedom (DOF) in Cartesian coordinates.

Each part of the model may be created separate from the assembled structure and added in the assembly phase. Each part is added to the assembled structure by defining boundary conditions and internal constraints on certain DOF of the part and on the global assembly. Two beams may be connected using the “TIE” command in ABAQUS, which constrains all DOF of the constrained nodes so that if the constrained node from one beam is translated or rotated, the constrained node from the other beam must translate or rotate in an identical fashion. Global constraints (boundary conditions) typically constrain DOF of nodes of the entire assembled model. Boundary conditions are created by setting DOF of a particular node equal to zero or by making a resultant force linearly proportional to the displacement or rotation of the node.

2.1.2.2 Structural analysis

Many FEA software programs exist to perform many types of analysis. Structural FEA, though only a subset of the available FEA, is a powerful tool for structural analysis. Typically, structural members are greatly simplified to evaluate the global response of the structure, but detailed analysis can be extremely useful when evaluating connections or specific structural details.

In most situations, static linear-elastic analysis is sufficient to determine structural behaviour. Many options exist for such analysis and static analysis is frequently used in structural FEA. In the event that a system susceptible to second order effects is exposed to large magnitude time variant forces, dynamic analysis or equivalent static is necessary. Structural dynamic analysis evaluates the time variant behaviour of a structure. Different time stepping routines may be used depending on required accuracy and available computational power. Dynamic analysis is quite common in the automotive and aerospace industries, but not as widely used in structural FEA since most structures are designed to resist time variant forces without experiencing significant motion or deformation. One exception is the dynamic response of slender bridges to wind and traffic. The structural integrity of all bridges must be verified when the structure is exposed to worst-case-scenario dynamic loading (though equivalent static loading may also be used). The characteristic natural frequencies (eigenfrequencies) are of interest because the eigenfrequencies and eigenmodes of a structure define the vibration behaviour of the structure. Thus, frequency analysis is

quite common, especially for large bridges. Frequency analysis should be carried out early in the design phase of second order structures. Large amplitude vibrations can be avoided by changing the vibration characteristics of the structure by adding damping, increasing stiffness and decreasing mass.

2.1.2.3 Elements

In order to model different physical phenomena, different FEM elements are used. In the simplest case, 1D linear elasticity, a 1 node spring and mass element with 1 DOF can be used. More complicated element types have more nodes with more DOF for each node and can represent increasingly complicated physical behaviour. Elements with polynomial shape functions, known as higher order elements, can model bending more accurately than linear elements. Structural FEA typically utilizes small, simple elements for global analysis, larger elements with more DOF for complicated local structural behaviour or a combination of simple and complicated elements to model both global and local structural behaviour.

Efficient modelling of global structural behaviour requires model simplification in order to reduce computational time and to permit calculation of eigenfrequencies and eigenmodes. The most common element types for modelling global behaviour are truss, beam, membrane and shell elements. Truss elements have 2 nodes with 1 DOF for each node and can only model axial force and axial deformation. Cables and truss structures may be modelled using truss elements if one is certain that no moment is transferred from the cable or truss and that the structural member is sufficiently slender that the stress distribution is sufficiently uniform. Beam elements can transfer axial force, shear and bending. The cross-sectional properties of the beam may be defined using standard types (such as I-profiles and box beams) in commercial FE software, or generalized sections can be defined with user input data for area moment of inertia about the primary and secondary axis. Integration points span the cross-section and are used to discretize the inertial properties of the cross-section for numerical integration. Euler-Bernoulli beam theory assumes that plane sections remain plane, neglecting rotatory inertia, principal shear deformation and combined rotatory inertia and shear deformation. Euler-Bernoulli beam elements are valid for slender beams (aspect ratio, length divided by height, greater than 10) loaded primarily in bending such that bending deformation is much greater than shear deformation. Timoshenko beam theory includes rotatory inertia, principal shear deformation and combined rotatory inertia and shear deformation. Timoshenko beam elements can more accurately model deep beams (aspect ratio greater than 2), where shear deformation and rotatory inertia should not be neglected. Derivations of Euler-Bernoulli and Timoshenko beam theory from governing partial differential equations of motion are available in Craig et al. (2006). The Galerkin method can be used to derive the finite element matrix equation for Euler-Bernoulli beam elements while the energy method can be used to derive the FE matrix equations for Timoshenko beam elements according to Kwon and Bang (2000).

Euler-Bernoulli beam theory,

$$\frac{\partial^2}{\partial x^2} \left(EI \frac{\partial^2 u}{\partial x^2} \right) - \left(p_y(x,t) - \rho A \frac{\partial^2 u}{\partial t^2} \right) = 0 \quad (2.1)$$

Timoshenko beam theory,

$$\begin{aligned} & \frac{\partial^2}{\partial x^2} \left(EI \frac{\partial^2 u}{\partial x^2} \right) - \left(p_y(x,t) - \rho A \frac{\partial^2 u}{\partial t^2} \right) - \rho I \frac{\partial^4 u}{\partial x^2 \partial t^2} \\ & + \frac{EI}{\kappa GA} \frac{\partial^2}{\partial x^2} \left(p_y(x,t) - \rho A \frac{\partial^2 u}{\partial t^2} \right) - \frac{\rho I}{\kappa GA} \frac{\partial^2}{\partial t^2} \left(p_y(x,t) - \rho A \frac{\partial^2 u}{\partial t^2} \right) = 0 \end{aligned} \quad (2.2)$$

Surfaces may be modelled in FEM with membrane and shell elements. A quadrilateral membrane element has 4 nodes with 2 in-plane DOF for each node. Membrane elements are capable of modelling in-plane forces and bending. If out of plane bending for thin plates should be modelled, plate elements that utilize classical Kirchoff plate theory are often used. Classical plate theory assumes plane stress or plane strain and an undeformed neutral plane of the plate. Plate elements can be used to evaluate buckling risk for slender plate structures and to find deformation of plates loaded transversely to the plate plane. A derivation of the FE formulation for plate elements with classical Kirchoff plate theory is available in Ottosen and Petersson (1992). The Galerkin method is used to derive the FE matrix equation for a classical Kirchoff plate element in Kwon and Bang (2000). Shell elements have curvature along the surface and have 5 DOF for each node, three translational DOF and two rotational DOF. The curved surface of shell elements enables the modelling of curved structural members without requiring as fine of a mesh as is needed when discretizing using plate elements. Furthermore, solid continuum elements may be degenerated into shell elements, thus reducing total model DOF while retaining model accuracy. The effect of transverse shear deformation may be included using Mindlin/Reissner plate theory; a derivation of the FE matrix equation using internal energy is available in Kwon and Bang (2000).

Classical Kirchoff plate theory,

$$\frac{\partial^4 u}{\partial x^4} + 2 \frac{\partial^4 u}{\partial x^2 \partial y^2} + \frac{\partial^4 u}{\partial y^4} - \frac{12(1-\nu^2)}{Et^3} q(x,y) = 0 \quad (2.3)$$

Once global behaviour is obtained by simplified global analysis, local analysis can be used to assess structural details. Local analysis of structural details can be used to find the stresses in regions with non-uniform stress distribution, such as structural connections. Solid (continuum) elements are useful for such general modelling. Brick and tetrahedral elements with linear-elastic material properties are commonly used, especially for 3D SLS analysis, but higher order continuum elements with specialized constitutive material relations can be used for specialized purposes. A typical example of a specialized structural analysis is FEA of a continuous reinforced concrete beam loaded until failure. The stresses are redistributed across the beam cross-section after concrete cracking initiates and the concrete-reinforcement bond properties determine the cracking pattern. For accurate analysis, the constitutive equations must include

non-linear crushing of the concrete, tensile softening of concrete, concrete-reinforcement bond slip and elastic-perfectly-plastic reinforcement steel stress vs. strain.

Special structural elements include springs, dashpots, point masses, point rotary inertias and rigid connections. These are especially useful for simplified global analysis, where a simplified model with beam elements does not adequately describe the dynamic behaviour of the structure. Springs and rigid connections can provide internal constraints and boundary conditions to more realistically model structural geometry (e.g. rigid elements of the width of a beam with full interaction with the beam element can provide internal connections). Point mass, point rotary inertia and dashpots change the dynamic properties of the structure and can be used to tune the modal mass and modal damping matrices to better correspond to measurements.

SLS behaviour is of primary interest and accurate FE modelling was accomplished by simplified global analysis with beam elements and linear-elastic constitutive relations.

2.1.2.4 Material properties

The stress-strain relationship is defined in the structural FEA according to the applicable material model. Isotropic material properties are used in this study and are the most common for FEA. Isotropic material properties are homogeneous and identical in all directions. Anisotropic materials are the most general and have material properties that depend on direction. Crystalline materials are anisotropic and material properties depend on crystalline plane and grain boundary orientation. Orthotropy is a special case of isotropy and orthotropic materials have different material properties in orthogonal directions. These include glass and carbon fiber composites, wood and rolled steel. Hooke's Law of linear elasticity describes the relationship between stress and strain,

$$\boldsymbol{\sigma} = \mathbf{E}\boldsymbol{\varepsilon} \quad (2.4)$$

Anisotropic stress vs. strain relation,

$$\begin{bmatrix} \sigma_{xx} \\ \sigma_{yy} \\ \sigma_{zz} \\ \sigma_{yz} \\ \sigma_{zx} \\ \sigma_{xy} \end{bmatrix} = \begin{bmatrix} E_{11} & E_{12} & E_{13} & E_{14} & E_{15} & E_{16} \\ E_{21} & E_{22} & E_{23} & E_{24} & E_{25} & E_{26} \\ E_{31} & E_{32} & E_{33} & E_{34} & E_{35} & E_{36} \\ E_{41} & E_{42} & E_{43} & E_{44} & E_{45} & E_{46} \\ E_{51} & E_{52} & E_{53} & E_{54} & E_{55} & E_{56} \\ E_{61} & E_{62} & E_{63} & E_{64} & E_{65} & E_{66} \end{bmatrix} \begin{bmatrix} \varepsilon_{xx} \\ \varepsilon_{yy} \\ \varepsilon_{zz} \\ \varepsilon_{yz} \\ \varepsilon_{zx} \\ \varepsilon_{xy} \end{bmatrix} \quad (2.5)$$

Isotropic stress vs. strain relation,

$$\begin{bmatrix} \sigma_{xx} \\ \sigma_{yy} \\ \sigma_{zz} \\ \sigma_{yz} \\ \sigma_{zx} \\ \sigma_{xy} \end{bmatrix} = \frac{E}{(1+\nu)(1-2\nu)} \begin{bmatrix} 1-\nu & \nu & \nu & 0 & 0 & 0 \\ \nu & 1-\nu & \nu & 0 & 0 & 0 \\ \nu & \nu & 1-\nu & 0 & 0 & 0 \\ 0 & 0 & 0 & 1-2\nu & 0 & 0 \\ 0 & 0 & 0 & 0 & 1-2\nu & 0 \\ 0 & 0 & 0 & 0 & 0 & 1-2\nu \end{bmatrix} \begin{bmatrix} \varepsilon_{xx} \\ \varepsilon_{yy} \\ \varepsilon_{zz} \\ \varepsilon_{yz} \\ \varepsilon_{zx} \\ \varepsilon_{xy} \end{bmatrix} \quad (2.6)$$

Structures analysed in the serviceability limit state (SLS) utilize a linear-elastic stress-strain relationship. This assumption allows for the calculation of deformations, natural frequencies, reaction forces, stresses and strains during the life of a structure. Linear-elastic modelling is useful for determining the onset of yielding, but it cannot always predict the failure mechanism of a structure.

Structures are normally designed in the ultimate limit state (ULS) to resist the rare load combination as designated in the structural design code. Perfect plasticity is a useful simplification assuming that the materials have sufficient ductility for ULS load-bearing capacity.

Modelling of reinforced concrete is especially difficult because the model must account for the softening plasticity of concrete while accounting for the plastic behaviour of the reinforcing steel and the concrete-steel bond. Such complicated behaviour requires a very specialized material model with a non-linear constitutive relation, thus simplifications are used whenever possible.

Various non-linear analysis techniques exist for other cases, though linear-elastic analysis remains the most popular and most useful analysis type.

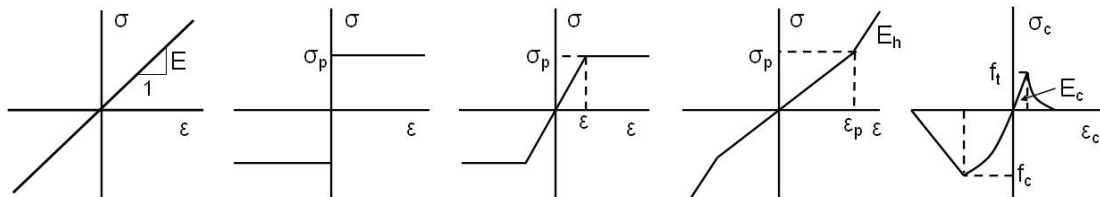


Figure 2.2 Stress vs. strain relationship for: linear elasticity, perfect plasticity, elastic-perfectly plastic, hardening plasticity and concrete softening.

2.1.2.5 Meshing

In order to discretize a model for numerical analysis, the continuous body must first be meshed into discrete finite elements. During the meshing process, simplifications are made for the geometry of the continuous body. At curves along the surface of the body, the discretized model will have discontinuities in curvature if flat elements are used. An increased mesh density reduces the modelling error due to curvature discontinuities but a fine mesh has more elements and more DOF, thus requires more

computational time. If the mesh density was infinite, the FE model geometry would be identical to the geometry of the continuous body, but such a system is not possible to model numerically. In reality, a balance exists between mesh density, desired model accuracy and computational time. As the element size is decreased, the FE response of a convergent FE model becomes increasingly accurate. During mesh refinement, an optimal mesh density is obtained when convergence is evident and the FE model is capable of modelling response to the desired accuracy.

2.1.3 FE general concepts

2.1.3.1 Equilibrium

Force and moment equilibrium must be satisfied for each element. The static bending moment of a symmetric beam section normal to the x-axis and loaded about the xz-plane may be expressed as in terms of the stress components,

$$M = \int_A z \sigma_{xx} dA \quad (2.7)$$

Vertical shear force in a beam may be expressed as,

$$V = \int_A \sigma_{xz} dA \quad (2.8)$$

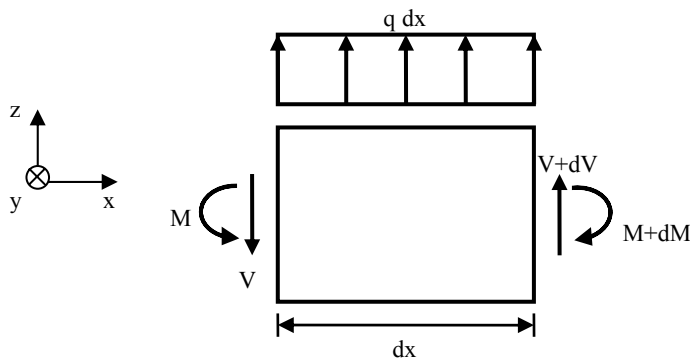


Figure 2.3 Infinitesimal beam segment.

Vertical force equilibrium of an infinitesimal beam segment,

$$\frac{dV}{dx} = -q \quad (2.9)$$

Moment equilibrium of the infinitesimal beam segment,

$$\frac{dM}{dx} = V \quad (2.10)$$

Thus the differential equation for moment as a function of applied load is obtained,

$$\frac{d^2 M}{dx^2} + q = 0 \quad (2.11)$$

Typical structural analysis employs matrix notation for the equation. For linear-elastic static analysis, the global force vector is the product of the global stiffness matrix and the nodal displacement.

$$\mathbf{K}\mathbf{u} = \mathbf{F} \quad (2.12)$$

In dynamic analysis, equilibrium equations account for body inertia, dissipative forces, internal loads carried by the structure and external loads (including reaction forces).

$$\mathbf{M}\ddot{\mathbf{u}} + \mathbf{C}\dot{\mathbf{u}} + \mathbf{K}\mathbf{u} = \mathbf{F}(t) \quad (2.13)$$

The characteristic bending frequencies of a structure occur at equilibrium of inertial forces and internal forces caused by the structural deformation. Ignoring dissipative forces (e.g. damping) and assuming harmonic free-vibration, the eigenfrequencies (natural frequencies) and corresponding eigenmodes of the structure are obtained as follows,

$$\mathbf{M}\ddot{\mathbf{u}} - \mathbf{K}\mathbf{u} = \mathbf{0} \quad (2.14)$$

Assuming harmonic free vibration,

$$\mathbf{u} = \mathbf{U} \cos(\varpi t + \alpha) \quad (2.15)$$

Taking the derivative with respect to time and substituting equation 2.9 into 2.8, the algebraic eigenvalue problem is obtained,

$$[\mathbf{K} - \varpi^2 \mathbf{M}] \mathbf{U} = \mathbf{0} \quad (2.16)$$

The nontrivial solution to equation 2.10 is obtained from the characteristic equation,

$$\det(\mathbf{K} - \varpi^2 \mathbf{M}) = 0 \quad (2.17)$$

For the eigenvalues, ϖ^2 , obtained from equation 2.11, the modal matrix contains the corresponding mode shapes, Φ ,

$$\Phi \equiv [\phi_1 \ \phi_2 \ \dots \ \phi_n] \quad (2.18)$$

The algebraic eigenvalue problem, equation 2.10, may be re-written for all n modes,

$$\mathbf{K}\Phi = \mathbf{M}\Phi\Lambda \quad (2.19)$$

With the corresponding eigenvalue matrix defined as, Λ ,

$$\Lambda \equiv \text{diag}(\varpi_1^2, \varpi_2^2, \dots, \varpi_n^2) \quad (2.20)$$

2.1.3.2 Kinematics

The kinematic relationship is assumed using theory. In the case of Euler-Bernoulli beam bending, the neutral axis is assumed to remain normal to beam cross sections during bending (thus neglecting shear deformation). Thus the longitudinal displacement, u_x , is related to deflection due to bending, u_z , for an infinitesimal beam segment as,

$$u_x = u_x^0 - z \frac{du_z}{dx} \quad 2.21$$

Considering the differential relationship between longitudinal displacement and longitudinal strain,

$$\varepsilon_{xx} = \frac{\partial u_x}{\partial x} \quad 2.22$$

With beam curvature defined as,

$$\kappa = \frac{d^2 u_z}{dx^2} \quad 2.23$$

Longitudinal strain (the only non-zero strain component) for an infinitesimal Euler-Bernoulli beam segment is related to deflection as,

$$\varepsilon_{xx} = \frac{du_x^0}{dx} - z \frac{d^2 u_z}{dx^2} \quad 2.24$$

$$\varepsilon_{yy} = \varepsilon_{zz} = \varepsilon_{xy} = \varepsilon_{yz} = \varepsilon_{xz} = 0 \quad 2.25$$

2.1.3.3 Constitutive relation

The relationship between stress and strain is defined by the constitutive relation (refer to Section 2.1.2.4). For Euler-Bernoulli beams, the linear elastic stress-strain relationship for isotropic materials described by Hooke's law is simplified due to kinematic assumptions,

$$\begin{bmatrix} \sigma_{xx} \\ \sigma_{yy} \\ \sigma_{zz} \\ \sigma_{yz} \\ \sigma_{zx} \\ \sigma_{xy} \end{bmatrix} = \frac{E}{(1+\nu)(1-2\nu)} \begin{bmatrix} 1-\nu & \nu & \nu & 0 & 0 & 0 \\ \nu & 1-\nu & \nu & 0 & 0 & 0 \\ \nu & \nu & 1-\nu & 0 & 0 & 0 \\ 0 & 0 & 0 & 1-2\nu & 0 & 0 \\ 0 & 0 & 0 & 0 & 1-2\nu & 0 \\ 0 & 0 & 0 & 0 & 0 & 1-2\nu \end{bmatrix} \begin{bmatrix} \varepsilon_{xx} \\ 0 \\ 0 \\ 0 \\ 0 \\ 0 \end{bmatrix} \quad 2.26$$

Often the uniaxial stress state is the only stress state of interest and is simplified as,

$$\sigma_{xx} = E\varepsilon_{xx} \quad 2.27$$

The preceding derivations as well as kinematic and constitutive derivations for plates are available in Ottosen and Petersson (1992).

2.1.3.4 Discretization

The finite element chosen to discretize a structural member must satisfy the completeness and compatibility requirements. A shape function is assigned to a finite element and is chosen to represent the behaviour of interest. For beam bending, completeness and compatibility are defined in Ottosen and Petersson (1992) as follows,

Completeness:

- The approximation for the deflection u_z must be able to represent an arbitrary rigid-body motion.
- The approximation for the deflection u_z must be able to represent an arbitrary curvature.

Compatibility:

- The approximation for the deflection u_z must vary continuously with continuous slopes over the element boundaries.

Shape functions describe the deflection of the beam element as a function of the longitudinal displacement. The “simplest possible beam element” capable of satisfying completeness and compatibility for Euler-Bernoulli beam theory is the cubic polynomial. Higher order polynomial terms are used for higher order elements.

2.1.3.5 Boundary Conditions

Global force equilibrium requires equilibrium of all forces and moments. The global force vector of equation 2.6 is the sum of the boundary force vector, \mathbf{F}_b , and the load vector, \mathbf{F}_l ,

$$\mathbf{Ku} = \mathbf{F} = \mathbf{F}_b + \mathbf{F}_l \quad 2.28$$

Static boundary conditions and kinematic boundary conditions constitute the global boundary conditions. For beam loading, the static boundary conditions are given by shear force, V , and moment, M , at the ends of the beam while the kinematic boundary conditions are described by the deflection, u_z , and slope, $\frac{du_z}{dx}$, at the ends of the beam.

2.2 Optimization

2.2.1 Optimization overview

In mathematics, optimization is the process of minimizing or maximizing a real function with respect to real or integer variables in a subspace. Many solution methods exist depending on the function of interest and subspace. The minimization of an objective function in a given subspace is especially useful when applied to the field of FEA. If the target responses of a FE model are compared with experimentally measured values, the residual is thus established and is a non-linear function of the input parameters. By minimizing the objective function that accounts for the residual of the response, with an optional regularization term, an FE model may be optimized.

2.2.2 Optimization general mathematical formulation

The general goal of optimization is to minimize or maximize an objective function. In this case, the residual is the difference between the calculated response of the system and the observed response of the system. The objective function is a function of the residual and the input parameters and can be nonlinear. The objective function is thereby minimized within an input parameter domain.

$$\min_{\Phi \in \mathbf{D}} \Pi(\Phi) \quad (2.29)$$

2.2.2.1 Global minimum vs. local minima

In the case of most deterministic optimization algorithms, local hill-climbing is used to find the location of a local minimum. Different algorithms utilize different strategies to maximize efficiency while traversing the objective space in search of the local minimum. One of the challenges of discrete optimization methods is to efficiently search for a local minimum in a region where the gradient of the objective function is near zero. Gradient based methods face ill-conditioning for the Jacobian and Hessian matrices and may encounter numerical difficulties at iteration steps. For such cases, conditioning should be monitored to ensure algorithm stability.

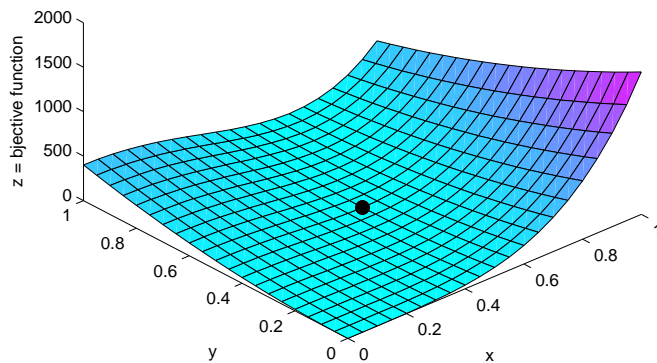


Figure 2.4 Surface plot of objective function (Rosenbrock banana function) used for testing local optimization algorithms (location of optimal solution shown with black dot).

Non-linear functions of many variables can contain many local minima in addition to the global minimum. Most deterministic algorithms will converge to the local minimum in the region of local convexity by local hill-climbing, but will fail to converge to the global minimum. When using a discrete function for which the analytical formulation is unknown, the shape of the objective function cannot be predicted and many local minima may exist. If the parameter space of the function is very large, finding a solution for global optimality is troublesome and can be computationally expensive. For such a problem, stochastic optimization methods are useful for determining the vicinity of a global optimum. The Nelder-Mead Simplex algorithm is capable of escaping local minima in some cases and can even handle discontinuities according to Coleman and Zhan (2007). Hybrid algorithms that utilize a rough stochastic global optimality search in combination with local hill-climbing for refinement of the final optimal solution are ideal for practical problems.

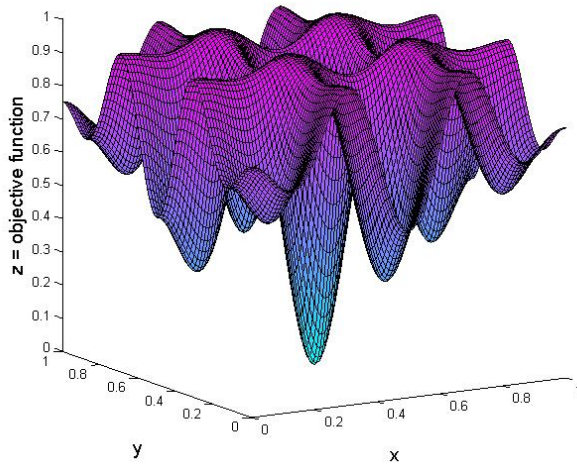


Figure 2.5 Surface plot of objective function with local minima and a unique global minimum.

For this project, a parameter response study was performed to explore the possibility of global minima, refer to Chapter 6.3. The existence of many local minima and flat objective space is very troublesome and is beyond the scope of this project.

2.2.3 Optimization – classical least squares estimate

In general, the responses of a system are some function of the input parameters. The simplest case is when the system is composed of a series of linear equations. The linear system may be expressed in matrix notation as,

$$\mathbf{S}\boldsymbol{\theta} = \mathbf{z} \quad (2.30)$$

Where,

$\boldsymbol{\theta}$ Vector of n input parameters, $[n \times 1]$

\mathbf{z} Vector of m responses (for measurement/observation), $[m \times 1]$

\mathbf{S} Sensitivity matrix relating the responses to the input parameters. This matrix is equivalent to the Jacobian matrix,

$$\mathbf{S} = \begin{bmatrix} \frac{\partial z_1}{\partial \theta_1} & \dots & \frac{\partial z_1}{\partial \theta_n} \\ \vdots & \ddots & \vdots \\ \frac{\partial z_m}{\partial \theta_1} & \dots & \frac{\partial z_m}{\partial \theta_n} \end{bmatrix} \quad (2.31)$$

In reality, measurement noise, disturbances in the environment of the experimental setup and modelling uncertainties exist for all systems. In order to account for errors, an error vector is introduced to the responses,

$$\mathbf{S}\boldsymbol{\theta} = \mathbf{z} - \mathbf{e} \quad (2.32)$$

The objective function represents the magnitude of the error of the response vector, defined as the difference between the observed responses compared with the expected value of the response,

$$\Pi(\mathbf{z}) = E \left\{ (\mathbf{z} - \mathbf{E}\{\mathbf{z}\})^T (\mathbf{z} - \mathbf{E}\{\mathbf{z}\}) \right\} \quad (2.33)$$

Expressed in terms of the measurement error,

$$\Pi(\mathbf{z}) = E \left\{ \mathbf{e}^T \mathbf{e} \right\} = E \left\{ \|\mathbf{e}\|^2 \right\} \quad (2.34)$$

The solution for equation (2.34) that minimizes the variance of the response vector is expressed using the Moore-Penrose pseudoinverse,

$$\hat{\boldsymbol{\theta}} = \mathbf{S}^+ \mathbf{z} \quad (2.35)$$

If the system of interest is overdetermined, meaning that the system has more observable responses than input parameters, then an exact solution is unlikely. This case requires more sensors than input parameter and produces a sensitivity matrix, \mathbf{S} , with linearly independent columns.

$$\mathbf{S}^+ = (\mathbf{S}^T \mathbf{S})^{-1} \mathbf{S}^T \quad (2.36)$$

In the event of an underdetermined system, an infinite number of input parameter combinations may be able to produce the observed response. For this case, equation (2.37) determines the solution that produces the smallest parameter change when compared with the initial input parameter vector. As such, the initial parameter vector estimate must be realistic. If the initial parameter vector estimate is close to the actual value, the calculated solution will be near the actual solution.

$$\mathbf{S}^+ = \mathbf{S}^T (\mathbf{S} \mathbf{S}^T)^{-1} \quad (2.37)$$

If the number of input parameters is identical to the number of output responses, the sensitivity matrix is square. If the rows and columns of the sensitivity matrix are linearly independent and it is positive definite, it may be inverted directly.

$$\mathbf{S}^+ = \mathbf{S}^{-1} \quad (2.38)$$

The MATLAB function ‘pinv’ computes the Moore-Penrose pseudoinverse described above using singular value decomposition. More information and a proof of the solution of the least squares estimate may be found in Söderström and Stoica (1989).

2.2.4 Optimization – Nelder-Mead simplex method

In the Nelder-Mead simplex method, the worst point of an n -dimensional simplex ($n + 1$ vertices) is reflected about the centroid of the remaining n points. For the simplified 2D ($n = 2$) simplex optimization, three points near a starting guess are evaluated (forming a triangle, a 2D simplex in the objective space). The three points are ordered according to the value of the objective function and the point with the maximum value for the objective function is reflected about the centroid of the remaining points (in this case, the axis connecting the remaining two points). This procedure is repeated until the optimization routine converges to the desired tolerance according to the prescribed optimality conditions. The Nelder-Mead simplex method for n -dimensional problems begins with a starting guess and perturbations near the starting guess that form the initial n -dimensional simplex to be evaluated. The value of the objective function at each vertex is evaluated and the vertices are organized in ascending order. The vertex with the highest value for the objective function is reflected about the centroid of the remaining vertices. If the reflected vertex has the minimum value of the objective function of all vertices, a minimum is expected to exist in the direction of the reflected vertex and the simplex is expanded in the direction of the reflected vertex. Simplex expansion increases the convergence rate of the algorithm by increasing step size along the search direction where a minimum is expected. Conversely, if the value for the objective function of the reflected vertex remains the maximum of all vertices, a minimum is assumed to exist within the simplex and the simplex is contracted. The iteration is thus completed and the search algorithm continues until the specified optimality conditions are satisfied.

Although the Nelder-Mead simplex algorithm is a sort of hill-climbing optimization routine, it is not gradient based and is thus less prone to numerical difficulties encountered with discretized gradient methods. For example, the simplex algorithm is more stable than gradient methods when searching for minima near discontinuities and asymptotes, where gradients calculated with the finite difference method are erroneous. When searching for a global minimum in a search space containing local minima, care must be taken when choosing the initial starting value and perturbation size. A small simplex will converge to a local minimum if all vertices are located within the convex subspace of the local minimum. If local minima are suspected to exist in the search space, many starting guesses across the search space should be evaluated to test for convergence. For information regarding Nelder-Mead simplex implementation in the MATLAB optimization toolbox, please refer to Coleman and Zhan (2007).

2.3 Statistics

For the scope of this project, a normal, or Gaussian, distribution is assumed for all measurements. This assumption is common in scientific and engineering practice and is assumed a priori. All statistical references and calculations in the report therefore correspond to the normal distribution. For more thorough statistical treatment of the measurements, small sample statistics with the Student's t -distribution could be considered for measurements with a low sampling rate and therefore a low sample population. The chi-square distribution is useful when evaluating the goodness of fit

of statistical data to a theoretical model. Further statistical analysis is recommended for future studies, but is beyond the scope of this project.

The standard deviation used when evaluating measurement statistics is the sample deviation of a non-infinite sample population and is defined as,

$$\sigma = \sqrt{\frac{1}{N-1} \sum_{i=1}^N (x_i - \bar{x})^2} \quad (2.39)$$

The mean value of the sample population of the measurement X is,

$$\bar{x} = \frac{1}{N} \sum_{i=1}^N x_i \quad (2.40)$$

The variance of the measurement X is therefore defined as,

$$\sigma^2 = E\{(X - \mu)^2\} \quad (2.41)$$

With,

$$\mu = E\{X\} \quad (2.42)$$

The probability distribution function (pdf) for the normal distribution (also referred to as the bell curve) is,

$$\text{pdf} = \frac{1}{\sigma\sqrt{2\pi}} \exp\left(-\frac{(x - \mu)^2}{2\sigma^2}\right) \quad (2.43)$$

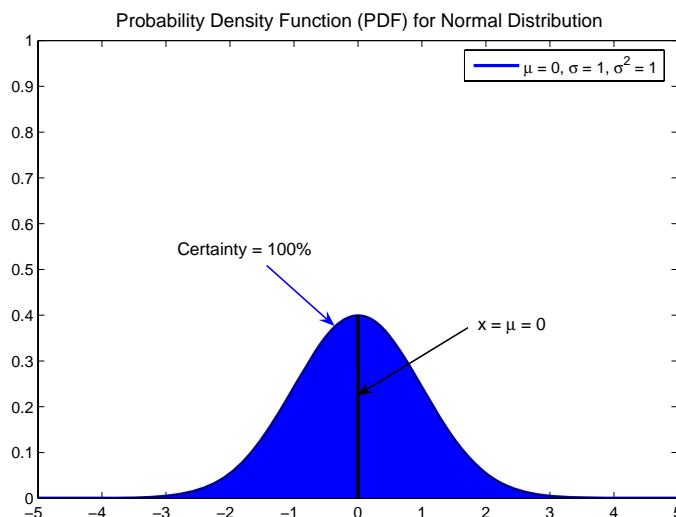


Figure 2.6 Plot of probability distribution function for normal distribution (bell curve).

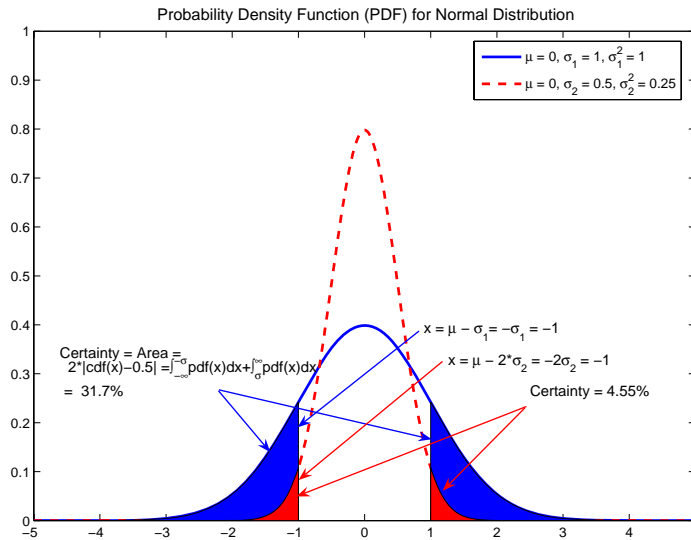


Figure 2.7 Plot of PDF exemplifying statistical properties for two statistical cases.

The cumulative distribution function (cdf) is the integral of the probability distribution function,

$$\text{cdf} = \int_{-\infty}^x \text{pdf} dx = \frac{1}{2} \left[1 + \text{erf} \left(\frac{x - \mu}{\sigma \sqrt{2}} \right) \right] \quad (2.44)$$

The error function, or Gauss error function, has the general form,

$$\text{erf}(x) = \frac{2}{\sqrt{\pi}} \int_0^x e^{-t^2} dt \quad (2.45)$$

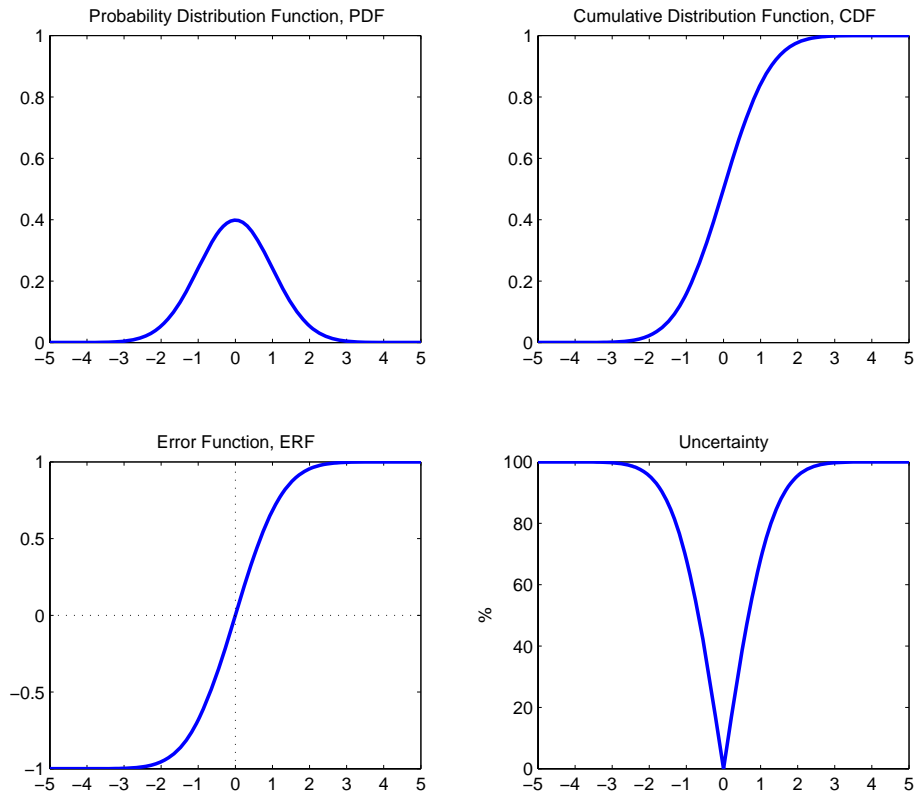


Figure 2.8 Clockwise from top left, plots of : PDF, CDF, ERF and uncertainty.

For this project, the uncertainty was defined as,

$$\text{uncertainty}(x) = |\text{erf}(x)| \tag{2.46}$$

Similarly, the certainty was defined as,

$$\text{certainty}(x) = 1 - |\text{erf}(x)| \tag{2.47}$$

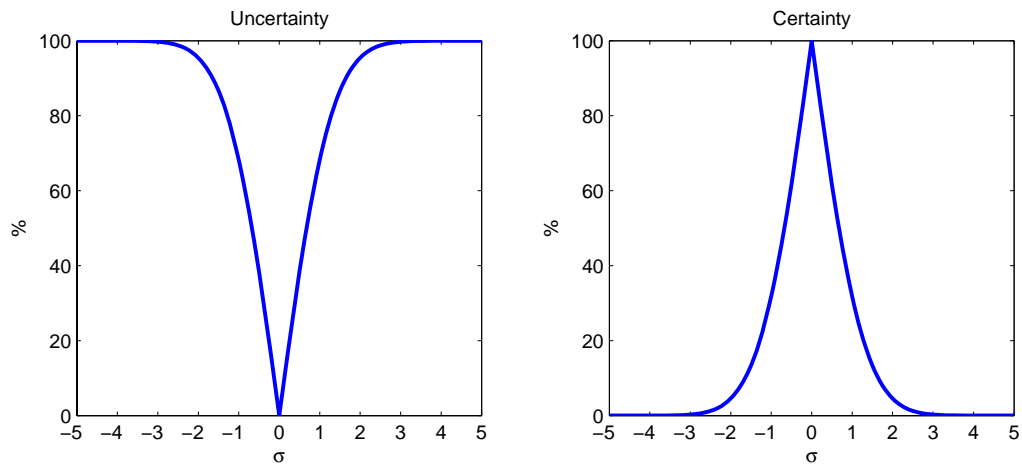


Figure 2.9 Plots of uncertainty and certainty.

The uncertainty and certainty functions will be used later for FE model evaluation and provide verification of FE model improvement. These functions also facilitated statistical analysis when comparing statistical data to the FE model and were used to identify load cases and measurements with poor statistical correlation.

2.4 Finite element model updating

2.4.1 FE model updating overview

Historically, FE model updating emerged in the 1990s as a tool for correcting invalid assumptions about a model using primarily vibration test data. FE model updating evaluates a FE model and compares the output target responses to experimental data. Uncertain input parameters are then iterated until more accurate target responses are obtained. Many iterations may be required for convergence, thus models should be simplified as much as possible in order to reduce the computational time at each of the iterations. The improved FE model can then be used for assessment of the structure. Improved modelling is of great importance to the design, construction and maintenance of civil engineering structures.

Both direct and sensitivity based FE model updating techniques exist and have been used in the fields of civil engineering, mechanical engineering and aeronautics. Direct FE model updating techniques can directly update the global mass and stiffness matrices in one step so that the FE model will be capable of reproducing the measured eigenfrequencies and mode shapes, though the resulting FE model may not maintain structural connectivity according to Jaishi and Ren (2005). Due to lack of mode shape data and the requirement of a meaningful result, direct FE model updating techniques are beyond the scope of this study. The sensitivity-based parameter updating approach is useful for identifying structural parameters that can directly affect the response characteristics of the structure. Traditionally, only dynamic responses are used for FE model updating, two examples include Zhang et al. (2001) and Zivanovic et al. (2007). FE model updating has been expanded to include static load tests for the present study. Thus, both the dynamic response and the results of static load tests were used for FE model updating.

Many modern major bridges are constructed with consideration of the entire service life and thus include sensors for monitoring strain, acceleration, temperature and wind data. The New Svinesund Bridge includes many sensors capable of remote monitoring that provide measurements that can be used for FE model updating. Such monitoring can be used for routine structural assessment with an updated FE model.

Detailed information regarding FE model updating is available in Friswell and Mottershead (1995).

2.4.2 FE model updating conceptual framework

The following flow chart demonstrates the concept of FE model updating. The FE model was first defined by the pre-processor (possibly in conjunction with FEM updating software) as described in Chapter 2.1.2. FE calculations were then executed by the FEA program in order to obtain output responses. Convergence was assessed by comparing output responses with measured values. The parameters were then updated and iterations were performed until the desired convergence was achieved.

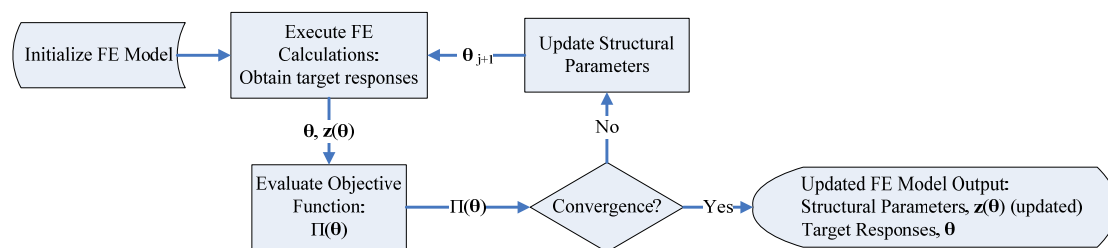


Figure 2.10 FE model updating conceptual flow chart.

For this particular study, the commercial program ABAQUS was used for FE calculations and MATLAB was used in conjunction with ABAQUS for pre-processing and post-processing. ABAQUS is a general FEM program which is able to do many types of analysis. An ABAQUS input file template (text format) that defined FE model geometry, material parameters, element types, meshing parameters, internal connections, boundary conditions, load cases and analysis types for pre-processing was supplemented with a custom MATLAB subroutine for writing updating parameter values to the ABAQUS parameter files. The basic data structure in MATLAB is the array, thus the program is highly optimized in order to handle arrays. MATLAB also utilizes many inbuilt toolboxes, such as the optimization toolbox which is suitable for this project. FE model updating iterations were performed by MATLAB using a script file and various MATLAB subroutines. MATLAB executed ABAQUS to perform FE calculations and used ABAQUS in conjunction with a custom FORTRAN subroutine to convert binary output to ASCII format compatible with MATLAB. By default, ABAQUS stores all data in binary format, since binary format requires less space for storage. The post processing program was written in FORTRAN code and was compiled and linked with ABAQUS library routines. The desired outputs were then compared with measured values to assess convergence. The Euclidean norm of a weighted error vector (formed as the difference between measured values and FE outputs) was compared to a tolerance for most subroutines. If

the response had not yet converged to the desired tolerance, selected parameters were updated using various FE model updating subroutines in MATLAB. The updated parameters were then included in the text input file using the ABAQUS input file template and the MATLAB subroutine for updating parameters. FE calculations were executed once again, thus iterating the FE model.

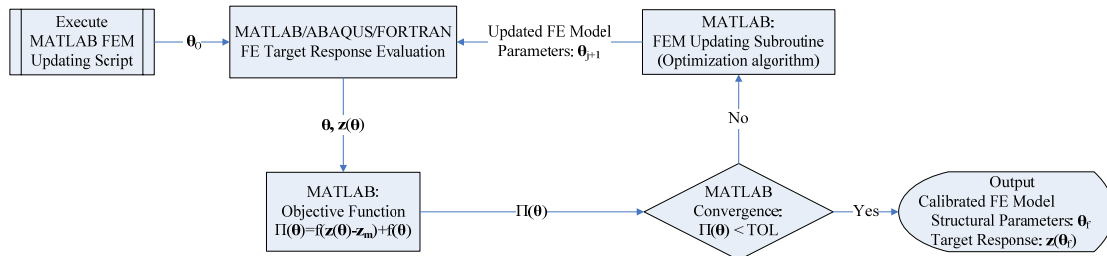


Figure 2.11 FE model updating flowchart showing MATLAB, ABAQUS and FORTRAN functions.

In this particular project, a FORTRAN post processing program obtained the requested output data from the results record, translated the binary format and wrote the data to a number of files in ASCII format. The output data from the post processing program was used in MATLAB in the optimization procedure. To be able to execute ABAQUS from MATLAB, a function was written in MATLAB code. The outline of the code is shown in Figure 2.12.

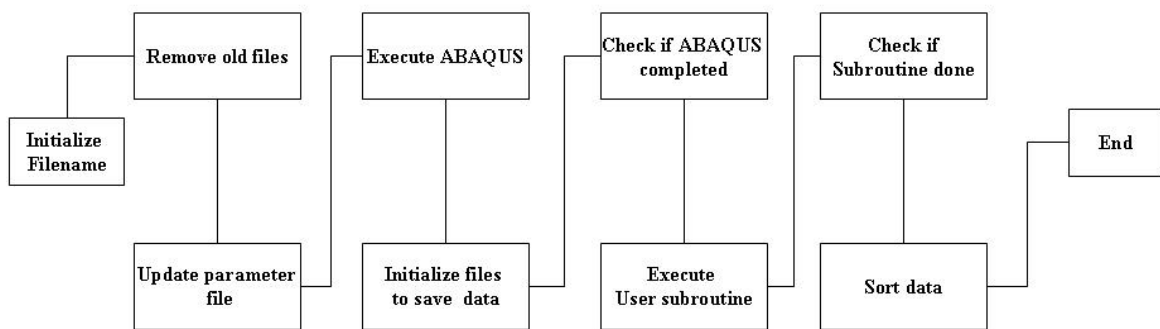


Figure 2.12 Flowchart showing how MATLAB and ABAQUS were linked for FE model updating.

2.4.3 Least squares FE model updating techniques

In order to define the FE updating procedure for the classical FE updating techniques introduced in this chapter, the notation for the updating parameters and response is defined below. The general goal of the updating procedures is to minimize the residual between the measured response and the FEM response. Chapter 2.4.3.1 – 2.4.3.8 discuss some least squares techniques for FE updating given different conditions. Each of the methods was verified using the simple beam model in

ABAQUS with FE updating equations implemented in MATLAB. Derivations of the classical FE updating equations and further information about FE model updating are available in Friswell and Mottershead (1995).

Measured response $[m \times I]$, \mathbf{z}_M ,

$$\mathbf{z}_M = [z_{1M} \quad z_{2M} \quad \dots \quad z_{mM}]^T \quad (2.48)$$

FE response at iteration j ,

$$\mathbf{z}_j = [z_{1,j} \quad z_{2,j} \quad \dots \quad z_{m,j}]^T \quad (2.49)$$

Initial value for updating parameter vector $[n \times I]$,

$$\boldsymbol{\theta}_0 = [\theta_{1,0} \quad \theta_{2,0} \quad \dots \quad \theta_{n,0}]^T \quad (2.50)$$

Updating parameter vector, $\boldsymbol{\theta}$,

$$\boldsymbol{\theta}_j = [\theta_{1,j} \quad \theta_{2,j} \quad \dots \quad \theta_{n,j}]^T \quad (2.51)$$

Often the updating parameter vector is normalized, $\boldsymbol{\Phi}$,

$$\boldsymbol{\Phi}_j = \left[\frac{\theta_{1,j}}{\theta_{1,0}} \quad \frac{\theta_{2,j}}{\theta_{2,0}} \quad \dots \quad \frac{\theta_{n,j}}{\theta_{n,0}} \right]^T \quad (2.52)$$

The updating parameters are normalized in order to overcome the problem with ill-conditioning which can occur when forming the sensitivity matrix. The normalized sensitivity matrix contains the first order derivatives of the responses and has to be calculated for each iteration step. The sensitivity matrix is also normalized to facilitate good conditioning and thus avoid numerical problems during calculation. A common way to calculate the derivatives numerically for the normalized sensitivity matrix is to use forward finite difference scheme presented below.

$$\mathbf{S}(i, j) = \frac{z_i(\phi_j + \Delta\phi_j) - z_i(j)}{(\phi_j + \Delta\phi_j) - \phi_j} \left(\frac{1}{z_{iM}} \right) \quad (2.53)$$

And in full matrix format

$$\mathbf{S} = \begin{pmatrix} \frac{\partial z_1}{\partial \phi_1} \left(\frac{1}{z_1} \right) & \dots & \frac{\partial z_1}{\partial \phi_n} \left(\frac{1}{z_1} \right) \\ \vdots & \ddots & \vdots \\ \frac{\partial z_m}{\partial \phi_1} \left(\frac{1}{z_m} \right) & \dots & \frac{\partial z_m}{\partial \phi_n} \left(\frac{1}{z_m} \right) \end{pmatrix} \quad (2.54)$$

In this case when the number of updating parameters (n) is less than the target responses (m), the sensitivity matrix becomes a non-square matrix with dimensions $[m \times n]$.

The updating equation is obtained by minimizing an objective function of the error, which is a penalty function,

$$\text{obj}(\delta\Phi) = \mathbf{e}^T \mathbf{e} \quad (2.55)$$

The error between the measured response and the FE response is given by,

$$\mathbf{e} = \mathbf{z}_M - (\mathbf{z}_j + \mathbf{S}\delta\Phi) \quad (2.56)$$

A non square matrix \mathbf{S} does not have an inverse in the conventional sense, but it is possible to define pseudo inverse, denoted by \mathbf{S}^+ , the pseudo inverse can be calculated according to equation (2.36) or equation (2.36). After having made an educated guess of the initial vector of the updating parameters, Φ_0 , the normalized updated parameters are updated according to the FE updating equation,

$$\Phi_{j+1} = \Phi_j + \mathbf{S}^+ \begin{pmatrix} \mathbf{z}_M - \mathbf{z}_j \\ \mathbf{z}_M \end{pmatrix} \quad (2.57)$$

The general formulation of the pseudo-inverse algorithm, equation (2.57) is equivalent to Gauss-Newton method in optimization, which uses a linear truncation of the Taylor Series expansion to solve for the next iteration. Only a very simple formulation was considered for this study, more robust Gauss-Newton formulations often utilize the line search method for step size control. For more information, refer to the Coleman and Zhan (2007).

2.4.3.1 Unweighted pseudo-inverse algorithm: more target responses than updating parameter

For the case of FE updating with more target responses than updating parameter, $m > n$, the equation set is over-determined and the solution is a least-squares minimization of the residual, which is solved in Chapter 2.2.3. Thus the pseudo-inverse is calculated according to equation (2.36) and the FE updating equation is,

$$\Phi_{j+1} = \Phi_j + (\mathbf{S}^T \mathbf{S})^{-1} \mathbf{S}^T \begin{pmatrix} \mathbf{z}_M - \mathbf{z}_j \\ \mathbf{z}_M \end{pmatrix} \quad (2.58)$$

2.4.3.2 Unweighted pseudo-inverse algorithm: more updating parameter than target responses

If more input parameters are used for updating than available output responses, $n > \hat{m}$, the model can often reproduce the measured responses exactly. The pseudo-

inverse is rank deficient and the equations for updating are under-determined, thus the unweighted pseudo-inverse method with more updating parameter than target responses is not capable of producing a unique solution. There can be an infinite number of input parameter combinations available that satisfy the convergence criteria and it is impossible to know which ones are correct without additional measurements to compare with the model response.

The updating parameter remain unchanged from the previous case, but now the measured response is reduced,

$$\mathbf{z}_M = [z_{1M} \quad z_{2M} \quad \dots \quad z_{\hat{m}M}]^T \quad (2.59)$$

FE response,

$$\mathbf{z}_j = [z_{1,j} \quad z_{2,j} \quad \dots \quad z_{\hat{m},j}]^T \quad (2.60)$$

For the case of the unweighted pseudo-inverse method with more updating parameter than target responses, the pseudo-inverse is defined according to equation (2.37) and iterations are made using equation (2.57),

$$\Phi_{j+1} = \Phi_j + \mathbf{S}^T (\mathbf{S}\mathbf{S}^T)^{-1} \begin{pmatrix} \mathbf{z}_M - \mathbf{z}_j \\ \mathbf{z}_M \end{pmatrix} \quad (2.61)$$

2.4.3.3 Unweighted pseudo-inverse algorithm: equal amount of target responses and updating parameters

For the case of the unweighted pseudo-inverse method with an equal amount of target responses and updating parameters, $\hat{m} = n$, the pseudo-inverse has full rank and the rows are linearly independent. A unique solution can be obtained for FE model updating. The pseudo-inverse is defined according to equation (2.38) and iterations are made using equation (2.57),

$$\Phi_{j+1} = \Phi_j + \mathbf{S}^{-1} \begin{pmatrix} \mathbf{z}_M - \mathbf{z}_j \\ \mathbf{z}_M \end{pmatrix} \quad (2.62)$$

2.4.3.4 Weighted response pseudo-inverse algorithm: more target responses than updating parameter

In reality, some target responses are measured more accurately than others, therefore weighting should be used to reflect the higher degree of confidence. The updating equations are obtained by minimizing an objective function of the weighted error, which is a penalty function,

$$\Pi(\delta\Phi) = \mathbf{e}^T \mathbf{W}_{zz} \mathbf{e} \quad (2.63)$$

The weighting matrix for response residual is often composed of the inverse of the response variance matrix. For the simple case of non-correlation of response variations, the variance matrix is diagonal and the weighting matrix is defined as,

$$\mathbf{W}_{zz} = \text{diag} \left(\left[\begin{array}{ccc} 1 & & \\ \sigma_{z_1}^2 & & \\ & 1 & \\ & \sigma_{z_2}^2 & \\ & & \dots \\ & & & 1 \\ & & & \sigma_{z_m}^2 \end{array} \right]^T \right) \quad (2.64)$$

The resulting FE updating equation for the normalized updating parameter is,

$$\Phi_{j+1} = \Phi_j + \left[\mathbf{S}_j^T \mathbf{W}_{zz} \mathbf{S}_j \right] \mathbf{S}_j^T \mathbf{W}_{zz} \begin{pmatrix} \mathbf{z}_M - \mathbf{z}_j \\ \mathbf{z}_M \end{pmatrix} \quad (2.65)$$

2.4.3.5 Weighted updating parameter change pseudo-inverse algorithm: more updating parameter than target responses

For an under-determined system of equations, the pseudo-inverse is rank deficient and an infinite number of combinations of input parameters will satisfy the convergence criteria and minimize the error as specified in equation (2.34). In such a case, a penalty term may be used for regularization. The penalty term is used to express the degree of confidence in the input parameters. For the case at hand, the weighting matrix for the updating parameters is chosen within a reasonable range.

It is reasonable to use a weighting matrix that is the inverse of the variance matrix. For non-correlated updating parameters,

$$\mathbf{W}_{\phi\phi} = \text{diag} \left(\left[\begin{array}{ccc} 1 & & \\ \sigma_{\phi_1}^2 & & \\ & 1 & \\ & \sigma_{\phi_2}^2 & \\ & & \dots \\ & & & 1 \\ & & & \sigma_{\phi_n}^2 \end{array} \right]^T \right) \quad (2.66)$$

The updating equations are obtained by solving the following constrained optimization problem,

$$\text{Minimize } \Pi(\delta\Phi) = \delta\Phi^T \mathbf{W}_{\phi\phi} \delta\Phi \quad \text{subject to } \delta\mathbf{z} = \mathbf{S}\delta\Phi \quad (2.67)$$

Solving the minimization equation above, the FE updating equation for the normalized updating parameter is obtained as,

$$\Phi_{j+1} = \Phi_j + \mathbf{W}_{\phi\phi}^{-1} \mathbf{S}_j^T \left[\mathbf{S}_j \mathbf{W}_{\phi\phi}^{-1} \mathbf{S}_j^T \right]^{-1} \begin{pmatrix} \mathbf{z}_M - \mathbf{z}_j \\ \mathbf{z}_M \end{pmatrix} \quad (2.68)$$

2.4.3.6 Weighted updating parameter change and weighted response pseudo-inverse algorithm

In some cases, even though more responses than updating parameters are available for updating, the pseudo-inverse still may be rank-deficient. If an FE model is used to reproduce the measured results of a structure, modelling limitations can prohibit exact reproduction of the measured responses. This presents a serious problem for FE updating because the updating algorithm will become unstable. It is therefore helpful to include the regularization term, $\delta\Phi^T \mathbf{W}_{\Phi\Phi} \delta\Phi$. This term controls the step size at each iteration by applying the weight to the updating parameter step, thus ensuring that the algorithm does not choose unrealistic step sizes.

The objective function to be minimized,

$$\Pi(\delta\Phi) = \mathbf{e}^T \mathbf{W}_{zz} \mathbf{e} + \delta\Phi^T \mathbf{W}_{\Phi\Phi} \delta\Phi \quad (2.69)$$

Solving the minimization of the equation above, the FE updating equation for the normalized updating parameter is,

$$\Phi_{j+1} = \Phi_j + \left[\mathbf{S}_j^T \mathbf{W}_{zz} \mathbf{S}_j + \mathbf{W}_{\Phi\Phi} \right]^{-1} \mathbf{S}_j^T \mathbf{W}_{zz} \begin{pmatrix} \mathbf{z}_M - \mathbf{z}_j \\ \boldsymbol{\sigma}_z \end{pmatrix} \quad (2.70)$$

2.4.3.7 Weighted updating parameter and weighted response pseudo-inverse algorithm

The weighted updating parameter change given by the previous algorithm improves the stability of the FE updating algorithm, but may not prohibit an unstable model from converging to meaningless results. In order to ensure that the FE updating algorithm does not stray far from reasonable input parameter estimates, the regularization parameter contributes to the objective function weighted according to the difference in the updating parameter at the current iteration and the initial value of the updating parameter. This term also improves the convexity of the objective space in the case of non-convexity when only the weighted response is considered.

The objective function to be minimized,

$$\Pi(\delta\Phi) = \mathbf{e}^T \mathbf{W}_{zz} \mathbf{e} + \left[\delta\Phi + (\Phi_j - \Phi_0) \right]^T \mathbf{W}_{\Phi\Phi} \left[\delta\Phi + (\Phi_j - \Phi_0) \right] \quad (2.71)$$

Minimizing the equation above, the FE updating equation for the normalized updating parameter is,

$$\Phi_{j+1} = \Phi_j + \left[\mathbf{S}_j^T \mathbf{W}_{zz} \mathbf{S}_j + \mathbf{W}_{\Phi\Phi} \right]^{-1} \left[\mathbf{S}_j^T \mathbf{W}_{zz} \begin{pmatrix} \mathbf{z}_M - \mathbf{z}_j \\ \mathbf{z}_M \end{pmatrix} - \mathbf{W}_{\Phi\Phi} (\Phi_j - \Phi_0) \right] \quad (2.72)$$

2.4.3.8 Minimum variance method

In the minimum variance method, the response of the FE model is regarded to be in the sample of measured data, thus it may be treated statistically. The goal of the minimum variance method is to minimize the variance between the model response and the measured response. A detailed explanation of the method and a derivation of the formulation is provided in Friswell and Mottershead (1995). The FE updating equations are summarized below,

$$\Phi_{j+1} = \Phi_j + (\mathbf{V}_j \mathbf{S}_j^T - \mathbf{D}_j) \mathbf{V}_{zj}^{-1} \begin{pmatrix} \mathbf{z}_M - \mathbf{z}_j \\ \mathbf{z}_M \end{pmatrix} \quad (2.73)$$

The variance of the response residual is quantified in the response variance matrix,

$$\mathbf{V}_{zj} = \mathbf{S}_j \mathbf{V}_j \mathbf{S}_j^T - \mathbf{S}_j \mathbf{D}_j - \mathbf{D}_j^T \mathbf{S}_j^T + \mathbf{V}_e \quad (2.74)$$

Which is obtained from,

$$\mathbf{V}_{zj} = E \left\{ (\mathbf{z}_m - \mathbf{z}_j) (\mathbf{z}_m - \mathbf{z}_j)^T \right\} \quad (2.75)$$

The variance matrix is defined in terms of the normalized measurement noise, \mathbf{e} ,

$$\mathbf{V}_e = E \{ \mathbf{e} \mathbf{e}^T \} \quad (2.76)$$

The variance of the parameter estimate is updated at each iteration,

$$\mathbf{V}_{j+1} = \mathbf{V}_j - [\mathbf{V}_j \mathbf{S}_j^T - \mathbf{D}_j] \mathbf{V}_{zj}^{-1} [\mathbf{V}_j \mathbf{S}_j^T - \mathbf{D}_j]^T \quad (2.77)$$

The correlation between the parameter estimate and the measurement noise is updated,

$$\mathbf{D}_{j+1} = \mathbf{D}_j + [\mathbf{V}_j \mathbf{S}_j^T - \mathbf{D}_j] \mathbf{V}_{zj}^{-1} [\mathbf{S}_j \mathbf{D}_j - \mathbf{V}_e]^T \quad (2.78)$$

2.4.4 FE model with Nelder-Mead simplex method

FE model updating of an FE model in ABAQUS coupled with MATLAB is facilitated using the MATLAB optimization toolbox. ABAQUS is a good choice for FEA due to the computational power, flexibility and efficiency of the program. Simple or complex FE models can be built and analyzed in ABAQUS with a wide selection of element types, material constitutive relations and analysis types. MATLAB is easy to work with for FE updating and optimization especially because of the inbuilt optimization toolbox which includes many robust, fully-tested optimization algorithms that are easy to use. The FE updating equations are generated automatically by the optimization algorithm as it iterates.

The objective of FE model updating is to update an FE model in order to reproduce the measured response of a structure. The objective function is used to quantify the performance of the model relative to the measured response and the input parameters. For least-squares optimization algorithms (Gauss-Newton and Levenberg-Marquardt), the objective function should be the weighted residual vector while a scalar objective function should be used for the Nelder-Mead Simplex algorithm and Quasi-Newton implementation in MATLAB. For this study, only the Nelder-Mead Simplex algorithm is presented. Optimization with the Quasi-Newton, Gauss-Newton and Levenberg-Marquardt methods is outside of the scope of the current study.

The response residual vector may be weighted to reflect the confidence in different measurements,

$$(\mathbf{z}_m - \mathbf{z}_j)^T \mathbf{W}_{zz} (\mathbf{z}_m - \mathbf{z}_j) \quad (2.79)$$

Regularization may be used to reflect the confidence in the updating parameters,

$$(\Phi_j - \Phi_0)^T \mathbf{W}_{\Phi\Phi} (\Phi_j - \Phi_0) \quad (2.80)$$

Thus the objective function may be formulated as (without regularization),

$$\Pi(\Phi_j) = (\mathbf{z}_m - \mathbf{z}(\Phi_j))^T \mathbf{W}_{zz} (\mathbf{z}_m - \mathbf{z}(\Phi_j)) \quad (2.81)$$

Thus the objective function may be formulated as (with regularization),

$$\Pi(\Phi_j) = (\mathbf{z}_m - \mathbf{z}(\Phi_j))^T \mathbf{W}_{zz} (\mathbf{z}_m - \mathbf{z}(\Phi_j)) + (\Phi_j - \Phi_0)^T \mathbf{W}_{\Phi\Phi} (\Phi_j - \Phi_0) \quad (2.82)$$

In order to use the inbuilt optimizations methods in the MATLAB optimization toolbox for FE model updating, send the function handle of the objective function as well as the initial updating parameter vector to the optimization subroutine with the proper optimization settings.

MATLAB syntax:

% Nelder-Mead Simplex Optimization (scalar objective function):

`[phi,objval,exitflat,output] = fminsearch(obj,phi0,options)`

3 FE Model Updating of a Simple Beam

In order to develop MATLAB subroutines for FE model updating, the simplified case of a simply supported beam was analyzed. The preliminary FE models were compared side-by-side and with analytical formulas in order to ensure accurate modelling. During the proof of concept stage, a very simple model is of great use because it may be used to identify errors early during the development of the subroutines that will be used for the bridge model later. Verification of convergence criteria for optimization routines and error checks for the MATLAB and FORTRAN subroutines are easier with a small, simple model as opposed to a large, computationally demanding numerical model.

3.1 Problem description

A simply supported steel beam of standard profile, IPE 180, with a length of 8 m was chosen for the analysis; see Figure 3.1 and Figure 3.2. The beam is loaded with a point load in the negative y-direction applied at the midpoint, see Figure 3.3. All motion is constrained to the x-y plane. Each support includes a vertical spring that only permits translational motion in the y-direction and a rotational spring that permits rotation about the z-axis. Shear deformation is neglected in analytical calculations due to the slenderness of the beam, as elastic bending deformation and elastic spring deformation are of much greater magnitude.

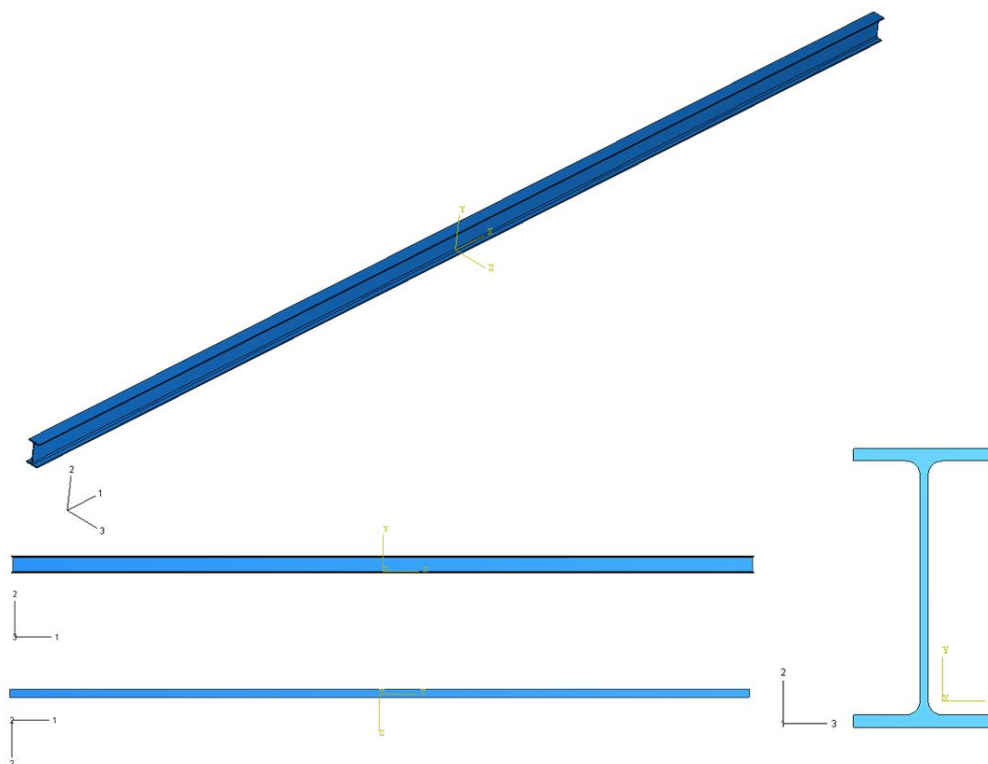


Figure 3.1 CAD drawings of the IPE 180 beam: isometric, side, top and front views (counter-clockwise from top).

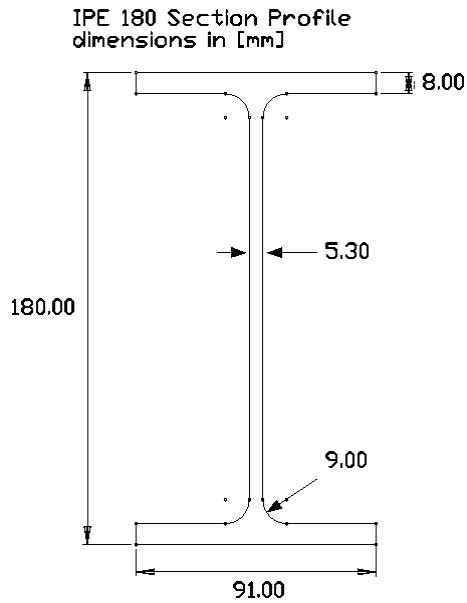


Figure 3.2 Section profile for IPE 180 beam.

In order to verify the FE models, hand calculations for the first four eigenfrequencies, midspan displacement, support displacement (linear spring deformation) and maximum flange strain were performed for the above model. The analytical solution for the first four eigenfrequencies and the midspan displacement were obtained using Euler-Bernoulli beam theory.

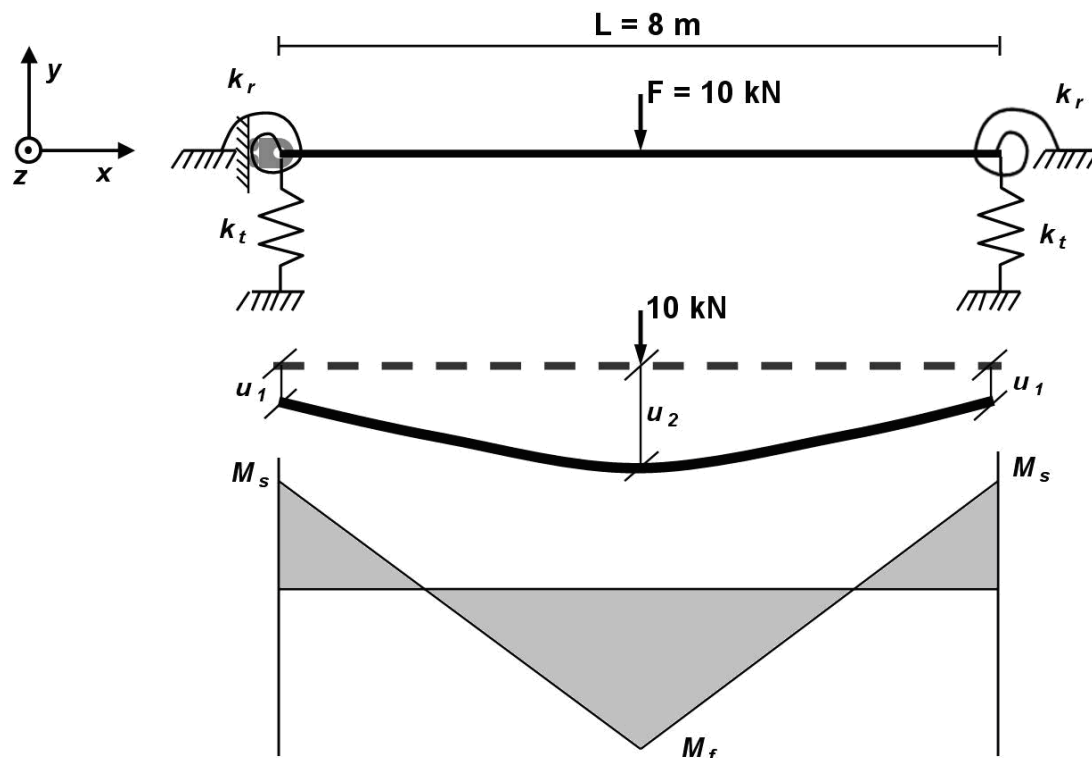


Figure 3.3 Sketch of IPE 180 beam with spring supports.

3.2 Numerical modelling

FE modelling provides a means of utilizing the computational power of computers to evaluate the results of numerical models quickly. For the present case, analytical equations become rather complicated with the introduction of springs to the boundary conditions, thus a numerical model is very useful.

3.2.1 Analytical formulas: MATLAB

The analytical solution was solved by hand from Euler-Bernoulli beam bending for the general case then implemented as a MATLAB subroutine for FE model verification. The derivation of the analytical solution is presented in Appendix A with the numerical implementation of the beam response as a MATLAB subroutine presented in Appendix C. The MATLAB beam response in Appendix C minimizes the determinant of the coefficient matrix for the eigensolution, as presented in Appendix B.

3.2.2 FE modelling: MATLAB

A preliminary study was conducted by Schlune (2007) using the CALFEM toolbox in MATLAB developed by Lund University (2002). The beam was discretized using 8 Euler-Bernoulli beam elements, each with length of 1 m. Linear elastic spring elements were used, one translational spring and one rotational spring, at each end of the beam. The boundary conditions were constrained according to Figure 3.3 and beam sectional constants were taken from wholesaler specifications, Bröderna Edstrand (2000)

3.2.3 FE modelling: ABAQUS

FE modelling in ABAQUS verified the calculation of eigenfrequencies, deflections and strains determined by the analytical equations and the CALFEM model in MATLAB. A total of 10 Timoshenko beam elements (element type B32), each with element length of 0.8 m were used to discretize the beam.

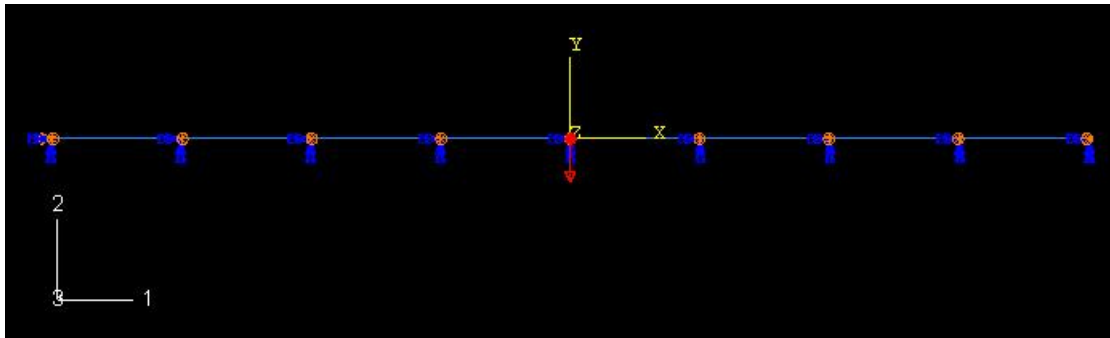


Figure 3.4 Simple beam element with point load and boundary conditions in ABAQUS.

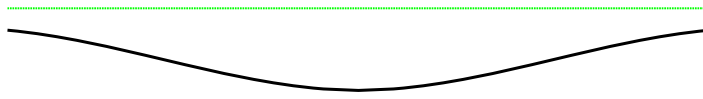


Figure 3.5 Bending of the beam due to point load from ABAQUS compared with undeformed beam (scale factor = 50, $u_1 = 18.77\text{mm}$ and $\sigma_{f,\text{max}} = 8.823\text{ kPa}$).

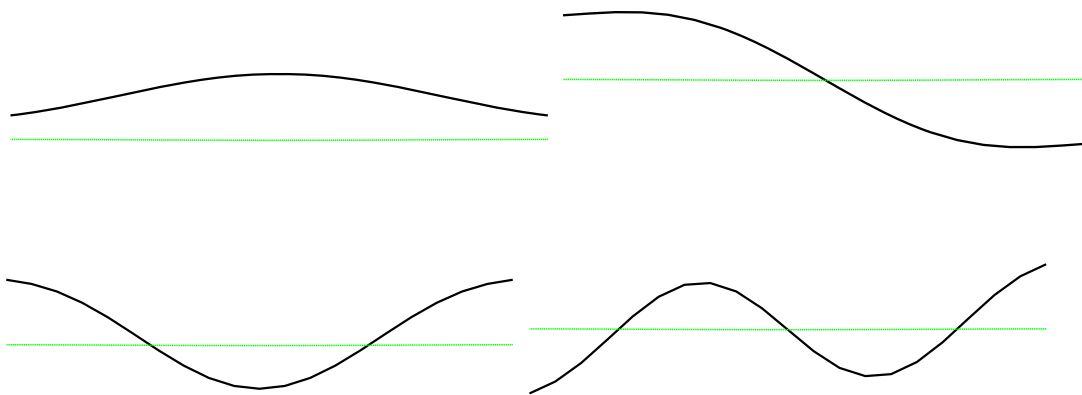


Figure 3.6 Natural modes 1 to 4 for simple beam in ABAQUS.

3.2.4 FE model verification

The tables below (Table 3.1 and Table 3.2) summarize the input parameters and target responses for the simply supported beam modelled using analytical formulas and FEM in MATLAB and ABAQUS. The “measured” input parameters are defined arbitrarily and produce the “measured” target responses of a simulated experiment.

Table 3.1 “Measured” input parameters for IPE 180 beam with spring supports.

	"Measured" Value	Units
Steel Elastic Modulus, E	210E9	N/m ²
Translational Spring Constant, k _t	1.00E+06	N/m
Rotational Spring Constant, k _r	5.00E+06	Nm/rad

Table 3.2 “Measured” target responses for IPE 180 beam.

Target Response	Analytical Formulas	MATLAB-CALFEM	ABAQUS	Units
f_{1m}	13.232	13.319	13.274	Hz
f_{2m}	26.353	26.491	26.496	Hz
f_{3m}	45.979	46.408	45.893	Hz
f_{4m}	83.723	84.882	82.298	Hz
u_{1m}	5.000	5.000	5.000	mm
u_{2m}	18.16	17.85	18.77	mm
ϵ_{1m}	0.0003649	0.0003549	0.0003486	mm/mm

The results obtained for the beam target response using FEA with CALFEM and ABAQUS were verified using analytical formulas. The input parameters in Table 3.1 may be considered as the “measured” parameters of the simulated experiment. The target responses presented in Table 3.2 are the “measured” target responses of the simulated experiment, the results obtained for the simulated IPE 180 beam with the “measured” input parameters.

3.3 FE model updating procedure

To simulate an experiment in FE model updating, the “measured” target responses were obtained using analytical formulas, CALFEM and ABAQUS with the “measured” input parameters described in section 3.2.4. The input parameters were then changed to simulate an educated guess based on the structural detail. By comparing the target responses from the model with guessed parameters with the “measured” target responses, the FE model updating procedure can then be used to iterate the input parameters. The subsequent output target responses are once again evaluated with the convergence criteria relative to the “experimental” target responses and iteration proceeds until convergence or until the maximum iteration count is reached. Such a procedure is conducted by Friswell and Mottershead (1995) with a cantilevered beam and is verified with a laboratory modal analysis test.

3.3.1 Least squares FE model updating techniques

3.3.2 Simple beam results: least squares FE model updating techniques

The FE model of the simple beam as defined in Chapter 3.2 was updated using the least squares FE updating techniques described in Chapter 2.4.3. The tabulated results are available in Appendix D. These analyses provided verification of the FE model updating approach using ABAQUS for FE calculations and MATLAB for FE model updating algorithm implementation.

The “measured values” were calculated by the FE model according to the input parameters given in Table 3.1. Since the FE model was used to produce the measured response vector, FE updating algorithms for full-rank systems were able to reproduce the measured response vector exactly and converge to the measured input updating parameters.

$$\mathbf{z}_m = [f_{1m} \ f_{2m} \ f_{3m} \ f_{4m} \ u_{1m} \ u_{2m} \ \varepsilon_{1m}]^T \quad (3.1)$$

FE response vector,

$$\mathbf{z}_j = [f_{1,j} \ f_{2,j} \ f_{3,j} \ f_{4,j} \ u_{1,j} \ u_{2,j} \ \varepsilon_{1,j}]^T \quad (3.2)$$

Updating parameter vector,

$$\boldsymbol{\theta}_j = [E_j \ k_{t,j} \ k_{r,j}]^T \quad (3.3)$$

Normalized updating parameter vector,

$$\boldsymbol{\Phi}_j = \left[\begin{array}{ccc} E_j / E_0 & k_{t,j} / k_t & k_{r,j} / k_r \end{array} \right]^T \quad (3.4)$$

3.3.2.1 Unweighted pseudo-inverse algorithm: more target responses than updating parameter

The FE updating procedure for the unweighted pseudo-inverse algorithm with more target responses than updating parameter was implemented with the entire response vector. The equation set was over-determined and the algorithm reproduced the measured values of the updating parameter vector and the response vector after 4 iterations. For the tabulated results of the analysis, refer to Table D.1 in Appendix D.1.

3.3.2.2 Unweighted pseudo-inverse algorithm: more updating parameter than target responses

In the case of the unweighted pseudo-inverse method with more updating parameter than target responses algorithm, the first two eigenfrequencies were used for FE updating. The updating parameter remained unchanged from the previous case, but now the response vector was reduced to,

$$\mathbf{z}_M = [f_{1M} \quad f_{2M}]^T \quad (3.5)$$

With the corresponding target responses,

$$\mathbf{z}_j = [f_{1,j} \quad f_{2,j}]^T \quad (3.6)$$

The measured values of the first two eigenfrequencies were reproduced exactly after 4 iterations, but the model did not converge as a whole. The final updating parameter values obtained by the model were not correct. This example was rank deficient and the equations for updating are under-determined, thus the unweighted pseudo-inverse method with more updating parameter than target responses did not converge to the full measured response. For the tabulated results of the analysis, refer to Table D.2 in Appendix D.1.

3.3.2.3 Unweighted pseudo-inverse algorithm: equal amount of target responses and updating parameters

For the unweighted pseudo-inverse algorithm with equal amount of target responses and updating parameters algorithm, the first three eigenfrequencies were used for FE updating. The updating parameter remained unchanged from the previous case, but now the response vector was reduced to,

$$\mathbf{z}_M = [f_{1M} \quad f_{2M} \quad f_{3M}]^T \quad (3.7)$$

$$\mathbf{z}_j = [f_{1,j} \quad f_{2,j} \quad f_{3,j}]^T \quad (3.8)$$

The FE model was used to produce the measured values of the response. The unique solution was obtained and the exact solution for the measured values of the updating

parameter vector and the response vector was obtained after 4 iterations. Without the presence of noise in the measured response, the complete response was produced. For the tabulated results of the analysis, refer to Table D.3 in Appendix D.1

3.3.2.4 Weighted response pseudo-inverse algorithm: more target responses than updating parameter

In order to test the weighted response pseudo-inverse algorithm with more updating parameter than target responses, realistic assumptions were made for the statistical variance of the response. The weighting matrix for the response residual was defined using the statistical variance.

Weighting matrix for response residual,

$$\mathbf{W}_{zz} = \text{diag} \left(\left[\begin{array}{ccccccc} 1 & 1 & 1 & 1 & 1 & 1 & 1 \\ \sigma_{f_1}^2 & \sigma_{f_2}^2 & \sigma_{f_3}^2 & \sigma_{f_4}^2 & \sigma_{u_1}^2 & \sigma_{u_2}^2 & \sigma_{\varepsilon_1}^2 \end{array} \right]^T \right) \quad (3.9)$$

The assumed coefficients of variation for frequencies are quite low,

$$COV_{f_1-f_4} = \frac{\sigma_{f_1}}{f_1} = \frac{\sigma_{f_2}}{f_2} = \frac{\sigma_{f_3}}{f_3} = \frac{\sigma_{f_4}}{f_4} = 0.01 = 1\% \quad (3.10)$$

The assumed coefficients of variation for displacement are higher than for frequencies,

$$COV_{u_1-u_2} = \frac{\sigma_{u_1}}{u_1} = \frac{\sigma_{u_2}}{u_2} = 0.05 = 5\% \quad (3.11)$$

The assumed coefficient of variation for strain is higher than for displacements,

$$COV_{\varepsilon_1} = \frac{\sigma_{\varepsilon_1}}{\varepsilon_1} = 0.10 = 10\% \quad (3.12)$$

Convergence of the algorithm occurred after 4 iterations and the exact solution for the measured values of the updating parameter vector and the response vector was obtained. Without the presence of noise in the measured response vector, this algorithm produced the exact solution. For the tabulated results of the analysis, refer to Table D.4 in Appendix D.1.

3.3.2.5 Weighted updating parameter change pseudo-inverse algorithm: more updating parameter than target responses

The weighted updating parameter change pseudo-inverse algorithm with more updating parameter than target responses, realistic assumptions were made for the

statistical variance of the updating parameter. The weighting matrix for the updating parameters was defined as the inverse of the variance matrix.

$$\mathbf{W}_{\Phi\Phi} = \text{diag} \left(\left[\begin{array}{ccc} 1 & 1 & 1 \\ \sigma_{\phi_1}^2 & \sigma_{\phi_2}^2 & \sigma_{\phi_3}^2 \end{array} \right]^T \right) \quad (3.13)$$

The modulus of elasticity of the steel has a very low variation due to high quality control standards. The standard deviation of the normalized steel elastic modulus is thus assumed to be,

$$\sigma_{\phi_1} = 0.03 = 3\% \quad (3.14)$$

The variation of the spring stiffness was assumed to be significantly higher than that of the elastic modulus of steel. In an actual experiment this could be caused by uncertain spring stiffness or uncertain degree of fixture to the beam. Standard deviations of the normalized spring stiffness,

$$\sigma_{\phi_2} = 1 = 100\% \quad (3.15)$$

$$\sigma_{\phi_3} = 1 = 100\% \quad (3.16)$$

This algorithm did not converge and the exact solution for the measured values of the updating parameter vector and the response vector was not obtained. The algorithm does not appear to be nearing convergence, this is due to the regularization. For the results of the analysis, refer to Table D.5 in Appendix D.1.

3.3.2.6 Weighted updating parameter change and weighted response pseudo-inverse algorithm

The weighting matrix for the response as defined in Chapter 3.3.2.4 and the weighting matrix for the updating parameter used in Chapter 3.3.2.5 were used with FE updating. As in Chapter 3.3.2.5, the regularization term prevented convergence to the exact solution, but the higher relative weight (lower relative variance) of the response caused the algorithm to more accurately reproduce the measured response. This is evident by comparing the Euclidean norm of the normalized response vector at the final iteration in Table D.5 to Table D.6. The value of the weighted response residual at the final iteration is,

$$\begin{aligned}
(\mathbf{z}_m - \mathbf{z}_{j=5})^\top \mathbf{W}_{zz} (\mathbf{z}_m - \mathbf{z}_{j=5}) &= \begin{pmatrix} \begin{bmatrix} 13.267 \\ 26.496 \\ 45.916 \\ 82.359 \\ 0.01877 \\ 0.00501 \\ 0.000348 \end{bmatrix} & - & \begin{bmatrix} 13.274 \\ 26.496 \\ 45.893 \\ 82.298 \\ 0.01877 \\ 0.00500 \\ 0.000349 \end{bmatrix} \end{pmatrix}^\top \text{diag} \left(\begin{bmatrix} 7.534 \\ 3.774 \\ 2.179 \\ 1.215 \\ 1066 \\ 4000 \\ 28690 \end{bmatrix} \right) \begin{pmatrix} \begin{bmatrix} 13.267 \\ 26.496 \\ 45.916 \\ 82.359 \\ 0.01877 \\ 0.00501 \\ 0.000348 \end{bmatrix} & - & \begin{bmatrix} 13.274 \\ 26.496 \\ 45.893 \\ 82.298 \\ 0.01877 \\ 0.00500 \\ 0.000349 \end{bmatrix} \end{pmatrix} \quad (3.17) \\
(\mathbf{z}_m - \mathbf{z}_{j=5})^\top \mathbf{W}_{zz} (\mathbf{z}_m - \mathbf{z}_{j=5}) &= 0.006043
\end{aligned}$$

For the tabulated results of the analysis, refer to Table D.6 in Appendix D.1.

3.3.2.7 Weighted updating parameter and weighted response pseudo-inverse algorithm

In order to test the affect of weighting the deviation of the updating parameter vector from the initial value, FE updating was implemented with the weighting matrix for the response as defined in Chapter 3.3.2.4 and the weighting matrix for the updating parameter used in Chapter 3.3.2.5. As in Chapter 3.3.2.5 and Chapter 3.3.2.6, the regularization term prevented convergence to the exact solution. When compared with the results, but the higher relative weight (lower relative variance) of the response caused the algorithm to more accurately reproduce the measured response. This is evident by comparing the Euclidean norm of the normalized response vector at the final iteration in Table D.6 to Table D.7. The value of the weighted response residual at the final iteration is,

$$\begin{aligned}
(\mathbf{z}_m - \mathbf{z}_{j=5})^\top \mathbf{W}_{zz} (\mathbf{z}_m - \mathbf{z}_{j=5}) &= \begin{pmatrix} \begin{bmatrix} 13.275 \\ 26.513 \\ 45.821 \\ 82.002 \\ 0.01884 \\ 0.00497 \\ 0.000352 \end{bmatrix} & - & \begin{bmatrix} 13.274 \\ 26.496 \\ 45.893 \\ 82.298 \\ 0.01877 \\ 0.00500 \\ 0.000349 \end{bmatrix} \end{pmatrix}^\top \text{diag} \left(\begin{bmatrix} 7.534 \\ 3.774 \\ 2.179 \\ 1.215 \\ 1066 \\ 4000 \\ 28690 \end{bmatrix} \right) \begin{pmatrix} \begin{bmatrix} 13.275 \\ 26.513 \\ 45.821 \\ 82.002 \\ 0.01884 \\ 0.00497 \\ 0.000352 \end{bmatrix} & - & \begin{bmatrix} 13.274 \\ 26.496 \\ 45.893 \\ 82.298 \\ 0.01877 \\ 0.00500 \\ 0.000349 \end{bmatrix} \end{pmatrix} \quad (3.18) \\
(\mathbf{z}_m - \mathbf{z}_{j=5})^\top \mathbf{W}_{zz} (\mathbf{z}_m - \mathbf{z}_{j=5}) &= 0.1189
\end{aligned}$$

Comparing the weighted response residual to that from the previous section, it is clear that the regularization term that weights the change of the updating parameter vector from the initial value reduces the ability of the FE model to reproduce the measured response. For the tabulated results of the analysis, refer to Table D.7 in Appendix D.1.

3.3.3 FE model updating with Nelder-Mead simplex method

In order to simply verify the effectiveness of the MATLAB optimization toolbox for FE updating, the Euclidean norm of the normalized response residual was chosen for a simple objective function for the response of the simple beam. As stated earlier, the FE model was used to generate the measured response, so the optimization algorithms should converge to the exact solution. The analyses in this chapter provide proof of concept for FE updating using ABAQUS for FEA and MATLAB for optimization.

$$\Pi(\Phi_j) = \sqrt{\sum_{i=1}^{N_z} \frac{(z_{mi} - z_i)^2}{z_{mi}^2}} = \left\| \frac{\mathbf{z}_m - \mathbf{z}(\Phi_j)}{\mathbf{z}_m} \right\| \quad (3.19)$$

MATLAB syntax:

```
% Response function: 'zIPE180(phi)' calls ABAQUS to execute FEA
z=@(phi)zIPE180(phi);

% Objective function: Euclidean norm of normalized response residual
obj=@(phi)norm((zm-z(phi))./zm);

% "Measured" response:
phim=[1.02888 2 2]';
zm=z(phim);

% Initial guess for updating parameter vector:
phi0=[1 1 1]';

% FE updating using Nelder-Mead Simplex optimization method
options=optimset('MaxFunEvals',100);
[phi,objval,exitflag,output]=fminsearch(obj,phi0,options);
```

The results for the MATLAB optimization using the Nelder-Mead simplex algorithm for FE updating are in Table D.9 to Appendix D.1.

3.4 Simple beam FE model updating results

Without noise, nearly all FE updating methods converged to the measured values, thus verifying the FE model updating procedure. When less response parameters than updating parameters were used for FE updating, the FE updating procedure converged quickly to a non-unique solution. The responses used for updating were reproduced exactly, but the entire updated response was not equal to the measured response.

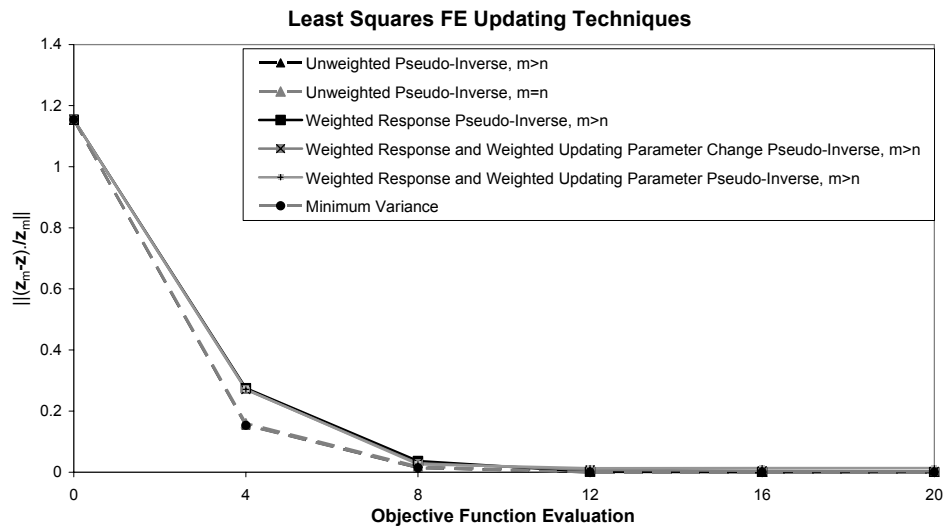


Figure 3.7 Convergence of normalized residual of response vector for least squares FE updating techniques (more response parameters than updating parameters).

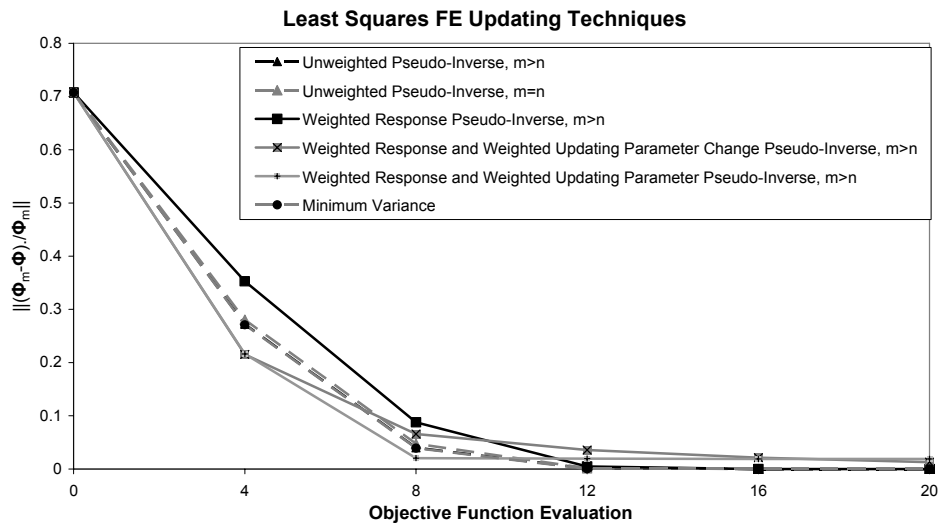


Figure 3.8 Convergence of normalized difference between updating parameter vector and measured parameter vector for least squares FE updating techniques (more response parameters than updating parameters).

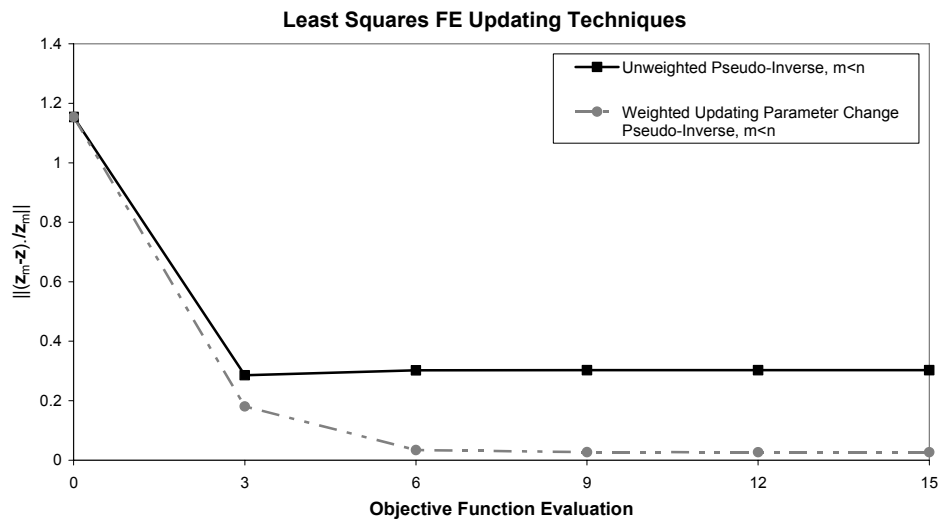


Figure 3.9 Normalized residual of response vector for least squares FE updating techniques (more updating parameters than response parameters).

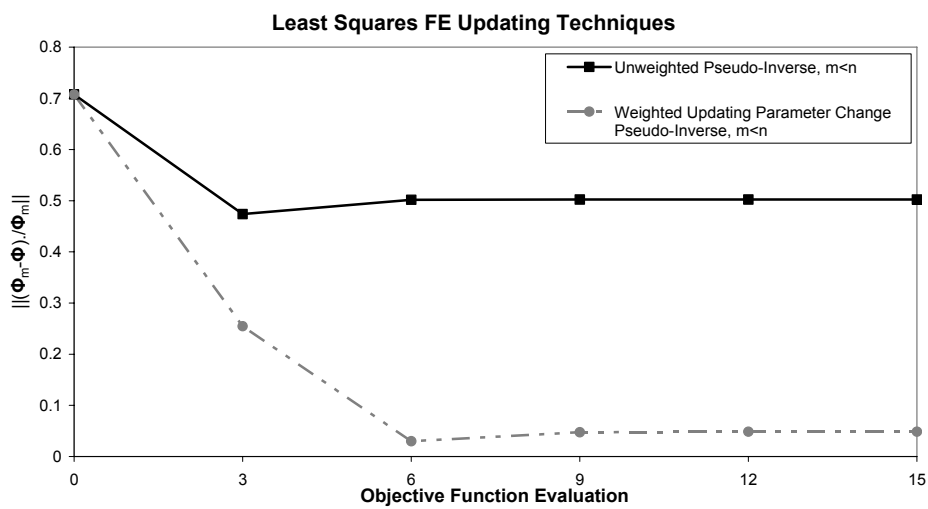


Figure 3.10 Normalized difference between updating parameter vector and measured parameter vector for least squares FE updating techniques (more updating parameters than response parameters).

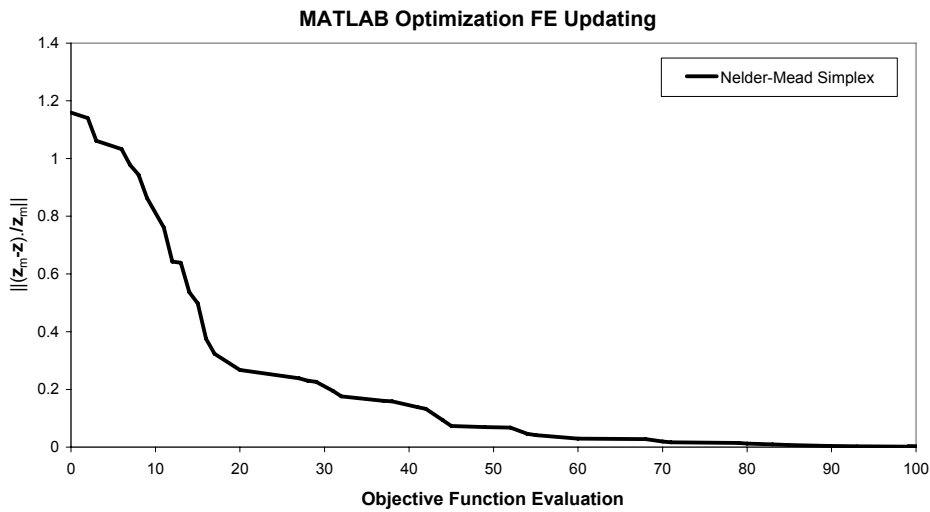


Figure 3.11 Convergence of normalized difference between updating parameter vector and measured parameter vector for MATLAB optimization FE updating using the Nelder-Mead Simplex method.

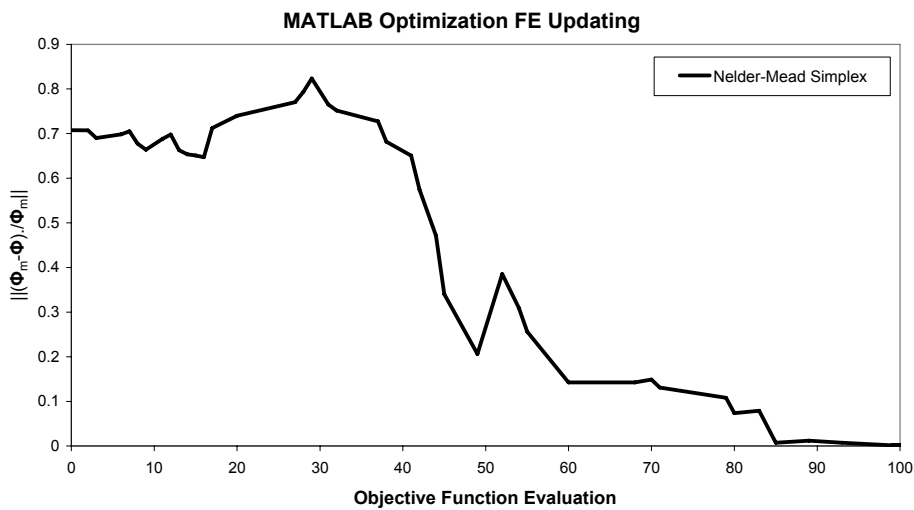


Figure 3.12 Convergence of normalized difference between updating parameter vector and measured parameter vector for MATLAB optimization FE updating using the Nelder-Mead Simplex method.

3.5 Noisy measurements

For the previous FE model updating studies, the FE model was used to produce the measured response, thus all of the FE updating techniques that did not include a regularization term converged to the analytical solution and reproduced the measured response exactly. In reality, experimental noise and modelling limitations will reduce the ability of the FE model to reproduce the experimental measurements. When experimental noise exists and more measurements that updating parameters are used, the FE model will not be able to reproduce the response exactly. In such a case, the FE model updating algorithms search for a solution to satisfy the optimality criteria.

For the investigation at hand, experimental noise was randomly added to the analytical FE response using a Gaussian normalized random distribution that was proportional to the assumed standard deviation of the measured response. Only the rotational and translational spring updating parameters were used for updating so that the results could be visualized.

Table 3.3 "Measured" input parameters for IPE 180 beam with spring supports for FE model updating with simulated experimental measurement noise.

	"Measured" Value		Initial Value	
Translational Spring Constant, k_t	$\varphi_{1m} = 2$	$\theta_{1m} = 1.0 \times 10^6$ N/m	$\varphi_1 = 1$	$\theta_1 = 5.0 \times 10^5$ N/m
Rotational Spring Constant, k_r	$\varphi_{2m} = 2$	$\theta_{2m} = 5.0 \times 10^6$ Nm/rad	$\varphi_2 = 1$	$\theta_2 = 2.5 \times 10^6$ Nm/rad

$$\sigma_{\varphi_1} = 1 = 100\% \quad (3.20)$$

$$\sigma_{\varphi_2} = 1 = 100\% \quad (3.21)$$

$$\mathbf{z}_m = \begin{bmatrix} 13.27 & \text{Hz} \\ 26.50 & \text{Hz} \\ 45.92 & \text{Hz} \\ 82.36 & \text{Hz} \\ 0.0188 & \varepsilon \\ 0.0050 & \varepsilon \\ 0.00035 & m \end{bmatrix} \quad (3.22)$$

$$\begin{aligned} \boldsymbol{\sigma}_z &= \begin{bmatrix} \frac{\sigma_{f_1}}{f_1} & \frac{\sigma_{f_2}}{f_2} & \frac{\sigma_{f_3}}{f_3} & \frac{\sigma_{f_4}}{f_4} & \frac{\sigma_{u_1}}{u_1} & \frac{\sigma_{u_2}}{u_2} & \frac{\sigma_{\varepsilon_1}}{\varepsilon_1} \end{bmatrix}^T \\ &= [0.01 \quad 0.01 \quad 0.01 \quad 0.01 \quad 0.05 \quad 0.05 \quad 0.10]^T \end{aligned} \quad (3.23)$$

$$\mathbf{z}_{m,noise} = \mathbf{z}_m + \text{randn}(7,1) \cdot \boldsymbol{\sigma}_z = \begin{bmatrix} (13.27)(1+0.01(-1.336)) & \text{Hz} \\ (26.50)(1+0.01(0.714)) & \text{Hz} \\ (45.92)(1+0.01(1.624)) & \text{Hz} \\ (82.36)(1+0.01(-0.692)) & \text{Hz} \\ (0.0188)(1+0.05(0.858)) & \varepsilon \\ (0.0050)(1+0.05(1.254)) & \varepsilon \\ (0.00035)(1+0.10(-1.594)) & \text{m} \end{bmatrix} = \begin{bmatrix} 13.10 & \text{Hz} \\ 26.69 & \text{Hz} \\ 46.64 & \text{Hz} \\ 81.73 & \text{Hz} \\ 0.0196 & \varepsilon \\ 0.0053 & \varepsilon \\ 0.00029 & \text{m} \end{bmatrix} \quad (3.24)$$

Three different least squares FE model updating techniques were implemented to study the affect of experimental noise. The unweighted pseudo-inverse algorithm with more responses than updating parameters (PI 1 in Table 3.4), the weighted updating parameter and weighted response pseudo-inverse technique (PI 2 in Table 3.4) and the minimum variance method were used with varying degrees of noise, starting with zero noise.

The Nelder-Mead simplex method was used to minimize the standard deviation objective function for the simple beam. The formulation of the objective function is very important as the set of updating parameters that minimize the objective function are considered the optimal updating parameters. For this case, the standard deviation objective function is used to express the average normalized deviation of the FEM response from the measured response.

Standard deviation objective function for response,

$${}^z \Pi_{\sigma} = \frac{\sum_{i=1}^{N_z} \sqrt{\frac{(z_{mi} - z_i)^2}{\sigma_{z_i}^2}}}{N_z} \quad (3.25)$$

In the objective function above, N_z is the length of the response vector, which is equal to the number of responses. If the standard deviation objective function for the response is minimized, the updated FE model is considered to be optimized with respect to the response with statistical consideration of the measured response. Experimental noise in the measured response will cause the FE updating algorithms to search for a set of parameter that best reproduce erroneous response. The solution may not be reasonable and if the experimental noise level is very high, the FE updating algorithms may become unstable. For such a case, regularization ensures that the final updating parameters do not significantly deviate from the best guess according to preliminary calculations.

In practice, the updating parameters represent uncertain structural parameters. Generally, there is a certain confidence associated with the uncertain structural parameters. The European structural code requires that the structural members are capable of satisfying the design requirements according to probabilistic criteria associated with the probabilistic distribution of the material parameter (such as strength) and the probabilistic criteria associated with the load combination. Building materials with very consistent material properties (i.e., steel) have a lower coefficient of variation and thus a lower partial safety coefficient than building materials that are known to vary, such as concrete according to EN 1992-1-1. In order to obtain an FE

model that minimizes the response residual without becoming unrealistic, a regularization term as a function of the updating parameters should be used.

The standard deviation regularization term for updating parameters,

$$\Phi_{\sigma} \Pi = \frac{\sum_{i=1}^2 \sqrt{\frac{(\phi_{0i} - \phi_i)^2}{\sigma_{\phi_i}^2}}}{2} \quad (3.26)$$

In this case, the optimal FE model (for the case of simulated experimental noise) was defined as that which minimized the deviation of the response and the deviation of the updating parameters with regard to statistical consideration of the response and statistical consideration of the updating parameters.

$$\sigma_{\sigma} \Pi = \frac{{}^z \Pi + \Phi_{\sigma} \Pi}{2} \quad (3.27)$$

The updating parameter vector for the optimal FE model with a noisy measured response is obtained by solving,

$$\min_{\Phi} \sigma_{\sigma} \Pi \quad (3.28)$$

In order to visualize the optimization procedure, the iteration steps are presented in Figure 3.13 in the normalized updating parameter space. The contours represent the magnitude of the standard deviation objective function of the response, $\sigma_{\sigma} \Pi$. At the “measured” normalized updating parameter vector ($\Phi_m = [2 \ 2]^T$), the objective function is minimized and the response is reproduced exactly. For the case without noise, $\sigma_{\sigma} \Pi$ was minimized to obtain the exact solution.

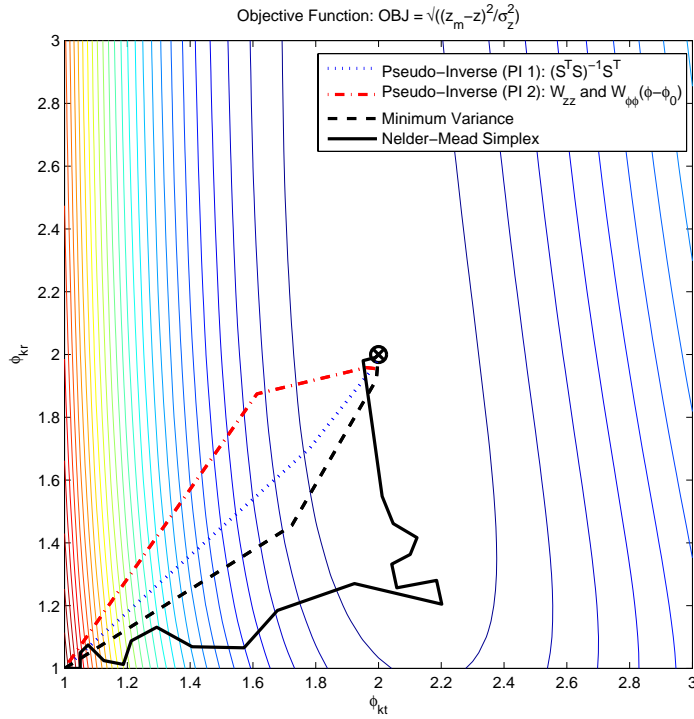


Figure 3.13 Plot of FE model updating iterations in updating parameter space without noise.

Table 3.4 Tabulated results of FE model updating for simple beam without noise.

	PI 2	PI 2	Minimum Variance	Nelder-Mead Simplex	\mathbf{z}_m
φ_1	2.000	2.003	2.000	2.000	2.000
φ_2	2.000	1.954	2.000	2.000	2.000
f_1	13.27	13.25	13.27	13.27	13.27
f_2	26.50	26.51	26.50	26.50	26.50
f_3	45.89	45.89	45.89	45.89	45.89
f_4	82.30	82.22	82.30	82.30	82.30
u_1	0.0188	0.0188	0.0188	0.0188	0.0188
u_2	0.0050	0.0050	0.0050	0.0050	0.0050
ε_1	0.00030	0.00030	0.00030	0.00030	0.00035

The results presented in Figure 3.13 and Table 3.4 were expected and are very similar to the convergence study previously presented. When experimental noise was added to the results in the manner described above, the solution to the minimization of the objective function of the response with regularization of the updating parameter produced the best results for the techniques used. In this case, the Nelder-Mead simplex method was used to minimize the standard deviation objective function for the response with regularization of the input parameters, σ_{Π} .

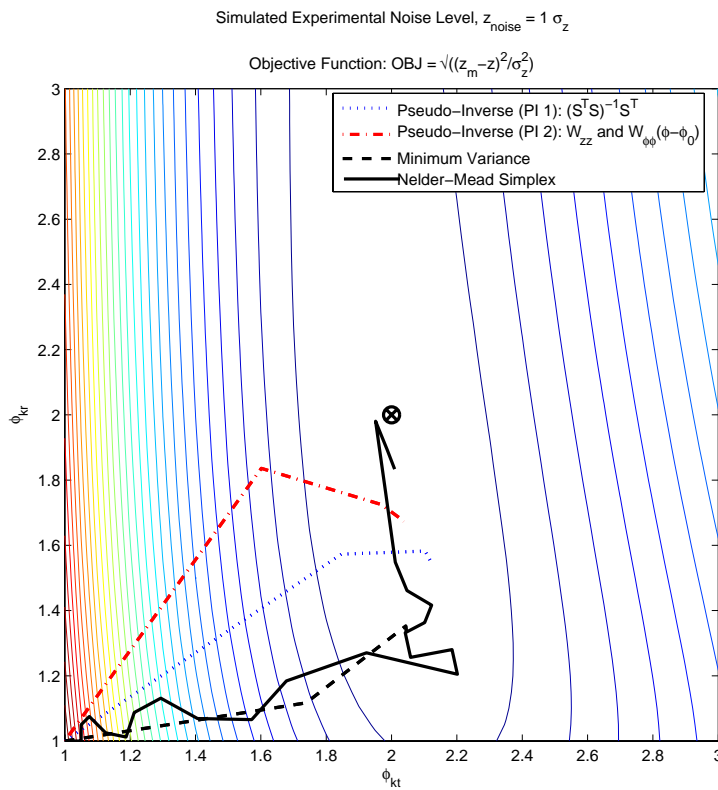


Figure 3.14 Plot of FE model updating iterations in updating parameter space with simulated experimental noise (noise level $\sim 1\sigma_z$).

Table 3.5 Tabulated results of FE model updating for simple beam with simulated experimental noise (noise level $\sim 1\sigma_z$).

	PI 1	PI 2	Minimum Variance	Nelder-Mead Simplex	\mathbf{z}_m	$\mathbf{z}_{m,noise}$
φ_1	2.118	2.037	2.049	2.009	2.000	
φ_2	1.554	1.673	1.319	1.834	2.000	
f_1	13.15	13.13	12.84	13.19	13.27	13.10
f_2	27.00	26.64	26.66	26.53	26.50	26.69
f_3	46.35	45.96	45.85	45.88	45.89	46.64
f_4	81.75	81.75	80.84	82.00	82.30	81.73
u_1	0.0194	0.0193	0.0202	0.0190	0.0188	0.0196
u_2	0.0047	0.0049	0.0049	0.0050	0.0050	0.0053
ε_1	0.00040	0.00040	0.00040	0.00040	0.00035	0.00029

When an extreme amount of noise ($5\text{randn}(7,1) \times \sigma_z$) was added to the response, the least squares FE updating methods did not converge as well as the Nelder-Mead simplex algorithm ($\min_{\Phi} \sigma \Pi$).

$$\mathbf{z}_{m,noise} = \mathbf{z}_m + 5\text{randn}(7,1) \times \sigma_z \quad (3.29)$$

The unweighted pseudo-inverse algorithm (PI 1) became unstable after two iterations. This was probably due to the linear approximation (truncation of the Taylor series after the first-order terms) used to solve for the next iteration. The weighted updating parameter and weighted response pseudo-inverse algorithm converged after nine iterations. The minimum variance algorithm became immediately unstable, iterating to an impossible value. Once again, the linear truncation of the Taylor series assumed by the minimum variance method is devastating when optimizing an objective function with considerable non-linear behaviour. The Nelder-Mead simplex was stable, converging after 24 iterations. The results of the analysis are presented in the table below.

Table 3.6 Tabulated results of FE model updating for simple beam with simulated noise (noise level $\sim 5\sigma_z$).

	PI 1	PI 2	Minimum Variance	Nelder-Mead Simplex	\mathbf{z}_m	$\mathbf{z}_{m,very\ noisy!}$
φ_1	2.603	2.229	1.799	1.984	2.000	
φ_2	0.426	0.922	-0.225	1.340	2.000	
f_1	11.56	12.54	---	12.73	13.27	12.39
f_2	28.50	27.37	---	26.23	26.50	27.44
f_3	48.25	46.59	---	45.56	45.89	49.62
f_4	78.93	80.09	---	81.95	82.30	79.45
u_1	0.0256	0.0215	---	0.0196	0.0188	0.0228
u_2	0.0038	0.0045	---	0.0050	0.0050	0.0066
ε_1	0.00040	0.00040	---	0.00038	0.00035	0.00007

3.6 Conclusions

The study of the simple beam provided proof of concept for FE model updating using ABAQUS coupled with MATLAB. Least squares FE updating techniques were implemented and verified. The Nelder-Mead Simplex algorithm in the MATLAB optimization toolbox was successfully implemented for FE updating. The importance of regularization was explored in Chapter 3.5 with the introduction of noise to the measured response. Many of the least squares algorithms were determined to be unstable when a significant level of noise was introduced to the measured response. This was believed to be caused by the linear truncation of the Taylor series for least squares solutions. Without considering higher order terms that are important for functions with considerable non-linear behaviour, the direct pseudo-inverse algorithms derived from least squares minimization were erratic when experimental noise was introduced to the system. No step-size controls were used for the least squares FE updating algorithms, such controls are in-built in the Gauss-Newton line-search non-linear least-squares minimization algorithm in the MATLAB optimization toolbox. Instability in the least squares FE updating routines that only considered the response emphasized the importance of using regularization and even establishing feasible limitations on the updating parameters for iterations. The Nelder-Mead simplex method available in the MATLAB optimization toolbox is robust and well-

developed when compared with the pseudo-inverse algorithms derived from least squares minimization.

Although all FE updating algorithms converged to reasonable results for the case of the simple beam without noise, the introduction of noise caused the unweighted pseudo-inverse algorithm and the minimum variance algorithm to become unstable. Experimental noise is known to exist for the case of the Svinesund bridge, so the unweighted pseudo-inverse algorithm was concluded to not be ideal for such a case. Furthermore, the response of the Svinesund bridge is suspected to be considerably non-linear and possibly non-convex and therefore optimization routines that utilize linear truncation of the Taylor series (such as direct least squares FE model updating techniques) are prone to instability. The Nelder-Mead simplex method was chosen for updating due to stability, convergence and ease of use for the case of the simple beam model. Although the simplex method requires more iterations for convergence than the least squares FE updating techniques, it does not require the calculation of the sensitivity matrix, which is computationally expensive due to the necessity of FE model response evaluation for each updating parameter for the finite difference method. Calculating FE model response in the FEA portion of FE updating using ABAQUS required much more time than the FE model updating procedures in MATLAB. This was because the system of equations solved during FEA was large and because ABAQUS must first be initialized by the operating system before FEA calculations can begin. As such, the number of objective function evaluations is decisive rather than the number of iterations when considering the time needed for FE updating.

The stability and ease of use of the FE model updating method were the determining factors when selecting a method for FE model updating of the Svinesund bridge. In conclusion, due to numerical stability and ease of use, the Nelder-Mead simplex method was determined to best satisfy the demands for an FE updating algorithm.

4 FE Modelling and Experimental Testing of the New Svinesund Bridge

4.1 FE modelling

Originally, the FE model for the bridge was created by the bridge contractor Bilfinger Berger (2003) for design purposes. For analysis, a new FE model was created using ABAQUS by Plos and Movaffaghi (2004) using indata files supplied by Bilfinger Berger (2004). The ABAQUS FE bridge model was shared by KTH and Chalmers for analysis and research purposes.

4.1.1 FE model description

The FE model of the completed bridge from Plos and Movaffaghi (2004) is shown in Figure 4.1. The FE model is defined using the standard international (SI) units in a Cartesian coordinate system with the x, y and z axes corresponding to axes 1, 2 and 3 in Figure 4.1. In total, the FE model of the permanent bridge structure contains 2393 elements, 1690 nodes and 11 724 DOF (the equation set is determined by the DOF). The total set of equations must be solved for the eigenfrequency calculations and for each static load case each time the response function is evaluated. In order to increase efficiency during optimization, all unnecessary output data was suppressed, thus reducing computational time. The calculation time for the response function for the bridge (executed from MATLAB with FEA completed by ABAQUS) was thus reduced from 45 seconds to 24 seconds.

To model the global behavior of the bridge while minimizing computational time, the FE model was simplified as much as possible. The utilization of beam elements instead of solid, continuum elements reduced the model complexity drastically. For the arch and bridge superstructure elements, first order (2 nodes) Timoshenko beam elements (ABAQUS element type: BEAM GENERAL SECTION) with linear material behavior and constant cross-section and material properties were placed along the neutral axes. These elements accurately model the global behavior of each section of the bridge with regards to normal force, bending moment, shear, stress, strain and shear deflection. The strains at various sensor locations were obtained from beam sectional points defined in the beam section of interest.

The carriageways of the superstructure were modeled as beam grid structures with three longitudinal beams with interacting top and bottom flanges to model the longitudinal walls within the box girder. Transversal stiffening beams are placed every four meters to model the internal transversal stiffening walls within the box girder superstructure.

Each supporting cable from the arch to the superstructure was modeled with a beam element of constant cross-section and constant material properties. Due to the low bending stiffness, a negligible moment is transferred from the cable to the arch or bridge superstructure. Each pair of cables attach to a transversal beam element at the carriageway. At the connection of the arch and cable, a very stiff element is used to

support the cables at the correct position relative to the arch neutral axis. The same stiff beam elements are used to connect the supports for the carriageways to the pier top.

Further information regarding the development of the FE model may be obtained from Plos and Movaffaghi (2004).

4.1.2 Boundary conditions and internal constraints

As is essential with all FE models, the boundary conditions and internal constraints were considered with utmost care as to ensure model accuracy. For foundations that are considered partially fixed, no translation or rotation was permitted for fixed DOF. Remaining DOF were constrained with linear elastic translational or rotational springs. For the model by Plos and Movaffaghi (2004), the abutments and the bearings at the tops of the piers for the support of the bridge superstructure were constrained such that translational and rotational DOF only permit motion allowed by the bearing design, see Figure 4.1 and Figure 5.10. An extensive description of the boundary conditions and internal connections for the initial ABAQUS model is described in Plos and Movaffaghi (2004).

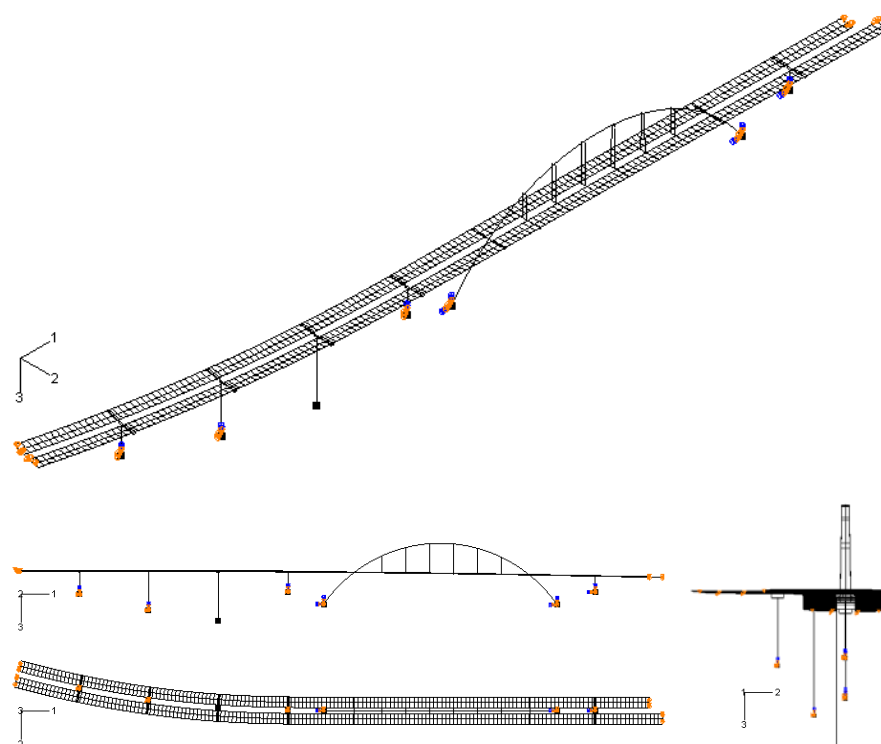


Figure 4.1 FE model of the New Svinesund Bridge: fixed DOF marked with red arrows (displacement) and blue arrows (rotation). Spring elements indicated by black boxes. Figure is used with permission from Plos and Movaffaghi (2004).

4.2 New Svinesund Bridge response

4.2.1 Permanent sensors

Structural monitoring of the New Svinesund Bridge is accomplished using sensors installed during construction. Data acquisition systems at the base of the arch on each side of the bridge record data. The bridge instrumentation system is capable of measuring strain, acceleration, temperature, wind speed and wind direction. The instrumentation of the arch includes 16 vibrating-wire strain gauges, 8 resistance strain gauges, 4 linear servo accelerometers installed in pairs to measure vertical and transversal acceleration, 28 temperature gauges in the same sections as the strain gauges and 1 outside temperature gauge with a 3-directional ultrasonic anemometer for measuring wind speed and direction. The suspended part of the bridge deck includes 2 sets of linear servo accelerometers: 2 accelerometers for measuring vertical acceleration of the deck and 1 accelerometer for measuring transversal acceleration of the deck. The forces of the first hangers are measured using 4 load cells. Linear variable differential transformer (LVDT) position sensors monitor the transversal movement of the bridge deck relative to the top of the piers. Further detail regarding instrumentation and measurements is detailed in Ülker-Kaustell and Karoumi (2006) and www.byv.kth.se/svinesund/instrumentation.htm.

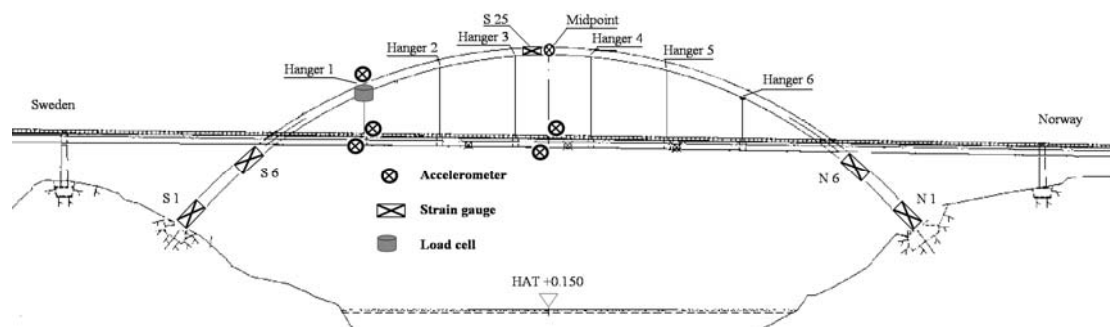


Figure 4.2 Figure showing the approximate locations for the different types of sensors.

4.2.2 Static load tests

The static load testing program was developed by Dr. Raid Karoumi at KTH and is presented in detail in Karoumi (2006) and Karoumi (2007). The static load tests consisted of 25 ton trucks parked in different positions to produce several static load patterns, the loading configuration is shown in Figure 4.3 with a yellow rectangle and red arrow representing each truck and its orientation. Chalmers performed static FE-analysis to provide the theoretical response prediction before actual load testing.

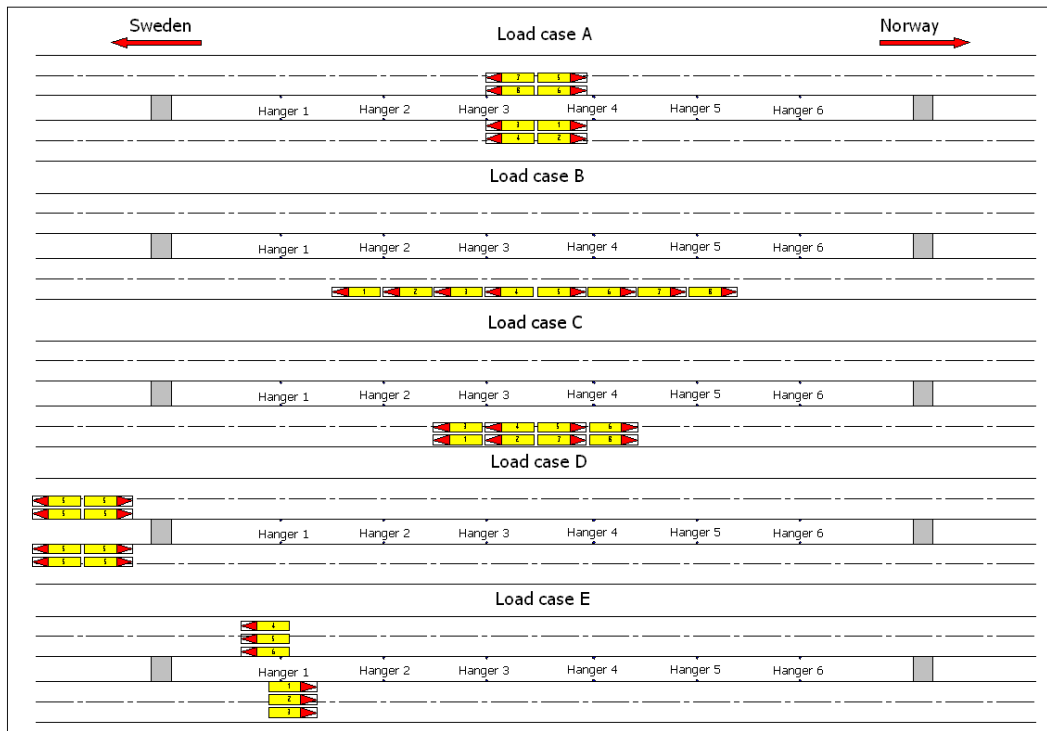


Figure 4.3 Loading configurations for load cases A-E.

4.2.3 Experimentally measured response

The experimentally measured response is composed of eigenfrequencies and static load case measurements. The eigenfrequencies were calculated by Ülker-Kaustell and Karoumi (2006) from 66 raw data files of ambient vibration acceleration measurements conducted during the time periods of June to August 2005 and November 2005 to January 2006. Static measurements were recorded during the load tests conducted during 18-19 May 2005. The static measurements included strains, displacements and hanger loads.

Temperature and wind speed were recorded during experimental measurements for eigenfrequency and static responses. For the static loads, the temperature effect was removed by linearly interpolation over the unloaded time intervals. Removal of the temperature effect from the acceleration data used to determine the eigenfrequencies

was not possible, thus experimental noise due to temperature variation is intrinsically evident in the eigenfrequency data. In order to minimize the experimental noise due to temperature variation, only the data from the 50 frequency measurements conducted during summer frequency measurement period were used for updating.

4.2.3.1 Experimentally measured eigenfrequencies

Acceleration measurements of ambient vibrations due to wind and traffic were obtained from the permanently installed accelerometers and were used to determine the measured eigenfrequencies. The permanently installed accelerometers provide reliable measurements for acceleration and are easily accessible for inspection, repair and replacement. Three different methods were utilized to obtain the eigenfrequencies from the acceleration data: maximum likelihood technique, random decrement technique and stochastic subspace identification technique. An example of a typical stabilization diagram from ARTEMIS for the stochastic subspace frequency identification method using acceleration measurements is presented in Figure 4.4. The peaks of the stabilization diagram correlate to the measurable eigenfrequencies of the bridge. The eigenfrequencies predicted by the methods were provided by KTH (2006) for statistical analysis. Of all of the frequency data available, the mean values of the frequency measurements conducted during the summer measurement period for all frequency identification methods were used in this report for FE model updating. As such, the mean measured frequencies presented in this report differ from the values presented in Ülker-Kaustell and Karoumi (2006). A temperature trend that cannot be easily removed is evident in the eigenfrequency data presented in Ülker-Kaustell and Karoumi (2006), thus the summer frequency measurements were chosen for FE model updating as to minimize temperature variation. This trend is believed to be caused by the temperature dependency of the asphalt elastic modulus, which is especially evident at temperatures below 10 °C (hence the winter frequency measurements were not considered for FE model updating). Further information regarding the asphalt elastic modulus is presented in Chapter 5.1.3.

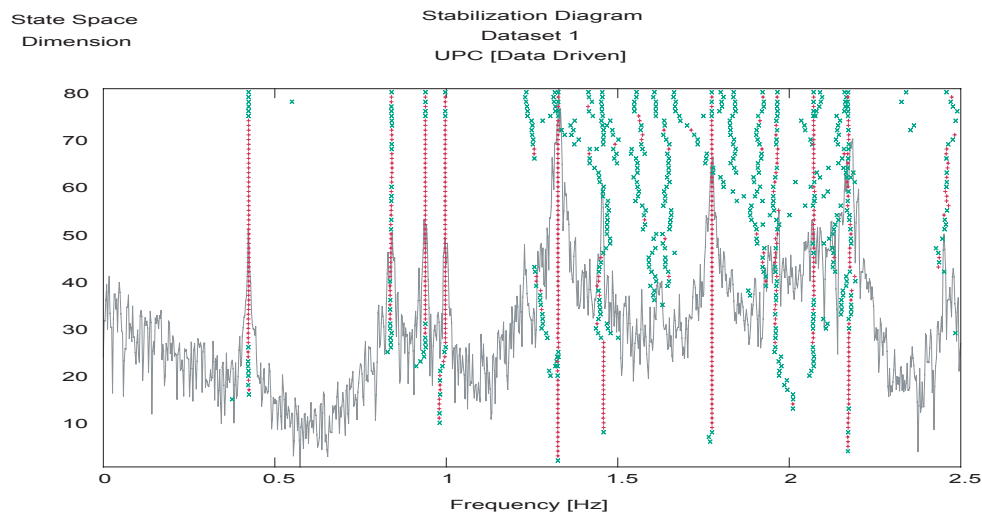


Figure 4.4 Typical stabilization diagram of accelerometer data as presented by ARTEMIS from Ülker-Kaustell and Karoumi (2006).



Figure 4.5 Accelerometer mounted inside of arch.

4.2.3.2 Experimentally measured strains

Permanently installed strain gauges in five arch cross sections (refer to Figure 4.2) provided strain data during load testing. Vibrating wire and resistance strain gauges were used in the same sections for strain output verification. The strain gauges cannot be replaced because they are attached to steel reinforcement bars in the arch and cast into the arch section. A study conducted by the Norwegian Geotechnical Institute, DiBiagio (2003), found that vibrating wire type strain gauges were still properly functioning after 27 years of continuous service, thus the measurement system is expected to be able to provide valuable data well into the life of the bridge.

Strain data was recorded at 1 Hz according to Karoumi (2007). The effect of temperature was removed using linear interpolation of the unloaded time intervals. The strain measurements for all measured arch sections are reported in Appendix F.2.

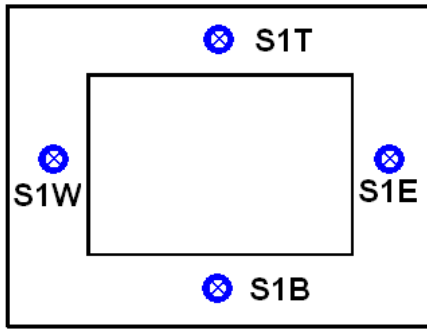


Figure 4.6 Approximate location of strain gauges in arch section S1 (near arch foundation, Swedish side).



Figure 4.7 NGI/Geonor P-300 vibrating wire type strain gauge installed in arch sections, James and Karoumi (2003), GEONOR (2007).

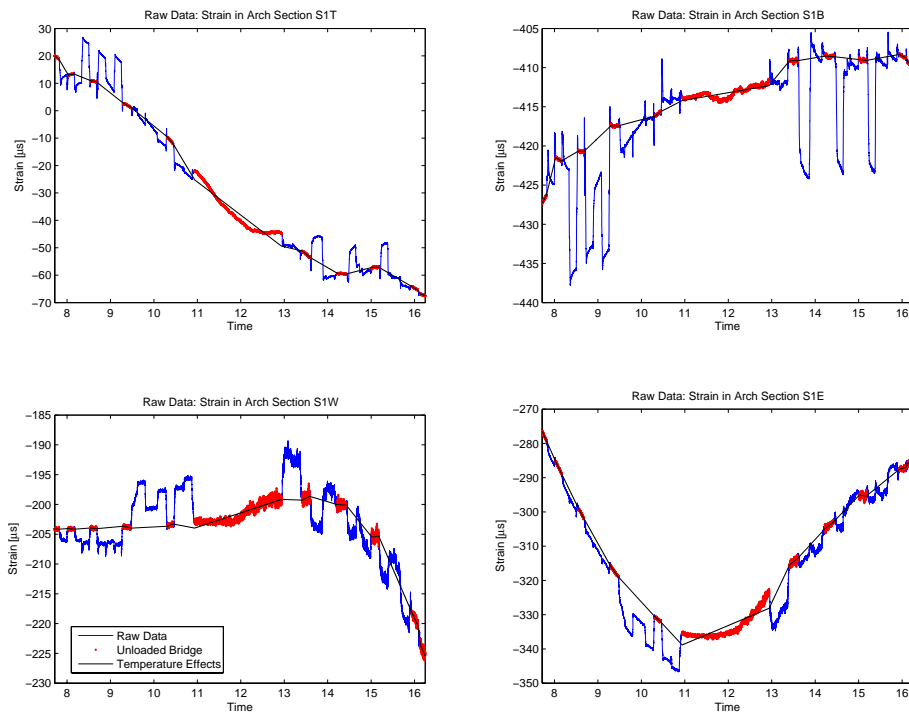


Figure 4.8 Measured strains in arch section S1 before temperature correction.

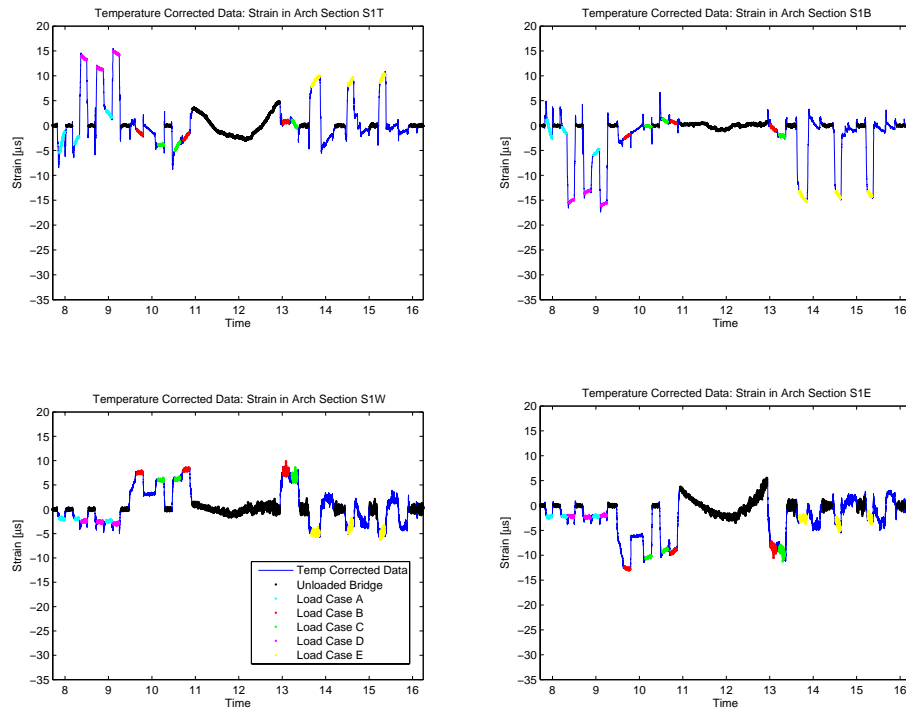


Figure 4.9 Measured strains in arch section S1 after temperature correction.

4.2.3.3 Experimentally measured displacements

FB Engineering performed the measuring of the displacement by utilizing six total stations of the type Leica TCA2003, see Figure 4.11. Two total stations were placed in line with pier five (Swedish side) one on each side of the arch and analogy for the Norwegian side, but instead in line with pier eight. In order to measure the vertical displacements in the carriageways thirty for this particular occasion, special made signals were placed on the edges of the carriageways, see Figure 4.10 and Figure 4.12. Each of the signals was constructed with two prisms on each side of the signal, the prisms were pointing in opposite direction. The purpose for the signals was only to measure the vertical movement of carriageways. A third pair of total stations was placed on a top of hill on the Norwegian side, northwest of the bridge. That particular pair mainly measured the longitudinal, transversal and vertical displacements of the arch. The signals for arch measurement were placed at quarter points above hanger 1 and hanger 6, a third signal was placed at the top of the arch. The measurement was taken within ten minutes for each loading case. All the equipment was calibrated before the measurements were taken.

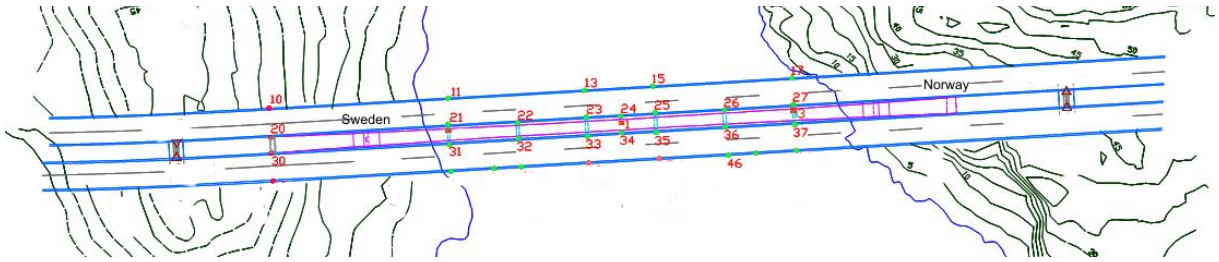


Figure 4.10 Figure showing location of the points at the carriageway for displacement measurements (top view of main span).



Figure 4.11 Figure showing total station placed on the hill northwest of the bridge, FB Engineering (2005).



Figure 4.12 Figure showing special made signal, FB Engineering (2005).

4.2.3.4 Experimentally measured hanger loads

During the static load tests, the hanger loads at hanger 1E and hanger 1W were recorded at a rate of 1 Hz, Karoumi (2007). Temperature effects were removed using linear interpolation of the unloaded time intervals as for the strain measurements. The load cells used to measure the hanger loads were calibrated before the static load tests

were performed using vibration measurements of the hangers with forced excitation under gravitational loading conditions, Karoumi and Andersson (2006).



Figure 4.13 Hanger 1E with load cells.

5 FE Model Manual Refinement of the New Svinesund Bridge through Structural Calculations

Although FE model updating is a powerful tool, manual model refinement is of great importance. Before FE model updating algorithms may be implemented, the FE model must be created and calibrated manually according to engineering judgement. Uncertain structural parameters should be investigated and a ‘best guess’ FE model should be used for FE model updating. FE model updating algorithms are useless if an FE model is used that cannot model the desired structural response. Modelling limitations should be sufficiently minimized before the updating parameters are calibrated with the FE model updating algorithm. The adjustments to uncertain structural parameters investigated in the preceding sections were progressively included in the FE model; the results of the study are tabulated in Appendix F.

5.1 Structural parameter investigation

5.1.1 Increase of arch section stiffness

The FE model implemented during the design phase of the New Svinesund Bridge was used to verify the structural capacity and performance as specified by the European and Swedish structural codes. The stiffness of the arch sections was calculated using the lower limit and thus did not consider the stiffness increase from concrete hydration and the stiffness contribution of the reinforcement. Such an assumption is common during design because it ensures that the actual structure will satisfy the design requirements. Thus the performance of the actual structure is often better than the model due to safe-side assumptions during modelling. Although conservative modelling techniques are common in design, the modelling parameters must be more realistic in order to accurately model the actual bridge response. Thus, the increased stiffness of the arch due to concrete hydration was calculated according to Eurocode 1992-1-1:2003,

Concrete class K70:

$$f_{cm}(t) = \beta_{cc}(t) f_{cm} \quad (5.1)$$

$$\beta_{cc}(t) = \exp \left\{ s \left[1 - \left(\frac{28}{t} \right)^{1/2} \right] \right\} \quad (5.2)$$

$$E_{cm}(t) = \left(\frac{f_{cm}(t)}{f_{cm}} \right)^{0.3} E_{cm} \quad (5.3)$$

Substituting equation (5.1) into equation (5.3),

$$E_{cm}(t) = [\beta_{cc}(t)]^{0.3} E_{cm} \quad (5.4)$$

Where,

$$f_{ck} = 49.5 \text{ MPa} \text{ characteristic compressive strength at 28 days} \quad (5.5)$$

$$f_{cm} = f_{ck} + 8 \text{ Mpa} = 57.5 \text{ MPa} \text{ mean compressive strength at 28 days} \quad (5.6)$$

$$E_{ck} = 37.5 \text{ GPa} \text{ characteristic modulus of elasticity at 28 days} \quad (5.7)$$

$$s = 0.25 \text{ coefficient for strength Class CEM42,5 N (Class N)} \quad (5.8)$$

$$t = 456 \text{ days} \text{ age of concrete at measurement tests} \quad (5.9)$$

$$\beta_{cc}(t) \text{ coefficient for concrete age} \quad (5.10)$$

In the serviceability limit state,

$$E_{cm} \approx E_{ck} = 37.5 \text{ GPa} \text{ mean modulus of elasticity at 28 days} \quad (5.11)$$

Thus, at the time of testing, the stiffness of the concrete due to hydration was,

$$E_{cm}(456) = 39.7 \text{ GPa} \quad (5.12)$$

$$\frac{E_{cm}(456) - E_{cm}}{E_{cm}} = 5.8\% \quad (5.13)$$

In addition to the increase in stiffness due to hydration, the stiffness of the arch section is increased due to reinforcement,

$$E_{eq} = \frac{E_{cm}A_c + E_{steel}A_{steel}}{A_c + A_{steel}} \quad (5.14)$$

Structural drawings were available for the 25 arch sections on the Swedish side. The area of reinforcement steel in each arch cross section was calculated using the number of reinforcement bars in each section and the dimensions of the section as specified by Billfinger Berger (2003b). The equivalent stiffness at each section was correlated to the corresponding beam element in the FE model using quadratic interpolation. Although the quadratic trend is not exact, it was the most reasonable approximation given the available information. Only a sample set of the structural drawings was available, thus the reinforcement layout was estimated using engineering judgement when only a partial set of structural drawings were available for a particular arch section. The scatter in the data in Figure 5.1 indicates that a better trend could be used if all of the structural drawings were available.

The equivalent stiffness near the arch base was calculated as,

$$A_{steel} = 78\phi 20 + 58\phi 32 = 0.0711 \text{ m}^2 \quad (5.15)$$

$$A_c = (6230 \text{ mm} \times 4231 \text{ mm}) - (3230 \text{ mm} \times 2000 \text{ mm}) = 19.9 \text{ m}^2 \quad (5.16)$$

$$E_{eq} = 40.43 \text{ GPa} \quad (5.17)$$

$$\frac{E_{eq}}{E_{cm}} = 7.8\% \quad (5.18)$$

The equivalent stiffness near the arch crown was calculated as,

$$A_{steel} = 204\phi 25 = 0.100 \text{ m}^2 \quad (5.19)$$

$$A_c = (4007 \text{ mm} \times 2714 \text{ mm}) - (2808 \text{ mm} \times 1804 \text{ mm}) = 5.8 \text{ m}^2 \quad (5.20)$$

$$E_{eq} = 43.29 \text{ GPa} \quad (5.21)$$

$$\frac{E_{eq}}{E_{cm}} = 15.44\% \quad (5.22)$$

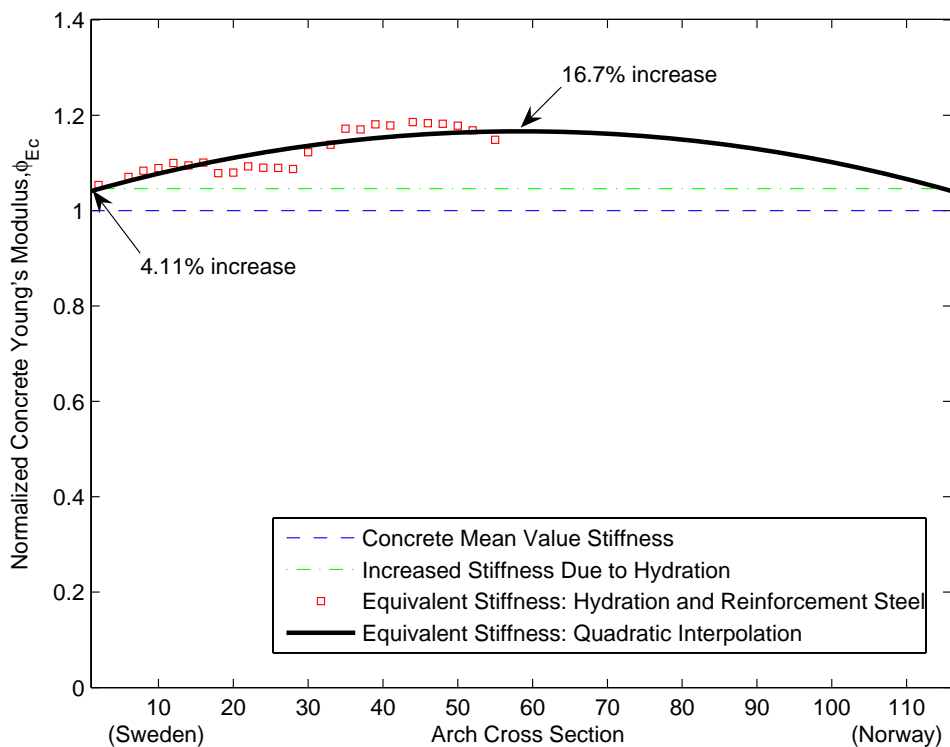


Figure 5.1 Variation of normalized concrete Young's modulus (elastic modulus), ϕ_{Ec} , across arch.

5.1.2 Asphalt mass

During FE modelling in the design phase, beam elements with equivalent sectional parameters were used to model the carriageway. The sectional area of the outer web was set to 0, $A_{web,o} = 0$, while the sectional area of the inner web was the equivalent area of the entire section, $A_{web,i} = A_{carr}$. No additional elements were used for modelling the self-weight of the asphalt layer, utilities (including internal walkways and drainage system) and railings, Billfinger Berger (2003a). Instead, a uniform load was applied to the longitudinal beam elements. These approximations are valid for verifying structural design codes, such as SLS deflection criteria, but, in reality, are simplified and do not represent the actual behaviour of the bridge. In order to calculate the eigenfrequencies of the bridge, the density of all carriageway elements was first set to zero and the equivalent mass was added to each element. The sum of the masses of the steel, asphalt layer, utilities and railing was distributed to each beam element. In such a way, the mass distribution was approximated.

When transferring the model from the designers model to ABAQUS for research purposes, realistic sectional properties were used for each longitudinal beam element of the carriageway. As such, the mass distribution of the steel in the carriageway was realistically modelled, Plos and Movaffaghi (2004). In order to include the mass of the non-structural members (asphalt layer, utilities and railings), discrete point mass elements were added at the nodes of intersection of the transversal stiffeners and longitudinal beams. These elements only approximate the mass distribution of non-load carrying members; they do not add stiffness to the carriageway. Load dividers were used to allocate the distributed mass of the non-load carrying members to the discrete point masses. Each element contributes an equivalent gravitational load to according to the load dividers presented in Figure 5.3.

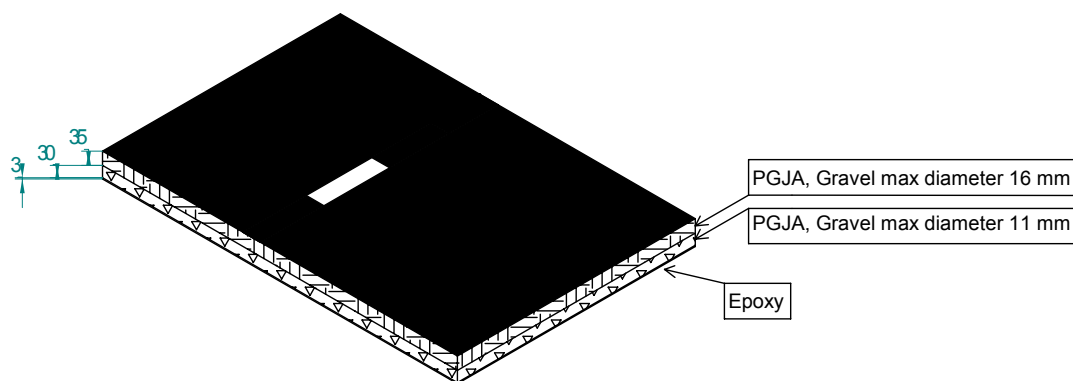


Figure 5.2 Drawing of asphalt layer.

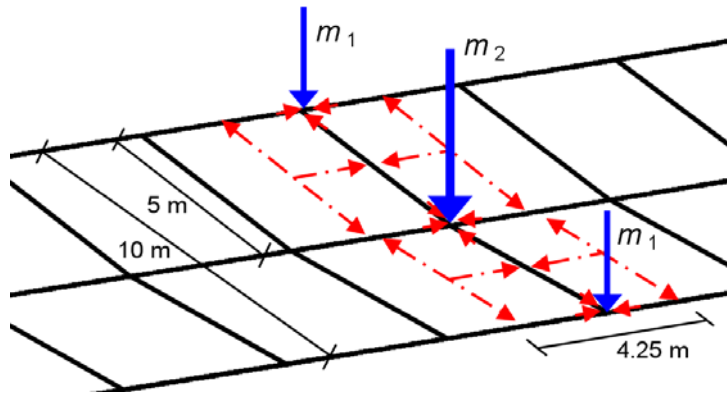


Figure 5.3 Load dividers for mass elements used to model non-structural members of the carriageway.

The discrete mass elements used to model the asphalt layer also included the masses of the utilities (internal walkways and drainage system) and the railings. Load dividers were set between beam elements in order to evenly distribute the mass of the non-structural members. The longitudinal load divider was placed in the middle between the outer beam elements and the central beam element, thus the spacing between the longitudinal load dividers and the longitudinal beam elements was 2.5 m. Transversal load dividers were placed in the middle between consecutive transversal stiffeners. The spacing between the transversal load dividers and the transversal beam elements was 4.25 m.

$$\rho_{railings} = \left(1.43 \frac{kN}{m}\right) \left(\frac{98.1kg}{1kN}\right) = 145.8 \frac{kg}{m} \quad (5.23)$$

$$\rho_{walkways} = 2 \left(0.5 \frac{kN}{m}\right) \left(\frac{98.1kg}{1kN}\right) = 102 \frac{kg}{m} \quad (5.24)$$

$$\rho_{drainage} = \left(0.5 \frac{kN}{m}\right) \left(\frac{98.1kg}{1kN}\right) = 56 \frac{kg}{m} \quad (5.25)$$

$$\rho_{asphalt} = \left(25 \frac{kN}{m^3}\right) (0.070m) (10m) \left(\frac{98.1kg}{1kN}\right) = 1717 \frac{kg}{m} \quad (5.26)$$

$$m_{tot} = \left(\rho_{railings} + \rho_{walkways} + \rho_{drainage} + \rho_{asphalt}\right) (s_{beams}) \quad (5.27)$$

$$m_{tot} = 8\,261 \text{ kg} \quad (5.28)$$

$$m_1 = 2\,065 \text{ kg} \quad (5.29)$$

$$m_2 = 4\,131 \text{ kg} \quad (5.30)$$

The addition of mass elements to the carriageway increased the hanger loads during gravitational loading. The resulting distribution of hanger loads is much more realistic and the FE hanger loads compare well with values reported in Karoumi and Andersson (2006). A discrepancy between the FE hanger loads and measured hanger

loads is evident at hanger 1 and hanger 6. This is probably due to the contribution of bending of the carriageway to the hangers nearest the carriageway-arch connection. Before the temporary hangers were removed during the final phase of the construction process, the axial force in each hanger was adjusted to the design value by adding steel plates at the support. Because the hangers are designed to uniformly carry the load from the carriageway when loaded, hanger 1 and hanger 6 are slightly prestressed and the increased hanger load is caused by negative bending of the carriageway. The difference between the measured value and the FE value for the average hanger load for hangers 2-5 is only 3.8% after adding mass elements to the FE model to account for the asphalt layer compared with a difference of 29.4% before the addition of the mass elements.

$$F_{hangFEM} = \frac{(F_{hang2W} + F_{hang2E} + \dots + F_{hang5W} + F_{hang5E})_{FEM}}{8} \quad (5.31)$$

$$F_{hang,measured} = \frac{(F_{hang2W} + F_{hang2E} + \dots + F_{hang5W} + F_{hang5E})_{measured}}{8} \quad (5.32)$$

Before adding point mass elements to FE model to account for the asphalt layer,

$$\frac{F_{hang,measured} - F_{hangFEM}}{F_{hang,measured}} = 29.1\%$$

After adding point mass elements to FE model to account for the asphalt layer,

$$\frac{F_{hang,measured} - F_{hangFEM}}{F_{hang,measured}} = 3.4\%$$

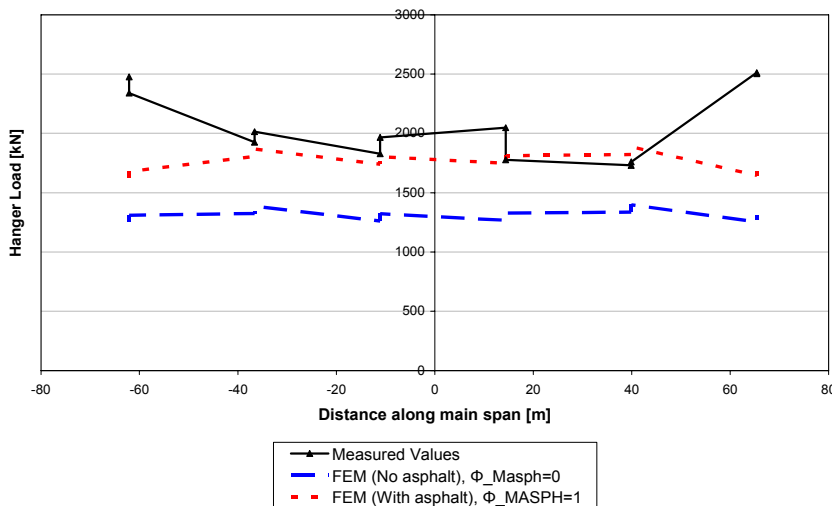


Figure 5.4 Experimentally measured hanger loads compared with calculated hanger loads using FEM with and without asphalt mass elements (initial FE model: $\phi_{Masph} = 0$, Model 3: $\phi_{Masph} = 1$) for gravitational loading.

Table 5.1 Tabulated values for measured and calculated hanger loads for gravitational loading.

		Hanger Loads					
		Measured F_m	FEM				
			$\phi_{Masph} = 0$		$\phi_{Masph} = 1$		
			F_{FEM}	$\frac{F_m - F_{FEM}}{F_m}$	F_{FEM}	$\frac{F_m - F_{FEM}}{F_m}$	
Hanger 1	W	2477 kN	1253 kN	49%	1621 kN	35%	
	E	2339 kN	1309 kN	44%	1679 kN	28%	
Hanger 2	W	1925 kN	1325 kN	31%	1806 kN	6%	
	E	2015 kN	1385 kN	31%	1867 kN	7%	
Hanger 3	W	1828 kN	1261 kN	31%	1740 kN	5%	
	E	1966 kN	1322 kN	33%	1803 kN	8%	
Hanger 4	W	2048 kN	1267 kN	38%	1748 kN	15%	
	E	1778 kN	1328 kN	25%	1811 kN	-2%	
Hanger 5	W	1730 kN	1337 kN	23%	1822 kN	-5%	
	E	1760 kN	1398 kN	21%	1886 kN	-7%	
Hanger 6	W	2512 kN	1253 kN	50%	1645 kN	35%	
	E	2504 kN	1312 kN	48%	1712 kN	32%	

5.1.3 Asphalt dynamic stiffness

Asphalt is a material that exhibits highly nonlinear behaviour. The Young's modulus is highly temperature dependent, but also depends on loading frequency and content parameters. In order to obtain an accurate initial estimate for the contribution of the asphalt stiffness to the bridge input parameters, a parametric study was conducted. The asphalt temperature data for the frequency measurements was not provided directly, thus it had to be estimated. The average temperature during the sampling period at each arch section was provided along with the frequency measurements obtained from the stabilization diagrams by KTH, Karoumi (2007). During the

summer frequency measurement period (June 14 to August 5, 2005), the asphalt temperature is assumed to vary throughout the day compared to the average arch temperature according to Figure 5.5. The relationship conservatively estimated based on engineering judgement and the temperature variation reported by KTH during load testing (May 2005).

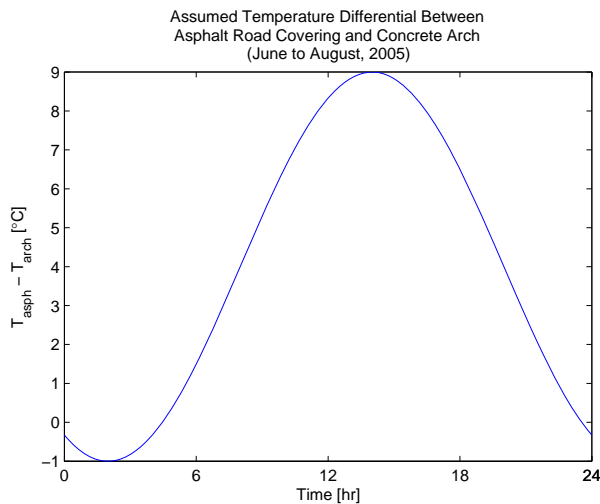


Figure 5.5 Estimated average variation of asphalt temperature compared with average arch temperature for frequency measurement summer period.

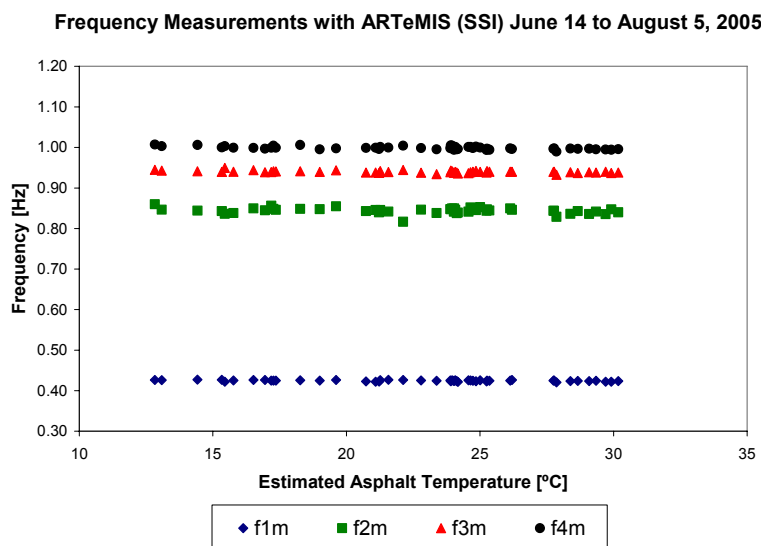


Figure 5.6 Measured frequency data (provided by KTH, Karoumi (2007)) versus estimated asphalt temperature for frequency measurement summer period.

In total, 50 frequency measurements for the summer frequency measurement period were recorded. The mean asphalt temperature was 22.72°C and the standard deviation was 4.73 °C during that period according to the relationship presented in Figure 5.5.

$$T = T_{asphalt,mean} = 22.72^{\circ}C$$

$$\sigma_T = \sigma_{T,asphalt} = 4.73^{\circ}C$$

The Young's modulus of asphalt is dependent on many parameters, including the temperature, loading frequency, pavement depth, aggregate size, bitumen content, percentage of air voids and bitumen viscosity. According to Cable et al. (2005),

$$\begin{aligned} \log_{10} (E_{Asph}) = & 5.553833 + 0.028829 \left(\frac{P_{200}}{F^{0.17033}} \right) - 0.03476 \cdot V_V \\ & + 0.070377 \cdot \eta + 0.931757 \cdot \left(\frac{1}{f^{0.02774}} \right) \\ & + \left(0.000005 - \frac{0.00189}{f^{1.1}} \right) \cdot T_{Asph}^{(1.3+0.49825 \cdot \log_{10}(f))} \cdot P_{Asph}^{0.5} \end{aligned} \quad (5.33)$$

where,

E_{Asph} = Young's modulus of asphalt [psi]

P_{200} = percent aggregate passing the #200 sieve [%]

f = loading frequency (~0.4 to 2.5 Hz for eigenfrequency analysis) [Hz]

V_V = percent air voids [%]

P_{Asph} = asphalt bitumen content, percent by weight of mix [%]

T_{Asph} = mean asphalt mix temperature at 1/3 depth [°F]

η = absolute viscosity at 70°F ($\approx 21^{\circ}C$) [10^6 poise]

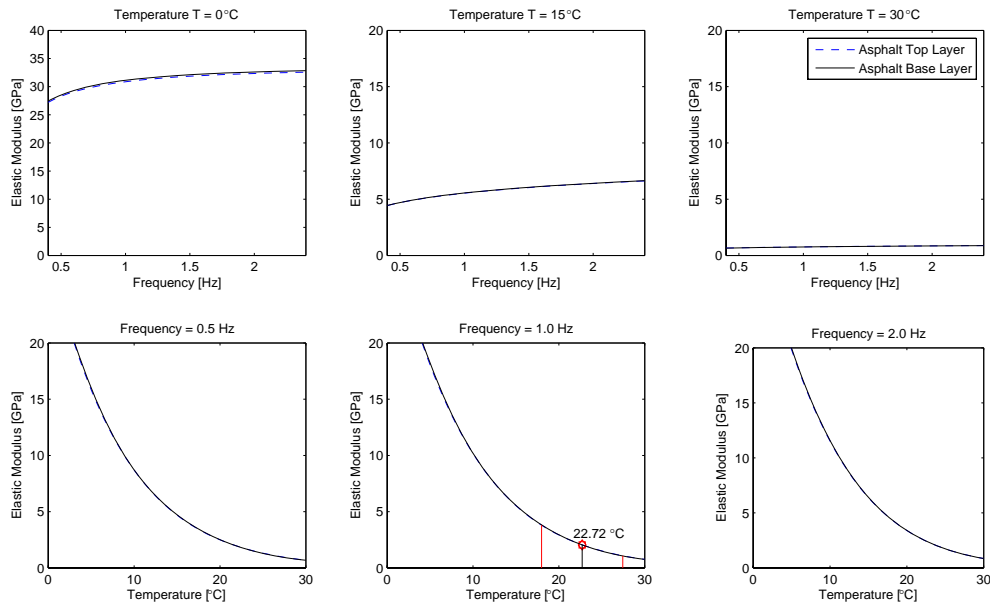


Figure 5.7 Variation of asphalt Young's modulus with respect to temperature and loading frequency.

Temperature and pressure units were changed to °C and MPa respectively for Figure 5.7 to avoid confusion. The frequency range of interest is within the first 20 eigenfrequencies of the bridge. Frequency excitations below the first eigenfrequency do not significantly contribute to the stabilization diagram since they occur below resonance. At higher frequencies, the frequency separation between consecutive modes is very small. In order to correlate eigenfrequencies above 1 Hz, a modal assurance criterion (MAC) study must be performed to ensure that the FEM eigenfrequencies correspond with the measured eigenfrequencies. Without a MAC matrix to correlate mode shapes, eigenfrequencies above 1 Hz cannot be used for FEM updating. Furthermore, it may be concluded from Figure 5.7 that the Young's Modulus of the asphalt does not vary significantly with frequency in the range of the first four eigenfrequencies for the temperature range for which the measurements were conducted. Since the first four eigenfrequencies are used for updating, the asphalt Young's Modulus at 1 Hz was concluded to satisfactorily represent a proper upper-bound estimation within this range. From Figure 5.7 it is also evident that the asphalt temperature influences the Young's modulus more drastically in the frequency range of interest far more than the excitation frequency.

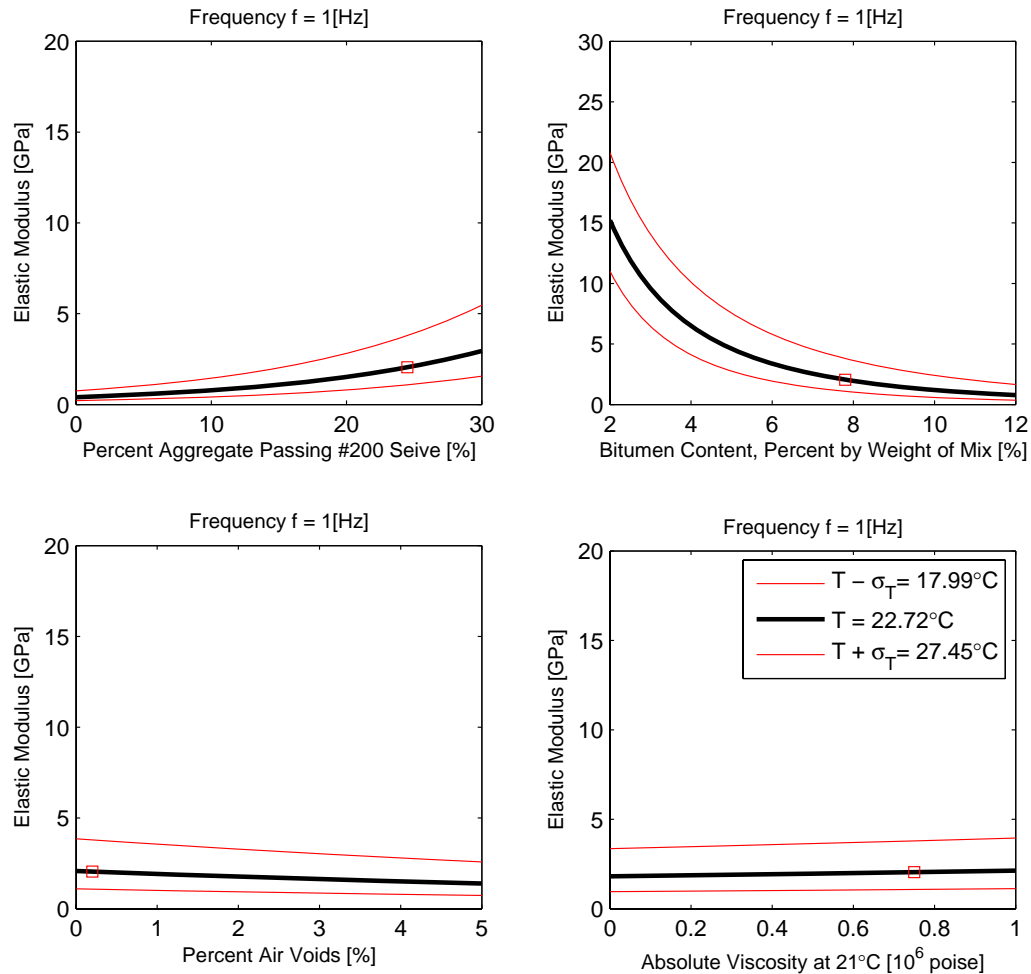


Figure 5.8 Variation of Young's modulus of asphalt to various parameters with loading frequency of 1 Hz.

During construction, high quality control standards ensure low variability in the asphalt content; nonetheless Figure 5.8 is used to demonstrate the possible variability of the asphalt Young's modulus with regards to asphalt content. The temperature of the asphalt greatly influences the dynamic stiffness, therefore the Young's modulus at $\pm\sigma_T$ is shown in Figure 5.8 as well.

During dynamic loading (eigenfrequency analysis in FEM), the dynamic stiffness of the asphalt contributes to the carriageway sectional parameters. At low temperatures, the dynamic stiffness of the asphalt is significantly greater than at higher temperatures, therefore it was necessary to study the contribution of the asphalt dynamic stiffness affects the carriageway sectional parameters. Sensitive parameters must be updated to account for the increase due to the contribution of the asphalt in dynamic loading, but insensitive carriageway sectional parameters are concluded to remain constant.

The equivalent stiffness of the carriageway due to the contribution of the asphalt stiffness during dynamic loading was calculated as,

$$E_{eq} = \frac{E_{steel}A_{carr} + E_{Asph}A_{Asph}}{A_{carr}} \quad (5.34)$$

Where A_{Asph} is the sectional area of the asphalt layer,

$$A_{Asph} = (65 \text{ mm})(10 \text{ m}) = 0.65 \text{ m}^2 \quad (5.35)$$

The equivalent bending inertia of the carriageway about the transverse axis was calculated as,

$$III_{eq} = \frac{E_{steel}III_{carr} + E_{Asph}III_{Asph}}{III_{carr}} \quad (5.36)$$

The parallel axis theorem was used to calculate the approximate inertia of the asphalt layer about the transverse axis,

$$III_{Asph} = A_{Asph} \left(1.5\text{m} + \frac{0.072\text{m}}{2} \right)^2 \quad (5.37)$$

The equivalent bending inertia of the carriageway about the vertical axis was calculated as,

$$I22_{eq} = \frac{E_{steel}I22_{carr} + E_{Asph}I22_{Asph}}{I22_{carr}} \quad (5.38)$$

The inertia of the asphalt layer about the vertical axis was calculated as,

$$I22_{Asph} = \frac{1}{12} \left(\frac{0.065\text{m}}{2} \right) \left(\frac{10\text{m}}{2} \right)^2 \quad (5.39)$$

The torsional inertia of the asphalt layer was calculated according to the perpendicular axis theorem,

$$J_{Asph} = III_{Asph} + I22_{Asph} \quad (5.40)$$

Thus the equivalent torsional inertia of the carriageway was calculated as,

$$J_{eq} = \frac{E_{steel}J_{carr} + E_{Asph}J_{Asph}}{J_{carr}} \quad (5.41)$$

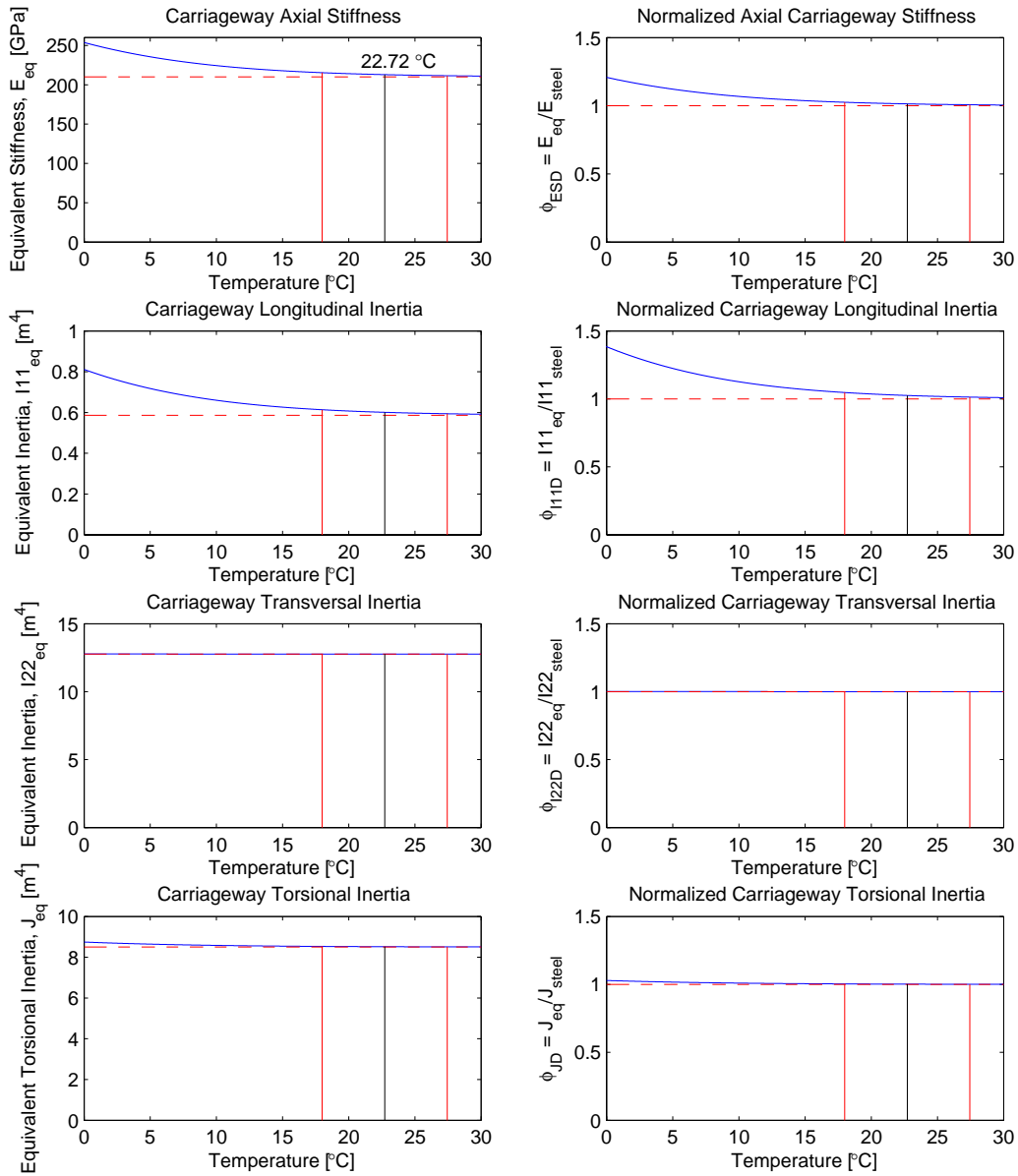


Figure 5.9 Variation of carriageway dynamic parameters with temperature.

The asphalt dynamic elastic modulus for the average asphalt temperature during frequency measurements and the carriageway sectional parameters for the carriageway section at mid-span were used for the preceding study. It was concluded that the axial stiffness of the carriageway (equivalent stiffness, E_{eq}) and the bending inertia of the carriageway about the transversal axis (equivalent inertia, $I_{11_{eq}}$) were sensitive to the contribution of the asphalt layer in dynamic loading. These parameters were therefore considered for FEM updating.

5.1.4 Arch-carriageway connection stiffness

Due to the high slenderness of the single arch, stability was crucial, so the carriageway was used to brace the arch. During the design phase, the arch to carriageway connection was considered to be fully constrained. This assumption was used during design to satisfy structural design criteria. During construction, the arch concrete was cast directly to the carriageway. At the concrete-steel interface, protrusions from the sheet steel of the carriageway wall ensured a strong bond between the concrete of the arch and the steel of the carriageway. Steel tendons were post-stressed to apply tensile force across the arch width from one carriageway to the other. The normal force due to the tendon force was assumed to ensure full restraint at the arch-carriageway interface.

In order to verify the design assumptions, linear-elastic spring elements were added to the FE model to connect the arch to the carriageway. The initial rotational stiffness of the spring elements was calculated using a very conservative estimate.

$$K_{a-carr} = G_c J_{a-carr} \quad (5.42)$$

The shear modulus of concrete, G_c , for this case,

$$G_c = \frac{E_c}{2(1+\nu_c)} = \frac{37.5 \text{ GPa}}{2(1+0.2)} = 15.6 \text{ GPa} \quad (5.43)$$

The torsional inertia of the connection was estimated very conservatively by assuming that only the equivalent of a ring of concrete approximately 10 cm wide with a radius of 1 m was resisting torsion,

$$J_{a-carr} \approx \frac{\pi}{2} \left((1.1\text{m})^4 - (1.0\text{m})^4 \right) \quad (5.44)$$

So, the initial conservative estimate for the rotational spring element to connect the arch to the carriageway was,

$$K_{a-carr} = 1.0 \times 10^{10} \text{ N/rad} \quad (5.45)$$

5.1.5 Static friction in bearings

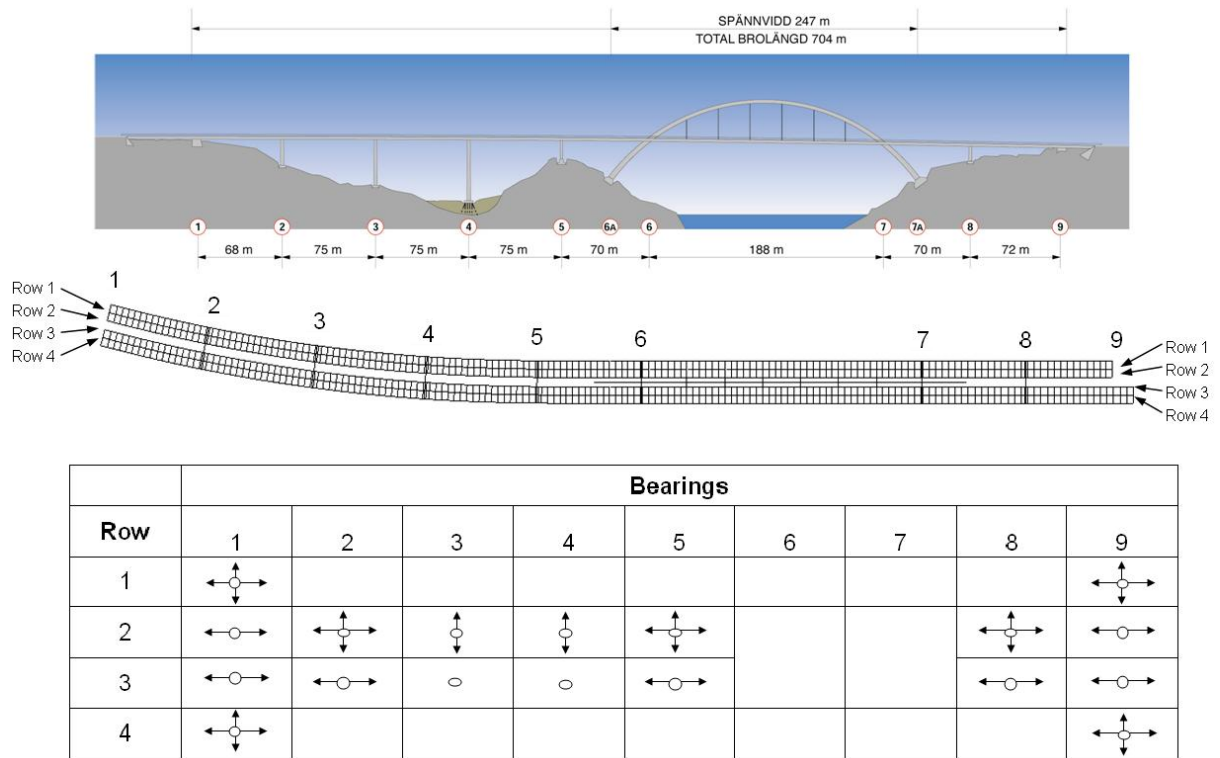


Figure 5.10 Permissible bearing translational movement according to Bilfinger Berger (2003b), bridge layout from www.vv.se/svinesund.

A discrepancy between the measured eigenfrequency for mode 2 and the FEM eigenfrequency was first reported by Ülker-Kaustell and Karoumi (2006) and believed to be caused by static friction. The increased normal force in the bearings due to prestressing increases the resistance in the bearing due to static friction. If the loading on the bridge is not sufficient to overcome the static friction resistance threshold, the bearing will not permit movement intended by the bearing design. Although spherical bearings have very low friction, the additional normal force provided by prestressing drastically increases the static friction in the bearing. In order to test the static friction hypothesis, the restraint condition for the bearings at the abutments and the piers was changed in order to simulate static friction. The restraints applied by Plos and Movaffaghi (2004) in accordance with the bearing design (see Figure 5.10) allowed rotation (DOF 4-6) and permissible translation (DOF 1-2) without any friction. Vertical motion (DOF 3) was restrained in the FE model due to prestressing. This initial case is presented as ‘FREE’ in Appendix E and model 1a in Chapter 5.2.2.1.

The spherical bearings used in the New Svinesund Bridge have a flat surface to allow for translational movement and a cupped surface for rotation, see Figure 5.11. The dimensions of the bearings are available in Figure 5.12 and Figure 5.13. A thorough study of the bearings was performed with the results presented in Appendix E.

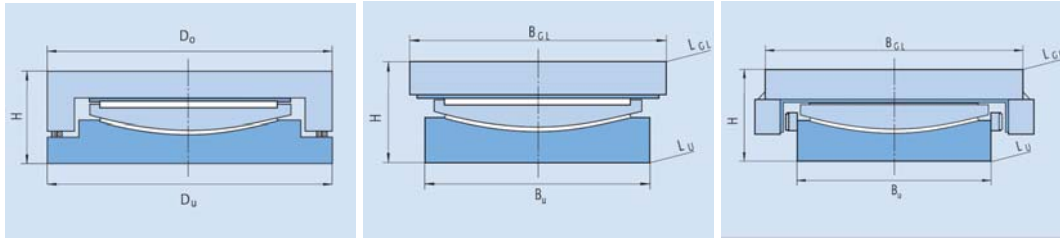


Figure 5.11 Fixed, generally mobile and unilaterally mobile spherical bearings for connection between pier and bridge superstructure, Maurer Söhne (2007).

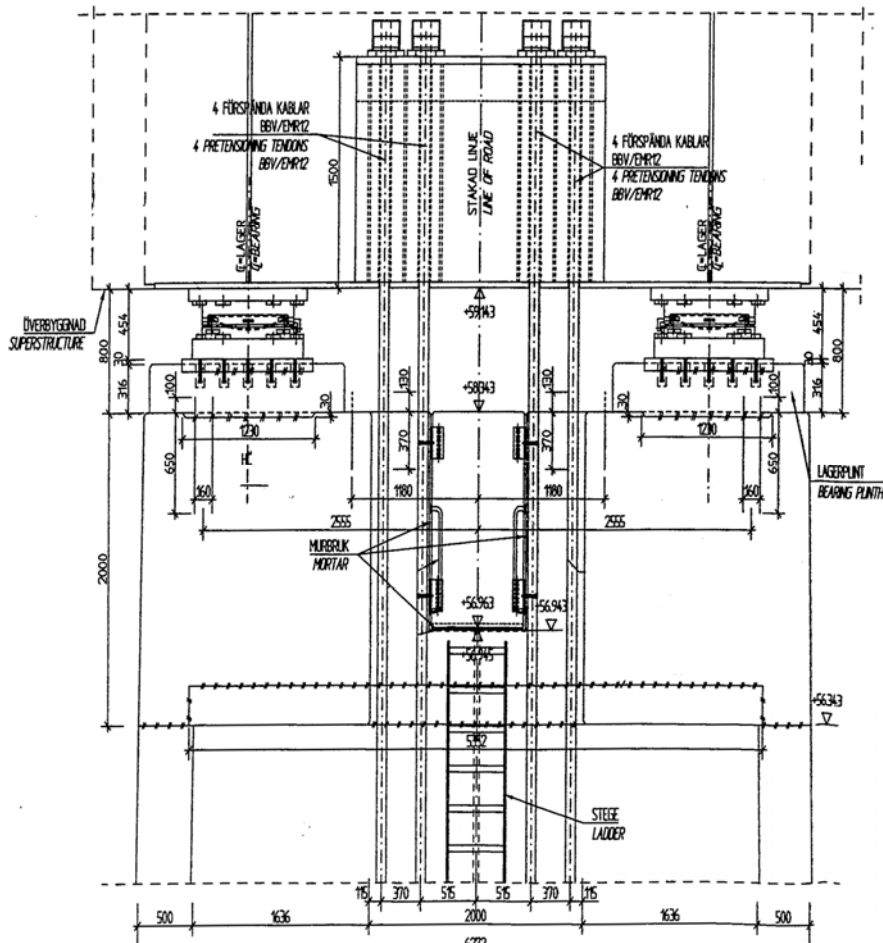


Figure 5.12 Structural drawing front view of pier to carriageway connection at pier 3 provided by Bilfinger Berger (2003a).

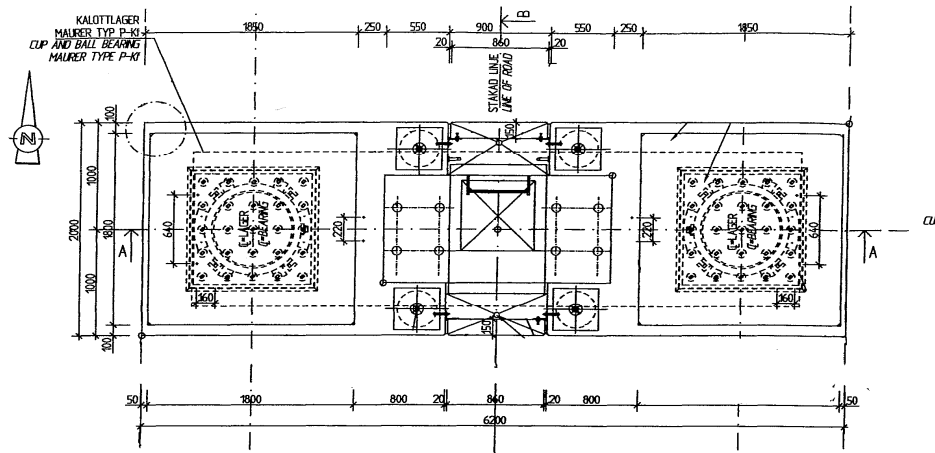


Figure 5.13 Structural drawing top view of pier to carriageway connection at pier 3 provided by Bilfinger Berger (2003a).

5.2 FE model evolution

5.2.1 Model 0: initial model

Fortunately, the initial FE model created by Bilfinger Berger (2004) for design and translated to ABAQUS by Plos and Movaffaghi (2004) for analysis was very detailed and capable of modelling the structural response for a vast range of load combinations and analysis types. Insufficient model accuracy of the second eigenfrequency and certain load combinations provided motivation for FE model updating. The first 20 eigenmodes for model 0 are presented in Figure 5.14 and Figure 5.15. Considerable movement at the bearing at pier 5 for eigenmode 2 is evident in Figure 5.14. The correlation between the experimentally measured eigenfrequencies and the frequencies for model 0 is good for modes 1,3 and 4, but the correlation is uncertain for mode 2 and modes 5 and higher.

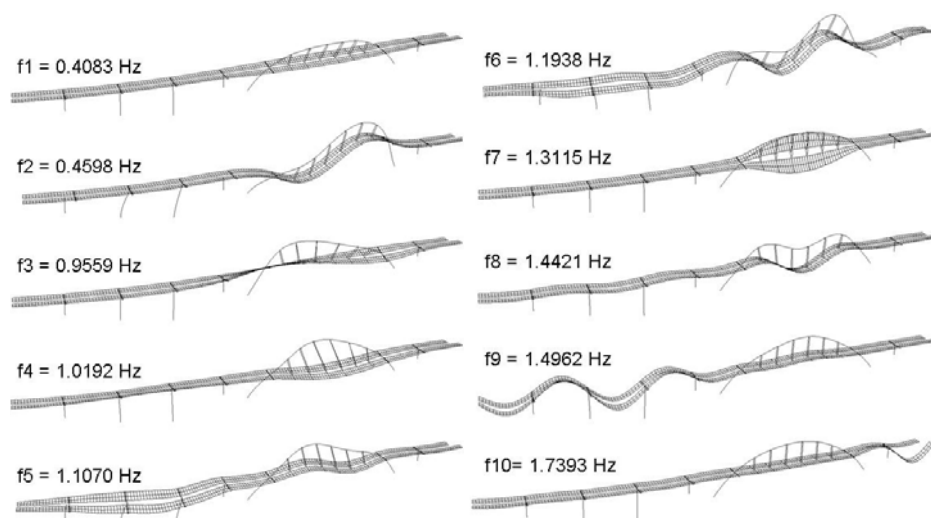


Figure 5.14 Eigenmodes 1-10 for model 0.

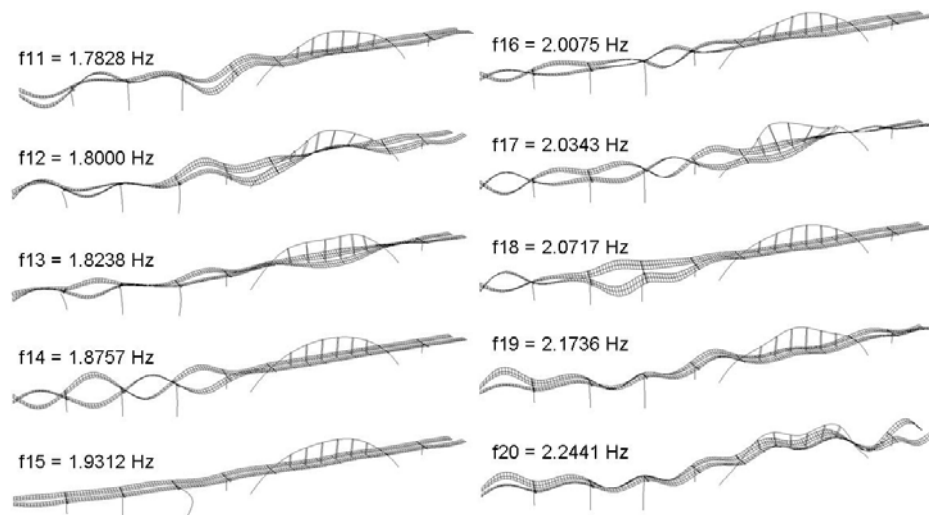


Figure 5.15 Eigenmodes 10-20 for model 0.

5.2.2 Model 1: boundary condition study

The discrepancy between Model 0 and the measurements for eigenmode 2 suggested that the bearings did not behave as intended in design. In order to model static friction in all bearings during the frequency analysis, the nodes of the pier were tied to the nodes of the bridge superstructure at the bearing location, thus restraining all translation and rotation (DOF 1-6). Thus for Model 1: Model 1a, Model 1b, Model 1c and Model 1d, the bearing constraints were tied for the frequency analysis. The frequency results for Model 1a, Model 1b, Model 1c and Model 1d were identical but each model used different bearing restraint conditions for the static load cases. Four restraint conditions were modelled for the static load cases in order to test the affect of static friction. Tabulated data and plots of the bearing forces for the restraint conditions are presented in Appendix E.

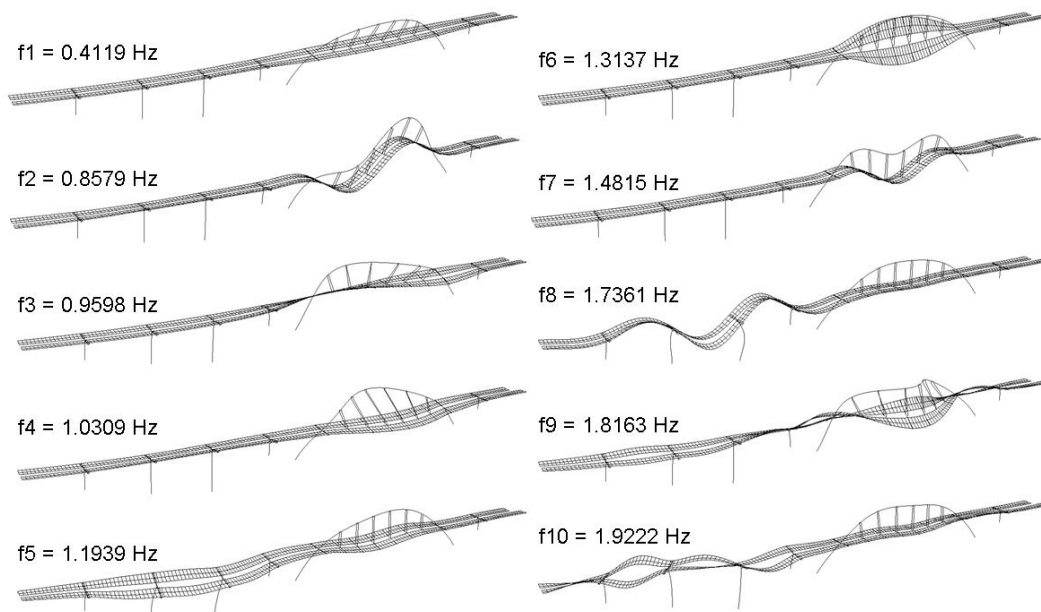


Figure 5.16 Eigenmodes 1-10 for model 1.

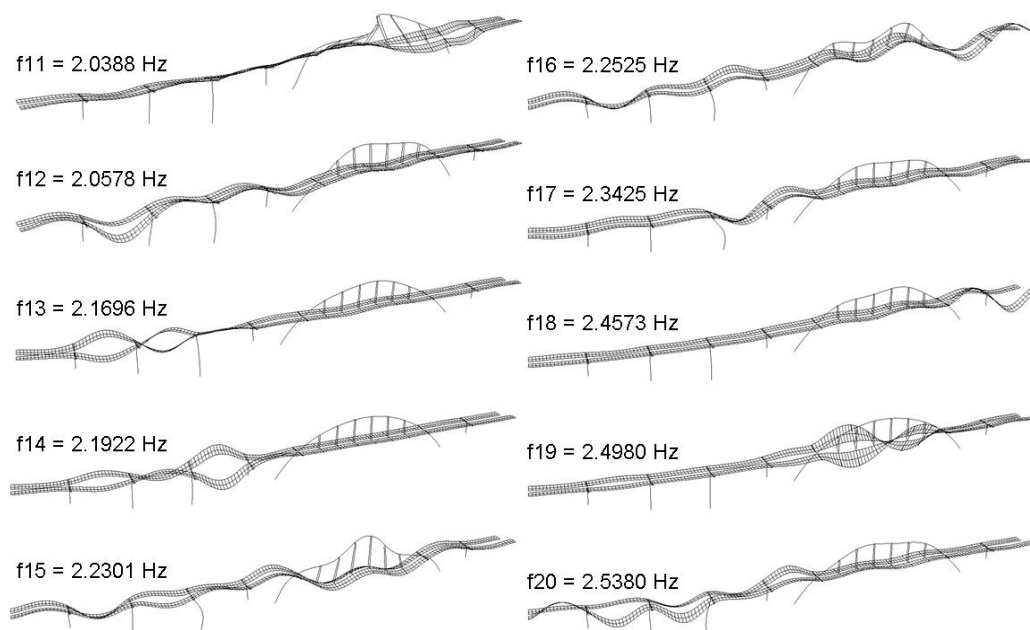


Figure 5.17 Eigenmodes 10-20 for model 1.

The most considerable change in the eigenfrequencies due to the fully constrained bearings occurs at eigenmode 2. The restraint increases the eigenfrequency from 0.460 Hz to 0.858 Hz. The change in bearing constraints therefore seems reasonable. The eigenfrequencies that correspond to measurable eigenmodes (modes with movement manifest in sensor locations) for model 0 and model 1 are presented in Table 5.2. During initial analysis, model 1 was very promising since the FE model predicted exactly 1 measurable eigenmode in the vicinity of each measured frequency. Although there were other eigenfrequencies between the measurable frequencies, the excitation location did not correspond with the sensor location, thus they would have not been measured. Examination of eigenmode 4 in Figure 5.16 with the location of accelerometers in Figure 4.2 demonstrates excitation of the transversally oriented

accelerometers in the arch crown and in the carriageway and thus a resonance peak is manifest in the stabilization diagram, Figure 4.4. Eigenmode 5 is the transverse oscillation of the carriageway over piers 3 and 4 and occurs at 1.194 Hz. No accelerometers were used in that section of the carriageway, therefore no resonant peak is manifest in the stabilization diagram. Eigenmode 6 is the torsional bending of the carriageways over the main span. This motion excited the vertically oriented accelerometers in the carriageways and thus was believed to correspond with the strong resonant peak at 1.335 Hz.

Table 5.2 Eigenfrequencies 1-8 from experimental measurements with possible corresponding eigenfrequencies from FE model 0 (free bearing constraints) and FE model 1 (tied bearing constraints).

Measured	Model 0	Model 1	Units
f_{1m} 0.425	f_1 0.408	f_1 0.412	Hz
f_{2m} 0.846	f_2 0.460	f_2 0.858	Hz
f_{3m} 0.940	f_3 0.956	f_3 0.960	Hz
f_{4m} 0.999	f_4 1.019	f_4 1.031	Hz
f_{5m} 1.335	f_5 1.107	f_6 1.314	Hz
	f_6 1.194		
f_{6m} 1.455	f_7 1.312	f_7 1.482	Hz
f_{7m} 1.781	f_8 1.442	f_9 1.816	Hz
f_{8m} 2.072	f_{12} 1.800	f_{11} 2.039	Hz
	f_{13} 1.824		
	f_{17} 2.034		

5.2.2.1 Model 1a: 'FREE'

Model 1a was termed 'FREE' because the bearings were allowed to move according to the design specifications for the static load cases. The bearings permitted motion according to the bearing design without friction for the static loads, but were fixed during the frequency analysis. Significant motion was present at the abutment bearings, at pier 2 and at pier 5. The longitudinal load was distributed to pier 3 and pier 4 due to longitudinal restraint. No bearing motion is present at piers 3 and 4; rather, deformation of the piers is evident by comparing the deformed bridge during loading to the undeformed bridge in Figure 5.18.

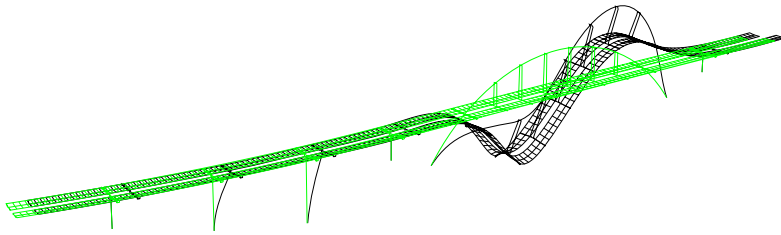


Figure 5.18 Deformation of bridge during load case E and for Model 1a: static bearing condition FREE (scale factor = 1500).

5.2.2.2 Model 1b: 'TIE'

Neglecting static friction during the static load cases was not reasonable, so the bearing forces were investigated by FEA. Although the sectional forces in the elements that connected the piers to the carriageway were lower than the calculated static friction, the sectional forces in the elements that connected the carriageway to the abutments were much greater than the calculated static friction in the abutment bearings. The normal force in the pier bearings was drastically increased due to prestressing, thus making the static friction threshold in the pier bearings significantly greater than in the abutment bearings. The high sectional forces in the abutment bearings and low sectional forces in the pier bearings are plotted relative to the static friction threshold in Figure 5.19.

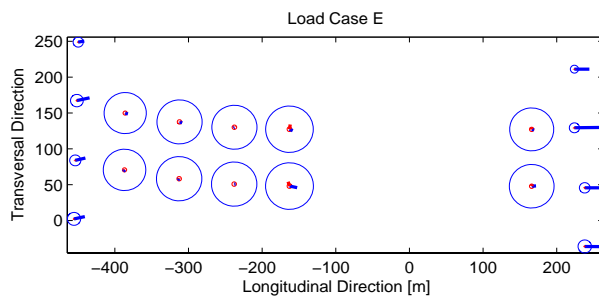


Figure 5.19 Plot of bearing forces and moments and static friction threshold for load case E and bearing condition TIE (sectional forces plotted with lines, static friction threshold plotted with circles).

5.2.2.3 Model 1c: 'PIER TIE'

Due to high sectional forces in the elements at the abutment bearings compared with the static friction threshold, Model 1b with bearing condition 'TIE' was not realistic. Upon overcoming the static friction in the abutment bearings, the bearings move freely until equilibrium is established. For all load cases, the sectional force in each abutment bearing element overcame the corresponding static friction threshold, thus the abutment bearings were allowed to function according to design for bearing condition 'PIER TIE'. By releasing the abutment bearings to move freely, the force was redistributed to the remaining bearings, particularly to the bearings at pier 5 and pier 8. The effect of the load redistribution was particularly evident for load case E.

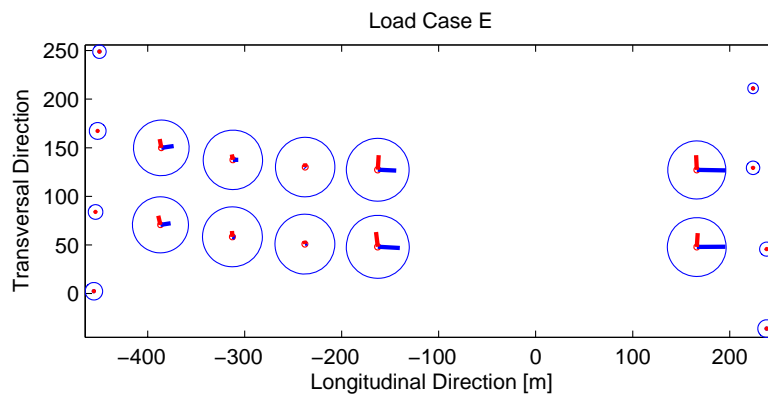


Figure 5.20 Plot of bearing forces and moments and static friction threshold for load case E and bearing condition PIER TIE (sectional forces plotted with lines, static friction threshold plotted with circles).

5.2.2.4 Model 1d: 'PIER TIE 58 FREE'

Although bearing condition 'PIER TIE' was assuredly more accurate than bearing conditions 'FREE' and 'TIE', the redistribution of bearing forces for load case E made the bearing condition at piers 5 and 8 uncertain. In order to further understand the structural behaviour of the bridge, the bearings at piers 5 and 8 were released and the load redistribution was studied in bearing condition 'PIER TIE 58 FREE'. The loads were redistributed primarily to piers 2 and 3. This result was not surprising since pier 4 is relatively flexible due to the pile foundation and the relatively high slenderness when compared with the shorter piers 2 and 3 (which have rock foundations).

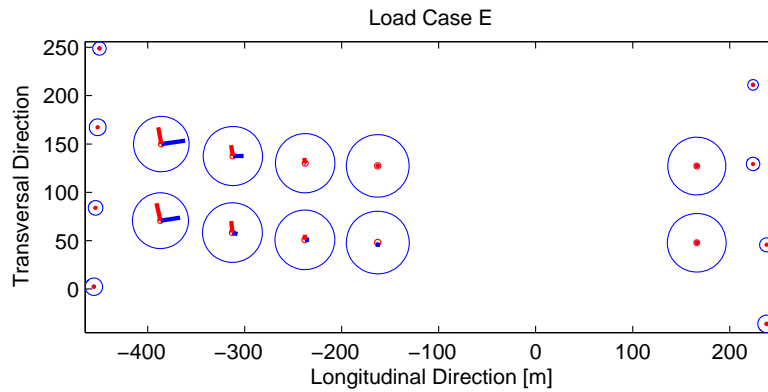


Figure 5.21 Plot of bearing forces and moments and static friction threshold for load case E and bearing condition PIER TIE 58 FREE (sectional forces plotted with lines, static friction threshold plotted with circles).

5.2.3 Model 2 to Model 7

Throughout Chapter 5, a detailed description has been made of each step of the model evolution. From the study of the boundary conditions it was concluded that Model 1c is the candidate which should be used for further development. In Model 2 the increased stiffness of the concrete in the arch is considered. This measure caused a dramatic change of the eigenfrequencies. It turned out after scrutinized the designer's documentation of bridge and the ABAQUS input files, that the mass of the asphalt layer not were taken in to account in the initial model which was done in Model 3. The first thought is that the asphalt layer does not contribute to any stiffness, but after careful investigation of the asphalts properties it was concluded that the stiffness certainly should be considered, which implies Model 4. In Model 5 a linear spring were implemented in the connections between the arch and the carriageways, the reason for implementing the springs was to investigate if the connections really was fixed or not. For same reason springs was implemented in the foundations of the arch in Model 6. The final step in the model evolution was to implement non-linear springs (Model 7). The non-linear springs is implemented to simulate the static friction in the bearings. The non-linear springs is implemented with high-stiffness until static friction threshold reached, then constant force (similar to elastic-perfectly plastic).

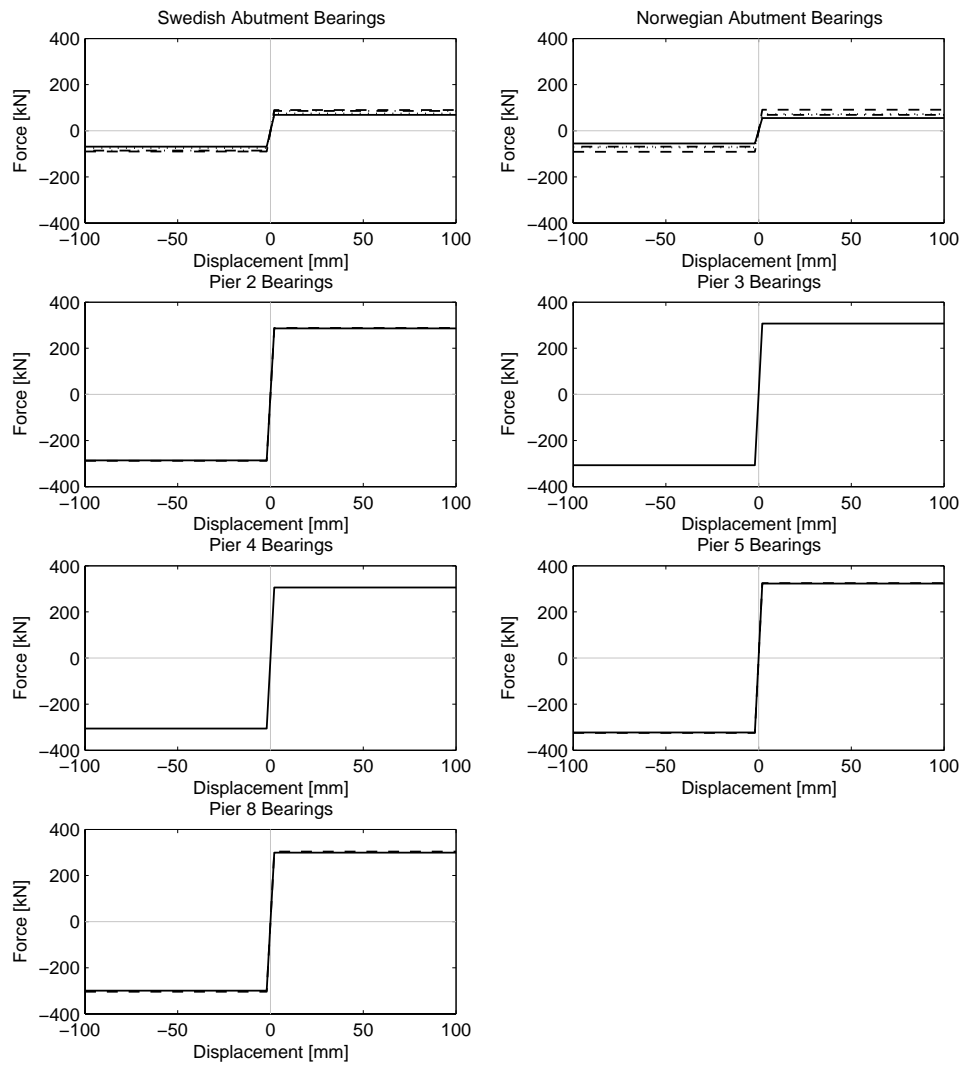


Figure 5.22 Plot of constitutive relationship for non-linear springs at bearings.

In Figure 5.23 below, the bearing force for load case A was below the static friction threshold, thus only small movement was evident at the bearing.

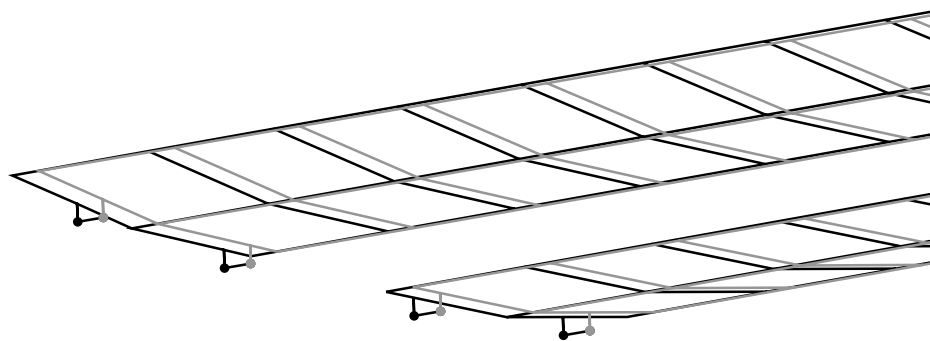


Figure 5.23 Figure showing displacement at the abutment on the Swedish side for load case A (scale 1500).

In Figure 5.24, the static friction threshold was overcome in the bearing for load case E, thus large displacement was evident.

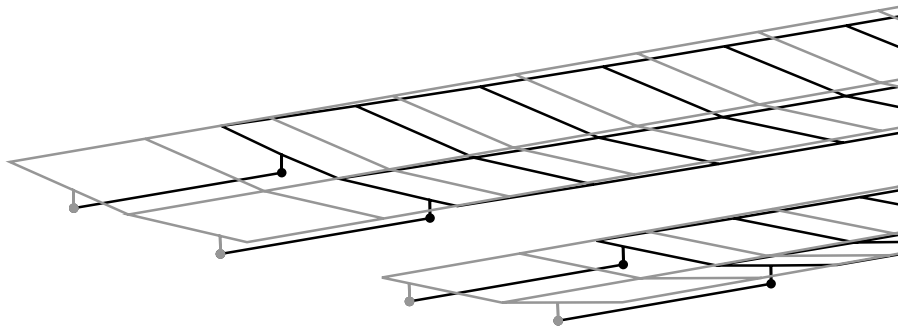


Figure 5.24 Figure showing displacement at the abutment on the Swedish side for load case E (scale 1500).

6 FE Model Manual Refinement of the New Svinesund Bridge through Parameter Sensitivity Analysis

6.1 Statistics for measurements

One of the significant challenges of this project was deciding how to apply weight to the response residual and the updating parameter change in a meaningful way. If only frequencies were used for FE model updating, the weighting of the response residual would be rather straightforward since the response residual could be normalized with the measured eigenfrequencies or using the standard deviations from the frequency measurements. In order to obtain an “optimal” model, the objective function had to compare the frequency, strain, displacement and hanger load measurements in a meaningful way while considering the values of the updating parameters. Furthermore, systematic error such as temperature effects and modelling limitations were known to limit the ability of the FE model to reproduce the measured response. Many objective functions were formulated in an attempt to understand the proper balance for the contribution of each type of response residual to the optimized FE model.

Using the data from the measurement project provided by Karoumi (2007) the statistical considerations for each type of measurement were scrutinized. The statistical data reported by Ülker-Kaustell and Karoumi (2006) and Karoumi and Andersson (2006) only considered typical values of the experimentally measured static response when calculating the standard deviation, experimental noise was not included. Experimental noise during loaded and unloaded measurement periods of the static response was included in the calculation of the standard deviations of the measurements for this study. In order to minimize the temperature effect on the frequency measurements, the frequency measurements from the winter measurement period were excluded for the scope of this study. Thus, the statistical data presented in this study does not exactly match the statistics reported by Ülker-Kaustell and Karoumi (2006) and Karoumi and Andersson (2006). Mean values for the standard deviations of each type of measurement are summarized in the table below.

Table 6.1 Average statistical data for experimentally measured responses (mean values of response or deviation vector \mathbf{x} denoted by \bar{x}).

	\bar{z}_m	$\bar{\sigma}_{std}$	$\bar{\sigma}_T$	$\bar{\sigma}_{no-load}$	$\bar{\sigma}_{sensor}$	$\bar{\sigma}_{model}$	$\bar{\sigma}_{tot}$	Units	$\frac{\bar{\sigma}_{tot}}{\bar{z}_m}$
Frequency, f	0.8024	0.0036	0.0029				0.0048	Hz	0.6%
Strain, ε	7.543	0.633		0.740	6.000	0.846	6.250	$\mu\text{m/m}$	82.9%
Displacement, u	7.919	1.297			1.346	1.010	2.466	mm	31.1%
Hanger Loads, F	131.9	2.3		3.3	10.8	16.3	21.1	kN	16.0%

The standard deviation of experimentally measured data, σ_{std} , was calculated from the spreadsheets provided by KTH (2007). Only the data from the summer the frequency measurements was used to calculate σ_{std} for frequency.

The frequency measurements were conducted at a different time than the static load tests, thus structural parameters for the frequency measurements and for the static load tests may not have been identical. Strains and hanger loads were measured continuously from permanently installed sensors at a rate of 1 Hz and the data was recorded by NGI using the permanent data acquisition system while FB Engineering was responsible for displacement measurements, Karoumi and Andersson (2006). Experimental noise was evident for all measurements and although efforts were put forth to remove systematic error, bias was still suspected in the measured static response. The sensor accuracy according to the manufacturer, σ_{sensor} , and a model correlation factor, σ_{model} , were included in the calculation of the deviation of the static load measurements in an effort to account for systematic error. Since the strains and hanger loads were measured continuously, the noise level during unloaded time periods could be calculated and included in the calculation of the total deviation, σ_{tot} .

As discussed in Chapter 5.1.3, the temperature of the arch was not consistent for each frequency measurement. The asphalt temperature was assumed to vary according to the arch temperature and the time of day, thus a range for the asphalt stiffness during ambient vibration measurements was determined. Since the eigenfrequencies depend on the asphalt stiffness, the deviation of the first four eigenfrequencies due to the expected deviation in the asphalt stiffness, σ_T , was calculated.

By minimizing experimental bias due to temperature for the static loads and by including experimental measurement noise, frequency variation due to temperature, sensor accuracy and model correlation, the total deviation was formulated.

Frequency deviation was calculated using the standard deviation of the measurements, σ_{std} , and the modelled deviation due to temperature variation, σ_T ,

$$\sigma_{tot,f} = \sqrt{\sigma_{std,f}^2 + \sigma_{T,f}^2} \quad (6.1)$$

Using the permanently installed strain gauges, the strains were measured continuously during all load tests. Strain deviation was calculated using the standard deviation of the measurements during loading, σ_{std} , and between load tests, $\sigma_{no-load}$, as well as the sensor deviation, σ_{sensor} , and a model correlation factor, σ_{model} ,

$$\sigma_{tot,\varepsilon} = \sqrt{\sigma_{std,\varepsilon}^2 + \sigma_{no-load,\varepsilon}^2 + \sigma_{sensor,\varepsilon}^2 + \sigma_{model,\varepsilon}^2} \quad (6.2)$$

The displacements were obtained with discrete measurements rather than a continuous signal, thus no data was available to determine the no-load deviation,

$$\sigma_{tot,u} = \sqrt{\sigma_{std,u}^2 + \sigma_{sensor,u}^2 + \sigma_{model,u}^2} \quad (6.3)$$

Hanger load deviation was calculated in the same way as the strain deviation,

$$\sigma_{tot,\varepsilon} = \sqrt{\sigma_{std,\varepsilon}^2 + \sigma_{no-load,\varepsilon}^2 + \sigma_{sensor,\varepsilon}^2 + \sigma_{model,\varepsilon}^2} \quad (6.4)$$

6.2 Objective function formulation for the New Svinesund bridge

According to Jaishi and Ren (2005), “the selection of the objective function to be minimized has a profound impact on the problem.” The purpose of the objective function is to provide a meaningful scalar or vector function for the optimization function to minimize. The updating parameter vector that minimizes the objective function is considered to be the optimal solution to the problem at hand.

Many FE model updating algorithms only consider a select number of the eigenfrequencies of the bridge for the response. In such a case, the Euclidean norm of the normalized frequency residual is suitable for the objective function. The response of the New Svinesund Bridge was not so simple, thus more robust objective functions were needed.

6.2.1 Standard deviation objective function

Since the response included frequencies, strains, displacements and hanger loads, the objective function needed to balance the residuals in a statistically significant manner. If the residual was scaled simply by dividing by the measured response, strain and displacement measurements near zero would be a source of numerical error when compiling the objective function. Instead, the residual was evaluated using the statistical significance of each measurement for the standard deviation, variance and uncertainty objective functions. Furthermore, only four eigenfrequencies were used for updating due the lack of a MAC matrix for the evaluation of eigenmodes above mode four, but the confidence in the eigenfrequency measurements was very high compared with the confidence in the strain, displacement and hanger load measurements due to the presence of experimental noise. If each parameter in the response vector were weighted equally, the strain and displacement responses would dominate the objective function and thus skew the results. Thus, objective functions were formulated in a manner as to balance the contributions of the frequency, strain, displacement and hanger load responses in a statistically meaningful manner.

The standard deviation objective function was used to express the objective function in terms of the response residual normalized by the standard deviation of the measured response.

Standard deviation objective function for frequency, \mathbf{f} (size, $[N_f \times 1]$),

$$\sigma^f \Pi = \frac{\sum_{i=1}^{N_f} \sqrt{\frac{(f_{mi} - f_i)^2}{\sigma_{f_i}^2}}}{N_f} \quad (6.5)$$

Standard deviation objective function for strain, $\boldsymbol{\varepsilon}$,

$$\sigma^\varepsilon \Pi = \frac{\sum_{i=1}^{N_\varepsilon} \sqrt{\frac{(\varepsilon_{mi} - \varepsilon_i)^2}{\sigma_{\varepsilon_i}^2}}}{N_\varepsilon} \quad (6.6)$$

Standard deviation objective function for displacement, \mathbf{u} ,

$$\sigma^u \Pi = \frac{\sum_{i=1}^{N_u} \sqrt{\frac{(u_{mi} - u_i)^2}{\sigma_{u_i}^2}}}{N_u} \quad (6.7)$$

Standard deviation objective function for hanger load, \mathbf{F} ,

$$\sigma^F \Pi = \frac{\sum_{i=1}^{N_F} \sqrt{\frac{(F_{mi} - F_i)^2}{\sigma_{F_i}^2}}}{N_F} \quad (6.8)$$

The standard deviation objective function for the response of the New Svinesund Bridge was defined as the mean deviation of each type of response,

$$\sigma^z \Pi = \frac{\sigma^f \Pi + \sigma^\varepsilon \Pi + \sigma^u \Pi + \sigma^F \Pi}{4} \quad (6.9)$$

The updating parameter vector, $\boldsymbol{\Phi}$, that will best reproduce the experimentally measured response (by minimizing the deviation of the response) is obtained by solving the standard deviation objective function for the response.

$$\min_{\boldsymbol{\Phi}} \sigma^z \Pi \quad (6.10)$$

In the study of the simple beam, the importance of regularization was established by including a high level of noise. The least squares updating algorithm without regularization was not stable, but the use of a weighted penalty for deviation from the initial updating parameter allowed the pseudo-inverse algorithm with a weighted response and weighted updating parameter to converge. The use of regularization is common for optimization when the stability of the optimization algorithm is a concern. For the case of the Svinesund bridge, the regularization term for the standard deviation objective function expressed the deviation of the iterated updating parameter vector from the initial guess based on engineering calculations in terms of the standard deviation of the updating parameter.

$$\Phi_{\sigma\Pi} = \frac{\sum_{i=1}^{N_{\phi}} \sqrt{\frac{(\phi_{0i} - \phi_i)^2}{\sigma_{\phi_i}^2}}}{N_{\phi}} \quad (6.11)$$

Considering the standard deviation of the response ($\mathbf{z}_j - \mathbf{z}_m$) with regularization added according to the deviation from the “best guess” updating parameter vector from engineering calculations ($\Phi_j - \Phi_0$), the objective function to be minimized represents the optimal model with regard to standard deviation. Generally, the regularization term is a penalty term that is multiplied by a scalar, α , that can be adjusted in order to ensure the stability of the objective function during optimization,

$$\Pi = {}^z\Pi + \alpha \Phi\Pi \quad (6.12)$$

For this study, the objective function of the response was weighted equally with the regularization function of the input parameters,

$$\sigma\Pi = \frac{{}^z\Pi + \Phi\Pi}{2} \quad (6.13)$$

Thus the minimization equation for the optimal model with regard to the response and the input parameters in terms of standard deviation is,

$$\min_{\Phi} \sigma\Pi \quad (6.14)$$

6.2.2 Variance objective function

In order to minimize the variance of the response with regard to the measured response and measured variance, the variance objective function was defined as follows.

Variance objective function for a type of measured response, ${}_1\hat{\mathbf{z}}$, (for response vector ${}_1\hat{\mathbf{z}}$ of size $[N_{1\hat{\mathbf{z}}} \times 1]$),

$${}_1\hat{\mathbf{z}}\Pi_v = \frac{\sum_{i=1}^{N_{1\hat{\mathbf{z}}}} \frac{({}_1\hat{\mathbf{z}}_{mi} - {}_1\hat{\mathbf{z}}_i)^2}{\sigma_{1\hat{\mathbf{z}}_i}^2}}{N_{1\hat{\mathbf{z}}}} \quad (6.15)$$

Thus variance objective function for the response is the mean of the variance objective functions for n types of measured responses.

$${}^z\Pi_v = \frac{{}_1\hat{\mathbf{z}}\Pi_v + {}_2\hat{\mathbf{z}}\Pi_v + \dots + {}_n\hat{\mathbf{z}}\Pi_v}{n} \quad (6.16)$$

For the case at hand, the types of measured responses include frequency (${}_1\hat{\mathbf{z}} = \mathbf{f}$), strain (${}_2\hat{\mathbf{z}} = \boldsymbol{\varepsilon}$), displacement (${}_3\hat{\mathbf{z}} = \mathbf{u}$) and hanger loads (${}_4\hat{\mathbf{z}} = \mathbf{F}$).

The regularization term was used to minimize the variance of the updating parameter vector the best guess from engineering calculations.

$$\Phi_v \Pi = \frac{\sum_{i=1}^{N_\phi} (\phi_{0i} - \phi_i)^2}{N_\phi \sigma_{\phi_i}^2} \quad (6.17)$$

Considering both response and the updating parameter, the variance objective function to be minimized in order to obtain the optimal FE model is,

$${}_v \Pi = \frac{{}_z \Pi + \Phi_v \Pi}{2} \quad (6.18)$$

The minimization equation to be solved for the optimal updating parameter vector, Φ , is,

$$\min_{\Phi} {}_v \Pi \quad (6.19)$$

6.2.3 Error objective function

While the standard deviation and variance objective functions account for the statistical significance of the response, \mathbf{z} , and the updating parameter, Φ , the error objective function may be used to express the mean error of the response.

Error objective function for a type of measured response, ${}_1\hat{\mathbf{z}}$,

$${}_{z/\Sigma|z_m} {}_1\hat{\mathbf{z}} \Pi = \frac{\sum_{i=1}^{N_{1\hat{\mathbf{z}}}} |{}_1\hat{z}_{mi} - {}_1\hat{z}_i|}{\sum_{i=1}^{N_{1\hat{\mathbf{z}}}} |{}_1\hat{z}_{mi}|} \quad (6.20)$$

Thus error objective function for the response is,

$${}_z \Pi = \frac{{}_{z/\Sigma|z_m} {}_1\hat{\mathbf{z}} \Pi + {}_{z/\Sigma|z_m} {}_2\hat{\mathbf{z}} \Pi + \dots + {}_{z/\Sigma|z_m} {}_n\hat{\mathbf{z}} \Pi}{n} \quad (6.21)$$

The regularization term for the updating parameter,

$${}_{z/\Sigma|z_m} \Phi \Pi = \frac{\sum_{i=1}^{N_{1\hat{\mathbf{z}}}} |\Phi_{0i} - \Phi_i|}{\sum_{i=1}^{N_{1\hat{\mathbf{z}}}} |\Phi_{0i}|} \quad (6.22)$$

For the regularization term above, the updating parameter vector should be normalized so that no single uncertain structural parameter will govern the behaviour of the objective function. Considering both the error of the response and the change in the updating parameter,

$${}_{z/\Sigma|z_m} \Pi = \frac{{}_z \Pi + {}_{z/\Sigma|z_m} \Phi \Pi}{2} \quad (6.23)$$

The minimization equation to be solved for the optimal updating parameter vector, Φ ,

$$\min_{\Phi} {}_{z/\Sigma|z_m} \Pi \quad (6.24)$$

6.2.4 Uncertainty objective function

During the experimental measurement phase, all precautions should be taken in order to eliminate measurement bias. Nonetheless, temperature, sensor bias, hysteresis and environmental factors can cause significant systematic error in the measurements. For such a case, the variance of the measurements may be low (high precision) while the actual error is high (low accuracy). For such measurements (often termed “outliers”) the standard deviation, variance and error objective functions apply significant weight and so will dominate the minimization function. Although the outlier cannot be modelled because it is an artefact of systematic error caused by experimental bias or numerical modelling limitations, it will contribute more to the objective function than the responses that can be accurately modelled. The outlier residual will be minimized at the cost of the more accurate measurements.

The uncertainty objective function has the benefit that all responses that deviate more than twice the standard deviation will contribute about the same to the objective function. In such a manner, more “certain” measurements will dominate the behaviour of the objective function.

Uncertainty objective function for a type of measured response, ${}_1 \hat{z}$,

$${}_{|\text{erf}|} {}_1 \hat{z} \Pi = \frac{\sum_{i=1}^{N_{1\hat{z}}} |\text{erf}|}{N_{1\hat{z}}} \quad (6.25)$$

Thus uncertainty objective function for the response is,

$${}_z \Pi = \frac{{}_1 \hat{z} \Pi + {}_2 \hat{z} \Pi + \dots + {}_n \hat{z} \Pi}{n} \quad (6.26)$$

Often the probability distribution for building materials is specified in structural codes or by the manufacturer in terms of the coefficient of variation (*COV*). The regularization term for the updating parameter,

$$|\text{erf}|^{\Phi} \Pi = \frac{\sum_{i=1}^{N_{1,\hat{z}}} |\text{erf}|}{N_{1,\hat{z}}} \quad (6.27)$$

Considering both the uncertainty of the response and the uncertainty of the updating parameter,

$$|\text{erf}| \Pi = \frac{|\text{erf}|^z \Pi + |\text{erf}|^{\Phi} \Pi}{2} \quad (6.28)$$

The minimization equation to be solved for the most certain updating parameter vector, Φ ,

$$\min_{\Phi} |\text{erf}| \Pi \quad (6.29)$$

Stochastic minimization algorithms are recommended to solve the minimization equation above. The uncertainty objective function accentuates the response where the agreement between the FE model response and the experimentally measured response is high, often with asymptotic behaviour. Gradient based algorithms that search for a flat (zero gradient) surface (such as the Quasi-Newton algorithm) should not be used to minimize the uncertainty objective function. Instead, the Nelder-Mead simplex method, global optimization routines (such as evolutionary, genetic or annealing algorithms) or hybrid algorithms are suggested in order to determine the global minimum in the feasible updating parameter space. The possibility of the presence of non-optimal local minima should be explored and a global optimality search should be performed if local minima are present during the parameter sensitivity study (refer to Figure 6.4).

6.3 Parameter sensitivity study

One of the primary challenges in FE model updating is determining which structural parameters should be updated. In order to determine which uncertain structural parameters should be updated, a parameter sensitivity study was performed. Uncertain structural parameters were iterated within a reasonable range and the response (dynamic and static) of the bridge was assessed at each iteration. The results of the structural parameter investigation, Chapter 5.1, were used to determine a starting guess for the uncertain structural parameters to be investigated. In order to quantify the residual the response at each iteration, objective functions defined in Chapter 6.1 were utilized. In some cases, a change to the updating parameter would reduce the frequency residual but increase the residual from the hanger load measurements. At that point, the statistical significance of each type of measurement was used to evaluate the response. Thus, error in measurements with a very low variance was weighted higher than error in measurements with higher variance. For example, frequency measurements had very low variation because the accelerometers are very accurate while the strain displacement and hanger load measurements were not weighted as heavily after considering measurement noise and sensor accuracy. Standard deviation, variance, error and uncertainty objective functions were all used

to evaluate the modelled response to changes in each updating parameter and the resulting plots were scrutinized to determine the optimal starting value of the normalized updating parameter vector for automated optimization (FE model updating). The modelled response with regard to each parameter and the significance of the normalized updating parameter value that minimizes each objective function is discussed in the proceeding sections.

Direct FE updating techniques directly change the mass and stiffness matrices so that the FE model will reproduce the frequencies of interest, but the resulting mass and stiffness matrices bear no relevance to the actual structural parameters of the bridge. Furthermore, direct FE model updating techniques only use dynamic response parameters such as frequencies, mode shapes and damping, thus the static response is not considered.

6.3.1 Concrete stiffness

The coefficient of variation of the elastic modulus of concrete is 0.15 according to Thelandersson (2004), therefore possible variation of the arch stiffness was considered during design. Structural design criteria require that the bridge satisfy SLS deflection limitations with a conservative estimate of the concrete elastic modulus (concrete elastic modulus design value) to account for possible variation. In order to model the actual performance of the bridge, the mean value for the elastic modulus was used. Furthermore, the increased arch stiffness due to concrete hydration and reinforcement was modelled using the results from the structural parameter investigation, Chapter 5.1.1. The objective function of the response as a function of the normalized updating parameter for the elastic modulus of concrete is presented below in Figure 6.1 and Figure 6.2.

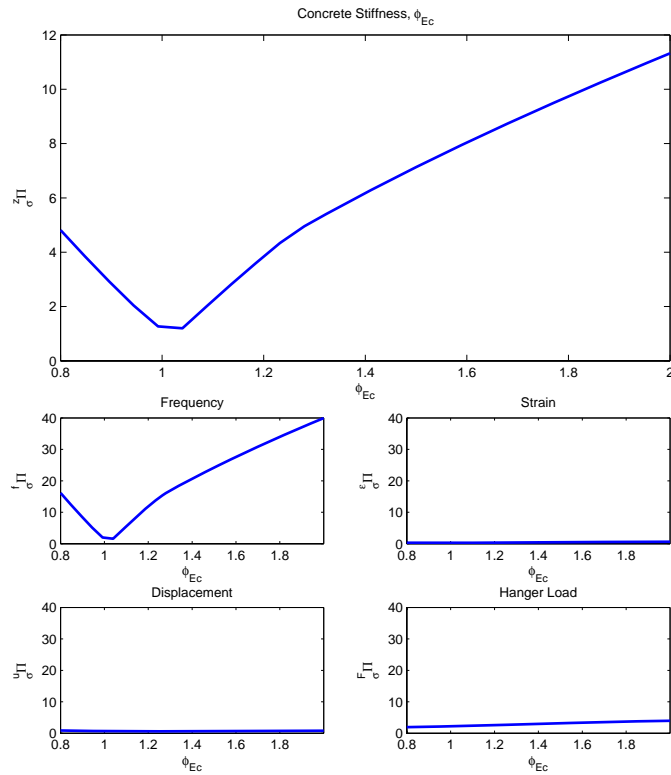


Figure 6.1 Standard deviation objective function plotted as a function of normalized stiffness of the concrete arch.

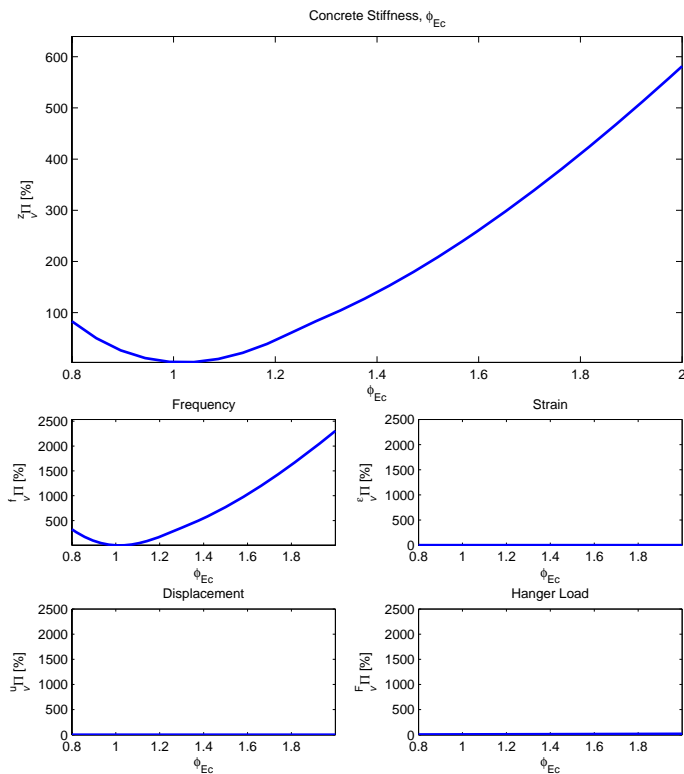


Figure 6.2 Variance objective function plotted as a function of normalized stiffness of the concrete arch.

From Figure 6.1 and Figure 6.2, it is clear that the initial guess for the equivalent elastic modulus of concrete as determined in the structural parameter investigation was quite accurate. The frequency portion of the response is especially sensitive to the arch stiffness, thus contributing dominating the behaviour of the variance and standard deviation objective functions. Bending of the arch is evident in all four bending modes that compose the frequency portion of the response, thus the dynamic response is highly sensitive to the arch stiffness.

The initial estimations of an increase to the concrete stiffness at the arch base of 4.1% and to the arch crown of 16.7% were slightly conservative, according to all objective functions used to analyse the response residual. According to the analysis, in order to better reproduce the measured response, the arch stiffness should be increased by about 2% ($\phi_{Ec} = 1.02$) of the value predicted by the structural parameter investigation (that is, $\phi_{Ecbase} = \phi_{Ec} \cdot \phi_{Ecbase0}$ and $\phi_{Eccrown} = \phi_{Ec} \cdot \phi_{Eccrown0}$). Thus the stiffness of the arch base should be increased by approximately 6.1% and the stiffness of the arch crown should be increased by approximately 19.0%. FE model updating procedures will use the values $\phi_{Ecbase} = 1.061$ and $\phi_{Eccrown} = 1.190$ for the values of the normalized updating parameters for the stiffness of the arch base and crown respectively.

6.3.2 Carriageway steel elastic modulus

Although the elastic modulus of steel has a considerably low coefficient of variation (0.03) compared with concrete (0.15), the objective functions of the response residual were evaluated for a feasible range of normalised steel stiffness. Of particular interest were the changes to the dynamic response and to the calculated hanger loads when the elastic modulus of steel was modified. The frequency, displacement and hanger loads are particularly sensitive to the elastic modulus of the steel and therefore govern the behaviour of the objective functions, as is evident in Figure 6.3 and Figure 6.4.

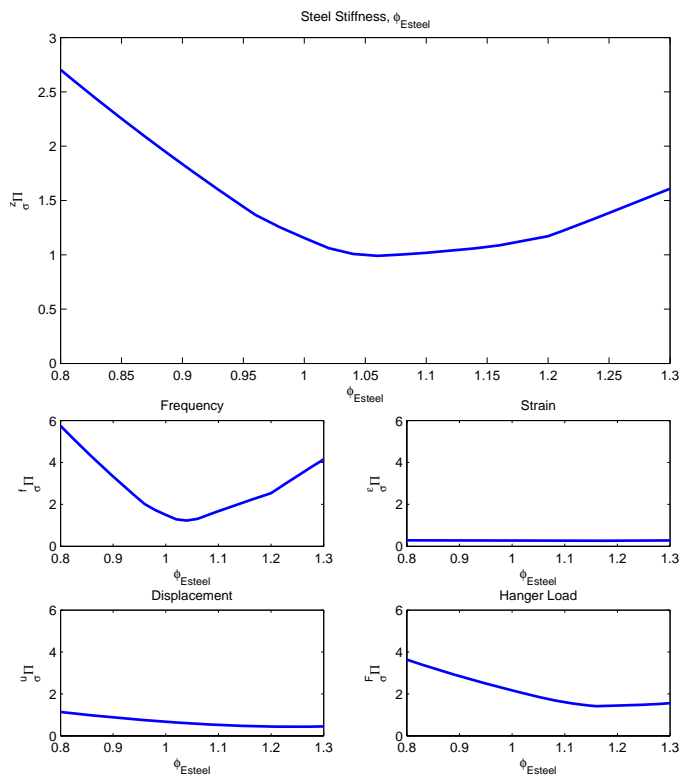


Figure 6.3 Standard deviation objective function plotted as a function of normalized elastic modulus of steel for the carriageway.

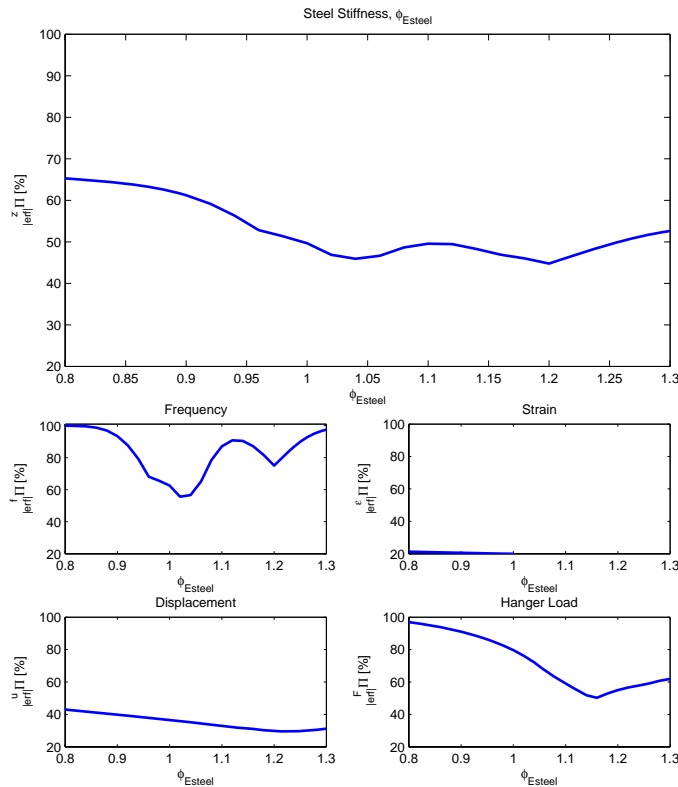


Figure 6.4 Uncertainty objective function plotted as a function of normalized elastic modulus of steel for the carriageway.

According to Figure 6.3, the mean deviation of the residual with respect to the standard deviation of the measured response is minimized at approximately $\phi_{Esteel} = 1.05$ for the frequency contribution to the objective function and $\phi_{Esteel} = 1.18$ for the hanger loads. Furthermore, the slope of the frequency portion of the objective function changes at about $\phi_{Esteel} = 1.18$. The strain measurements are not sensitive to the elastic modulus of the steel in the carriageway.

Two local minima are evident in the uncertainty plot, Figure 6.4, one at approximately $\phi_{Esteel} = 1.05$ and the other at approximately $\phi_{Esteel} = 1.16$. The uncertainty of the frequency measurements is minimized at $\phi_{Esteel} = 1.05$ while the uncertainty of the hanger loads is minimized at $\phi_{Esteel} = 1.16$, thus the optimal normalized updating parameter is unclear from the plot of the superposition of the mean uncertainty of each type of measurement.

It is very important for an engineer to scrutinize the results of a parameter optimization study to ensure the feasibility of the outcome. In this case, the frequency measurements were statistically more reliable due to low measurement noise than the hanger loads. Also, the FE model was considered to be “very good” at modelling dynamic response and only “good” at modelling static response, such as hanger loads. The magnitude of the frequency contribution to the standard deviation objective function, Figure 6.3, suggests that the local minimum that optimizes the frequency response is more important than that for the hanger loads. Though the uncertainty objective function considers the standard deviation of each measured response

parameter, it is not useful when comparing response parameters with different units (such as frequency [Hz] and hanger loads [kN]). The uncertainty objective function is most useful when evaluating the validity of the FE model for each measured response parameter. The uncertainty of the response is a normalized value from 0 to 1 (0 to 100%), thus it is intrinsically unweighted. If the uncertainty objective function is to be used for updating, the normalized value should be weighted in order to reflect the confidence in each measured parameter.

The aberrations in the objective functions at approximately $\phi_{Steel} = 1.16$ suggest interesting structural behaviour at an increase in carriageway stiffness. This is believed to be due to the stiffness contribution of the railings to the carriageway. Although the railings are securely fastened (using bolts) to the carriageway in order to prevent catastrophe in the case of vehicle accidents, they are not designed to carry structural load. Nonetheless, when assessing the actual behaviour of the bridge for FE model validation, the contribution of the railing certainly contributes to the response. The additional stiffness provided by the railing reduces the hanger loads in the actual bridge, thus the FE model overestimates the hanger loads. Though the mass of the railings is included in the mass elements that represent the asphalt layer, utilities and railings, the stiffness contribution to the carriageway is not. The railings increase the stiffness and bending inertia of the carriageway, which increases the eigenfrequency of the carriageway and decreases the hanger loads. Additional beam elements could be included in order to model the railings, but should not be considered when evaluating the bridge performance with regard to the SLS and ULS design criteria. Instead of adding beam elements to the model to represent the railing, the sectional properties of the longitudinal beam elements of the carriageway were modified. All factors that affect the actual bridge performance must be considered when evaluating the validity of an FE model, but the contribution of non-structural members to the structural response should not be included when verifying design criteria.



Figure 6.5 Although the railing does not contribute to the structural integrity of the bridge, it contributes to the stiffness of the carriageway and therefore affects the measured response.

6.3.3 Asphalt mass

In order to calibrate the masses of the discrete mass elements from Chapter 5.1.2, the value of a normalized updating parameter, ϕ_{Masph} , was iterated within a reasonable range. The response residual was evaluated and the value that minimized the standard deviation objective function was chosen for FE model updating. Only the frequency response contributed to the objective function, the strain, displacement and hanger load responses were unchanged by the addition of mass elements to the FE model.

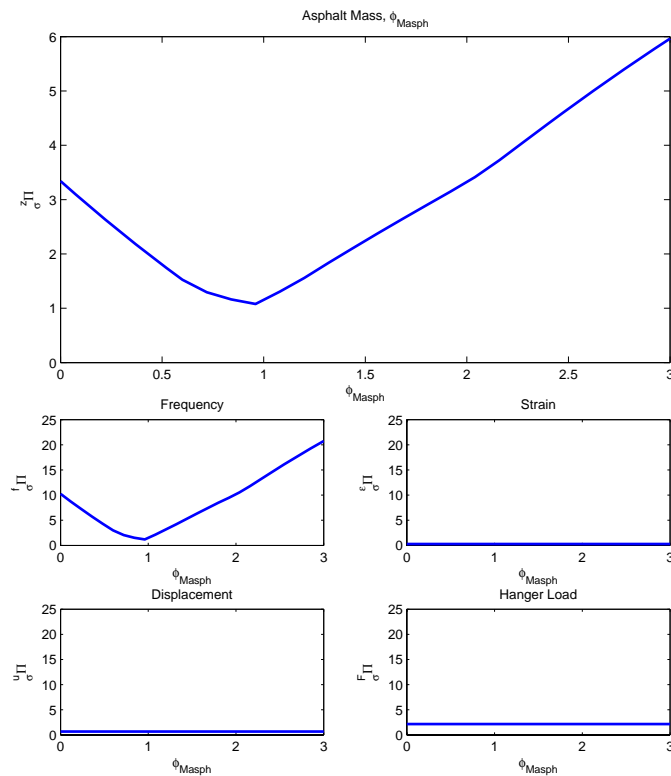


Figure 6.6 Standard deviation objective function plotted as a function of normalized mass of the non-structural members of the carriageway.

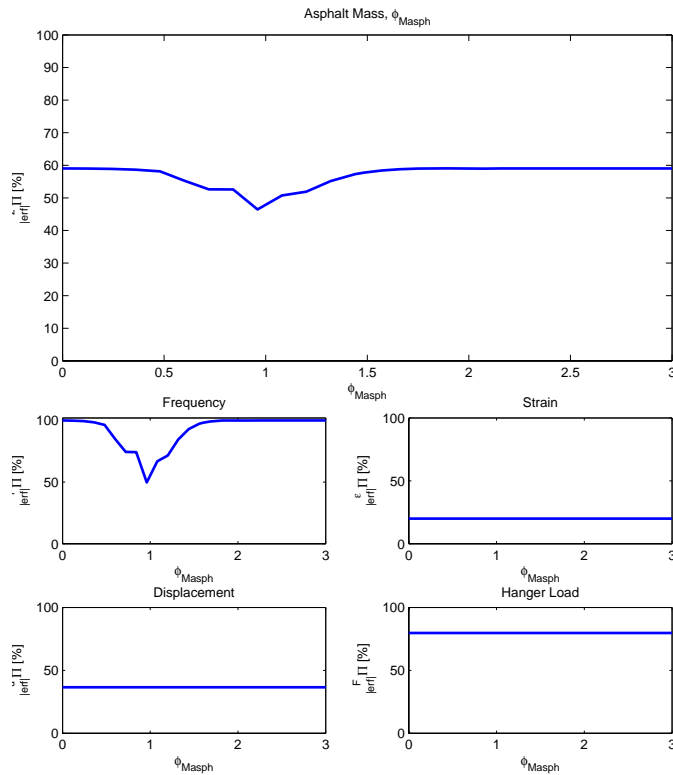


Figure 6.7 Uncertainty objective function plotted as a function of normalized mass of the non-structural members of the carriageway.

According to Figure 6.6 and Figure 6.7, the residual of the response is minimized at approximately $\phi_{Masph} = 0.95$. Thus it is clear that the estimation of the mass of the non-structural members during the structural parameter study was quite accurate. During construction, quality control standards ensure that the thickness of the asphalt layer will not significantly vary from one section of the carriageway to another. For this study, the asphalt thickness was considered to be perfectly consistent and the mass of the asphalt layer, utilities and railings was equally distributed across the length of the carriageway. In reality, some variance is to be expected, but is not likely to significantly affect the structural response of the bridge. The normalized updating parameter for the non-structural member mass for the starting values used in automated FE model updating was therefore the value that best minimized the response objective functions, $\phi_{Masph} = 0.95$.

6.3.4 Asphalt stiffness

Due to visco-elastic rate-dependent material behaviour, the contribution of the asphalt layer to the bridge was difficult to model. In order to simplify analysis, the sectional properties of the carriageway were modified for frequency analysis. The stiffness of asphalt concrete is related to the forcing frequency, thus for very low frequency loading (as is the case for static load testing), the asphalt stiffness is essentially zero. So, the asphalt layer was considered to have no affect on the response due to static loading. Thus, only the frequency response was affected by the stiffness of the asphalt layer.

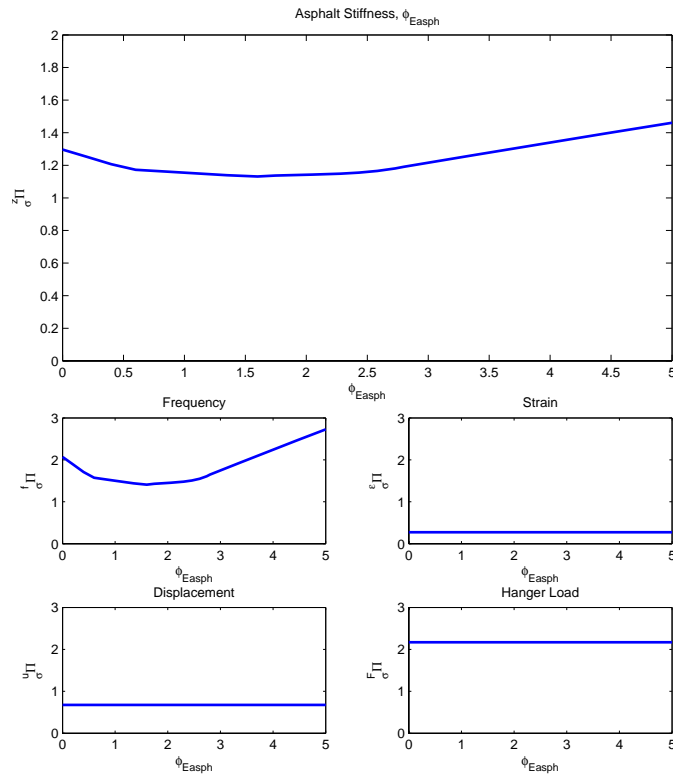


Figure 6.8 Standard deviation objective function plotted as a function of normalized elastic modulus of the asphalt layer of the carriageway deck.

According to the results of the parameter sensitivity study for the elastic modulus of the asphalt layer of the carriageway deck, the frequency response residual was minimized at approximately $\phi_{Easph} = 1.6$. The asphalt stiffness did not contribute the static response due to the low loading frequency, thus the strains, displacements and hanger loads were not sensitive to the asphalt stiffness. A constitutive model for asphalt concrete was used to predict the stiffness of the asphalt layer at the mean estimated asphalt temperature during frequency measurements. The asphalt stiffness determined during the structural parameter study, 4.9 GPa, was conservative according to the parameter response study and an increase of about 60% to 7.8 GPa minimizes the objective function by optimizing the frequency response. The asphalt stiffness of 7.8 GPa was not measured directly and should not be used for other analyses. It is a sort of calculation artefact only used for modelling vibrations on the order of 1 Hz at a temperature of approximately 22.7 °C. Other parameters which are not directly considered in the FE model affect the frequency response of the bridge, including the stiffness contribution of the railing to the carriageway during vibration measurements. If the non-structural members are modelled directly, the actual asphalt stiffness may be calculated more precisely using the frequency response but such analysis is beyond the scope of this study.

6.3.5 Arch-carriageway connection stiffness

In order to determine whether the actual behaviour of the connection permits rotation during normal loading conditions (SLS), the rotational stiffness of the connection was simulated across a wide range of values. The initial estimate of the rotational stiffness (with a corresponding normalized updating parameter value, $\phi_{Ka-carr} = 1$) was very conservative, as is described in Chapter 5.1.4. Very low rotational stiffness ($\phi_{Ka-carr} = 10^{-10}$) was used to model a hinge while a very high rotational stiffness ($\phi_{Ka-carr} = 10^{+10}$) was used to model full interaction between the arch and carriageway during frequency measurements and static load testing.

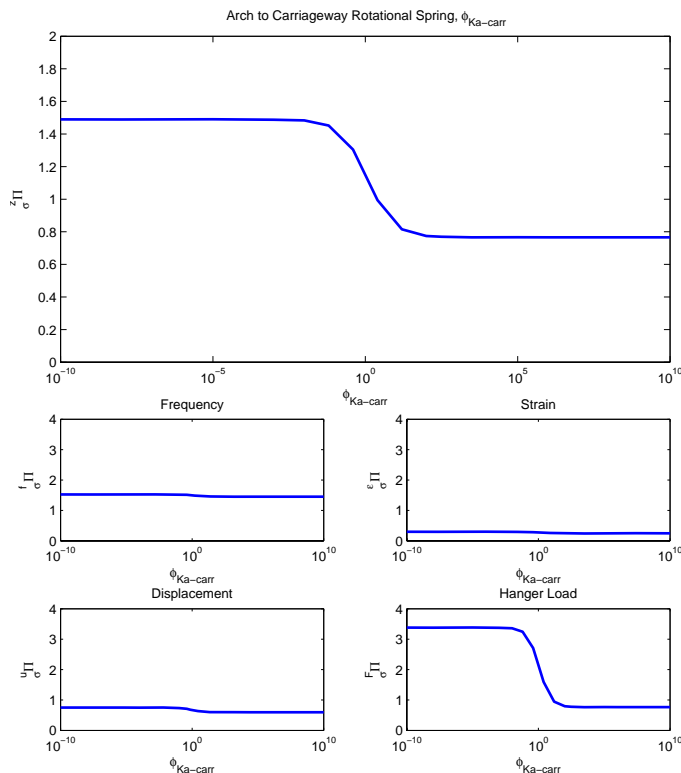


Figure 6.9 Standard deviation objective function plotted as a function of normalized rotational spring stiffness for the arch to carriageway connection (logarithmic scale for x-axis).

According to the parameter response study for the arch to carriageway connection, the objective function of the response residual is minimized for very high rotational spring stiffness. It is clear from Figure 6.9 that the frequency, strains and displacements responses are not as sensitive to the rotational stiffness of the arch to carriageway connection as are the hanger loads. Thus the hanger loads are the most sensitive to the rotational stiffness of the connection. At a rotational stiffness on the order of $K_{a-carr} = 5 \times 10^{11} \text{ N/rad}$ ($\phi_{Ka-carr} = 500$), which is approximately the rotational stiffness of a connection with full-interaction, the objective function of the response residual is minimized. The normal force due to the tendons should further increase the rotational stiffness, thus the actual rotational stiffness is suspected to be

above $\phi_{Ka-carr} = 500$. There is no change in the response for rotational stiffness for $K_{a-carr} \geq 5 \times 10^{11} \text{ N/rad}$, which is not surprising since the connection may be considered to be fully constrained at that point. Furthermore, the results of this study verify the design assumption that the connection was fully constrained. Further SLS analysis may be conducted using high-stiffness dummy elements to model the connection or using rotational springs with $K_{a-carr} \geq 5 \times 10^{11} \text{ N/rad}$, but ULS models should not rely on such elements to model the connection.

Due to the updating parameter insensitivity for $\phi_{Ka-carr} \geq 500$, the arch to carriageway connection was not used for automated FE model updating. Instead, the value was set to $\phi_{Ka-carr} = 500$.

6.3.6 Arch foundation stiffness

During design, the arch foundation was modelled as fixed for all DOF except for the rotation around the bridge transverse axis, where the rotational stiffness was modelled using a linear spring. The stiffness of the springs for the Swedish and Norwegian arch foundations were calculated by Bilfinger Berger (2002, 2003). Different stiffness values were used during arch launching and for the permanent arch structure. For this study, only the rotational stiffness for the permanent structure were considered.

It was of research interest to see if more accurate values for the rotational stiffness of the arch foundations could be extrapolated by comparing the FE model response with a range of stiffness values to the measured response of the bridge for frequencies and during load testing. From the plot of the error objective function of the response residual, Figure 6.10, it is clear that that the response is not sensitive to the rotational stiffness of the arch foundation about the transverse axis. The error remains relatively constant when different values are used for the normalized rotational spring stiffness of the arch foundation updating parameter, ϕ_{Ka-f} . Because the FE response was not sensitive to the arch foundation rotational stiffness, ϕ_{Ka-f} was not updated in this study.

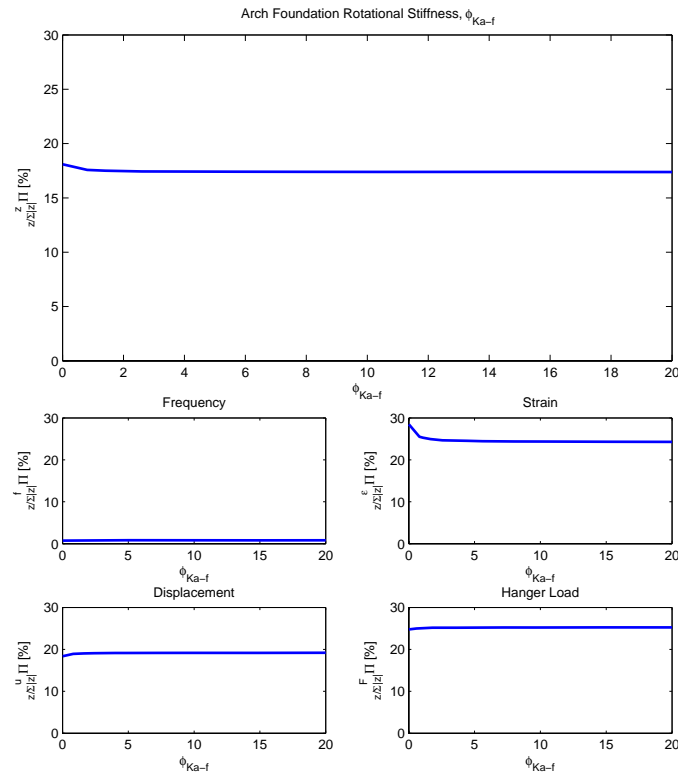


Figure 6.10 Error objective function plotted as a function of normalized rotational spring stiffness for the arch foundation.

6.3.7 Bearing static friction

Accurate modelling of boundary conditions is among the most difficult and important tasks for FE modelling. In many cases, free, pinned or fully-fixed boundary conditions are used for the FE model to simulate the actual boundary conditions. Such assumptions always use simplified models of the real structural behaviour to facilitate calculations. In many cases, simplified boundary conditions are capable of accurate modelling the structural behaviour, but the simplifications should be properly motivated with engineering considerations.

In the case at hand, the use of simplified boundary conditions was not possible. The results of the structural parameter study for the bearings in Chapter 5.2.2 and Appendix E demonstrated that the static friction of the bearings must be accounted for by the FE model in order to ensure accurate FE modelling. Non-linear joint elements were used to simulate static friction at the bearings. The constitutive models used for the non-linear spring elements are presented in Figure 5.22. The normalized updating parameter adjusted the magnitude of the static friction threshold (plateau in Figure 5.22). Values from a very low static friction coefficient (thus simulating a frictionless bearing, $\phi_{K_{bear}} = 0.001$, $\mu_s \approx 0$) to a very high static friction coefficient ($\phi_{K_{bear}} = 6$, $\mu_s \approx 0.20$) were simulated and the residual of the response was evaluated using the error objective function.

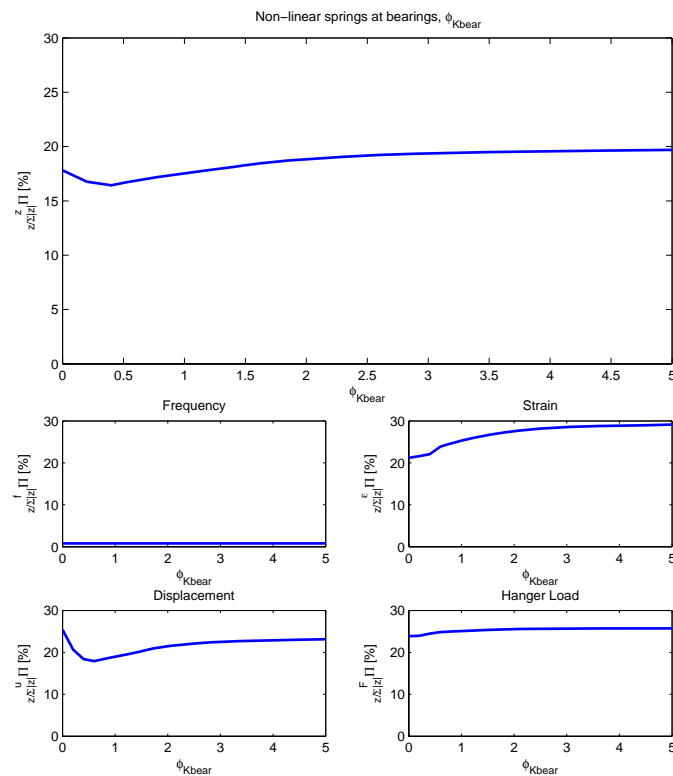


Figure 6.11 Error objective function plotted as a function of normalized bearing static friction threshold.

According to Figure 6.11, the initial estimation of the bearing static friction (estimated using the bearing kinetic friction provided by the bearing manufacturer) was too high. The displacement response residual was minimized at approximately $\phi_{Kbear} = 0.5$, but the hanger load and strain responses were minimized at $\phi_{Kbear} \approx 0$. The results were contradictory, thus the statistical weight of each type of measurement was considered when choosing an initial value for the normalized bearing static friction threshold for automatic FE model updating. Thus, the value of $\phi_{Kbear} = 0.001$ was chosen as an initial estimation for the optimization procedure. Due to the bearing assumptions from Appendix E, the bearings were tied for the frequency analysis, thus the non-linear joint elements were not used when modelling the eigenfrequencies. It may be seen from Figure 6.11 that the frequency response is not sensitive the static friction threshold modelled using non-linear joint elements.

6.3.8 Carriageway longitudinal stiffeners

During the design of the bridge, quality control ensured accurate carriageway section dimensions. In order to extrapolate the dimensions of the carriageway longitudinal stiffeners that optimize the response, the carriageway sectional parameters (sectional area, longitudinal bending inertia, transversal bending inertia and torsional inertia) were changed to reflect changes in the dimensions of the stiffeners. This analysis also provided verification that the correct sectional parameters were used for the initial model of the bridge.

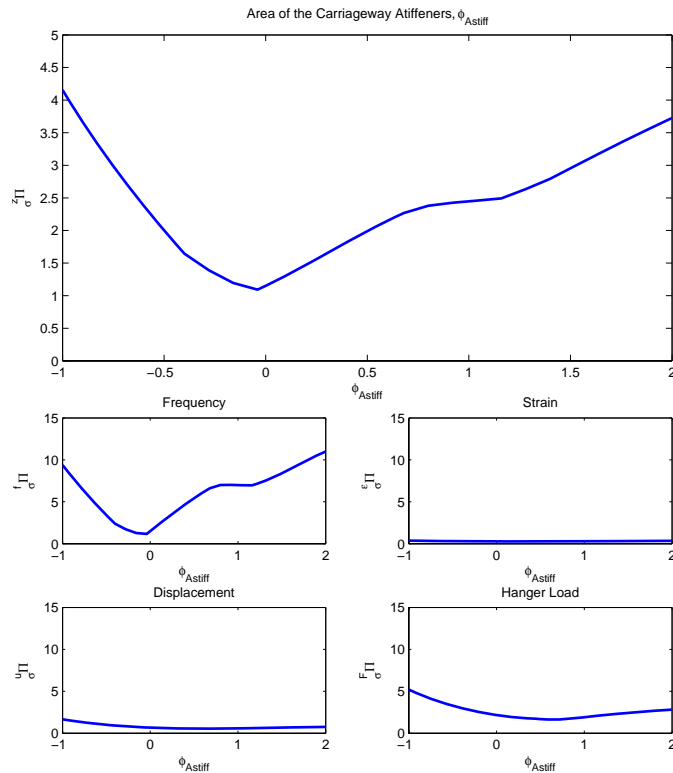


Figure 6.12 Standard deviation objective function plotted as a function of normalized increase of carriageway longitudinal stiffener sectional area.

From Figure 6.12, it is clear that the total response is optimized at $\phi_{Astiff} = 0$, which represents no change to the carriageway sectional parameters. The frequency response governs the standard deviation objective function (which is a function of the response residual and the normalized increase to the stiffener area) and is optimized at $\phi_{Astiff} = 0$. The strain response is not sensitive to the stiffener area. The displacement response is optimized at $\phi_{Astiff} \approx 0.5$ while the hanger load response is optimized at $\phi_{Astiff} \approx 0.7$.

In order to understand the discrepancy between the optimal results for the frequency, displacement and hanger load responses, the stiffness contribution of the railing must be considered. As was discussed in Chapter 6.3.2, the contribution of the railing to the carriageway is difficult to model. The initial model did not consider the stiffness contribution to the carriageway provided by the railing, which is a usual assumption during design but does not necessarily reflect the actual structural behaviour of the bridge. Thus the improved response at $\phi_{Astiff} \approx 0.5-1$ for the frequency, displacement and hanger loads is likely due to the railing. Further manual model refinement by including beam elements for the railing is suggested, but is beyond the scope of this study. The railing beam elements should only be used in the FE model used during model calibration and should be removed for verification of SLS and ULS design criteria as the railing is not designed to provide structural load-carrying capacity. The normalized updating parameter for the increase of the carriageway longitudinal stiffener sectional area, ϕ_{Astiff} , was included for automated FE model updating, but the

results should be treated very carefully in future analysis. An initial value, $\phi_{Astiff} = 0$, was chosen based on the results of the parameter sensitivity study and engineering judgement.

6.3.9 Parameter sensitivity study results

The results of the parameter sensitivity study were analysed and a starting guess for the automated FE model updating parameter vector, manually tuned updating parameter vector, was chosen. The manually tuned updating parameter vector was the result of the manual model refinement and represents a best guess input vector before automated optimization. From this point, the utilization of automated non-linear optimization techniques is required to minimize the objective function and thus determine an optimal FE model.

Table 6.2 Tabulated updating parameter results.

		Updating parameter		Initial value (Model 0)	Structural parameter study (Chapter 5.1)		Parameter response study (Chapter 5.3)	
		Φ	θ	θ	$\Phi_{0,initial}$	$\theta_{0,initial}$	Φ_0	θ_0
Concrete elastic modulus, E_c	Arch base	ϕ_1	θ_1	37.5 GPa	1.041	39.0 GPa	1.062	39.8 GPa
	Arch crown			37.5 GPa	1.167	43.8 GPa	1.190	44.6 GPa
Carriageway steel elastic modulus, E_{steel}		ϕ_2	θ_2	210 GPa	1	220.5 GPa	1	210 GPa
Asphalt mass, M_{asph}	Central beam	ϕ_3	θ_3	---	1	4131 kg	0.95	3924 kg
	Outer beam			---		2065 kg		1962 kg
Asphalt elastic modulus, E_{asph}		ϕ_4	θ_4	---	1	4.9 GPa	1.6	7.8 GPa
Arch-carriageway rotational connection stiffness, K_{a-carr}		ϕ_5	θ_5	---	1	10^{10} N/rad	500	5.0×10^{12} N/rad
Arch foundation rotational connection stiffness, K_{a-f}	Sweden	ϕ_6	θ_6	1	1	1.5×10^{11} N/rad	1	1.5×10^{11} N/rad
	Norway					1.5×10^{11} N/rad		1.5×10^{11} N/rad
Bearing static friction, F_s	Piers	ϕ_7	θ_7	---	1	300 kN	0.2	60 kN
	Abutments			---		80 kN		16 kN
Carriageway longitudinal stiffener area, A_{stiff}		ϕ_8	θ_8	---	0	0 m ²	0	0 m ²

6.4 Revised FE model

6.4.1 Eigenfrequencies

For ambient vibrations caused by low-amplitude loading, the static friction threshold in the bearings is greater than the reaction force at the bearing, thus the connection at the bearings may be considered as fully restrained. Large amplitude loading (from wind, heavy traffic or temperature change) is sufficient to overcome the static friction in some or all of the bearings, but the reaction forces at the bearings must be evaluated for all loading configurations.

The time-variant magnitude of loading due to wind and normal traffic for ambient vibration acceleration measurements is unknown; thus there is insufficient data to determine whether the static friction threshold for translation and rotation in the bearings was overcome during measurements. Eigenmode 2 and higher-order eigenmodes were determined to depend on boundary conditions and connection restraints, thus the frequency associated with a particular eigenmode changes if the boundary conditions or connection restraints are changed. The frequency shift due to the change in boundary conditions is evident by comparing eigenmode 2 for Model 0 and Model 1. Although the mode shape does not considerably change, a large frequency shift is present due to the restraint at the bearings.

One must exercise care when comparing eigenmodes for systems with different boundary conditions and connection restraints because the imposition of such restraints changes the dynamic space spanned by the DOF in the eigenvalue equation, equation (2.19). By changing the boundary conditions and the restraints, the entire system changes and the shape of the eigenmodes may change as well. This effect is quite different than introducing a scalar multiplier to the stiffness or mass matrices of the system, which will change the eigenvalue without changing eigenmode shape. Nonetheless, the comparison of eigenmodes with nearly identical shapes for different boundary conditions and restraint cases is reasonable for the eigenmodes considered in this study since the analyzed shapes are quite similar and correspond well with accelerometer locations.

Close examination of the stabilization diagrams presented in Ülker-Kaustell and Karoumi (2006) reveals higher relative uncertainty in the higher order experimentally measured eigenmodes, see Figure 4.4. With unknown loading configuration and magnitude for ambient vibration testing, the forces at the bearings likely exceeded the static friction in some bearings during some time intervals during testing. In such a case, the restraint condition at the bearings is a function of time variant load configuration and magnitude. Changing the restraint condition of the system as a function of time changes the dynamic properties of the system; thus changing the eigenfrequencies during testing. If such a speculation is correct, eigenmodes of different load-dependent systems were measured during ambient vibration testing and the unique set of eigenmodes for each system cannot be distinguished. Therefore it is possible that eigenfrequencies corresponding to those from measurable modes in Model 0 and Model 1 exist in the ambient vibration data.

After thorough investigation of the effect of static friction in the bearings, the fully constrained bearing condition was chosen to model frequency response for FEM updating. This model had exactly one eigenfrequency in close proximity to each

eigenfrequency determined by experimental measurements for modes 1 to 4, thus assuring reasonable correlation between eigenfrequencies from experimental measurements and from FEA. Unfortunately no mode shape data was available. If mode shapes are considered, the MAC matrix may be constructed and eigenfrequencies from higher order eigenmodes may be included in future FE model updating. The eigenfrequency data for the FE model with revised bearing constraints is presented in Table 6.3 and Figure 6.14.

Table 6.3 Eigenfrequencies 1-4 from experimental measurements vs. FE Model 0 and FE Model 7.

Eigenfrequency	Experimentally Measured	FE Model 0 (Initial)	FE Model 7 (revised)	Units
Mode 1: f_1	0.4249	0.4083	0.4253	Hz
Mode 2: f_2	0.8459	0.4598	0.8531	Hz
Mode 3: f_3	0.9402	0.9559	0.9366	Hz
Mode 4: f_4	0.9988	1.0192	0.9871	Hz

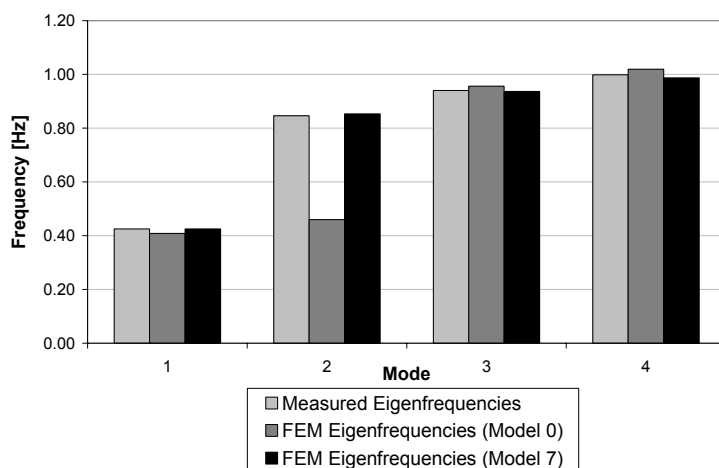


Figure 6.13 Eigenfrequency comparison: modes 1-4 from experimental measurements vs. FE Model 0 and FE Model 7.

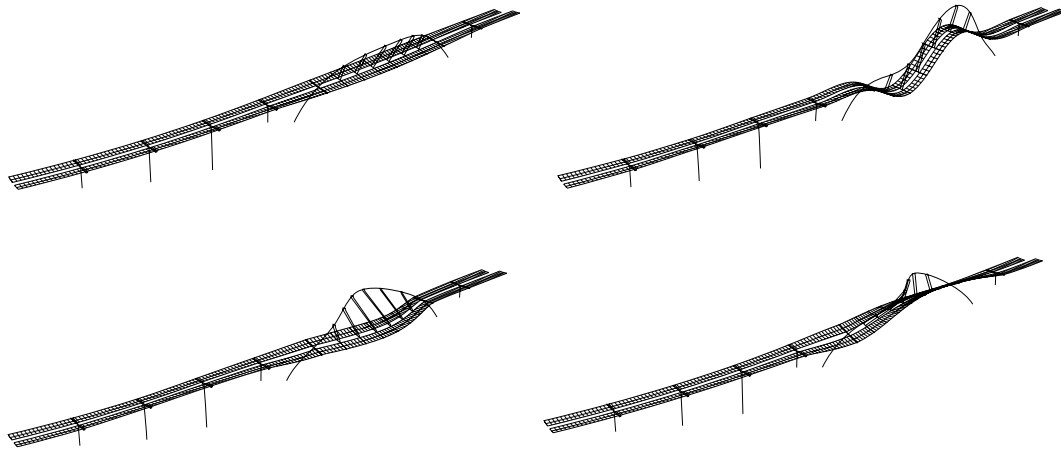


Figure 6.14 Eigenmode shapes 1-4 for FE model updating.

Increased interaction between the bridge superstructure and the pier is caused by the static friction from the increased normal force in the bearing due to prestressing. Since eigenfrequency measurements were obtained from low amplitude ambient vibrations, static friction was probably not overcome by the small excitations of normal traffic and wind. Hence, the eigenfrequencies obtained from the stabilization diagrams corresponded with the FE model with tied bearings for frequency analysis. Though this result changes the FE modelled bridge behaviour in the service state, the structural integrity is believed to remain unchanged because the static friction in the bearing will certainly be overcome in the ultimate limit state (ULS), thus leaving the ULS design load-carrying mechanism valid.

6.4.2 Strains

The strains have been measured in five different sections; the one at the foundation on the Swedish side is referred to as S1, the one in the connection between the arch and the carriageway is referred to as S6, at the midpoint of the arch is called S25, at the connection between the arch and the carriageway on the Norwegian side, N6, and at the arch foundation on the Norwegian side, N1. The strains on the Norwegian side follow same pattern as on the Swedish side, see Figure G.9 to Figure G.12. The agreement between the FEA strains and the experimentally measured strains improved when non-linear springs were introduced to the model.

Systematic error is suspected in the strain gauge measurements near the arch to carriageway connections (at sections S6 and N6), near the arch foundations (S1 and N1) and in the top strain gauge at the midpoint of the arch (section S25). Although linear interpolation was used to remove temperature effects, a trend that may have been caused by temperature was still evident for some of the strain measurements. A correlation between the strain measurements during the unloaded time periods and the temperature measurements in each arch section could be used to obtain a more accurate strain profile due to temperature effects, but such analysis is beyond the scope of this project.

A discontinuous stress field is suspected near the arch to carriageway connections, at the arch foundations and at the access hatch at the top of the arch. According to Engström (2006), the stress field in concrete structures is discontinuous near boundary conditions and points of load application. According to elastic field theory, the stress field in an elastic body requires a distance that is determined by the structure geometry to become fully-developed. Because arch sections S1, S6, N6 and N25 are located near boundaries and points of load application, it is likely that the strain gauges are located in discontinuous stress fields. The FE model uses beam elements with a linear elastic material constitutive relation for the concrete arch, thus assuming idealized structural behaviour. Boundary conditions and applied loads act on individual nodes in the FE model, thus the stress field is idealized and is only suitable for modelling the arch strain in arch segments that are located at a sufficient distance from any point loads, connections or boundaries. Arch segment S25 is located midway between hangers 3 and 4, thus the strain measurements from the bottom, east and west strain gauges were less prone to systematic error due to a discontinuous stress field. An access hatch is located at the top of the arch, thus the stress field is discontinuous in the top section of arch segment S25 and the strain measurement was therefore prone to systematic error.

With the measurement data from the static load cases and the FE model at hand, lingering systematic error caused by remaining temperature effects, possible sensor bias, other environmental factors and modelling limitations likely exists. All attempts were made within the scope of this project to remove systematic error, but the removal of all systematic error was not possible. Nonetheless, the agreement between the experimentally measured strains and the FEA strains improved through systematic manual model refinement.

6.4.3 Displacements

Displacement was measured at many points during the static load tests. The agreement between the FE modelled displacements and the measured displacements improved with manual FE model refinements. Primarily, the increased accuracy was due to the non-linear springs at the bearings. The mean deviation of the FEM displacements is tabulated in Table G.3 and the mean relative error of the FEM displacements is tabulated in Table G.4 .

6.4.4 Hanger loads

Hanger loads in Hangers 1E and 1W were measured continuously during the static load tests. The manual model refinements slightly decreased the accuracy of the FE model for hanger loads, which is evident in Table G.3 and Table G.4 in Appendix G. This may be due to the introduction of the spring at the arch to carriageway connection. From the parameter sensitivity analysis, the connection was determined to be rigid. Therefore the springs introduce modelling error, though the modelling error is minimized for sufficiently high rotational spring stiffness. In Appendix F.4, the discrepancy between the measured and FEM hanger loads increased due to the addition of springs in Model 6.

7 FE Model Updating of the New Svinesund Bridge

7.1 Calculations

All calculations involved for FE model updating of the New Svinesund Bridge were carried out on the computing cluster, "Ada", which consists of 252 nodes with 4 xeon 5160 Woodcrest 3 GHz dual, dual core processors with 4 GB RAM each. Optimization subroutines for FE model updating were written and compiled in MATLAB version 7.4 using the MATLAB optimization toolbox. Input files were used for FE model definition and FEA calculations were completed by ABAQUS version 6.5-6. The FORTRAN subroutine for reading the binary output from ABAQUS was compiled on an INTEL compiler, version 9.1. For more information regarding the computing cluster, refer to <http://www.unicc.chalmers.se>.

7.2 Results

Many possible objective functions were proposed in Chapter 6.2 to weigh the frequency, strain, displacement and hanger load response. Each objective function has certain advantages and certain disadvantages for FE model updating, though the standard deviation and error objective functions are perhaps the easiest to understand. If only one type of response is considered for FE model updating, the updating parameters will be optimized with regard to that response. For each type of response, different objective functions were used for optimization in order to determine which analysis would produce the best model. The results are summarized in sections below.

7.2.1 Frequency optimization

Dynamic FE model updating with eigenfrequencies is the most common type of FE model updating in practice. For the New Svinesund bridge, the global stiffness and global mass matrices of the FE model were updated using the sensitivity approach in order to best reproduce the measured eigenfrequencies. The standard deviations of the measurements were considered using the standard deviation objective function. The standard deviation objective function of the frequency was formulated using the first four eigenfrequencies.

$${}_{\sigma}^f \Pi = \frac{\sum_{i=1}^4 \sqrt{\frac{(f_{mi} - f_i)^2}{\sigma_{f_i}^2}}}{4} \quad (7.1)$$

The FE model was optimized to reproduce the measured eigenfrequencies,

$$\min_{\Phi} {}_{\sigma}^f \Pi \quad (7.2)$$

The eigenfrequencies were sensitive to some of the uncertain structural parameters, thus the updating parameters used included the arch base stiffness, arch crown stiffness, carriageway steel stiffness, non-structural member mass, asphalt stiffness and carriageway stiffener area. In case of unconstrained minimization presented above, the set of updating parameters, Φ , that best reproduced the experimentally measured response were the solution to equation (7.2). The statistical confidence in the updating parameters was accounted for using regularization.

$$\Phi_{\sigma\Pi} = \frac{\sum_{i=1}^6 \sqrt{\frac{(\phi_{0i} - \phi_i)^2}{\sigma_{\phi_i}^2}}}{6} \quad (7.3)$$

By introducing regularization to the standard deviation objective function, the statistical confidence in the calculations from Chapter 5 and the parameter sensitivity study from Chapter 6 were included.

$$\sigma_{\Pi} = \frac{f_{\sigma\Pi} + \Phi_{\sigma\Pi}}{2} \quad (7.4)$$

The updated FE model was optimized to reproduce the response while minimizing the updating parameter change from the “best guess” determined by calculations and the parameter sensitivity study.

$$\min_{\Phi} \sigma_{\Pi} \quad (7.5)$$

In both cases, equation (7.2) and equation (7.5), the first four eigenfrequencies of the FE model were improved with respect to the measured frequencies. The FE model optimized for response reproduced the experimentally measured response slightly better than the optimized model that included regularization, though the updating parameters were less realistic.

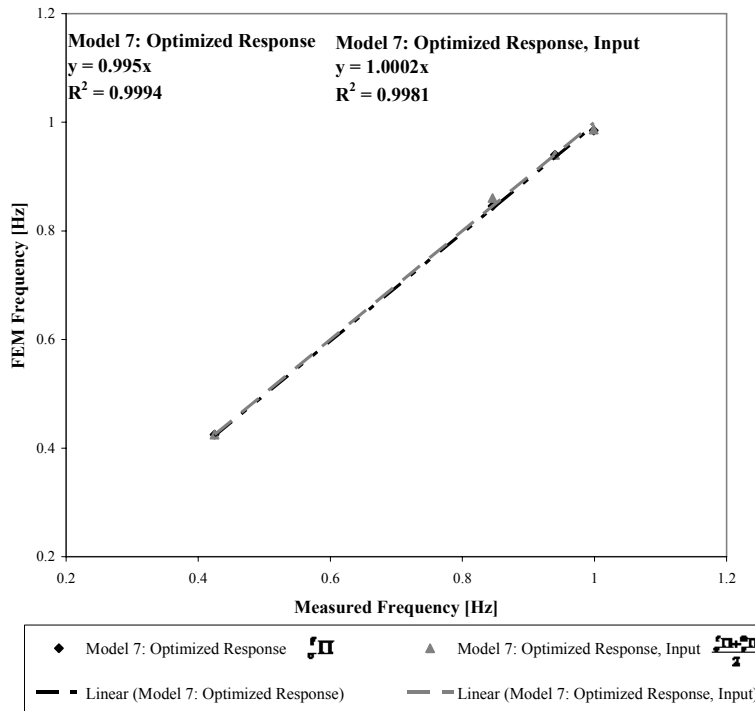


Figure 7.1 Optimized eigenfrequencies with and without regularization.

According to the FE model optimized for response, the stiffness of the arch base was increased from 106% to 121% while the stiffness of the arch crown was reduced from 119% to 100%. The mass of the non-structural members changed from 95% (determined in the parameter sensitivity study) to 90%. The asphalt stiffness and carriageway stiffener area were virtually unchanged but the carriageway steel stiffness was reduced to 96%.

For the FE model optimized for response with regularization of the updating parameters, the stiffness of the arch base remained virtually unchanged at 106% while the stiffness of the arch crown was reduced from 119% to 114% of the original value. The mass of the non-structural members, the asphalt stiffness, carriageway stiffener area and carriageway steel elastic modulus remained virtually unchanged from the values obtained using manual model refinement.

In order to determine if the solution to equation (7.2) was unique, the starting guess for the updating parameter vector was changed and the model was optimized with respect to response. Two cases were used to test for the existence of local minima, $\hat{\Phi}_0 = 0.5\Phi_0$ and $\hat{\Phi}_0 = 2\Phi_0$. In both cases, the optimization converged after about 150 objective function evaluations using the Nelder-Mead Simplex non-linear optimization algorithm, which corresponded to about 40 iterations.

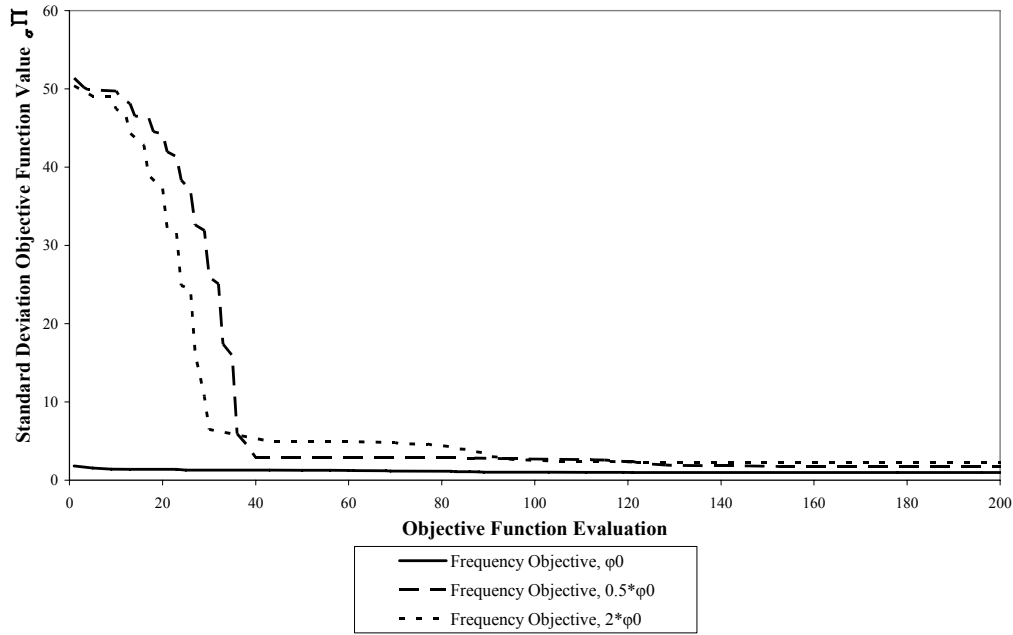


Figure 7.2 Convergence of frequency optimization to non-unique results for different updating parameter initial starting guesses.

The converged results were non-unique for $\hat{\Phi}_0 = 0.5\Phi_0$ and $\hat{\Phi}_0 = 2\Phi_0$, demonstrating the existence of local minima for the standard deviation frequency objective function in the updating parameter space. From Figure 7.2, it may be seen that although the minimization converged for $\hat{\Phi}_0 = 0.5\Phi_0$ and $\hat{\Phi}_0 = 2\Phi_0$, the converged solutions were not even as good as the starting guess obtained from manual refinement.

Due to the existence of local minima, a good starting value for the updating parameter vector, Φ_0 , was essential for optimization. Manual refinement using engineering calculations and a parameter sensitivity study were used to obtain an initial updating parameter vector, Φ_0 , for non-linear optimization. If only the response was considered, the optimized model was unrealistic, but the use of regularization of the updating parameters considering the “best guess” determined from manual model refinement produced an optimized FE model with more realistic updating parameters.

7.2.2 Strain optimization

By comparing the calculated strain simulated using the manually refined FE model with the measured strains from the load tests, the FE model was optimized to reduce the mean relative error expressed using the error objective function.

$$\frac{\epsilon \Pi}{z/\Sigma|z_m|} = \frac{\sum_{i=1}^{95} |\epsilon_{mi} - \epsilon_i|}{\sum_{i=1}^{95} |\epsilon_{mi}|} \quad (7.6)$$

The FE modelled strain response was only sensitive to the arch base stiffness, arch crown stiffness, pier bearing static friction threshold and abutment bearing static friction threshold. The updating parameter vector which best reduced the mean relative error for strain objective function was obtained using the Nelder-Mead Simplex non-linear optimization algorithm.

$$\min_{\Phi} \frac{\sum |z_m|}{\sum |z_m|} \epsilon \Pi \quad (7.7)$$

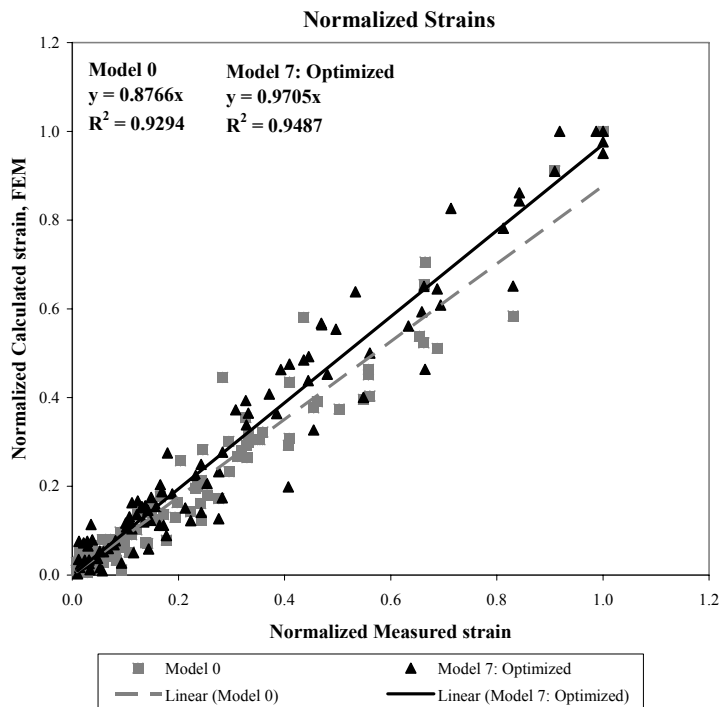


Figure 7.3 Comparison of optimized FE model strain response and initial FE model strain response with measured strain response.

Although the mean relative error for strain was reduced by approximately 5% for Model 7 using optimization, the agreement between the optimized model strains and the experimentally measured strains was not significantly better than for the initial FE model, Model 0. Additionally, the variation of the concrete stiffness along the arch profile optimized for strains was not realistic. For Model 7 optimized for strain, the stiffness of the arch base was reduced to 77% while the stiffness of the arch crown was increased to 123%. The static friction threshold of the abutment bearings was reduced to zero while the static friction threshold for the pier bearings was optimized at 56% of the calculated sliding friction (compared with 20% determined from the parameter sensitivity study).

As discussed earlier, systematic error, experimental noise and modelling limitations reduce the accuracy of the FE modelled strains. The strain gauges in the arch are located in arch sections near the arch bases and near the arch to carriageway connections, thus the stress profile is affected by local disturbances and should not be considered to be fully developed. Points of load application, internal restraints and boundary conditions are known regions of discontinuous stress fields, Engström (2006) Beam elements, which assume a linear stress distribution, were used to model

the concrete arch. As such, the modelled strains were simplified and idealized near the arch bases and the arch to carriageway connections. Thus, considering experimental error and modelling limitations, the results for the optimized FE model were not surprising.

To reduce the systematic error caused by the discontinuous stress field, the strains measured in arch section S25, located in the arch crown, were used for FE model updating. As was the case when all strains were used for FE model updating, no significant improvement was obtained from the optimization.

7.2.3 Displacement optimization

In much the same way as for strain, the FE modelled displacements at measured nodes were optimized with respect to the experimentally measured displacements. The mean relative error was calculated using the error objective function.

$$\min_{z/\Sigma|z_m} \frac{\sum_{i=1}^{155} |u_{mi} - u_i|}{\sum_{i=1}^{155} |u_{mi}|} \quad (7.8)$$

The FE modelled displacement response was only sensitive to the pier bearing static friction threshold, abutment bearing static friction threshold and the stiffness of the carriageway. The optimized updating parameters were obtained by minimizing the error objective function for displacement.

$$\min_{\Phi} \min_{z/\Sigma|z_m} \frac{\sum_{i=1}^{155} |u_{mi} - u_i|}{\sum_{i=1}^{155} |u_{mi}|} \quad (7.9)$$

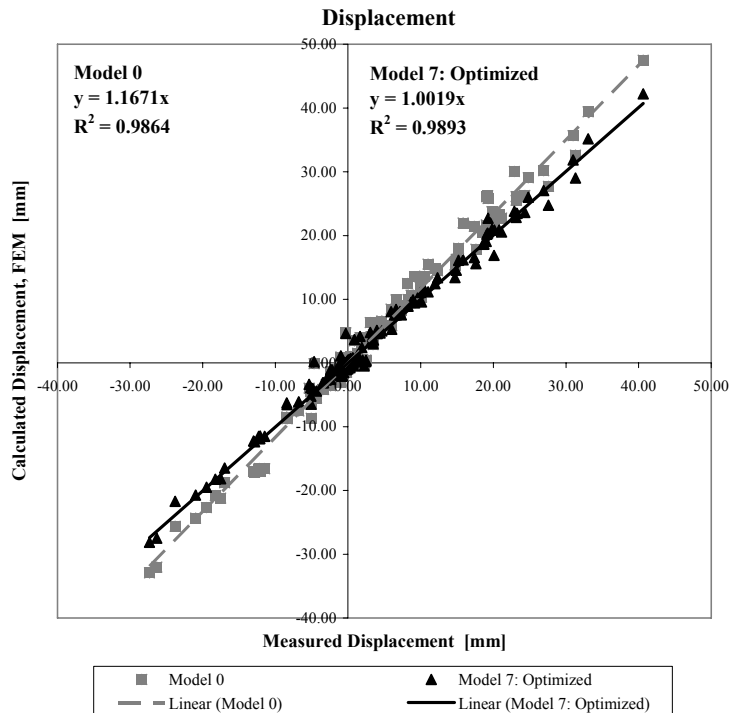


Figure 7.4 Comparison of optimized FE model normalized displacements and initial FE model normalized displacements with normalized measured displacements.

The correlation between the calculated displacements for the static load tests using the initial FE model, Model 0, and the experimentally measured displacements was quite good. Optimization of Model 7 reduced the mean relative error of the displacements by approximately 7% and thus improved the correlation to the experimentally measured measurements.

Scatter is still evident in Figure 7.4, which is most likely due to measurement noise. According to the FE model optimized for displacements, the static friction threshold at the abutment bearings was zero. The static friction threshold at the pier bearings was 78% of the approximated value calculated using from the kinetic friction. The normalized updating parameters for the bearings were realistic, especially when compared with the parameter sensitivity analysis and the results from the strain optimization. The elastic modulus of the steel for the carriageway was increased by 18%, which was not considered realistic. Rather, it is likely that the increased stiffness of the carriageway required to optimize the displacement measurements was caused by the contribution of the railing to the response of the bridge during static load testing.

As discussed in Chapter 6.3.2, the railing was suspected to contribute to both the dynamic and static structural behaviour of the bridge. In order to account for this contribution, the carriageway steel stiffness and the carriageway sectional parameters were permitted to change in a realistic way. The stiffness of the railing was not included in the FE model during the design of the bridge, though the railing certainly affected the measured response. Due to bolted connections, the railing elements are difficult to include in the FE model. For the case at hand, when the FE model was optimized for frequency, the stiffness of the carriageway was found to decrease by

4%. When the same FE model was optimized for displacement the carriageway stiffness increased by 18%. It is possible that during ambient vibration testing, the bolted connections for the railing were sufficiently loose as to not transmit any load while during static load testing, the applied loads were high enough to close the gaps in the bolted joints and thus transmit structural load through the railing. It is necessary to consider the contribution of non-structural members to the structural behaviour for FE model updating, but any beneficial structural contribution should be removed from the FE model for SLS structural assessment in order to ensure that design FE model remains conservative.

7.2.4 Hanger load optimization

The hanger loads in hangers 1E and 1W were measured with load cells during the static load tests. Temperature effects were removed from the data as for strain measurements and the manually refined FE model, Model 7, was optimized with regard to the standard deviations of the measurements for the 5 load cases.

$$F_{\sigma} \Pi = \frac{\sum_{i=1}^{10} \sqrt{\frac{(F_{mi} - F_i)^2}{\sigma_{F_i}^2}}}{10} \quad (7.10)$$

The FE model was optimized to reproduce the measured hanger loads,

$$\min_{\Phi} F_{\sigma} \Pi \quad (7.11)$$

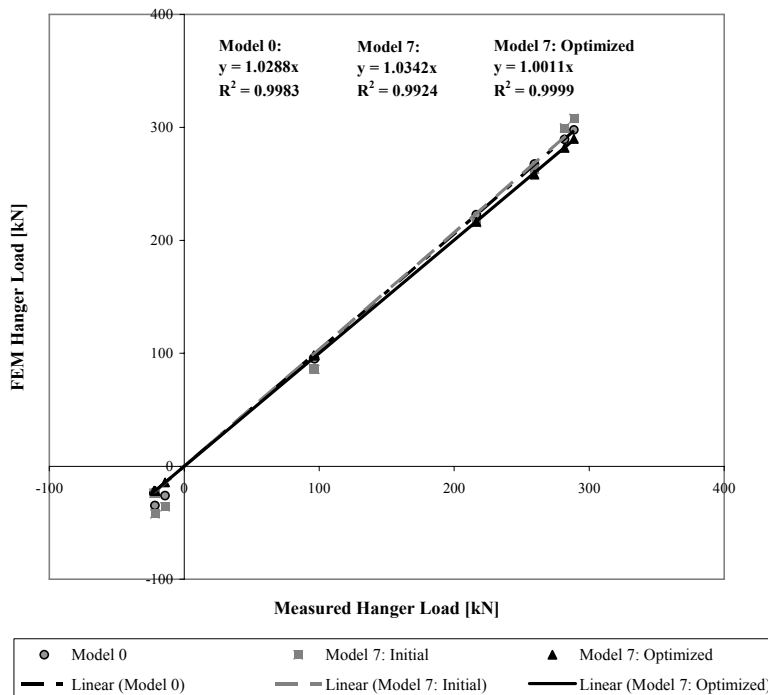


Figure 7.5 Comparison of FE model hanger loads before and after optimization and from the initial FE model with measured hanger loads.

From Figure 7.5, it is apparent that the initial FE model was quite accurate. Nonetheless, the optimized FE model yielded a closer correlation to the measured hanger loads. The stiffness of the arch base, stiffness of the arch crown, carriageway steel stiffness, carriageway stiffener area, and the static friction thresholds at the abutment and pier bearings were updated during optimization. The carriageway stiffener area and static friction thresholds and the bearings remained virtually unchanged. The stiffness of the arch base decreased from 106% to 102%, while the stiffness of the arch crown decreased from 119% to 105%. The carriageway steel elastic modulus increased by 10%, which was more conservative than the result obtained for the displacement optimization.

Once again, the stiffness contribution of the railing was believed to affect the measured response. As was discussed in the previous section, the contribution of non-structural members to the structural behaviour of the bridge is very difficult to model, especially for simple models. Although the design model of the bridge should be conservative, the FE model used for updating should be as realistic as possible and thus include all elements that contributed to the response during experimental measurements.

7.2.5 FE model optimization

In Chapter 7.2.1 to Chapter 7.2.4, the FE model was optimized for each type of response, \hat{z} , individually. The significance of the resulting updating parameter vector was discussed for each case. When the FE model was optimized for displacements and hanger loads, the carriageway stiffness was increased, which contradicted the updating results for the FE model optimized for frequency. In order to obtain an optimized FE model for all measured responses with consideration of the deviation of the updating parameter vector from the “best guess” determined from manual model refinements, the FE model was optimized with statistical consideration of the response and the updating parameters. The standard deviation objective function with and without regularization was used. The total deviation for each of the response as specified in Table 6.2 was used for σ_z as to reduce the effect of systematic error in the strain and displacement measurements on the final result without neglecting the strain and displacement response altogether. Thus, for an arbitrary response, ${}_1\hat{z}$, the contribution to the response objective function was formulated as,

$${}_1\hat{z}\Pi_{\sigma} = \frac{\sum_{i=1}^{N_{1\hat{z}}} \sqrt{\frac{({}_1\hat{z}_{mi} - {}_1\hat{z}_i)^2}{\sigma_{1\hat{z}_i}^2}}}{N_{1\hat{z}}} \quad (7.12)$$

The minimization equation was solved for the optimal updating parameter vector,

$$\min_{\Phi} {}_z\Pi_{\sigma} \quad (7.13)$$

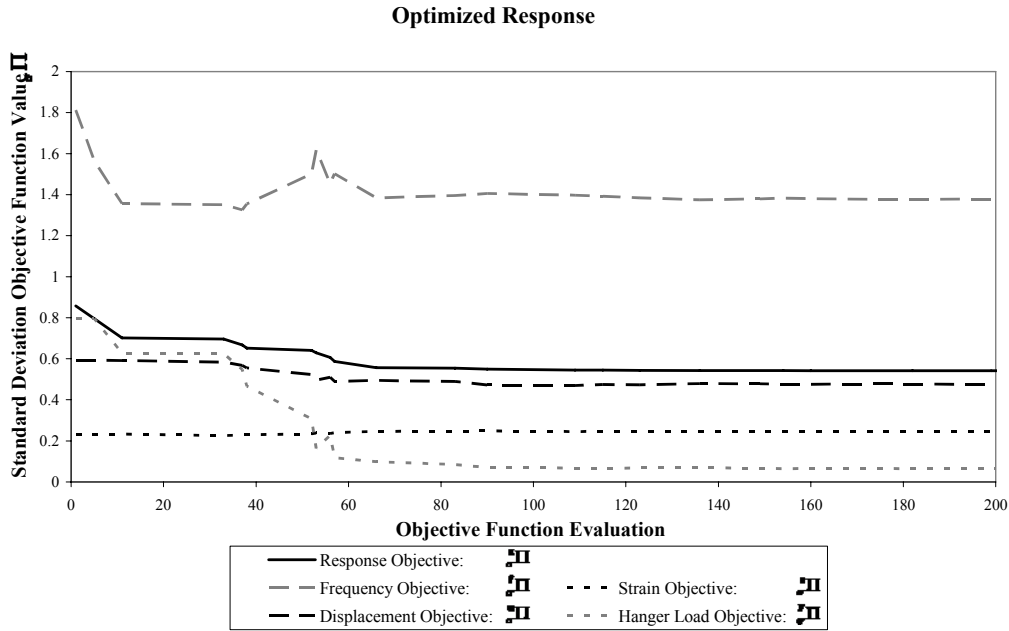


Figure 7.6 Convergence of optimization of mean response with frequency, strain, displacement and hanger load contribution to objective function.

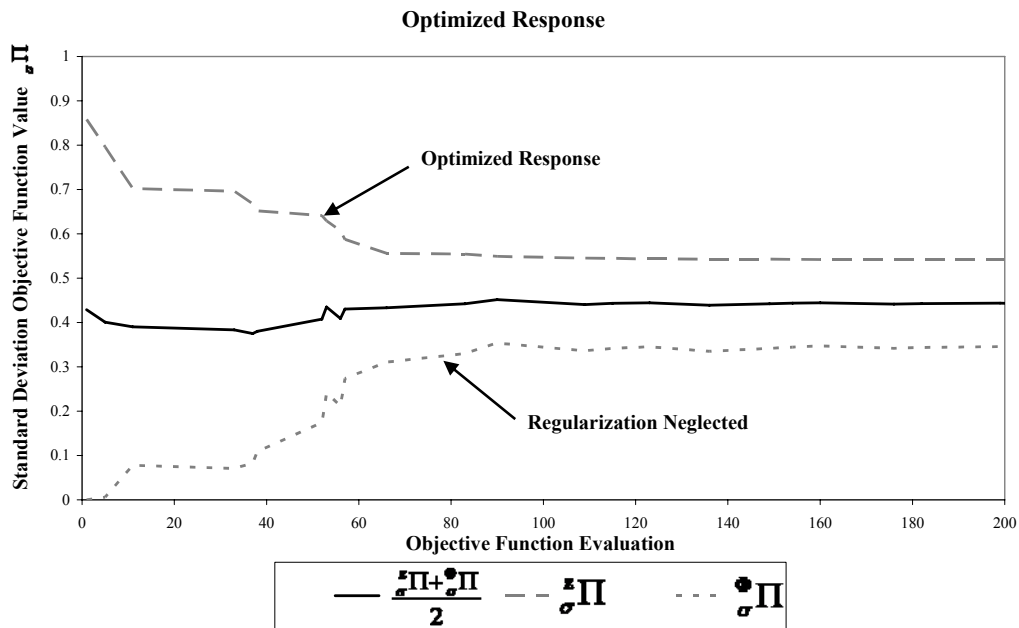


Figure 7.7 Convergence of optimization of mean response.

From Figure 7.6, it is clear that the frequency and hanger load response dominate the objective function. The displacement objective function is also reduced during the minimization. The strain response was not improved when all responses were considered for minimization. From Figure 7.7, it is clear that without including regularization, the updating parameters deviate from the “best guess” obtained through manual model refinements including engineering calculations and the parameter sensitivity analysis. All of the normalized updating parameters of interest determined from the parameter sensitivity study were optimized to obtain the best

possible response. The stiffness of the arch base increased from 106.2% to 114.5% while the stiffness of the arch crown decreased from 119% to 103.2%. These results are similar to those presented in the non-regularized frequency optimization presented previously. The normalized updating parameter for the asphalt mass increased from 0.95 to 1.02 while the normalized updating parameter for the asphalt stiffness decreased from 1.60 to 1.41. The normalized updating parameters for the static friction in the bearings and for the sectional area of carriageway stiffeners remained virtually unchanged. The elastic modulus of the steel of the carriageway increased by roughly 11% which was most likely due to the hanger load contribution to the objective function. From the parameter sensitivity study and the hanger load optimization analysis, the contribution of the railing to the structural behaviour of the bridge was evident, though difficult to quantify. A more realistic FE model should include railing elements for the static load simulations, though the beneficial contribution of the railings to the carriageway stiffness should be neglected in the design FE model so that the structural design criteria is verified conservatively.

In order to regularize the objective function, the deviation from the “best guess” updating parameter vector obtained from manual model, Table 6.2, formed the regularization term.

$$\Phi_{\sigma} \Pi = \frac{\sum_{i=1}^{N_{\phi}} \sqrt{\frac{(\phi_{0i} - \phi_i)^2}{\sigma_{\phi_i}^2}}}{N_{\phi}} \quad (7.14)$$

The standard deviation objective function considered both the response residual and the updating parameter deviation,

$$\sigma_{\sigma} \Pi = \frac{\sigma_{\sigma} \Pi + \Phi_{\sigma} \Pi}{2} \quad (7.15)$$

The optimal FE model for the New Svinesund bridge minimized the standard deviation objective function,

$$\min_{\Phi} \sigma_{\sigma} \Pi \quad (7.16)$$

Optimized Response with Regularization of Updating Parameters

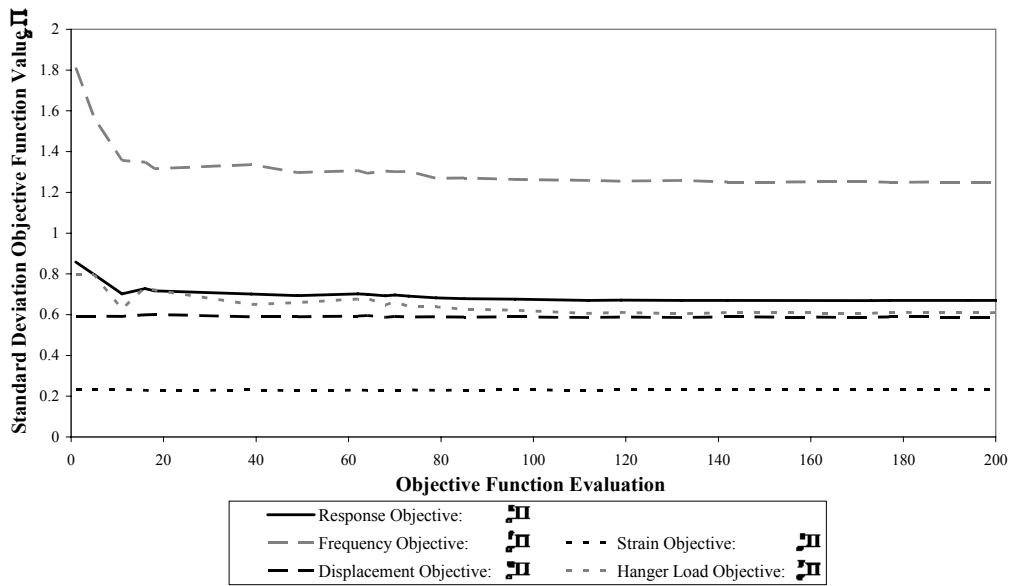


Figure 7.8 Convergence of optimization of regularized mean response with frequency, strain, displacement and hanger load contribution to objective function.

Optimized Response with Regularization of Updating Parameters

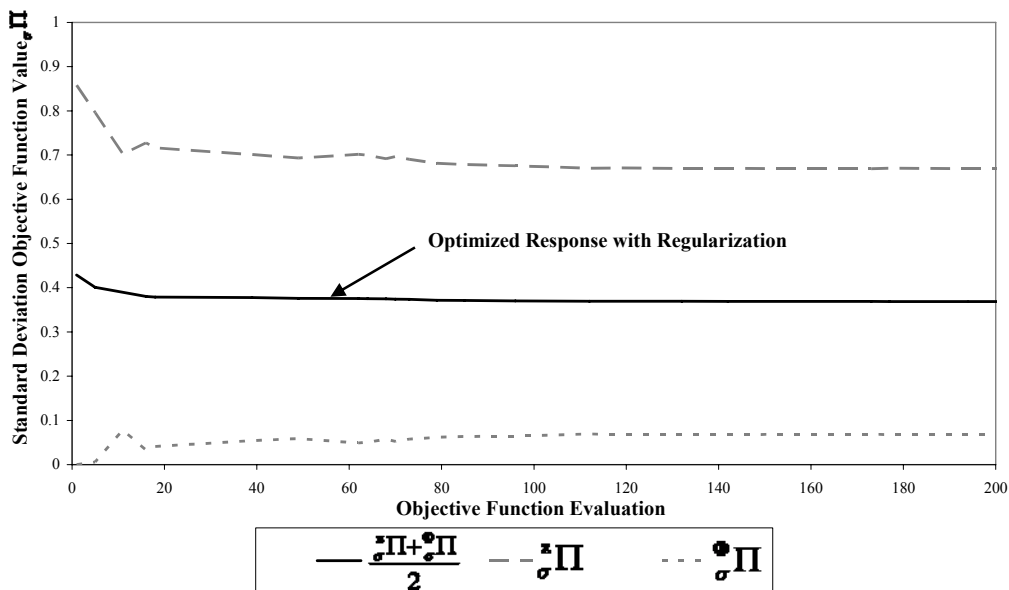


Figure 7.9 Convergence of optimization of regularized mean response.

When regularization was included in the objective function formulation, the response improved, though not as much as when regularization was neglected. While most of the normalized updating parameters did not significantly deviate from the initial values, the normalized stiffness of the arch crown decreased from 1.19 to 1.133. As discussed earlier, the stiffness of the arch crown was reduced for the frequency optimization without regularization. This may be due to the opening of micro-cracks during ambient vibration testing. Without further measurements and load tests, it is

difficult to substantiate a significant deviation from the calculated increase in the arch crown stiffness. The optimization results presented in this study should be considered when simulating the realistic performance of the bridge, but should not be used for structural assessment.

7.3 Results summary

The results from the FE model updating analyses are presented in the tables below. From the previous analyses, it was shown that although different results were obtained when the FE model was optimized for different types of response, the overall response could be improved when the residuals from all responses were accounted for in the objective function used for optimization. The statistical deviations of the measurements were used for weighting of the different responses in the objective function. Improvements to the FE model made using manual refinements were essential to obtain the “best guess” to be used for the initial updating parameter vector for optimization. Regularization ensured that the resulting updating parameter vector was reasonable. For more plots and tabulated results, please refer to Appendix K.

8 Conclusions

8.1 Discussion of FE model updating of the New Svinesund Bridge

The FE model of the New Svinesund bridge was updated through systematic manual model refinement and non-linear optimization. The resulting FE model included more realistic structural parameters and an improved response when compared with the original FE model of the bridge.

Manual model refinement was essential for the case of the New Svinesund bridge because of modelling limitations present in the initial FE model. Structural calculations were used to obtain more realistic estimates of uncertain structural parameters, which were further calibrated by comparing the modelled response with the measured response in the parameter sensitivity study. Several objective functions were developed to evaluate the modelled response with regard to the measured response. The advantages and disadvantages of each type of objective function were considered with regard to statistical considerations of the measured response parameters. All objective functions were used to assess the bridge response sensitivity to the uncertain structural parameters, though only the most useful results were presented. Important findings regarding the bridge behaviour were obtained from the parameter sensitivity study and were considered for optimization.

Using primarily the data obtained from the hanger loads during the static load tests, the rigidity of the arch to carriageway connection was verified. The sensitivity of the measured response to the arch foundation stiffness was found to be insufficient for FE model updating, thus the arch foundation stiffness calculated during design could not be verified. The contribution of non-structural members including the asphalt layer and the railings was investigated in the parameter response study and found to be important when assessing the actual response of the bridge.

For each type of response, a set of normalized updating parameters was obtained through optimization. Finally, the FE model was optimized for the entire measured response, including strains, displacements and hanger loads from the static load tests and frequencies from ambient vibration testing. The resulting FE model included more realistic values for uncertain structural parameters and was capable of better modelling the measured response.

8.2 Recommendations for further FE model updating for the New Svinesund Bridge

In order to further reduce the uncertainty of the FE model and to better understand the capability of FE model updating, further studies are recommended. The updated FE model obtained through this study is a sort of “footprint” model for further studies.

Including eigenmodes above modes 1 to 4 would be useful for dynamic FE model updating and would increase the confidence in the FE model for dynamic analysis. Mode shapes are required for mode pairing above mode 4 and to formulate the MAC matrix. Thus, further research including dynamic testing is recommended in order to obtain mass-normalized mode shapes that may be used for FE model updating.

Although the loading configuration and sensor system used for static load testing was useful for verifying the rigidity of the arch to carriageway connection, the transverse rotational stiffness of the arch foundation could not be verified. Uncertain structural parameters should be identified before static load testing and the static load configuration should first be simulated using the FE model to ensure that the uncertain structural parameters activate the measurable response. Temporary longitudinal displacement transducers at the bearings are recommended for future static load tests. Externally mounted strain gauges should be installed on the inside and outside surfaces of the concrete arch at some of the sections where the permanently installed strain gauges are located. The external strain gauges should be calibrated before and after load testing. The function of these strain gauges would primarily be calibration of the permanently installed resistance strain gauges in order to eliminate systematic error.

Experimental noise should be considered when comparing measurements with different units and the response residual should be statistically weighted to reflect the confidence in each type of measurement. The standard deviation of the experimentally measured response, sensor accuracy, sensor calibration and the modelling limitations should all be considered when comparing measurements of different types. The variation of the uncertain structural parameters should be established according to the probabilistic distribution. When formulating the objective function, the response should be statistically weighted in a reasonable manner. A regularization term should consider the deviation of the updating parameters from the “best guess” according to engineering calculations and a sensitivity analysis. The final FE model should be optimized with respect to the measured response vector and the “best guess” updating parameter vector determined systematically by engineering calculations and a parameter sensitivity analysis.

8.3 FE model updating for improved structural assessment

The use of FEM for structural assessment is valuable, especially for complex structures where strict design guidelines are not available. A holistic FE modelling perspective should be adopted from the early stages of design through the service life of a bridge. FE model updating using frequency and static response can be used to improve the agreement of the updated FE model with the experimentally measure response. The updated FE model then ensures the validity of the more conservative design FE model when verifying design criteria and the assessment FE model for structural assessment. In order to ensure the validity of the FE model updating procedure, certain guidelines should be followed.

During the initial FE modelling phase, the structural designer should create an initial FE model that is sufficiently robust to be used to verify design criteria and for structural assessment during the service life of the bridge. The geometry, element types and mesh are defined for the initial model. Material properties and element sectional data should be tabulated to facilitate FE model updating.

Initial FE Model:

- Created in design phase, not changed during service life
- Geometry
- Element types
- Mesh

The design FE model is derived from the initial FE model. While the geometry, element types and mesh remain unchanged, the boundary conditions and material properties are assigned according to design criteria.

Design FE Model (conservative):

- Used to verify design criteria
- Geometry, element types and mesh remain unchanged
- Boundary conditions
 - According to design criteria, assumptions on the safe side
- Material properties
 - According to design values
 - Material strength: 5% fractile
 - Material stiffness: mean values

Due to conservative assumptions, often the design FE model and assessment FE model can not accurately model SLS loads. If the difference between the measured response and the FEA response is considerable, the validity of the design and assessment FE models is suspect. In order to verify the conservative FE models, an update FE model, which is derived from the same initial FE model as both the design and the assessment FE models, is used. The update FE model has realistic material properties and boundary conditions and is updated using manual model refinement and optimization to better reproduce the measured response.

Update FE Model (realistic):

- Used to verify design FE model and to obtain an improved assessment FE model
- Updated using results of dynamic and static load testing
- Boundary conditions
 - Updated spring stiffness for abutments or foundations modelled with springs
 - Tied boundary conditions for prestressed bearings during ambient vibration frequency measurements
 - Static friction in bearings simulated using non-linear spring elements
- Material properties
 - Engineering calculations
 - Increased concrete stiffness due to hydration
 - Increased concrete stiffness due to reinforcement
 - Asphalt stiffness for dynamic loading
 - Parameter sensitivity analysis
- Non-structural elements
 - Asphalt layer
 - Railings

For structural assessment, a conservative FE model is used which includes improved boundary conditions and material properties from the update FE model, but does not include non-structural elements. The assessment FE model provides the level of safety as specified in the structural assessment codes but includes increased knowledge gained from load tests and material tests. Reduced or increased material properties are included to model concrete cracking, increased concrete hydration, steel corrosion, etc. that have occurred with time.

Assessment FE Model (conservative):

- Check structural capacity in accordance with structural assessment
- Geometry, element types and mesh remain unchanged
- Boundary conditions
 - According to updated model, conservative with respect to response in ULS
- Material properties
 - According to structural assessment codes with respect to material tests made
 - Reduced or increased material properties if necessary
 - Concrete cracking
 - Steel corrosion
 - Fatigue

In order to measure the dynamic and static response so that the update FE model may be calibrated and the design and assessment FE models may be verified, a sensor system is required. The permanent sensor system is designed before bridge

construction and is simulated in the update FE model in order to ensure that the necessary response can be measured.

Permanent sensor system:

- Measure dynamic and static response
- Calibrate sensors for static load tests using temporary sensor system
- Continuously record data during static load tests
- Accelerometers
 - Verify that the location of sensors corresponds with important eigenmodes
 - Full-scale dynamic test
 - Snap-back
 - Snap-through
 - Shaker
 - Ambient vibrations testing
 - Monitor temperature of structural members and asphalt layer
- Strain gauges
 - Located in uniform stress field away from discontinuous stress field caused by point loads, internal restraints and boundary conditions
 - Temperature gauges to monitor temperature effects
 - External strain gauges for calibration
- Load cells
 - Calibrated using temporary sensors (hanger frequency to determine load)

In addition to the permanently installed sensor system, a temporary sensor system is used to gather additional information about the bridge response during load test. If a permanent sensor system for FE model updating was not installed during construction, the temporary sensor system can provide the measured response for FE model updating.

Temporary sensor system:

- Measure dynamic response
 - Additional accelerometers to measure mode shapes
- Measure static response
 - Displacement measurements with total stations
 - Displacement gauges installed at bearings to determine realistic boundary conditions
 - External strain gauges for calibration of permanent reinforcement strain gauges
 - Additional temperature gauges to remove temperature trends

The load tests should first be simulated using the FE model to ensure that the necessary response to be measured will be activated. By simulating the load tests and the response, a parameter sensitivity study should be conducted to determine if the response is sufficiently sensitive to the uncertain structural parameters. FE model

updating may then be evaluated by introducing noise to the simulated “measured” response to see if the “measured” parameters may be obtained.

Load Tests:

- Simulate load tests using FE model before full-scale load testing
- Designed to activate response that is necessary to determine uncertain structural parameters
- Loading configurations randomized to reduce systematic error

8.3.1 Design

During the design stage, the realistic behaviour of the bridge should be considered for FE modelling. The “design model” should be conservative, thus assuming worst-case material properties and boundary conditions for worst-case loading configurations in order to satisfy SLS and ULS design criteria. Simultaneously, a similar FE model should be created with identical geometry, element types and mesh for FE model updating. The “update model” should utilize realistic values for material properties and boundary conditions.

The sensor system and load tests should be modelled so that the measured response may be simulated. If the uncertain structural parameters cannot be determined from the measurable response, the sensor system and load tests should be redesigned.

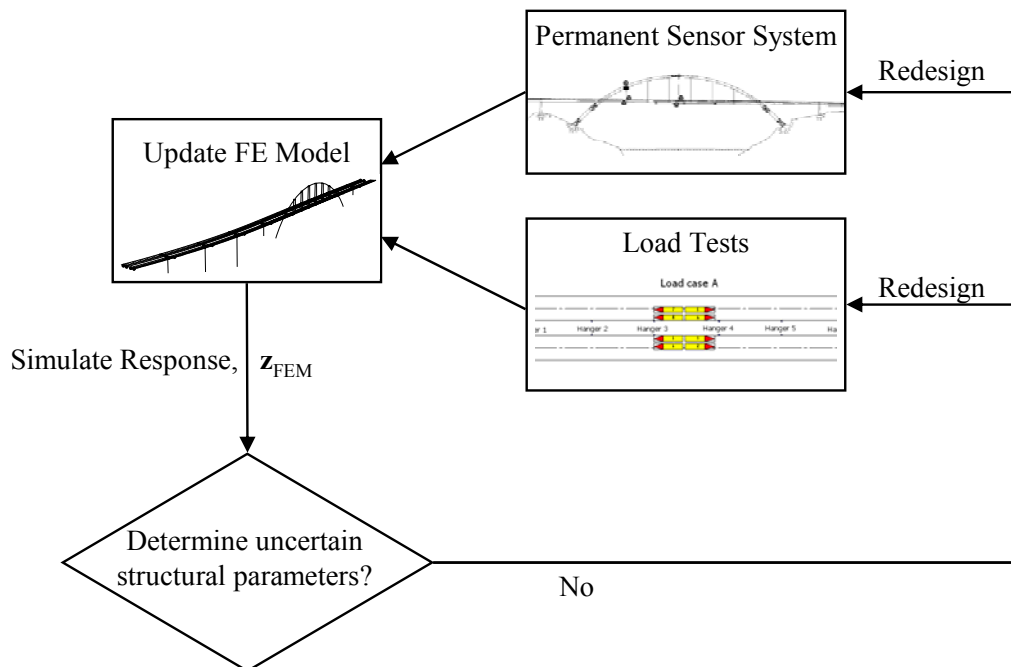


Figure 8.1 Conceptual framework for design of sensor system and load tests.

8.3.2 Service life

During the service life of the bridge, FE model updating can be used to calibrate the update FE model so that it accurately models the performance of the bridge. Dynamic and static load testing is used to activate the measurable response so that uncertain structural parameters may be determined using the response.

The design FE model is validated after the uncertain structural parameters have been determined and the update FE model has been calibrated through FE model updating. The confidence in the design FE model for verifying structural design criteria is increased once it has been validated.

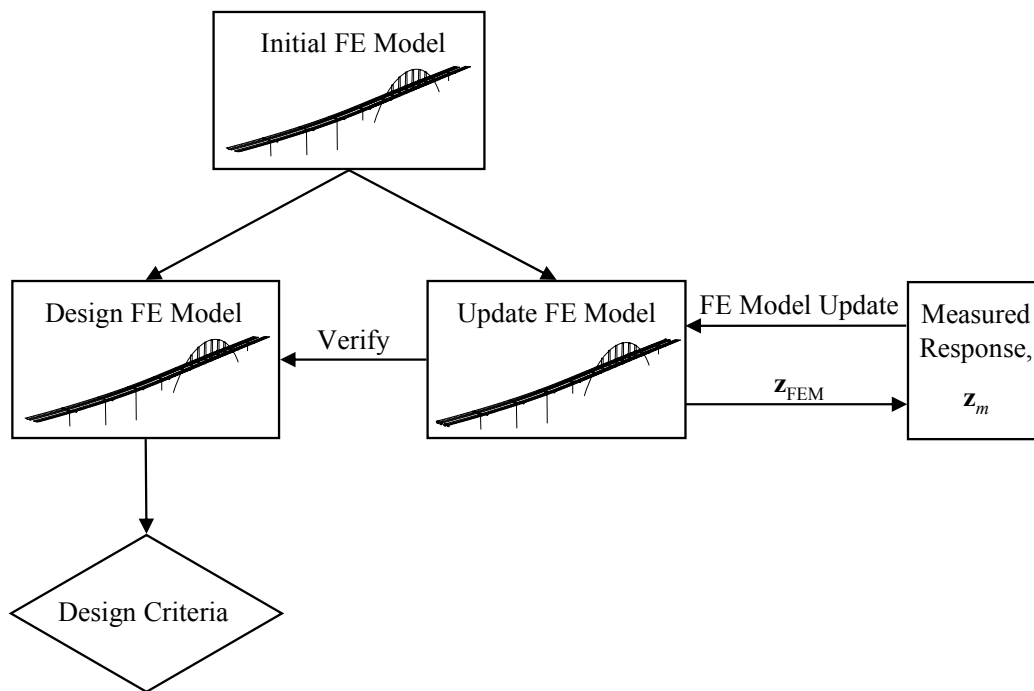


Figure 8.2 Conceptual framework for implementation of FE model updating using dynamic and static load tests to verify design FE model.

Routine structural assessment requires the validation of the residual structural capacity. The load carrying capacity in accordance with structural assessment criteria must be verified, often using a conservative FE model. The update FE model is required to verify the assessment FE model, which may not accurately model the real response of the bridge due to conservative assumptions. The update FE model can be updated through realistic manual model refinements and optimization with regard to the response measured at the time of structural assessment.

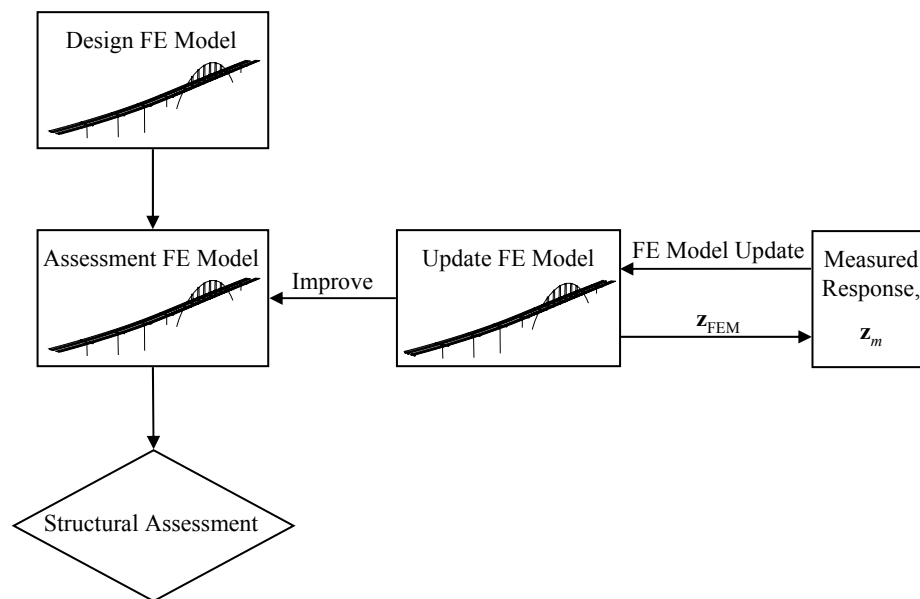


Figure 8.3 Conceptual framework for service life implementation of FE model updating using dynamic and static load tests for improved structural assessment.

9 References

ABAQUS (2006): Abaqus Standard: User's manual, Hibbitt Karlsson & Sorensen, Pawtucket, R. I., 2006.

Austrell P-E, m. f. l. (2004): Calfem, A finite element toolbox version 3.4, Lund, 2004.

Bilfinger Berger. (2003a). "14-1319-1 BRO ÖVER IDEFJORDEN (NY SVINESUNDSBRO) VID BJÄLLVARPET Å VÄG E6, Plan och sektioner." 113k2005, ed., Vägverket, Region Väst.

Bilfinger Berger (2003b): K Comparative Analysis of global System for Design of SubStructure K4 Calculation of Eigenfrequencies. Billfinger Berger AG.

Bilfinger Berger (2003c): K Comparative Analysis of global System for Design of Substructure K2 Static System. 110K11302, Mannheim.

Billfinger Berger. (2004). "Indata files for the structural model of the New Svinesund Bridge." Mannheim, Text files obtained by e-mail from Bilfinger Berger AG.

Bröderna Edstrand. (2000). "BEs Lilla Röda."

Cable J. K., Fanous F. S., Ceylan H., Wood D., Frentress D., Tabbert T., Oh S.-Y. and Gopalakrishnan K. (2005): Design and Construction Procedures for Concrete Overlay and Widening of Existing Pavements. FHWA DTFH61-01-X-00042 (Project 6) IHRB Project TR-511, Iowa State University, Ames.

Coleman T. F. and Zhan Y. (2007). "Optimization Toolbox User's Guide." The MathWorks, Inc.

Craig R. R., Kurdila A. and Craig R. R. (2006): Fundamentals of structural dynamics, John Wiley, Hoboken, N.J., 2006.

DiBiagio E. (2003): A Case study of Vibrating-Wire Sensors That Have Vibrated Continuously For 27 Years. Norwegian Geotechnical Institute (NGI).

Engström B. (2006): Design analysis of deep beams and other discontinuity regions, Chalmers University of Technology, Göteborg, 2006.

Friswell M. I. and Mottershead J. E. (1995): Finite element model updating in structural dynamics, Kluwer Academic Publishers, Dordrecht; Boston, 1995.

GEONOR. (2007). "GEONOR P-300 REINFORCEMENT STRAIN GAUGE for reliable stress/strain monitoring."

Jaishi B., Kim H.-J., Kim M. K., Ren W.-X. and Lee S.-H. (2007): Finite element model updating of concrete-filled steel tubular arch bridge under operational condition using modal flexibility. Mechanical Systems and Signal Processing, Vol. 21, No. 6, pp. 2406-2426.

James G. and Karoumi R. (2003): Monitoring of the new Svinesund bridge, Tekniska högsk., Stockholm, 2003.

Johansson S. (2005): SVINESUNDBRON BELASTNINGSPROV, STATISKA TESTER GEODETISKA MÄTNINGAR. 1650971, FB ENGINEERING AB, Göteborg.

Karoumi R. (2007). "Excel files with measured data for Svinesund bridge." KTH, Stockholm, Data files obtained by e-mail.

Karoumi R. and Andersson A. (2007): Load Testing of the New Svinesund Bridge: Presentation of results and theoretical verification of bridge behaviour. TRITA-BKN. Rapport 96, KTH Byggetenskap, Stockholm.

Kwon Y. W. and Bang H. (2000): The finite element method using MATLAB, CRC Press, Boca Raton, 2000.

MAURE RSÖHNE. (2003). "Fixed spherical bearing."

MAURE RSÖHNE. (2007). "MAURER MSM Sliding Bearings."

Ottosen N. and Petterson H. (1992): Introduction to the Finite Element Method, Prentice Hall Europe, 1992.

Plos M. and Movaffaghi H. (2004): Finite Element Analysis of the New Svinesund Bridge. 04:12, Chalmers University of Technology, Göteborg, Sweden.

Södersten T. and Stoica P. (1989): System Identification, Prentice Hall, 1989.

Thelandersson S. (2004): Assessment of material property data for structural analysis of nuclear containments, Lund University Division of Structural Engineering, Lund, 2004.

Ülker-Kaustell M. and Karoumi R. (2006): Monitoring of the New Svinesund Bridge - Report 3: The influence of temperature, wind and damages on the dynamic properties of the bridge. TRITA-BKN. Rapport 99, KTH Byggetenskap, Stockholm.

Zhang Q. W., Chang T. Y. P. and Chang C. C. (2001): Finite-element model updating for the Kap Shui Mun cable-stayed bridge. Journal of Bridge Engineering, Vol. 6, No. 4, pp. 285.

Zivanovic S., Pavic A. and Reynolds P. (2007): Finite element modelling and updating of a lively footbridge: The complete process. Journal of Sound and Vibration, Vol. 301, No. 1-2, pp. 126.

Appendix A. Simple Beam FE Model Verification

Relevant parameters for IPE 180 simply supported beam,

$$E = 210 \text{ GPa}$$

$$I = 13.17\text{E}6 \text{ mm}^4$$

$$A = 2395 \text{ mm}^2$$

$$k_t = 1.0\text{E}6 \text{ N/m}$$

$$k_r = 5.0\text{E}6 \text{ N*m/rad}$$

$$\rho = 7700 \text{ kg/m}^3$$

$$L = 8 \text{ m}$$

$$P = 10 \text{ kN}$$

Bernoulli-Euler beam theory,

$$\frac{\partial^2}{\partial x^2} \left(EI \frac{\partial^2 u}{\partial x^2} \right) + \rho A \frac{\partial^2 u}{\partial t^2} = p(x, t) \quad (\text{A.1})$$

An important result of the Euler-Bernoulli beam equation is,

$$\theta_B - \theta_A = \int_A^B \frac{M(x)}{EI} dx \quad (\text{A.2})$$

In this case for static loading,

$$\theta_B = \frac{du}{dx} \left(x = L/2 \right) = 0 \quad (\text{A.3})$$

$$M(x) = \left(\frac{M_f - M_s}{L/2} \right) (x) + M_s \quad (\text{A.4})$$

$$\theta_A = \frac{M_s}{k_r} \quad (\text{A.5})$$

Integrating equation (A.2) and substituting equation (A.3), equation (A.4) and equation (A.5), the field moment is obtained as,

$$M_f = \frac{PL(Lk_r + 4EI)}{8Lk_r + 16EI} \quad (\text{A.6})$$

The elastic stress and strain profile across the section at midspan,

$$\sigma_{f,\max} = \frac{M_f}{\left(\frac{I_x}{h/2}\right)} \quad (\text{A.7})$$

$$\varepsilon_1 = \frac{\sigma_{f,\max}}{E} \quad (\text{A.8})$$

Deflection of each of the vertical springs is simply calculated using symmetry,

$$u_s = \frac{(P/2)}{k_t} \quad (\text{A.9})$$

For deflection at the midspan,

$$u_f = u_s + \int_A^B \frac{M(x) \cdot x}{EI} dx \quad (\text{A.10})$$

In order to determine the first four eigenfrequencies, consider free vibration,

$$p(x,t) = 0 \quad (\text{A.11})$$

$$\frac{\partial^2}{\partial x^2} \left(EI \frac{\partial^2 u}{\partial x^2} \right) + \rho A \frac{\partial^2 u}{\partial t^2} = 0 \quad (\text{A.12})$$

Which may be written as,

$$(EIU'')'' + \rho A \ddot{u} = 0 \quad (\text{A.13})$$

Assume harmonic transient motion,

$$u = U(x) \cos(\omega t - \alpha) \quad (\text{A.14})$$

$$\frac{\partial^2 u}{\partial t^2} = \ddot{u} = -\omega^2 U(x) \cos(\omega t - \alpha) \quad (\text{A.15})$$

Differentiate with respect to position,

$$\begin{aligned}\frac{\partial u}{\partial x} &= U'(x)\cos(\varpi t - \alpha) \\ &\vdots\end{aligned}\tag{A.16}$$

Thus the eigenvalue equation is obtained by eliminating $\cos(\varpi t - \alpha)$ from the expression,

$$(EIU'')'' + \rho A \varpi^2 U = 0\tag{A.17}$$

Free vibration of uniform beam with eigenvalue defined per unit length as,

$$\lambda^4 = \varpi^2 \frac{\rho A}{EI}\tag{A.18}$$

$$\frac{\partial^4 U}{\partial x^4} - \lambda^4 U = 0\tag{A.19}$$

Assuming a general solution for $U(x)$,

$$U(x) = Ae^{\lambda x} + Be^{-\lambda x} + C \sin(\lambda x) + D \cos(\lambda x)\tag{A.20}$$

$$U'(x) = \lambda(Ae^{\lambda x} - Be^{-\lambda x} + C \cos(\lambda x) - D \sin(\lambda x))\tag{A.21}$$

$$U''(x) = \lambda^2(Ae^{\lambda x} + Be^{-\lambda x} - C \sin(\lambda x) - D \cos(\lambda x))\tag{A.22}$$

$$U'''(x) = \lambda^3(Ae^{\lambda x} - Be^{-\lambda x} - C \cos(\lambda x) + D \sin(\lambda x))\tag{A.23}$$

For the beam with vertical and rotational springs at each end,

Boundary conditions: $x = 0$

$$k_t U(0) + EIU'''(0) = 0\tag{A.24}$$

$$k_r U'(0) - EIU''(0) = 0\tag{A.25}$$

Boundary conditions: $x = L$

$$k_t U(L) - EIU'''(L) = 0\tag{A.26}$$

$$k_r U'(L) + EIU''(L) = 0\tag{A.27}$$

With,

$$K_T = \frac{k_t}{EI} \text{ and } K_R = \frac{k_r}{EI}\tag{A.28}$$

Evaluating the boundary conditions and forming a coefficient matrix,

$$\begin{bmatrix} K_T + \lambda^3 & K_T - \lambda^3 & -\lambda^3 & K_T \\ \lambda K_R - \lambda^2 & -\lambda K_R - \lambda^2 & \lambda K_R & \lambda^2 \\ K_T e^{L\lambda} - \lambda^3 e^{\lambda L} & K_T e^{-\lambda L} + \lambda^3 e^{-\lambda L} & K_T \sin(\lambda L) + \lambda^3 \cos(\lambda L) & K_T \cos(\lambda L) - \lambda^3 \sin(\lambda L) \\ \lambda K_R e^{L\lambda} + \lambda^2 e^{L\lambda} & -\lambda K_R e^{-L\lambda} + \lambda^2 e^{-L\lambda} & \lambda K_R \cos(\lambda L) - \lambda^2 \sin(\lambda L) & -\lambda K_R \sin(\lambda L) - \lambda^2 \cos(\lambda L) \end{bmatrix} \begin{pmatrix} A \\ B \\ C \\ D \end{pmatrix} = \begin{pmatrix} 0 \\ 0 \\ 0 \\ 0 \end{pmatrix}$$

The eigenvalues are obtained by finding λ such that the determinant of the coefficient matrix is zero,

$$\begin{vmatrix} K_T + \lambda^3 & K_T - \lambda^3 & -\lambda^3 & K_T \\ \lambda K_R - \lambda^2 & -\lambda K_R - \lambda^2 & \lambda K_R & \lambda^2 \\ K_T e^{L\lambda} - \lambda^3 e^{\lambda L} & K_T e^{-\lambda L} + \lambda^3 e^{-\lambda L} & K_T \sin(\lambda L) + \lambda^3 \cos(\lambda L) & K_T \cos(\lambda L) - \lambda^3 \sin(\lambda L) \\ \lambda K_R e^{L\lambda} + \lambda^2 e^{L\lambda} & -\lambda K_R e^{-L\lambda} + \lambda^2 e^{-L\lambda} & \lambda K_R \cos(\lambda L) - \lambda^2 \sin(\lambda L) & -\lambda K_R \sin(\lambda L) - \lambda^2 \cos(\lambda L) \end{vmatrix} = 0$$

When evaluated numerically for the problem at hand,

$$\lambda_1 = 0.4663$$

$$\lambda_2 = 0.6539$$

$$\lambda_3 = 0.8637$$

$$\lambda_4 = 1.1655$$

With the first four eigenfrequencies,

$$f_1 = 13.23 \text{ Hz}$$

$$f_2 = 26.35 \text{ Hz}$$

$$f_3 = 45.98 \text{ Hz}$$

$$f_4 = 83.72 \text{ Hz}$$

Appendix B. MATLAB Subroutine: Eigenfrequency Verification of Simple Beam

```

function R=IPE180EIGdet (f,E,kt,kr)
% Pseudo Inverse Algorithm for Simply Supported Beam
% 2007-08-21
% Fredrik Jonsson and David Johnson
%
% Function to determine the absolute value of the determinant of the
% coefficient matrix for the IPE180 beam with spring supports. Local
% minima correspond to the eigenfrequencies of the beam. This function may
% be minimized or iterated over a frequency domain that includes the
% eigenfrequency of interest in order to determine the first four
% eigenfrequencies. Otherwise it may be plotted over the frequency range of
% interest in order to graphically determine local minimums.
%
% Example:
% >> f_eig1 = fminsearch(@(f) IPE180EIGdet(f,E,kt,kr), 10)
% f_eig1 =
%    13.2314
%
% >> f_eig2 = fminsearch (@(f) IPE180EIGdet(f,E,kt,kr), 25)
% f_eig2 =
%    26.3528
%
% Graphically (use semilog-y):
% figure(1)
% >> fplot(@(f) IPE180EIGdet(f,E,kt,kr), [1 100])
%
% INPUT:
% f    frequency (Hz)
% OUTPUT:
% R    absolute value of determinant of coefficient matrix

I = (13.17E6)*(0.001)^4;           % Area moment of inertia (from beam table)

KT = kt/(E*I);
KR = kr/(E*I);
L = 8;                           % Beam length
rho = 7700;                       % Steel density
A = 2395*(0.001)^2;              % Cross-sectional area (from beam table)

w = f*2*pi();                    % Frequency: Hz to rad/sec
x = ((w^2)*rho*A/(E*I))^(0.25);  % Eigenfrequency to eigenvalue

R = det([KT+x^3                  KT-x^3          ...
        -x^3                    KT;            ...
        KR*x-x^2                -KR*x-x^2       ...
        KR*x                    +x^2;           ...
        KT*exp(x*L)-x^3*exp(x*L)  KT*exp(-x*L)+x^3*exp(-x*L) ...
        KT*sin(x*L)+x^3*cos(x*L)  KT*cos(x*L)-x^3*sin(x*L);
        KR*x*exp(x*L)+x^2*exp(x*L) -KR*x*exp(-x*L)+x^2*exp(-x*L) ...
        KR*x*cos(x*L)-x^2*sin(x*L) -KR*x*sin(x*L)-x^2*cos(x*L)]);

R=abs(R);

```

Appendix C. MATLAB Subroutine: Beam Response

```

function zbeam=beamresponse(phi)
% Beam properties      (Initial guess: phi=[1 1 1])
%                    ('Measured': phi=[1.0288 2 2]):
E = (210E9/1.02888)*phi(1);    % Steel modulus of elasticity [N/m^2]
kt = 5.0E5*phi(2);           % Translational spring stiffness [N/m]
kr = 2.5E6*phi(3);           % Rotational spring stiffness [N*m/rad]
P=10E3;                       % Applied point force, -y direction [N]
L=8;                           % Beam length (must be same as in IPE180EIGdet!)
I=13.17E6*0.001^4;           % Area moment of inertia for IPE 180
zbeam=zeros(7,1);

fguess=5;                       % Start with a guess of first eigenfrequency
fcount = 1;
df = 2;                          % Assume that eigenfrequencies are separated by df

% Eigenfrequency calculations
while zbeam(1) < 1
    % Find first eigenfrequency by finding f such that: det(coeff matrix)=0
    f = fminsearch(@(f) IPE180EIGdet(f,E,kt,kr), fguess);
    zbeam(fcount) = f;
    fguess = fguess+df;
end

while fcount < 4
    % Find eigenfrequencies 2-4
    f = fminsearch(@(f) IPE180EIGdet(f,E,kt,kr), fguess);
    if zbeam(fcount)+df < f
        fcount = fcount+1;
        zbeam(fcount) = f;
    end
    fguess=fguess+df;
end

u2=(P/2)/kt;                    % Deflection of translational springs
Mf=(P*L)*(L*kr+4*E*I)/(8*L*kr+16*E*I); % Maximum field moment
Ms=Mf-P*L/4;                    % Maximum support moment
sig=Mf/(I/90E-3);               % Maximum stress (bottom flange, midspan)
eps=sig/E;                      % Maximum strain (bottom flange, midspan)
u1=u2+L^2/(E*I)*(Mf/12+Ms/24); % Midspan deflection

zbeam(5:7)=[u1 u2 eps];

```

Appendix D. FE Model Updating of Simple Beam

D.1 Simple beam results: classical FE updating techniques

Table D.1 Results for the unweighted pseudo-inverse algorithm with more target responses than updating parameter.

Input Parameter	Initial Value	Iteration Number					Measured Values
		1	2	3	4	5	
$\varphi_1 = E_j/E_0$	1.000	1.068	1.026	1.029	1.029	1.029	1.029
$\varphi_2 = k_{t,j}/k_{t,0}$	1.000	1.778	1.991	2.000	2.000	2.000	2.000
$\varphi_3 = k_{r,j}/k_{r,0}$	1.000	1.509	1.921	1.998	2.000	2.000	2.000
$\ (\Phi_{ref} - \Phi_j)/\Phi_{ref}\ $	0.708	0.272	0.040	0.001	0.000	0.000	
Target Response							
$z_1 = f_1$	10.415	12.690	13.209	13.273	13.274	13.274	13.274
$z_2 = f_2$	20.436	25.494	26.437	26.496	26.496	26.496	26.496
$z_3 = f_3$	38.710	44.866	45.782	45.892	45.893	45.893	45.893
$z_4 = f_4$	74.755	81.489	82.029	82.294	82.298	82.298	82.298
$z_5 = u_1$	0.02688	0.01998	0.01895	0.01877	0.01877	0.01877	0.01877
$z_6 = u_2$	0.01000	0.00563	0.00502	0.00500	0.00500	0.00500	0.00500
$z_7 = \varepsilon_1$	0.000389	0.000348	0.000351	0.000349	0.000349	0.000349	0.000349
$\ (z_m - z_j)/z_m\ $	1.154	0.154	0.014	0.000	0.000	0.000	0.000

Table D.2 Results for the unweighted pseudo-inverse algorithm with more updating parameter than target responses.

Input Parameter	Initial Value	Iteration Number					Measured Values
		1	2	3	4	5	
$\varphi_1 = E_j/E_0$	1.000	1.368	1.454	1.455	1.455	1.455	1.029
$\varphi_2 = k_{t,j}/k_{t,0}$	1.000	1.671	1.770	1.771	1.771	1.771	2.000
$\varphi_3 = k_{r,j}/k_{r,0}$	1.000	1.404	1.479	1.480	1.480	1.480	2.000
$\ (\Phi_{ref} - \Phi_j)/\Phi_{ref}\ $	0.708	0.474	0.502	0.502	0.502	0.502	
Target Response							
$z_1 = f_1$	10.415	12.895	13.269	13.274	13.274	13.274	13.274
$z_2 = f_2$	20.436	25.726	26.485	26.496	26.496	26.496	26.496
$z_3 = f_3$	38.710	47.008	48.393	48.414	48.414	48.414	45.893
$z_4 = f_4$	74.755	88.152	90.701	90.739	90.739	90.739	82.298
$z_5 = u_1$	0.02688	0.01830	0.01728	0.01726	0.01726	0.01726	0.01877
$z_6 = u_2$	0.01000	0.00599	0.00565	0.00565	0.00565	0.00565	0.00500
$z_7 = \varepsilon_1$	0.000389	0.000284	0.000267	0.000267	0.000267	0.000267	0.000349
$\ (z_m - z_j)/z_m\ $	1.154	0.286	0.302	0.303	0.303	0.303	0.000

Table D.3 Results for the unweighted pseudo-inverse algorithm with equal amount of target responses and updating parameters.

Input Parameter	Initial Value	Iteration Number					Measured Values
		1	2	3	4	5	
$\varphi_1 = E_j/E_0$	1.000	1.090	1.023	1.029	1.029	1.029	1.029
$\varphi_2 = k_{t,j}/k_{t,0}$	1.000	1.762	1.992	2.000	2.000	2.000	2.000
$\varphi_3 = k_{r,j}/k_{r,0}$	1.000	1.506	1.906	1.997	2.000	2.000	2.000
$\ (\Phi_{ref} - \Phi_j)/\Phi_{ref}\ $	0.708	0.280	0.047	0.002	0.000	0.000	
Target Response							
$z_1 = f_1$	10.415	12.702	13.195	13.273	13.274	13.274	13.274
$z_2 = f_2$	20.436	25.477	26.430	26.496	26.496	26.496	26.496
$z_3 = f_3$	38.710	44.994	45.750	45.892	45.893	45.893	45.893
$z_4 = f_4$	74.755	81.994	81.924	82.293	82.298	82.298	82.298
$z_5 = u_1$	0.02688	0.01983	0.01900	0.01877	0.01877	0.01877	0.01877
$z_6 = u_2$	0.01000	0.00568	0.00502	0.00500	0.00500	0.00500	0.00500
$z_7 = \varepsilon_1$	0.000389	0.000342	0.000352	0.000349	0.000349	0.000349	0.000349
$\ (z_m - z_j)/z_m\ $	1.154	0.160	0.019	0.000	0.000	0.000	0.000

Table D.4 Results for the weighted response pseudo-inverse algorithm with more target responses than updating parameter.

Input Parameter	Initial Value	Iteration Number					Measured Values
		1	2	3	4	5	
$\varphi_1 = E_j/E_0$	1.000	1.152	1.035	1.029	1.029	1.029	1.029
$\varphi_2 = k_{t,j}/k_{t,0}$	1.000	1.607	1.949	2.000	2.000	2.000	2.000
$\varphi_3 = k_{r,j}/k_{r,0}$	1.000	1.465	1.832	1.990	2.000	2.000	2.000
$\ (\Phi_{ref} - \Phi_j)/\Phi_{ref}\ $	0.708	0.353	0.088	0.005	0.000	0.000	
Target Response							
$z_1 = f_1$	10.415	12.494	13.115	13.268	13.274	13.274	13.274
$z_2 = f_2$	20.436	24.815	26.262	26.493	26.496	26.496	26.496
$z_3 = f_3$	38.710	44.705	45.627	45.885	45.893	45.893	45.893
$z_4 = f_4$	74.755	82.953	81.974	82.274	82.298	82.298	82.298
$z_5 = u_1$	0.02688	0.01993	0.01912	0.01879	0.01877	0.01877	0.01877
$z_6 = u_2$	0.01000	0.00622	0.00513	0.00500	0.00500	0.00500	0.00500
$z_7 = \varepsilon_1$	0.000389	0.000327	0.000350	0.000349	0.000349	0.000349	0.000349
$\ (z_m - z_j)/z_m\ $	1.154	0.275	0.036	0.001	0.000	0.000	0.000

Table D.5 Results for the weighted updating parameter change pseudo-inverse algorithm with more updating parameter than target responses.

Input Parameter	Initial Value	Iteration Number					Measured Values
		1	2	3	4	5	
$\varphi_1 = E_j/E_0$	1.000	1.000	1.000	1.000	1.000	1.000	1.029
$\varphi_2 = k_{t,j}/k_{t,0}$	1.000	1.791	2.012	2.020	2.020	2.020	2.000
$\varphi_3 = k_{r,j}/k_{r,0}$	1.000	1.539	1.983	2.074	2.077	2.077	2.000
$\ (\Phi_{ref} - \Phi_j)/\Phi_{ref}\ $	0.708	0.255	0.030	0.047	0.049	0.049	
Target Response							
$z_1 = f_1$	10.415	12.591	13.214	13.273	13.274	13.274	13.274
$z_2 = f_2$	20.436	25.342	26.453	26.496	26.496	26.496	26.496
$z_3 = f_3$	38.710	44.234	45.629	45.699	45.700	45.700	45.893
$z_4 = f_4$	74.755	79.739	81.474	81.658	81.663	81.663	82.298
$z_5 = u_1$	0.02688	0.02056	0.01907	0.01891	0.01890	0.01890	0.01877
$z_6 = u_2$	0.01000	0.00558	0.00497	0.00495	0.00495	0.00495	0.00500
$z_7 = \varepsilon_1$	0.000389	0.000368	0.000358	0.000356	0.000356	0.000356	0.000349
$\ (z_m - z_j)/z_m\ $	1.154	0.181	0.034	0.027	0.027	0.027	0.000

Table D.6 Results for the weighted updating parameter change and weighted response pseudo-inverse algorithm.

Input Parameter	Initial Value	Iteration Number					Measured Values
		1	2	3	4	5	
$\varphi_1 = E_j/E_0$	1.000	1.048	1.047	1.040	1.036	1.033	1.029
$\varphi_2 = k_{t,j}/k_{t,0}$	1.000	1.613	1.952	1.993	1.996	1.998	2.000
$\varphi_3 = k_{r,j}/k_{r,0}$	1.000	1.814	1.883	1.932	1.960	1.976	2.000
$\ (\Phi_{ref} - \Phi_j)/\Phi_{ref}\ $	0.708	0.215	0.066	0.036	0.021	0.013	
Target Response							
$z_1 = f_1$	10.415	12.539	13.176	13.252	13.262	13.267	13.274
$z_2 = f_2$	20.436	24.558	26.319	26.496	26.497	26.496	26.496
$z_3 = f_3$	38.710	43.905	45.792	45.953	45.931	45.916	45.893
$z_4 = f_4$	74.755	81.151	82.423	82.461	82.399	82.359	82.298
$z_5 = u_1$	0.02688	0.02009	0.01890	0.01878	0.01878	0.01877	0.01877
$z_6 = u_2$	0.01000	0.00620	0.00512	0.00502	0.00501	0.00501	0.00500
$z_7 = \varepsilon_1$	0.000389	0.000346	0.000345	0.000346	0.000347	0.000348	0.000349
$\ (z_m - z_j)/z_m\ $	1.154	0.270	0.029	0.008	0.005	0.003	0.000

Table D.7 Results for the weighted updating parameter and weighted response pseudo-inverse algorithm.

Input Parameter	Initial Value	Iteration Number					Measured Values
		1	2	3	4	5	
$\varphi_1 = E_j/E_0$	1.000	1.048	1.021	1.016	1.016	1.016	1.029
$\varphi_2 = k_{t,j}/k_{t,0}$	1.000	1.612	1.962	2.012	2.013	2.013	2.000
$\varphi_3 = k_{r,j}/k_{r,0}$	1.000	1.813	2.000	2.027	2.024	2.024	2.000
$\ (\Phi_{ref} - \Phi_j)/\Phi_{ref}\ $	0.708	0.216	0.020	0.019	0.019	0.019	
Target Response							
$z_1 = f_1$	10.415	12.537	13.197	13.275	13.275	13.275	13.274
$z_2 = f_2$	20.436	24.552	26.289	26.508	26.513	26.513	26.496
$z_3 = f_3$	38.710	43.899	45.604	45.816	45.821	45.821	45.893
$z_4 = f_4$	74.755	81.146	81.941	82.002	82.002	82.002	82.298
$z_5 = u_1$	0.02688	0.02010	0.01895	0.01883	0.01884	0.01884	0.01877
$z_6 = u_2$	0.01000	0.00620	0.00510	0.00497	0.00497	0.00497	0.00500
$z_7 = \varepsilon_1$	0.000389	0.000346	0.000351	0.000352	0.000352	0.000352	0.000349
$\ (z_m - z_j)/z_m\ $	1.154	0.271	0.026	0.013	0.013	0.013	0.000

Table D.8 Results for the minimum variance algorithm.

Input Parameter	Initial Value	Iteration Number					Measured Values
		1	2	3	4	5	
$\varphi_1 = E_j/E_0$	1.000	1.068	1.026	1.029	1.029	1.029	1.029
$\varphi_2 = k_{t,j}/k_{t,0}$	1.000	1.779	1.991	2.000	2.000	2.000	2.000
$\varphi_3 = k_{r,j}/k_{r,0}$	1.000	1.511	1.922	1.999	1.999	1.999	2.000
$\ (\Phi_{ref} - \Phi_j)/\Phi_{ref}\ $	1.028	0.393	0.046	0.000	0.000	0.000	
Target Response							
$z_1 = f_1$	10.415	12.692	13.211	13.274	13.274	13.274	13.274
$z_2 = f_2$	20.436	25.499	26.439	26.497	26.496	26.496	26.496
$z_3 = f_3$	38.710	44.872	45.784	45.894	45.893	45.893	45.893
$z_4 = f_4$	74.755	81.494	82.031	82.298	82.298	82.298	82.298
$z_5 = u_1$	0.02688	0.01997	0.01895	0.01877	0.01877	0.01877	0.01877
$z_6 = u_2$	0.01000	0.00562	0.00502	0.00500	0.00500	0.00500	0.00500
$z_7 = \varepsilon_1$	0.000389	0.000348	0.000351	0.000349	0.000349	0.000349	0.000349
$\ (\mathbf{z}_m - \mathbf{z}_j)/\mathbf{z}_m\ $	2.241	0.304	0.033	0.000	0.000	0.000	0.000

D.2 Simple beam results: FE updating with ABAQUS and MATLAB optimization toolbox

Table D.9 Results for the Nelder-Mead simplex algorithm in MATLAB.

Input Parameter	Initial Value	Iteration Number					Measured Values
		1	2	5	20	100	
$\varphi_1 = E_j/E_0$	1.000	1.000	1.000	1.017	1.311	1.029	1.029
$\varphi_2 = k_{t,j}/k_{t,0}$	1.000	1.050	1.050	1.167	2.089	2.000	2.000
$\varphi_3 = k_{r,j}/k_{r,0}$	1.000	1.000	1.000	0.967	0.693	2.000	2.000
$\ (\Phi_{ref} - \Phi_j)/\Phi_{ref}\ $	0.708	0.690	0.690	0.664	0.710	0.000	
Target Response							
$z_1 = f_1$	10.415	10.564	10.564	10.872	12.512	13.274	13.274
$z_2 = f_2$	20.436	20.813	20.813	21.692	27.709	26.496	26.496
$z_3 = f_3$	38.710	39.060	39.060	39.979	47.964	45.893	45.893
$z_4 = f_4$	74.755	74.955	74.955	75.699	84.739	82.298	82.298
$z_5 = u_1$	0.02688	0.02641	0.02641	0.02543	0.02063	0.01877	0.01877
$z_6 = u_2$	0.01000	0.00952	0.00952	0.00857	0.00479	0.00500	0.00500
$z_7 = \varepsilon_1$	0.000389	0.000389	0.000389	0.000386	0.000330	0.000349	0.000349
$\ (\mathbf{z}_m - \mathbf{z}_j)/\mathbf{z}_m\ $	1.154	1.056	1.056	0.858	0.151	0.000	0.000

Appendix E. New Svinesund Bridge Bearing Friction Study

In order to determine the proper boundary conditions and internal constraints, a parametric study of the bearings was performed. Karoumi and Andersson (2006) strongly recommend updating and enhancement of a developed FE model due to poor agreement between the measured response and the initial FE model for some load cases. Specifically, the simplified modelling of the boundary conditions in the initial FE model is suspect and further study was recommended.

During preliminary analysis, the bridge designers verified the global system in the ULS and SLS with regard to the frictional forces in the bearings according to BRO 94 21.24. The analysis performed was to verify the structural integrity for the worst case loading condition including bearing friction. Such analysis is required during design, but the assumptions made did not reflect the actual bearing conditions during experimental load testing.

In order to investigate the actual behaviour of the bearings for each load case, the magnitude of the frictional force at each bearing was calculated and compared with the sectional force of the bearing element. The bearing friction coefficient (material: MSM) was calculated according to the bearing manufacturer. According the bearing manufacturer, MSM performs better for continuous loads at low temperatures, large bearing displacements and fast sliding velocities than conventional PTFE. The equations provided by the bearing manufacturer are for calculating the bearing friction coefficient at a sliding speed of 15 mm/s, no data was published for the static friction coefficient. The sliding friction coefficient was therefore used as an initial guess for calculating the static friction coefficient.

During load testing, the air temperature ranged from about 10° C to 15° C while the road temperature ranged from about 5° C to 25° C, therefore the equation for the bearing friction coefficient for temperatures above -5° C was used. According to the bearing manufacturer, MAURER SÖHNE (2007), the maximum bearing frictional coefficient for temperatures above -5° C may be calculated as,

$$0.015 \leq \mu_{\max} = \frac{1.2}{15 + \sigma_{MSM} [MPa]} \leq 0.06 \quad 9.1$$

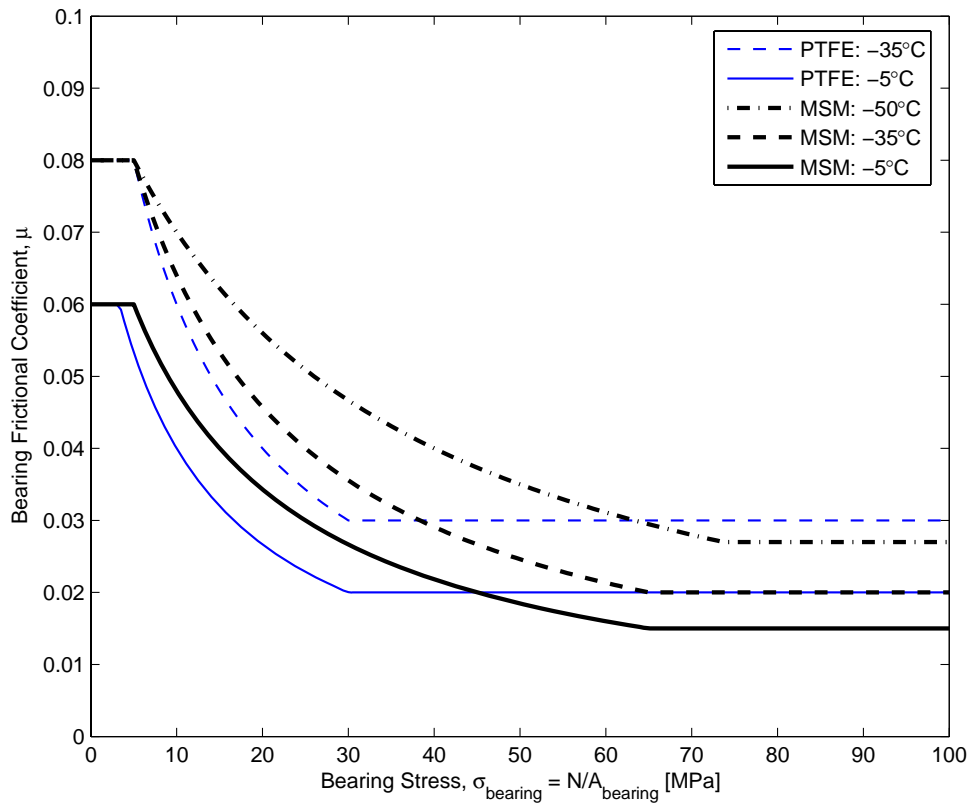


Figure E.1 Variation of bearing frictional coefficient according to bearing manufacturer.

The normal force in each pier bearing is equal to the normal force in each bearing element calculated during gravitational loading and half of the prestressing force for the pier. The normal force in the bearings at the abutment is equal to the normal force in the abutment bearing element calculated during gravitational loading.

$$N = F_{grav} + F_{prestess} \quad 9.2$$

$$\sigma_{bearing} = \frac{N}{A_{bearing}} \quad 9.3$$

Table E.1 Normal force in bearings.

	Gravity [kN]	Prestress [kN]	Normal Force [kN]	Bearing Stress [MPa]	μ_{static}	F_{static} [kN]
Abut 1:	1155		1155	3.2	6.0%	69.3
	1440		1440	4.0	6.0%	86.4
	1256		1256	3.5	6.0%	75.4
	1497		1497	4.2	6.0%	89.8
Pier 2:	5739	4860	10599	29.4	2.7%	286.2
	5987	4860	10847	30.1	2.7%	288.4
Pier 3:	5908	7290	13198	36.7	2.3%	306.6
	6170	7290	13460	37.4	2.3%	308.3
Pier 4:	5880	7290	13170	36.6	2.3%	306.4
	6138	7290	13428	37.3	2.3%	308.1
Pier 5:	5665	10400	16065	44.6	2.0%	323.3
	5967	10400	16367	45.5	2.0%	324.8
Pier 8:	4846	7290	12136	33.7	2.5%	299.0
	5475	7290	12765	35.5	2.4%	303.6
Abut 2:	912		912	2.5	6.0%	54.7
	1149		1149	3.2	6.0%	68.9
	1205		1205	3.3	6.0%	72.3
	1513		1513	4.2	6.0%	90.8

The maximum bearing friction coefficient as specified by the bearing manufacturer is used to calculate an initial guess for the bearing static friction force threshold,

$$F_{\text{static}} = N \cdot \mu_{\text{max}} \quad 9.4$$

The bearing static moment threshold is calculated using the static friction force threshold and the radius of curvature of the bearing,

$$M_{static} = F_{static} \cdot r \quad 9.5$$

The following plots and tables show the static friction force threshold and static friction moment threshold as well as the bearing resultant force and bearing resultant moment,

$$F_{bearing} = \sqrt{F_{bearing, longitudinal}^2 + F_{bearing, transversal}^2} \quad 9.6$$

$$M_{bearing} = \sqrt{M_{bearing, longitudinal}^2 + M_{bearing, transversal}^2} \quad 9.7$$

For all loading cases where the bearing resultant force was on the same order of magnitude as the bearing static friction force threshold, the bearing resultant moment far exceeded the static friction moment threshold. This is evident in the plots below. Thus the bearing static friction force threshold was the governing factor for the structural behaviour of the bearings during the load tests.

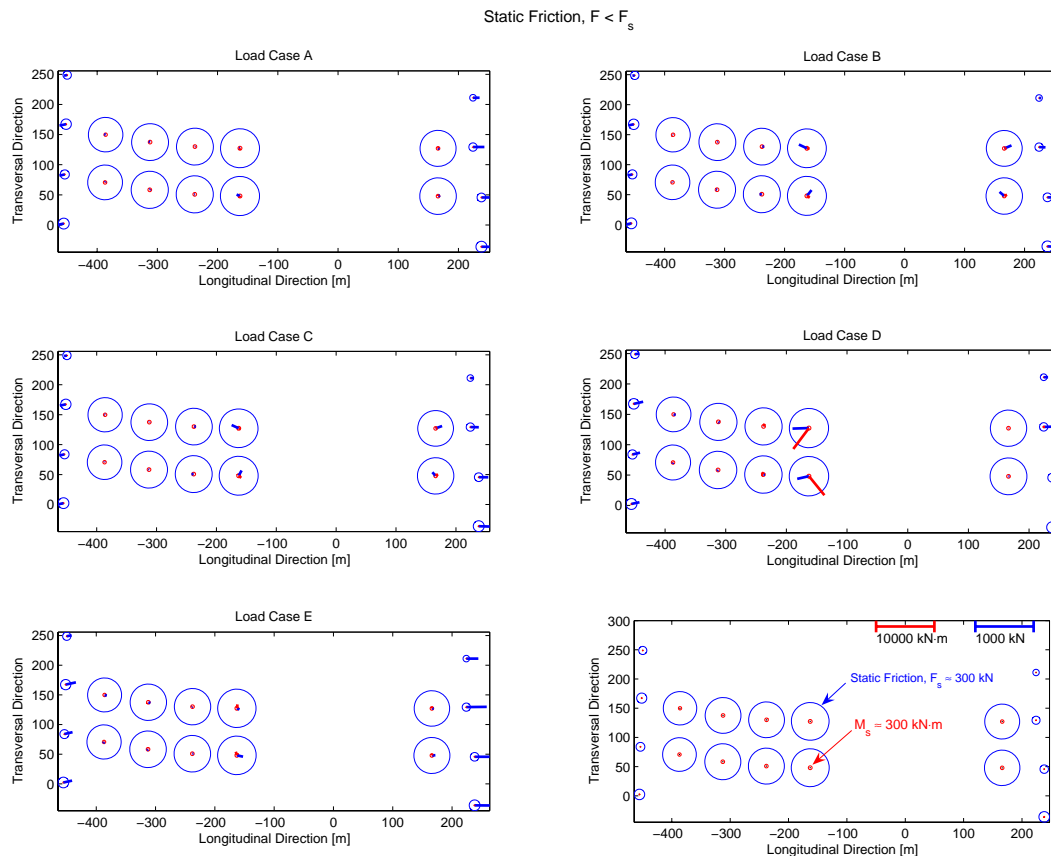


Figure E.2 Plot of bearing forces and moments and static friction threshold for bearing condition TIE.

Table E.2 Bearing forces and bearing static friction force threshold for all load cases for bearing condition TIE.

Static Friction, $F < F_s$											
Load Case:	A			B		C		D		E	
	F_{static} [kN]	$F_{bearing}$ [kN]	$\frac{F_{bearing}}{F_{static}}$								
Abut 1:	69	275	398%	54	78%	50	72%	75	109%	84	121%
	86	261	302%	113	131%	104	121%	158	183%	176	203%
	75	237	314%	92	121%	89	119%	128	170%	142	188%
	90	216	241%	97	108%	94	104%	136	151%	151	168%
Pier 2:	286	160	56%	25	9%	14	5%	35	12%	39	14%
	288	22	8%	18	6%	11	4%	23	8%	29	10%
Pier 3:	307	16	5%	23	8%	9	3%	24	8%	37	12%
	308	29	9%	17	5%	14	5%	21	7%	27	9%
Pier 4:	306	47	15%	10	3%	33	11%	4	1%	17	5%
	308	54	17%	13	4%	37	12%	27	9%	20	6%
Pier 5:	323	171	53%	19	6%	130	40%	270	84%	48	15%
	325	75	23%	62	19%	100	31%	199	61%	107	33%
Pier 8:	299	172	58%	25	8%	116	39%	4	1%	32	11%
	304	56	19%	37	12%	81	27%	16	5%	59	20%
Abut 2:	55	536	979%	109	198%	60	109%	72	131%	203	370%
	69	567	823%	189	274%	142	206%	122	177%	345	501%
	72	453	627%	137	189%	159	221%	90	124%	251	348%
	91	447	492%	137	151%	183	202%	92	101%	255	280%

Abutments, $F > F_s = 0$ Piers, $F < F_s$

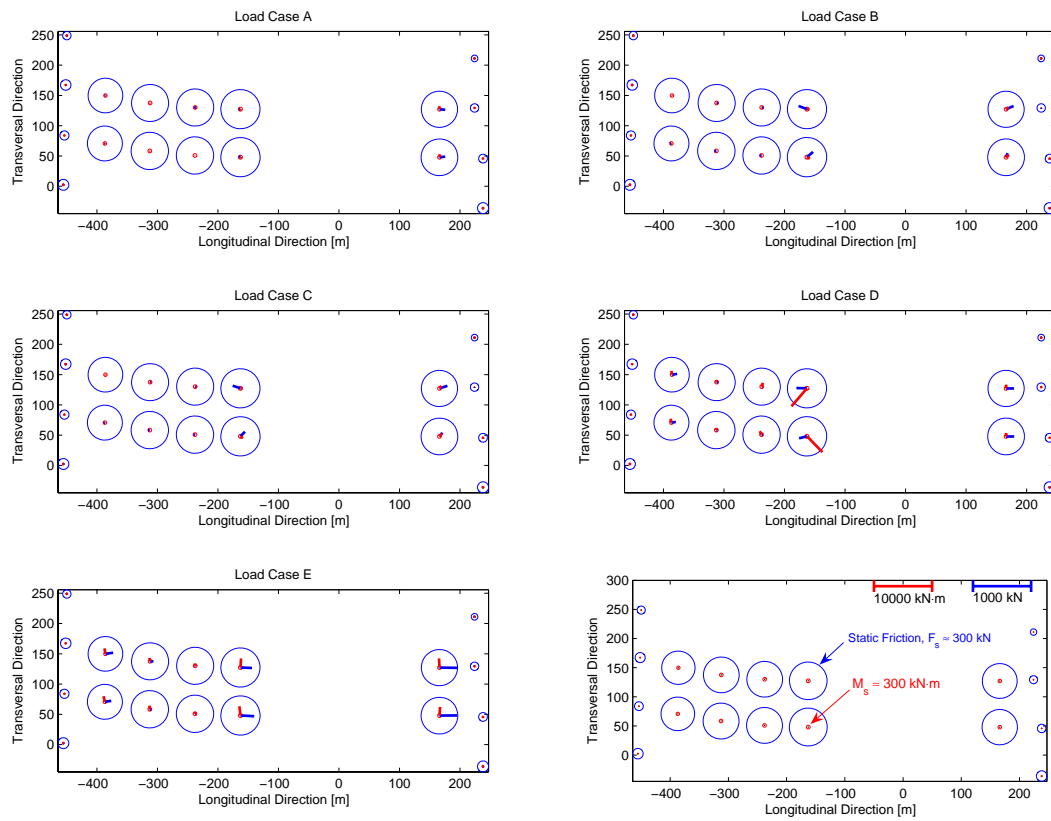


Figure E.3 Plot of bearing forces and moments and static friction threshold for bearing condition PIER TIE.

Table E.3 Bearing forces and bearing static friction force threshold for all load cases for bearing condition PIER TIE.

Abutments, $F > F_s = 0$		Piers, $F < F_s$									
Load Case:	A			B		C		D		E	
	F_{static} [kN]	$F_{bearing}$ [kN]	$\frac{F_{bearing}}{F_{static}}$								
Abut 1:	69	0	0%	0	0%	0	0%	0	0%	0	0%
	86	14	16%	1	1%	0	0%	3	3%	4	5%
	75	4	5%	1	1%	1	1%	3	4%	4	6%
	90	0	0%	0	0%	0	0%	0	0%	0	0%
Pier 2:	286	123	43%	16	6%	3	1%	85	30%	128	45%
	288	265	92%	14	5%	26	9%	74	26%	106	37%
Pier 3:	307	54	17%	7	2%	19	6%	26	8%	56	18%
	308	41	13%	4	1%	29	9%	22	7%	29	9%
Pier 4:	306	37	12%	1	0%	25	8%	15	5%	12	4%
	308	32	10%	3	1%	28	9%	24	8%	24	8%
Pier 5:	323	160	49%	30	9%	135	42%	176	54%	191	59%
	325	118	36%	32	10%	106	33%	136	42%	228	70%
Pier 8:	299	152	51%	97	33%	138	46%	131	44%	298	100%
	304	238	79%	94	31%	79	26%	134	44%	296	98%
Abut 2:	55	0	0%	0	0%	0	0%	0	0%	0	0%
	69	11	16%	2	3%	11	16%	6	9%	13	18%
	72	1	1%	2	3%	14	19%	5	7%	10	14%
	91	0	0%	0	0%	0	0%	0	0%	0	0%

Abutments and Piers 5 & 8, $F > F_s = 0$ Piers 2,3 & 4, $F < F_s$

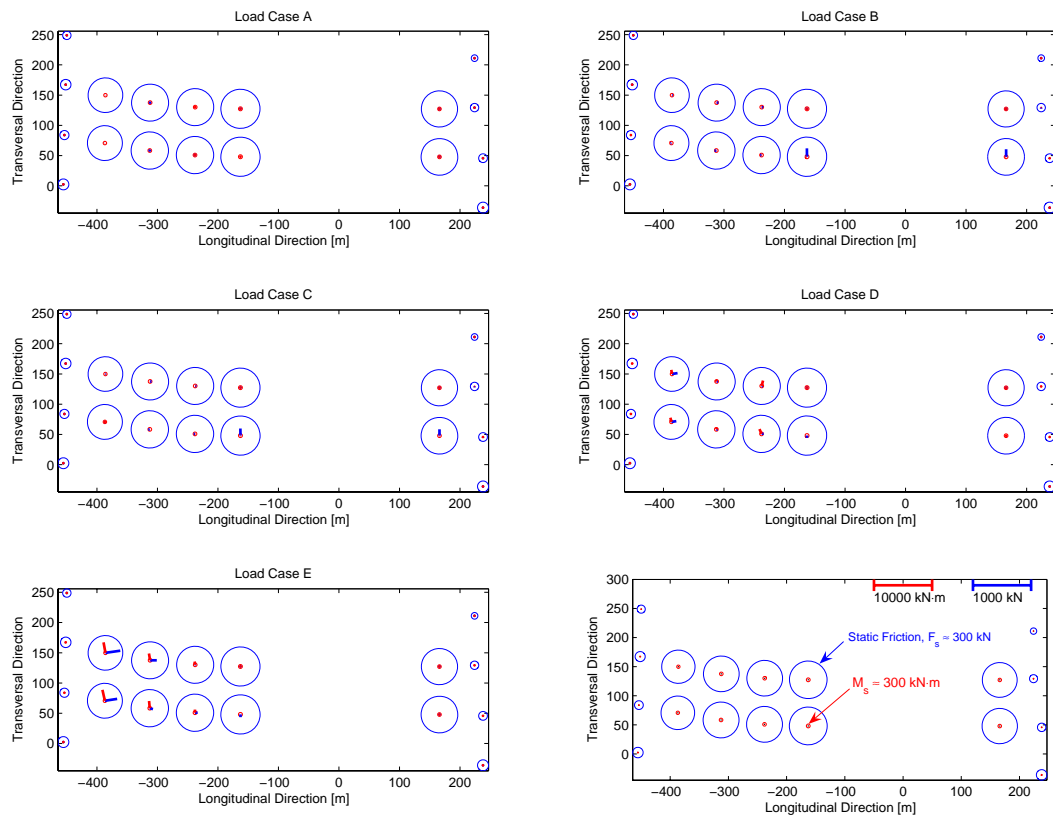


Figure E.4 Plot of bearing forces and moments and static friction threshold for bearing condition PIER TIE 58 FREE.

Table E.4 Bearing forces and bearing static friction force threshold for all load cases for bearing condition PIER TIE 58 FREE.

Abutments and Piers 5 & 8, $F > F_s = 0$		Piers 2,3 & 4, $F < F_s$									
Load Case:	A			B		C		D		E	
	F_{static} [kN]	$F_{bearing}$ [kN]	$\frac{F_{bearing}}{F_{static}}$	$F_{bearing}$ [kN]	$\frac{F_{bearing}}{F_{static}}$	$F_{bearing}$ [kN]	$\frac{F_{bearing}}{F_{static}}$	$F_{bearing}$ [kN]	$\frac{F_{bearing}}{F_{static}}$	$F_{bearing}$ [kN]	$\frac{F_{bearing}}{F_{static}}$
Abut 1:	69	0	0%	0	0%	0	0%	0	0%	0	0%
	86	12	14%	0	0%	0	0%	3	4%	8	10%
	75	2	2%	0	0%	0	1%	3	4%	8	11%
	90	0	0%	0	0%	0	0%	0	0%	0	0%
Pier 2:	286	131	46%	2	1%	10	4%	92	32%	248	87%
	288	253	88%	2	1%	14	5%	81	28%	205	71%
Pier 3:	307	65	21%	1	0%	24	8%	22	7%	111	36%
	308	41	13%	1	0%	25	8%	25	8%	55	18%
Pier 4:	306	27	9%	1	0%	21	7%	19	6%	10	3%
	308	13	4%	1	0%	21	7%	34	11%	43	14%
Pier 5:	323	0	0%	0	0%	0	0%	0	0%	0	0%
	325	15	4%	2	0%	118	36%	38	12%	45	14%
Pier 8:	299	0	0%	0	0%	0	0%	0	0%	0	0%
	304	77	25%	1	0%	107	35%	0	0%	1	0%
Abut 2:	55	0	0%	0	0%	0	0%	0	0%	0	0%
	69	32	47%	1	2%	15	22%	1	1%	2	2%
	72	13	19%	1	1%	11	15%	1	1%	1	2%
	91	0	0%	0	0%	0	0%	0	0%	0	0%

Appendix F. Model Evolution

F.1 Eigenfrequencies

Table F.1 Eigenfrequencies 1-4 from experimental measurements and nine modified FE models.

Eigenfrequency, Response [Hz]											
z_m	z_0	z_{1A}	z_{1B}	z_{1C}	z_{1D}	z_2	z_3	z_4	z_5	z_6	z_7
0.4249	0.4085	0.4121	0.4121	0.4121	0.4121	0.4306	0.4250	0.4259	0.4068	0.4253	0.4253
0.8459	0.5205	0.8614	0.8614	0.8614	0.8614	0.8972	0.8518	0.8582	0.8135	0.8531	0.8531
0.9402	0.9571	0.9608	0.9608	0.9608	0.9608	0.9999	0.9354	0.9388	0.9083	0.9366	0.9366
0.9988	1.0221	1.0323	1.0323	1.0323	1.0323	1.0616	0.9851	0.9876	0.9489	0.9871	0.9871

Table F.2 Eigenfrequencies 1-4 from experimental measurements compared with the improved models absolute error

Eigenfrequency, Absolute error [Hz]										
$ z_m - z_0 $	$ z_m - z_{1A} $	$ z_m - z_{1B} $	$ z_m - z_{1C} $	$ z_m - z_{1D} $	$ z_m - z_2 $	$ z_m - z_3 $	$ z_m - z_4 $	$ z_m - z_5 $	$ z_m - z_6 $	$ z_m - z_7 $
0.0164	0.0127	0.0127	0.0127	0.0127	0.0057	0.0002	0.0011	0.0181	0.0005	0.0005
0.3254	0.0156	0.0156	0.0156	0.0156	0.0513	0.0060	0.0123	0.0323	0.0073	0.0073
0.0169	0.0206	0.0206	0.0206	0.0206	0.0597	0.0047	0.0014	0.0318	0.0036	0.0036
0.0233	0.0335	0.0335	0.0335	0.0335	0.0628	0.0137	0.0112	0.0499	0.0118	0.0118

Table F.3 Eigenfrequencies 1-4 from experimental measurements compared with the improved models relative error

Eigenfrequency, Relative Error										
$\frac{ z_m - z_0 }{\max(z_m)}$	$\frac{ z_m - z_{1A} }{\max(z_m)}$	$\frac{ z_m - z_{1B} }{\max(z_m)}$	$\frac{ z_m - z_{1C} }{\max(z_m)}$	$\frac{ z_m - z_{1D} }{\max(z_m)}$	$\frac{ z_m - z_2 }{\max(z_m)}$	$\frac{ z_m - z_3 }{\max(z_m)}$	$\frac{ z_m - z_4 }{\max(z_m)}$	$\frac{ z_m - z_5 }{\max(z_m)}$	$\frac{ z_m - z_6 }{\max(z_m)}$	$\frac{ z_m - z_7 }{\max(z_m)}$
1.6%	1.3%	1.3%	1.3%	1.3%	0.6%	0.0%	0.1%	1.8%	0.0%	0.0%
32.6%	1.6%	1.6%	1.6%	1.6%	5.1%	0.6%	1.2%	3.2%	0.7%	0.7%
1.7%	2.1%	2.1%	2.1%	2.1%	6.0%	0.5%	0.1%	3.2%	0.4%	0.4%
2.3%	3.4%	3.4%	3.4%	3.4%	6.3%	1.4%	1.1%	5.0%	1.2%	1.2%

F.2 Strains

Table F.4 Strain at the foundation measured and computed responses for load cases A, B, C, D, E in ascending order, section S1

Strain at foundation of the arch on the Swedish side [$\mu\text{m}/\text{m}$]												
	z_m	z_0	z_{1A}	z_{1B}	z_{1C}	z_{1D}	z_2	z_3	z_4	z_5	z_6	z_7
A	-0.96	-1.69	-1.69	-2.59	-3.29	-1.48	-2.58	-2.58	-2.58	-2.53	-1.90	-2.02
	-2.63	-2.16	-2.16	-1.30	-0.63	-2.36	-1.08	-1.08	-1.08	-1.36	-1.73	-1.63
	-2.13	-1.98	-1.98	-1.99	-2.00	-1.97	-1.88	-1.88	-1.88	-1.99	-1.86	-1.88
	-2.19	-1.88	-1.88	-1.90	-1.93	-1.87	-1.79	-1.79	-1.79	-1.90	-1.77	-1.77
B	-0.92	-2.48	-2.48	-3.22	-3.81	-2.33	-3.14	-3.14	-3.14	-2.67	-2.08	-2.20
	-0.69	-1.56	-1.56	-0.85	-0.29	-1.70	-0.69	-0.69	-0.69	-1.37	-1.70	-1.60
	7.82	6.12	6.12	5.98	5.88	6.12	5.86	5.86	5.86	6.05	6.02	6.11
	-10.08	-10.16	-10.16	-10.05	-9.98	-10.15	-9.69	-9.69	-9.69	-10.10	-9.81	-9.91
C	-2.54	-1.89	-1.89	-2.75	-3.42	-1.69	-2.73	-2.73	-2.73	-2.57	-1.95	-2.07
	-0.41	-2.01	-2.01	-1.19	-0.54	-2.20	-0.98	-0.98	-0.98	-1.36	-1.72	-1.62
	6.26	4.95	4.95	4.82	4.74	4.94	4.74	4.74	4.74	4.87	4.87	4.94
	-9.55	-8.85	-8.85	-8.76	-8.71	-8.83	-8.44	-8.44	-8.44	-8.80	-8.54	-8.63
D	13.17	11.12	11.12	10.05	6.29	8.93	9.66	9.66	9.66	2.55	6.02	3.79
	-14.71	-14.31	-14.31	-13.06	-9.52	-12.25	-12.47	-12.47	-12.47	-5.98	-9.00	-7.18
	-2.67	-1.26	-1.26	-1.23	-1.31	-1.31	-1.14	-1.14	-1.14	-1.36	-1.19	-1.34
	-2.16	-1.93	-1.93	-1.78	-1.92	-2.01	-1.67	-1.67	-1.67	-2.07	-1.79	-2.05
E	9.16	16.93	16.93	1.30	-6.20	10.01	1.77	1.77	1.77	-2.94	3.07	3.61
	-14.11	-22.08	-22.08	-7.60	-0.53	-15.62	-7.65	-7.65	-7.65	-3.63	-8.87	-9.25
	-4.49	-2.77	-2.77	-3.28	-3.43	-2.91	-3.06	-3.06	-3.06	-3.36	-3.02	-2.97
	-2.79	-2.39	-2.39	-3.03	-3.30	-2.70	-2.82	-2.82	-2.82	-3.21	-2.77	-2.67

Table F.5 Absolute error, at the foundation of the arch on the Swedish side for load cases A, B, C, D, E in ascending order, section S1

Absolute Error [$\mu\text{m}/\text{m}$]											
	$ z_m - z_0 $	$ z_m - z_{1A} $	$ z_m - z_{1B} $	$ z_m - z_{1C} $	$ z_m - z_{1D} $	$ z_m - z_2 $	$ z_m - z_3 $	$ z_m - z_4 $	$ z_m - z_5 $	$ z_m - z_6 $	$ z_m - z_7 $
A	0.73	0.73	1.63	2.34	0.52	1.63	1.63	1.63	1.57	0.94	1.07
	0.46	0.46	1.32	2.00	0.27	1.55	1.55	1.55	1.27	0.89	1.00
	0.16	0.16	0.14	0.14	0.16	0.26	0.26	0.26	0.15	0.27	0.25
	0.31	0.31	0.29	0.26	0.32	0.40	0.40	0.40	0.29	0.42	0.42
B	1.56	1.56	2.30	2.88	1.40	2.22	2.22	2.22	1.75	1.16	1.27
	0.88	0.88	0.16	0.39	1.02	0.01	0.01	0.01	0.69	1.01	0.92
	1.70	1.70	1.84	1.94	1.70	1.96	1.96	1.96	1.77	1.80	1.71
	0.09	0.09	0.03	0.09	0.07	0.38	0.38	0.38	0.02	0.27	0.17
C	0.65	0.65	0.21	0.88	0.85	0.19	0.19	0.19	0.03	0.59	0.46
	1.61	1.61	0.78	0.14	1.79	0.57	0.57	0.57	0.95	1.32	1.21
	1.32	1.32	1.44	1.52	1.32	1.53	1.53	1.53	1.39	1.39	1.33
	0.70	0.70	0.79	0.84	0.72	1.11	1.11	1.11	0.75	1.01	0.92
D	2.05	2.05	3.12	6.88	4.24	3.52	3.52	3.52	10.62	7.15	9.38
	0.40	0.40	1.65	5.19	2.46	2.24	2.24	2.24	8.73	5.71	7.53
	1.41	1.41	1.44	1.36	1.36	1.53	1.53	1.53	1.31	1.48	1.34
	0.23	0.23	0.37	0.24	0.14	0.48	0.48	0.48	0.09	0.37	0.10
E	7.76	7.76	7.87	15.36	0.85	7.39	7.39	7.39	12.11	6.09	5.56
	7.97	7.97	6.51	13.58	1.51	6.46	6.46	6.46	10.48	5.24	4.86
	1.72	1.72	1.21	1.06	1.58	1.43	1.43	1.43	1.13	1.47	1.52
	0.41	0.41	0.23	0.50	0.10	0.03	0.03	0.03	0.42	0.02	0.12

Table F.6 Relative error, at the foundation of the arch on the Swedish side, section S1

Relative Error											
	$\frac{ z_m - z_{0I} }{\max(z_m)}$	$\frac{ z_m - z_{1A} }{\max(z_m)}$	$\frac{ z_m - z_{1B} }{\max(z_m)}$	$\frac{ z_m - z_{1C} }{\max(z_m)}$	$\frac{ z_m - z_{1D} }{\max(z_m)}$	$\frac{ z_m - z_{2I} }{\max(z_m)}$	$\frac{ z_m - z_{2J} }{\max(z_m)}$	$\frac{ z_m - z_{3I} }{\max(z_m)}$	$\frac{ z_m - z_{3J} }{\max(z_m)}$	$\frac{ z_m - z_{4I} }{\max(z_m)}$	$\frac{ z_m - z_{4J} }{\max(z_m)}$
A	2.3%	2.3%	5.0%	7.2%	1.6%	5.0%	5.0%	5.0%	4.9%	2.9%	3.3%
	1.4%	1.4%	4.1%	6.2%	0.8%	4.8%	4.8%	4.8%	3.9%	2.8%	3.1%
	0.5%	0.5%	0.4%	0.4%	0.5%	0.8%	0.8%	0.8%	0.4%	0.8%	0.8%
	1.0%	1.0%	0.9%	0.8%	1.0%	1.2%	1.2%	1.2%	0.9%	1.3%	1.3%
B	4.8%	4.8%	7.1%	8.9%	4.3%	6.9%	6.9%	6.9%	5.4%	3.6%	3.9%
	2.7%	2.7%	0.5%	1.2%	3.1%	0.0%	0.0%	0.0%	2.1%	3.1%	2.8%
	5.3%	5.3%	5.7%	6.0%	5.3%	6.1%	6.1%	6.1%	5.5%	5.6%	5.3%
	0.3%	0.3%	0.1%	0.3%	0.2%	1.2%	1.2%	1.2%	0.1%	0.8%	0.5%
C	2.0%	2.0%	0.6%	2.7%	2.6%	0.6%	0.6%	0.6%	0.1%	1.8%	1.4%
	5.0%	5.0%	2.4%	0.4%	5.5%	1.8%	1.8%	1.8%	3.0%	4.1%	3.7%
	4.1%	4.1%	4.5%	4.7%	4.1%	4.7%	4.7%	4.7%	4.3%	4.3%	4.1%
	2.2%	2.2%	2.4%	2.6%	2.2%	3.4%	3.4%	3.4%	2.3%	3.1%	2.8%
D	6.3%	6.3%	9.6%	21.3%	13.1%	10.9%	10.9%	10.9%	32.8%	22.1%	29.0%
	1.2%	1.2%	5.1%	16.0%	7.6%	6.9%	6.9%	6.9%	27.0%	17.7%	23.3%
	4.4%	4.4%	4.5%	4.2%	4.2%	4.7%	4.7%	4.7%	4.1%	4.6%	4.1%
	0.7%	0.7%	1.1%	0.7%	0.4%	1.5%	1.5%	1.5%	0.3%	1.1%	0.3%
E	24.0%	24.0%	24.3%	47.5%	2.6%	22.8%	22.8%	22.8%	37.4%	18.8%	17.2%
	24.6%	24.6%	20.1%	42.0%	4.7%	20.0%	20.0%	20.0%	32.4%	16.2%	15.0%
	5.3%	5.3%	3.7%	3.3%	4.9%	4.4%	4.4%	4.4%	3.5%	4.5%	4.7%
	1.3%	1.3%	0.7%	1.6%	0.3%	0.1%	0.1%	0.1%	1.3%	0.1%	0.4%

Table F.7 Strain at the connection Arch/Carriageway, measured and computed responses for load cases A, B, C, D, E in ascending order, section S6

Strain at Connection of the arch and the Carrigeway, Swedish side [$\mu\text{m}/\text{m}$]												
	z_m	z_0	z_{1A}	z_{1B}	z_{1C}	z_{1D}	z_2	z_3	z_4	z_5	z_6	z_7
A	-7.52	-7.44	-7.44	-7.42	-7.63	-7.45	-6.82	-6.82	-6.82	-7.89	-7.09	-7.11
	1.68	2.07	2.07	1.99	2.14	2.11	1.87	1.87	1.87	2.46	2.19	2.19
	-3.07	-2.73	-2.73	-2.76	-2.79	-2.71	-2.52	-2.52	-2.52	-2.75	-2.48	-2.50
	-2.31	-2.64	-2.64	-2.67	-2.70	-2.63	-2.44	-2.44	-2.44	-2.67	-2.41	-2.43
B	-7.86	-4.71	-4.71	-4.70	-4.86	-4.72	-4.31	-4.31	-4.31	-5.19	-4.62	-4.63
	-1.54	-0.96	-0.96	-1.03	-0.91	-0.94	-0.91	-0.91	-0.91	-0.49	-0.51	-0.52
	16.27	14.21	14.21	14.10	14.04	14.22	12.92	12.92	12.92	14.33	13.19	13.24
	-21.43	-19.88	-19.88	-19.83	-19.82	-19.87	-18.14	-18.14	-18.14	-20.01	-18.32	-18.39
C	-8.22	-6.84	-6.84	-6.82	-7.02	-6.85	-6.26	-6.26	-6.26	-7.30	-6.55	-6.58
	0.76	1.40	1.40	1.32	1.46	1.43	1.24	1.24	1.24	1.82	1.60	1.59
	13.22	11.71	11.71	11.60	11.55	11.72	10.63	10.63	10.63	11.79	10.86	10.89
	-18.05	-17.15	-17.15	-17.11	-17.11	-17.14	-15.65	-15.65	-15.65	-17.28	-15.81	-15.88
D	-22.25	-19.42	-19.42	-17.98	-17.63	-19.19	-16.66	-16.66	-16.66	-12.17	-11.98	-12.53
	18.14	15.33	15.33	14.11	13.39	14.88	13.17	13.17	13.17	7.53	8.15	8.12
	-3.47	-1.99	-1.99	-1.88	-2.06	-2.10	-1.69	-1.69	-1.69	-2.27	-1.88	-2.18
	-0.76	-2.10	-2.10	-1.99	-2.18	-2.21	-1.80	-1.80	-1.80	-2.37	-1.95	-2.23
E	17.74	15.05	15.05	14.75	15.23	15.49	13.73	13.73	13.73	13.86	12.06	12.48
	-26.86	-22.19	-22.19	-23.77	-24.98	-23.39	-21.86	-21.86	-21.86	-23.31	-20.03	-20.25
	-2.92	-3.69	-3.69	-4.58	-4.94	-4.05	-4.13	-4.13	-4.13	-4.79	-4.06	-4.02
	-3.62	-3.45	-3.45	-4.43	-4.81	-3.85	-4.00	-4.00	-4.00	-4.66	-3.91	-3.75

Table F.8 Absolute error, at the connection Arch/Carriageway, section S6

Absolute Error [$\mu\text{m}/\text{m}$]											
	$ z_m-z_0 $	$ z_m-z_{1A} $	$ z_m-z_{1B} $	$ z_m-z_{1C} $	$ z_m-z_{1D} $	$ z_m-z_2 $	$ z_m-z_3 $	$ z_m-z_4 $	$ z_m-z_5 $	$ z_m-z_6 $	$ z_m-z_7 $
A	0.08	0.08	0.10	0.11	0.07	0.70	0.70	0.70	0.37	0.43	0.41
	0.39	0.39	0.31	0.46	0.43	0.19	0.19	0.19	0.79	0.51	0.51
	0.34	0.34	0.31	0.28	0.35	0.55	0.55	0.55	0.31	0.58	0.57
	0.33	0.33	0.36	0.39	0.32	0.12	0.12	0.12	0.36	0.10	0.12
B	3.15	3.15	3.16	3.00	3.15	3.56	3.56	3.56	2.67	3.24	3.23
	0.58	0.58	0.51	0.63	0.60	0.63	0.63	0.63	1.05	1.03	1.02
	2.06	2.06	2.17	2.23	2.05	3.35	3.35	3.35	1.94	3.08	3.03
	1.55	1.55	1.61	1.61	1.56	3.29	3.29	3.29	1.42	3.11	3.04
C	1.38	1.38	1.39	1.20	1.37	1.95	1.95	1.95	0.91	1.66	1.64
	0.64	0.64	0.56	0.70	0.67	0.49	0.49	0.49	1.06	0.84	0.84
	1.51	1.51	1.61	1.66	1.50	2.58	2.58	2.58	1.43	2.36	2.32
	0.90	0.90	0.94	0.94	0.92	2.40	2.40	2.40	0.78	2.24	2.17
D	2.83	2.83	4.26	4.61	3.05	5.59	5.59	5.59	10.07	10.27	9.72
	2.81	2.81	4.03	4.75	3.26	4.97	4.97	4.97	10.61	9.98	10.02
	1.48	1.48	1.59	1.40	1.37	1.77	1.77	1.77	1.19	1.59	1.29
	1.34	1.34	1.23	1.42	1.45	1.04	1.04	1.04	1.61	1.19	1.48
E	2.69	2.69	2.99	2.51	2.25	4.01	4.01	4.01	3.89	5.69	5.26
	4.67	4.67	3.09	1.88	3.47	5.00	5.00	5.00	3.56	6.83	6.62
	0.77	0.77	1.66	2.02	1.13	1.21	1.21	1.21	1.87	1.14	1.10
	0.17	0.17	0.81	1.19	0.22	0.37	0.37	0.37	1.04	0.29	0.13

Table F.9 Relative error, at the connection Arch/Carriageway, section S6

Relative Error											
	$\frac{ z_m - z_{0L} }{\max(z_m)}$	$\frac{ z_m - z_{1A} }{\max(z_m)}$	$\frac{ z_m - z_{1B} }{\max(z_m)}$	$\frac{ z_m - z_{1C} }{\max(z_m)}$	$\frac{ z_m - z_{1D} }{\max(z_m)}$	$\frac{ z_m - z_{2L} }{\max(z_m)}$	$\frac{ z_m - z_{3L} }{\max(z_m)}$	$\frac{ z_m - z_{4L} }{\max(z_m)}$	$\frac{ z_m - z_{5L} }{\max(z_m)}$	$\frac{ z_m - z_{6L} }{\max(z_m)}$	$\frac{ z_m - z_{7L} }{\max(z_m)}$
A	0.2%	0.2%	0.3%	0.3%	0.2%	2.2%	2.2%	2.2%	1.1%	1.3%	1.3%
	1.2%	1.2%	1.0%	1.4%	1.3%	0.6%	0.6%	0.6%	2.4%	1.6%	1.6%
	1.1%	1.1%	1.0%	0.9%	1.1%	1.7%	1.7%	1.7%	1.0%	1.8%	1.8%
	1.0%	1.0%	1.1%	1.2%	1.0%	0.4%	0.4%	0.4%	1.1%	0.3%	0.4%
B	9.8%	9.8%	9.8%	9.3%	9.7%	11.0%	11.0%	11.0%	8.3%	10.0%	10.0%
	1.8%	1.8%	1.6%	1.9%	1.9%	1.9%	1.9%	1.9%	3.2%	3.2%	3.2%
	6.4%	6.4%	6.7%	6.9%	6.3%	10.4%	10.4%	10.4%	6.0%	9.5%	9.4%
	4.8%	4.8%	5.0%	5.0%	4.8%	10.2%	10.2%	10.2%	4.4%	9.6%	9.4%
C	4.3%	4.3%	4.3%	3.7%	4.2%	6.0%	6.0%	6.0%	2.8%	5.1%	5.1%
	2.0%	2.0%	1.7%	2.2%	2.1%	1.5%	1.5%	1.5%	3.3%	2.6%	2.6%
	4.7%	4.7%	5.0%	5.1%	4.6%	8.0%	8.0%	8.0%	4.4%	7.3%	7.2%
	2.8%	2.8%	2.9%	2.9%	2.8%	7.4%	7.4%	7.4%	2.4%	6.9%	6.7%
D	8.7%	8.7%	13.2%	14.3%	9.4%	17.3%	17.3%	17.3%	31.1%	31.7%	30.0%
	8.7%	8.7%	12.4%	14.7%	10.1%	15.4%	15.4%	15.4%	32.8%	30.9%	31.0%
	4.6%	4.6%	4.9%	4.3%	4.2%	5.5%	5.5%	5.5%	3.7%	4.9%	4.0%
	4.1%	4.1%	3.8%	4.4%	4.5%	3.2%	3.2%	3.2%	5.0%	3.7%	4.6%
E	8.3%	8.3%	9.2%	7.8%	7.0%	12.4%	12.4%	12.4%	12.0%	17.6%	16.3%
	14.5%	14.5%	9.6%	5.8%	10.7%	15.5%	15.5%	15.5%	11.0%	21.1%	20.5%
	2.4%	2.4%	5.1%	6.2%	3.5%	3.8%	3.8%	3.8%	5.8%	3.5%	3.4%
	0.5%	0.5%	2.5%	3.7%	0.7%	1.2%	1.2%	1.2%	3.2%	0.9%	0.4%

Table F.10 Strain at the Arch/Midpoint, measured and computed responses for load cases A, B, C, D, E in ascending order, section S25

Strain at Midpoint of the arch [$\mu\text{m}/\text{m}$]												
	z_m	z_0	z_{1A}	z_{1B}	z_{1C}	z_{1D}	z_2	z_3	z_4	z_5	z_6	z_7
A	-32.35	-38.00	-38.00	-37.81	-37.50	-38.01	-33.81	-33.81	-33.81	-37.49	-33.81	-33.82
	13.25	16.54	16.54	16.25	15.79	16.54	15.49	15.49	15.49	15.76	15.46	15.48
	-10.72	-11.39	-11.39	-11.43	-11.49	-11.39	-9.75	-9.75	-9.75	-11.50	-9.77	-9.76
	-9.53	-11.44	-11.44	-11.48	-11.55	-11.44	-9.80	-9.80	-9.80	-11.56	-9.82	-9.81
B	-21.44	-24.89	-24.89	-24.74	-24.49	-24.89	-22.04	-22.04	-22.04	-24.47	-22.03	-22.03
	3.99	5.21	5.21	4.98	4.63	5.21	5.22	5.22	5.22	4.56	5.17	5.18
	-10.30	-10.65	-10.65	-10.69	-10.71	-10.65	-9.13	-9.13	-9.13	-10.78	-9.20	-9.19
	-6.60	-9.79	-9.79	-9.82	-9.89	-9.79	-8.37	-8.37	-8.37	-9.86	-8.34	-8.34
C	-29.41	-34.61	-34.61	-34.43	-34.13	-34.61	-30.77	-30.77	-30.77	-34.12	-30.77	-30.77
	10.58	13.50	13.50	13.22	12.79	13.50	12.75	12.75	12.75	12.76	12.71	12.73
	-11.29	-11.59	-11.59	-11.63	-11.66	-11.59	-9.93	-9.93	-9.93	-11.72	-9.99	-9.98
	-7.96	-10.73	-10.73	-10.77	-10.85	-10.73	-9.18	-9.18	-9.18	-10.82	-9.15	-9.15
D	-1.02	-0.88	-0.88	-0.62	-0.47	-0.83	-0.59	-0.59	-0.59	-0.46	-0.62	-0.70
	2.20	2.16	2.16	1.70	1.53	2.12	1.50	1.50	1.50	1.71	1.71	1.96
	0.52	0.61	0.61	0.51	0.49	0.60	0.42	0.42	0.42	0.57	0.50	0.59
	0.34	0.61	0.61	0.52	0.52	0.61	0.43	0.43	0.43	0.62	0.52	0.60
E	-0.32	-0.58	-0.58	0.19	0.71	-0.44	0.28	0.28	0.28	0.72	0.27	0.23
	-4.45	-5.65	-5.65	-6.56	-7.24	-5.77	-5.74	-5.74	-5.74	-7.35	-5.83	-5.78
	-1.83	-3.04	-3.04	-3.12	-3.19	-3.05	-2.67	-2.67	-2.67	-3.24	-2.71	-2.70
	-2.33	-3.07	-3.07	-3.09	-3.14	-3.03	-2.65	-2.65	-2.65	-3.19	-2.69	-2.71

Table F.11 Strain absolute error Arch/Midpoint, measured and computed responses for load cases A, B, C, D, E in ascending order, section S25

Absolute Error [$\mu\text{m/m}$]											
	$ z_m-z_0 $	$ z_m-z_{1A} $	$ z_m-z_{1B} $	$ z_m-z_{1C} $	$ z_m-z_{1D} $	$ z_m-z_2 $	$ z_m-z_3 $	$ z_m-z_4 $	$ z_m-z_5 $	$ z_m-z_6 $	$ z_m-z_7 $
A	5.66	5.66	5.46	5.15	5.66	1.47	1.47	1.47	5.15	1.46	1.47
	3.29	3.29	3.00	2.55	3.30	2.25	2.25	2.25	2.52	2.21	2.24
	0.67	0.67	0.71	0.77	0.67	0.97	0.97	0.97	0.78	0.95	0.96
	1.90	1.90	1.95	2.01	1.90	0.27	0.27	0.27	2.03	0.28	0.27
B	3.45	3.45	3.30	3.05	3.45	0.60	0.60	0.60	3.03	0.59	0.59
	1.22	1.22	1.00	0.64	1.22	1.24	1.24	1.24	0.58	1.18	1.19
	0.35	0.35	0.38	0.40	0.35	1.17	1.17	1.17	0.47	1.10	1.11
	3.19	3.19	3.22	3.29	3.19	1.77	1.77	1.77	3.26	1.74	1.74
C	5.20	5.20	5.01	4.72	5.20	1.36	1.36	1.36	4.71	1.36	1.36
	2.92	2.92	2.64	2.21	2.92	2.17	2.17	2.17	2.18	2.13	2.16
	0.29	0.29	0.34	0.37	0.29	1.36	1.36	1.36	0.42	1.30	1.31
	2.77	2.77	2.81	2.89	2.78	1.22	1.22	1.22	2.87	1.20	1.20
D	0.14	0.14	0.40	0.55	0.19	0.43	0.43	0.43	0.56	0.39	0.32
	0.04	0.04	0.50	0.67	0.08	0.70	0.70	0.70	0.49	0.49	0.24
	0.09	0.09	0.01	0.03	0.08	0.09	0.09	0.09	0.06	0.01	0.07
	0.27	0.27	0.18	0.18	0.28	0.09	0.09	0.09	0.28	0.18	0.26
E	0.26	0.26	0.51	1.03	0.12	0.60	0.60	0.60	1.04	0.60	0.55
	1.20	1.20	2.11	2.79	1.32	1.29	1.29	1.29	2.90	1.38	1.33
	1.21	1.21	1.28	1.36	1.22	0.83	0.83	0.83	1.41	0.88	0.86
	0.74	0.74	0.76	0.81	0.70	0.31	0.31	0.31	0.86	0.36	0.38

Table F.12 Strain relative error Arch/Midpoint, measured and computed responses for, measured and computed responses for load cases A, B, C, D, E in ascending order, section S25

Relative Error											
	$\frac{ z_m - z_0 }{\max(z_m)}$	$\frac{ z_m - z_{1A} }{\max(z_m)}$	$\frac{ z_m - z_{1B} }{\max(z_m)}$	$\frac{ z_m - z_{1C} }{\max(z_m)}$	$\frac{ z_m - z_{1D} }{\max(z_m)}$	$\frac{ z_m - z_2 }{\max(z_m)}$	$\frac{ z_m - z_3 }{\max(z_m)}$	$\frac{ z_m - z_4 }{\max(z_m)}$	$\frac{ z_m - z_5 }{\max(z_m)}$	$\frac{ z_m - z_6 }{\max(z_m)}$	$\frac{ z_m - z_7 }{\max(z_m)}$
A	17.5%	17.5%	16.9%	15.9%	17.5%	4.5%	4.5%	4.5%	15.9%	4.5%	4.6%
	10.2%	10.2%	9.3%	7.9%	10.2%	6.9%	6.9%	6.9%	7.8%	6.8%	6.9%
	2.1%	2.1%	2.2%	2.4%	2.1%	3.0%	3.0%	3.0%	2.4%	2.9%	3.0%
	5.9%	5.9%	6.0%	6.2%	5.9%	0.8%	0.8%	0.8%	6.3%	0.9%	0.8%
B	10.7%	10.7%	10.2%	9.4%	10.7%	1.9%	1.9%	1.9%	9.4%	1.8%	1.8%
	3.8%	3.8%	3.1%	2.0%	3.8%	3.8%	3.8%	3.8%	1.8%	3.7%	3.7%
	1.1%	1.1%	1.2%	1.2%	1.1%	3.6%	3.6%	3.6%	1.5%	3.4%	3.4%
	9.9%	9.9%	9.9%	10.2%	9.9%	5.5%	5.5%	5.5%	10.1%	5.4%	5.4%
C	16.1%	16.1%	15.5%	14.6%	16.1%	4.2%	4.2%	4.2%	14.6%	4.2%	4.2%
	9.0%	9.0%	8.2%	6.8%	9.0%	6.7%	6.7%	6.7%	6.7%	6.6%	6.7%
	0.9%	0.9%	1.0%	1.1%	0.9%	4.2%	4.2%	4.2%	1.3%	4.0%	4.1%
	8.6%	8.6%	8.7%	8.9%	8.6%	3.8%	3.8%	3.8%	8.9%	3.7%	3.7%
D	0.4%	0.4%	1.2%	1.7%	0.6%	1.3%	1.3%	1.3%	1.7%	1.2%	1.0%
	0.1%	0.1%	1.6%	2.1%	0.3%	2.2%	2.2%	2.2%	1.5%	1.5%	0.7%
	0.3%	0.3%	0.0%	0.1%	0.3%	0.3%	0.3%	0.3%	0.2%	0.0%	0.2%
	0.8%	0.8%	0.5%	0.6%	0.9%	0.3%	0.3%	0.3%	0.9%	0.6%	0.8%
E	0.8%	0.8%	1.6%	3.2%	0.4%	1.9%	1.9%	1.9%	3.2%	1.8%	1.7%
	3.7%	3.7%	6.5%	8.6%	4.1%	4.0%	4.0%	4.0%	9.0%	4.3%	4.1%
	3.7%	3.7%	4.0%	4.2%	3.8%	2.6%	2.6%	2.6%	4.3%	2.7%	2.7%
	2.3%	2.3%	2.4%	2.5%	2.2%	1.0%	1.0%	1.0%	2.7%	1.1%	1.2%

Table F.13 Strain at the connection Arch/Carriageway, measured and computed responses for load cases A, B, C, D, E in ascending order, section N6

Strain at Connection of the arch and the Carrigeway, Norweigan side [$\mu\text{m}/\text{m}$]												
	z_m	z_0	z_{1A}	z_{1B}	z_{1C}	z_{1D}	z_2	z_3	z_4	z_5	z_6	z_7
A	-10.74	-12.01	-12.01	-12.18	-13.35	-11.96	-11.13	-11.13	-11.13	-13.70	-11.51	-11.79
	5.37	6.71	6.71	7.14	8.61	6.63	6.52	6.52	6.52	8.95	6.97	7.24
	-4.60	-2.70	-2.70	-2.57	-2.42	-2.71	-2.35	-2.35	-2.35	-2.42	-2.32	-2.33
	-3.16	-2.60	-2.60	-2.46	-2.33	-2.61	-2.25	-2.25	-2.25	-2.33	-2.22	-2.22
B	-7.85	-8.11	-8.11	-8.26	-9.20	-8.07	-7.53	-7.53	-7.53	-9.70	-8.02	-8.25
	1.21	2.51	2.51	2.87	4.04	2.45	2.61	2.61	2.61	4.59	3.20	3.42
	14.94	14.84	14.84	14.87	14.93	14.83	13.56	13.56	13.56	15.21	13.84	13.88
	-21.16	-20.44	-20.44	-20.26	-20.10	-20.45	-18.48	-18.48	-18.48	-20.32	-18.66	-18.71
C	-10.61	-11.11	-11.11	-11.28	-12.40	-11.07	-10.30	-10.30	-10.30	-12.78	-10.70	-10.97
	4.81	5.75	5.75	6.16	7.56	5.68	5.62	5.62	5.62	7.94	6.10	6.36
	11.61	12.25	12.25	12.31	12.41	12.24	11.22	11.22	11.22	12.62	11.46	11.49
	-18.06	-17.62	-17.62	-17.42	-17.25	-17.63	-15.90	-15.90	-15.90	-17.45	-16.06	-16.10
D	3.93	3.88	3.88	3.52	2.07	3.37	3.21	3.21	3.21	2.31	4.00	3.20
	-5.12	-4.78	-4.78	-4.16	-2.25	-4.01	-3.81	-3.81	-3.81	-2.44	-4.59	-3.58
	0.23	-0.41	-0.41	-0.30	-0.06	-0.28	-0.28	-0.28	-0.28	-0.03	-0.26	-0.15
	-1.12	-0.48	-0.48	-0.35	-0.12	-0.35	-0.32	-0.32	-0.32	-0.11	-0.32	-0.23
E	-5.74	-3.00	-3.00	-6.49	-10.10	-4.59	-5.98	-5.98	-5.98	-10.12	-5.95	-6.46
	3.00	-0.44	-0.44	5.39	10.09	1.97	4.92	4.92	4.92	10.10	5.09	5.41
	-2.34	-1.62	-1.62	-0.45	0.11	-1.21	-0.44	-0.44	-0.44	0.09	-0.35	-0.46
	-1.26	-1.82	-1.82	-0.64	-0.12	-1.41	-0.62	-0.62	-0.62	-0.12	-0.51	-0.60

Table F.14 Absolute error, at the connection Arch/Carriageway, section N6

Absolute Error [$\mu\text{m/m}$]											
	$ z_m - z_0 $	$ z_m - z_{1A} $	$ z_m - z_{1B} $	$ z_m - z_{1C} $	$ z_m - z_{1D} $	$ z_m - z_2 $	$ z_m - z_3 $	$ z_m - z_4 $	$ z_m - z_5 $	$ z_m - z_6 $	$ z_m - z_7 $
A	1.27	1.27	1.44	2.62	1.22	0.39	0.39	0.39	2.96	0.77	1.05
	1.34	1.34	1.78	3.24	1.27	1.15	1.15	1.15	3.59	1.61	1.87
	1.89	1.89	2.02	2.18	1.88	2.24	2.24	2.24	2.18	2.28	2.27
	0.56	0.56	0.70	0.84	0.55	0.91	0.91	0.91	0.83	0.95	0.94
B	0.26	0.26	0.41	1.35	0.23	0.31	0.31	0.31	1.86	0.17	0.40
	1.29	1.29	1.65	2.82	1.24	1.40	1.40	1.40	3.38	1.98	2.20
	0.10	0.10	0.08	0.01	0.11	1.38	1.38	1.38	0.27	1.10	1.06
	0.71	0.71	0.90	1.06	0.70	2.67	2.67	2.67	0.83	2.49	2.44
C	0.51	0.51	0.67	1.79	0.46	0.31	0.31	0.31	2.17	0.09	0.37
	0.94	0.94	1.36	2.75	0.87	0.82	0.82	0.82	3.14	1.30	1.55
	0.64	0.64	0.70	0.80	0.63	0.39	0.39	0.39	1.01	0.15	0.13
	0.44	0.44	0.63	0.81	0.43	2.16	2.16	2.16	0.60	2.00	1.95
D	0.05	0.05	0.41	1.86	0.56	0.72	0.72	0.72	1.63	0.07	0.73
	0.34	0.34	0.96	2.87	1.11	1.31	1.31	1.31	2.68	0.53	1.54
	0.65	0.65	0.53	0.29	0.51	0.51	0.51	0.51	0.26	0.49	0.39
	0.64	0.64	0.78	1.00	0.77	0.80	0.80	0.80	1.02	0.80	0.90
E	2.74	2.74	0.75	4.36	1.15	0.24	0.24	0.24	4.39	0.21	0.72
	3.45	3.45	2.39	7.09	1.03	1.92	1.92	1.92	7.09	2.09	2.40
	0.72	0.72	1.89	2.45	1.14	1.90	1.90	1.90	2.43	1.99	1.88
	0.56	0.56	0.62	1.14	0.15	0.65	0.65	0.65	1.14	0.76	0.66

Table F.15 Relative error, at the connection Arch/Carriageway, section N6

Relative Error											
	$\frac{ z_m - z_{0L} }{\max(z_m)}$	$\frac{ z_m - z_{1A} }{\max(z_m)}$	$\frac{ z_m - z_{1B} }{\max(z_m)}$	$\frac{ z_m - z_{1C} }{\max(z_m)}$	$\frac{ z_m - z_{1D} }{\max(z_m)}$	$\frac{ z_m - z_{2L} }{\max(z_m)}$	$\frac{ z_m - z_{3L} }{\max(z_m)}$	$\frac{ z_m - z_{4L} }{\max(z_m)}$	$\frac{ z_m - z_{5L} }{\max(z_m)}$	$\frac{ z_m - z_{6L} }{\max(z_m)}$	$\frac{ z_m - z_{7L} }{\max(z_m)}$
A	3.9%	3.9%	4.5%	8.1%	3.8%	1.2%	1.2%	1.2%	9.2%	2.4%	3.3%
	4.1%	4.1%	5.5%	10.0%	3.9%	3.6%	3.6%	3.6%	11.1%	5.0%	5.8%
	5.9%	5.9%	6.3%	6.7%	5.8%	6.9%	6.9%	6.9%	6.7%	7.0%	7.0%
	1.7%	1.7%	2.2%	2.6%	1.7%	2.8%	2.8%	2.8%	2.6%	2.9%	2.9%
B	0.8%	0.8%	1.3%	4.2%	0.7%	1.0%	1.0%	1.0%	5.7%	0.5%	1.2%
	4.0%	4.0%	5.1%	8.7%	3.8%	4.3%	4.3%	4.3%	10.4%	6.1%	6.8%
	0.3%	0.3%	0.2%	0.0%	0.3%	4.3%	4.3%	4.3%	0.8%	3.4%	3.3%
	2.2%	2.2%	2.8%	3.3%	2.2%	8.3%	8.3%	8.3%	2.6%	7.7%	7.6%
C	1.6%	1.6%	2.1%	5.5%	1.4%	0.9%	0.9%	0.9%	6.7%	0.3%	1.1%
	2.9%	2.9%	4.2%	8.5%	2.7%	2.5%	2.5%	2.5%	9.7%	4.0%	4.8%
	2.0%	2.0%	2.2%	2.5%	1.9%	1.2%	1.2%	1.2%	3.1%	0.5%	0.4%
	1.4%	1.4%	2.0%	2.5%	1.3%	6.7%	6.7%	6.7%	1.9%	6.2%	6.0%
D	0.2%	0.2%	1.3%	5.8%	1.7%	2.2%	2.2%	2.2%	5.0%	0.2%	2.3%
	1.1%	1.1%	3.0%	8.9%	3.4%	4.0%	4.0%	4.0%	8.3%	1.6%	4.8%
	2.0%	2.0%	1.6%	0.9%	1.6%	1.6%	1.6%	1.6%	0.8%	1.5%	1.2%
	2.0%	2.0%	2.4%	3.1%	2.4%	2.5%	2.5%	2.5%	3.1%	2.5%	2.8%
E	8.5%	8.5%	2.3%	13.5%	3.6%	0.7%	0.7%	0.7%	13.6%	0.6%	2.2%
	10.7%	10.7%	7.4%	21.9%	3.2%	5.9%	5.9%	5.9%	21.9%	6.4%	7.4%
	2.2%	2.2%	5.8%	7.6%	3.5%	5.9%	5.9%	5.9%	7.5%	6.2%	5.8%
	1.7%	1.7%	1.9%	3.5%	0.5%	2.0%	2.0%	2.0%	3.5%	2.3%	2.1%

Table F.16 Strain at the foundation measured and computed responses for load cases A, B, C, D, E in ascending order, section N1

Strain at foundation of the arch on the Norweigan side [$\mu\text{m}/\text{m}$]												
	z_m	z_0	z_{1A}	z_{1B}	z_{1C}	z_{1D}	z_2	z_3	z_4	z_5	z_6	z_7
A	-7.22	-5.41	-5.41	-3.94	-1.70	-5.61	-3.93	-3.93	-3.93	-1.80	-3.21	-3.04
	-2.32	-1.93	-1.93	-1.85	-1.77	-1.94	-1.75	-1.75	-1.75	-1.78	-1.73	-1.75
	-2.40	-1.87	-1.87	-1.78	-1.69	-1.87	-1.68	-1.68	-1.68	-1.68	-1.66	-1.65
B	-5.56	-5.18	-5.18	-3.99	-2.20	-5.32	-3.92	-3.92	-3.92	-1.81	-2.92	-2.77
	7.64	7.61	7.61	7.57	7.43	7.60	7.28	7.28	7.28	7.57	7.45	7.49
	-11.43	-11.59	-11.59	-11.43	-11.14	-11.59	-10.92	-10.92	-10.92	-11.26	-11.02	-11.08
C	-4.37	-5.35	-5.35	-3.94	-1.82	-5.53	-3.93	-3.93	-3.93	-1.80	-3.14	-2.97
	6.39	6.22	6.22	6.21	6.11	6.21	5.98	5.98	5.98	6.22	6.11	6.14
	-10.65	-10.06	-10.06	-9.89	-9.62	-10.06	-9.45	-9.45	-9.45	-9.73	-9.54	-9.59
D	-8.92	-6.55	-6.55	-5.18	-1.28	-4.55	-4.96	-4.96	-4.96	-0.82	-4.38	-2.41
	-0.92	-0.22	-0.22	-0.13	0.03	-0.13	-0.13	-0.13	-0.13	0.07	-0.11	-0.06
	-0.72	-0.31	-0.31	-0.23	-0.12	-0.24	-0.22	-0.22	-0.22	-0.13	-0.23	-0.16
E	-21.50	-26.81	-26.81	-10.28	-1.30	-20.45	-10.10	-10.10	-10.10	-1.43	-7.64	-8.13
	-1.88	-1.09	-1.09	-0.30	0.06	-0.78	-0.30	-0.30	-0.30	0.06	-0.24	-0.39
	0.25	-1.06	-1.06	-0.41	-0.14	-0.87	-0.41	-0.41	-0.41	-0.14	-0.34	-0.35

Table F.17 Absolute error, at the foundation of the arch on the Norwegian side for load cases A, B, C, D, E in ascending order, section N1

Absolute Error [$\mu\text{m}/\text{m}$]											
	$ z_m - z_0 $	$ z_m - z_{1A} $	$ z_m - z_{1B} $	$ z_m - z_{1C} $	$ z_m - z_{1D} $	$ z_m - z_2 $	$ z_m - z_3 $	$ z_m - z_4 $	$ z_m - z_5 $	$ z_m - z_6 $	$ z_m - z_7 $
A	1.81	1.81	3.28	5.52	1.61	3.29	3.29	3.29	5.42	4.01	4.18
	0.39	0.39	0.47	0.55	0.38	0.57	0.57	0.57	0.54	0.59	0.57
	0.54	0.54	0.62	0.72	0.53	0.72	0.72	0.72	0.72	0.74	0.75
B	0.39	0.39	1.58	3.36	0.25	1.64	1.64	1.64	3.75	2.64	2.80
	0.03	0.03	0.07	0.21	0.04	0.35	0.35	0.35	0.07	0.19	0.14
	0.16	0.16	0.01	0.29	0.16	0.51	0.51	0.51	0.17	0.41	0.35
C	0.98	0.98	0.42	2.55	1.17	0.44	0.44	0.44	2.56	1.22	1.40
	0.17	0.17	0.18	0.29	0.19	0.41	0.41	0.41	0.17	0.28	0.25
	0.59	0.59	0.76	1.03	0.59	1.20	1.20	1.20	0.92	1.11	1.06
D	2.37	2.37	3.74	7.64	4.37	3.96	3.96	3.96	8.10	4.53	6.51
	0.70	0.70	0.79	0.95	0.79	0.79	0.79	0.79	0.99	0.81	0.86
	0.41	0.41	0.48	0.59	0.47	0.49	0.49	0.49	0.58	0.48	0.56
E	5.31	5.31	11.22	20.21	1.06	11.40	11.40	11.40	20.07	13.86	13.38
	0.79	0.79	1.58	1.94	1.10	1.58	1.58	1.58	1.93	1.64	1.49
	1.32	1.32	0.66	0.39	1.12	0.66	0.66	0.66	0.39	0.60	0.60

Table F.18 Relative error, at the foundation of the arch on the Norwegian side, section N1

Relative Error											
	$\frac{ z_m - z_{1A} }{\max(z_m)}$	$\frac{ z_m - z_{1B} }{\max(z_m)}$	$\frac{ z_m - z_{1C} }{\max(z_m)}$	$\frac{ z_m - z_{1D} }{\max(z_m)}$	$\frac{ z_m - z_2 }{\max(z_m)}$	$\frac{ z_m - z_3 }{\max(z_m)}$	$\frac{ z_m - z_4 }{\max(z_m)}$	$\frac{ z_m - z_5 }{\max(z_m)}$	$\frac{ z_m - z_6 }{\max(z_m)}$	$\frac{ z_m - z_7 }{\max(z_m)}$	
A	5.6%	5.6%	10.1%	17.1%	5.0%	10.2%	10.2%	10.2%	16.8%	12.4%	12.9%
	1.2%	1.2%	1.5%	1.7%	1.2%	1.8%	1.8%	1.8%	1.7%	1.8%	1.8%
	1.7%	1.7%	1.9%	2.2%	1.6%	2.2%	2.2%	2.2%	2.2%	2.3%	2.3%
B	1.2%	1.2%	4.9%	10.4%	0.8%	5.1%	5.1%	5.1%	11.6%	8.2%	8.7%
	0.1%	0.1%	0.2%	0.7%	0.1%	1.1%	1.1%	1.1%	0.2%	0.6%	0.4%
	0.5%	0.5%	0.0%	0.9%	0.5%	1.6%	1.6%	1.6%	0.5%	1.3%	1.1%
C	3.0%	3.0%	1.3%	7.9%	3.6%	1.4%	1.4%	1.4%	7.9%	3.8%	4.3%
	0.5%	0.5%	0.6%	0.9%	0.6%	1.3%	1.3%	1.3%	0.5%	0.9%	0.8%
	1.8%	1.8%	2.4%	3.2%	1.8%	3.7%	3.7%	3.7%	2.8%	3.4%	3.3%
D	7.3%	7.3%	11.6%	23.6%	13.5%	12.2%	12.2%	12.2%	25.0%	14.0%	20.1%
	2.2%	2.2%	2.4%	2.9%	2.5%	2.4%	2.4%	2.4%	3.0%	2.5%	2.6%
	1.3%	1.3%	1.5%	1.8%	1.5%	1.5%	1.5%	1.5%	1.8%	1.5%	1.7%
E	16.4%	16.4%	34.7%	62.5%	3.3%	35.2%	35.2%	35.2%	62.1%	42.9%	41.4%
	2.4%	2.4%	4.9%	6.0%	3.4%	4.9%	4.9%	4.9%	6.0%	5.1%	4.6%
	4.1%	4.1%	2.1%	1.2%	3.5%	2.0%	2.0%	2.0%	1.2%	1.8%	1.9%

F.3 Displacements

Table F.19 Displacement in the arch

		Displacement in the arch [mm]											
		z_m	z_0	z_{1A}	z_{1B}	z_{1C}	z_{1D}	z_2	z_3	z_4	z_5	z_6	z_7
Δx of Arch at hanger 1	A	-2.05	-1.94	-1.94	-2.32	-2.71	-1.86	-2.16	-2.16	-2.16	-2.73	-2.11	-2.18
	B	-1.53	-1.03	-1.03	-1.34	-1.66	-0.97	-1.25	-1.25	-1.25	-1.68	-1.21	-1.28
	C	-2.35	-1.73	-1.73	-2.09	-2.47	-1.66	-1.95	-1.95	-1.95	-2.49	-1.91	-1.99
	D	0.56	0.72	0.72	0.54	-0.76	-0.02	0.61	0.61	0.61	-0.61	1.52	0.14
	E	11.03	15.50	15.50	9.67	6.95	13.10	9.16	9.16	9.16	6.94	9.67	10.08
Δy of Arch at hanger 1	A	-0.77	-0.05	-0.05	-0.05	-0.05	-0.05	-0.04	-0.04	-0.04	-0.05	-0.04	-0.05
	B	8.68	10.64	10.64	10.55	10.49	10.63	9.82	9.82	9.82	10.68	10.01	10.07
	C	7.15	9.06	9.06	8.99	8.94	9.06	8.37	8.37	8.37	9.10	8.53	8.58
	D	-0.49	0.15	0.15	0.13	0.15	0.17	0.13	0.13	0.13	0.18	0.14	0.16
	E	0.57	-0.10	-0.10	-0.04	0.00	-0.04	-0.03	-0.03	-0.03	0.00	-0.04	-0.08
Δz of Arch at hanger 1	A	-0.78	-2.17	-2.17	-2.64	-3.16	-2.08	-2.46	-2.46	-2.46	-3.15	-2.38	-2.47
	B	-0.83	-0.70	-0.70	-1.08	-1.51	-0.64	-1.03	-1.03	-1.03	-1.49	-0.95	-1.03
	C	-2.13	-1.83	-1.83	-2.28	-2.78	-1.75	-2.13	-2.13	-2.13	-2.77	-2.05	-2.14
	D	0.33	-0.17	-0.17	-0.33	-1.84	-1.02	-0.19	-0.19	-0.19	-1.89	0.55	-1.06
	E	15.83	21.97	21.97	15.11	11.91	19.22	14.21	14.21	14.21	12.05	14.78	15.30
Δx of Arch at midpoint	A	1.06	1.04	1.04	0.68	0.26	1.10	0.64	0.64	0.64	0.25	0.69	0.63
	B	0.18	0.81	0.81	0.51	0.18	0.85	0.49	0.49	0.49	0.17	0.53	0.47
	C	0.36	0.97	0.97	0.63	0.23	1.03	0.60	0.60	0.60	0.22	0.64	0.58
	D	1.28	0.88	0.88	0.65	-0.43	0.28	0.68	0.68	0.68	-0.43	1.32	0.23
	E	8.19	12.47	12.47	7.61	5.29	10.53	7.23	7.23	7.23	5.30	7.68	8.02
Δy of Arch at midpoint	A	0.40	-0.07	-0.07	-0.07	-0.07	-0.07	-0.07	-0.07	-0.07	-0.08	-0.07	-0.08
	B	17.62	17.86	17.86	17.75	17.60	17.85	16.37	16.37	16.37	17.93	16.67	16.74
	C	14.72	15.39	15.39	15.30	15.17	15.38	14.10	14.10	14.10	15.44	14.36	14.41
	D	0.28	0.13	0.13	0.12	0.15	0.15	0.11	0.11	0.11	0.18	0.13	0.14
	E	0.65	-0.03	-0.03	0.05	0.10	0.04	0.05	0.05	0.05	0.10	0.04	-0.03

Δz of Arch at midpoint	A	11.97	14.80	14.80	14.61	14.24	14.80	13.35	13.35	13.35	14.27	13.40	13.39
	B	6.62	9.94	9.94	9.79	9.50	9.93	8.94	8.94	8.94	9.53	9.00	8.99
	C	10.52	13.62	13.62	13.44	13.10	13.62	12.29	12.29	12.29	13.13	12.34	12.33
	D	0.99	0.74	0.74	0.47	0.41	0.76	0.40	0.40	0.40	0.22	0.26	0.42
	E	-0.77	-1.23	-1.23	-1.59	-2.00	-1.16	-1.49	-1.49	-1.49	-1.94	-1.38	-1.39
Δx of Arch at hanger 6	A	3.50	4.49	4.49	3.98	3.35	4.56	3.74	3.74	3.74	3.35	3.81	3.73
	B	1.90	3.05	3.05	2.64	2.14	3.10	2.49	2.49	2.49	2.13	2.55	2.48
	C	3.16	4.15	4.15	3.66	3.07	4.21	3.44	3.44	3.44	3.06	3.51	3.43
	D	1.33	1.53	1.53	1.14	-0.20	0.80	1.13	1.13	1.13	-0.20	1.92	0.68
	E	9.16	13.56	13.56	7.53	4.56	11.22	7.21	7.21	7.21	4.57	7.76	8.16
Δy of Arch at hanger 6	A	0.06	-0.04	-0.04	-0.04	-0.04	-0.04	-0.04	-0.04	-0.04	-0.05	-0.04	-0.05
	B	8.28	9.94	9.94	9.87	9.74	9.94	9.20	9.20	9.20	9.91	9.36	9.40
	C	6.64	8.48	8.48	8.42	8.30	8.47	7.84	7.84	7.84	8.45	7.98	8.01
	D	-0.44	0.04	0.04	0.04	0.06	0.05	0.04	0.04	0.04	0.04	0.08	0.05
	E	0.70	0.01	0.01	0.05	0.08	0.04	0.04	0.04	0.04	0.04	0.07	-0.01
Δz of Arch at hanger 6	A	-4.33	-5.50	-5.50	-4.94	-4.31	-5.58	-4.63	-4.63	-4.63	-4.31	-4.67	-4.61
	B	-3.01	-3.39	-3.39	-2.93	-2.42	-3.44	-2.77	-2.77	-2.77	-2.40	-2.79	-2.73
	C	-4.85	-4.99	-4.99	-4.46	-3.86	-5.07	-4.19	-4.19	-4.19	-3.85	-4.22	-4.16
	D	-2.38	-1.38	-1.38	-0.99	0.51	-0.54	-1.01	-1.01	-1.01	0.57	-1.72	-0.33
	E	-12.14	-17.01	-17.01	-10.16	-6.89	-14.33	-9.69	-9.69	-9.69	-6.94	-10.16	-10.66

Table F.20 Displacement, absolute error in the arch

		Absolute Error [mm]										
		$ z_m - z_0 $	$ z_m - z_{1A} $	$ z_m - z_{1B} $	$ z_m - z_{1C} $	$ z_m - z_{1D} $	$ z_m - z_2 $	$ z_m - z_3 $	$ z_m - z_4 $	$ z_m - z_5 $	$ z_m - z_6 $	$ z_m - z_7 $
Δx of Arch at hanger 1	A	0.11	0.11	0.26	0.66	0.19	0.10	0.10	0.10	0.68	0.06	0.13
	B	0.51	0.51	0.20	0.12	0.56	0.28	0.28	0.28	0.14	0.32	0.25
	C	0.61	0.61	0.25	0.12	0.68	0.39	0.39	0.39	0.15	0.44	0.36
	D	0.16	0.16	0.02	1.32	0.58	0.05	0.05	0.05	1.17	0.96	0.42
	E	4.48	4.48	1.36	4.08	2.08	1.86	1.86	1.86	4.09	1.36	0.95
Δy of Arch at hanger 1	A	0.73	0.73	0.73	0.73	0.73	0.73	0.73	0.73	0.72	0.73	0.73
	B	1.96	1.96	1.87	1.80	1.95	1.14	1.14	1.14	2.00	1.33	1.39
	C	1.92	1.92	1.85	1.79	1.91	1.22	1.22	1.22	1.95	1.38	1.43
	D	0.65	0.65	0.63	0.65	0.66	0.62	0.62	0.62	0.67	0.63	0.66
	E	0.67	0.67	0.61	0.57	0.61	0.60	0.60	0.60	0.57	0.61	0.65
Δz of Arch at hanger 1	A	1.39	1.39	1.86	2.38	1.30	1.67	1.67	1.67	2.37	1.60	1.69
	B	0.13	0.13	0.26	0.68	0.19	0.20	0.20	0.20	0.66	0.13	0.20
	C	0.30	0.30	0.15	0.65	0.38	0.00	0.00	0.00	0.64	0.07	0.02
	D	0.50	0.50	0.66	2.17	1.35	0.52	0.52	0.52	2.22	0.21	1.39
	E	6.14	6.14	0.72	3.92	3.39	1.62	1.62	1.62	3.78	1.06	0.54
Δx of Arch at midpoint	A	0.02	0.02	0.38	0.79	0.04	0.41	0.41	0.41	0.80	0.37	0.43
	B	0.63	0.63	0.33	0.00	0.67	0.31	0.31	0.31	0.01	0.35	0.29
	C	0.61	0.61	0.27	0.13	0.67	0.24	0.24	0.24	0.14	0.28	0.22
	D	0.39	0.39	0.62	1.70	1.00	0.59	0.59	0.59	1.71	0.04	1.04
	E	4.29	4.29	0.57	2.90	2.34	0.95	0.95	0.95	2.88	0.50	0.16
Δy of Arch at midpoint	A	0.47	0.47	0.47	0.47	0.47	0.47	0.47	0.47	0.48	0.47	0.48
	B	0.24	0.24	0.13	0.02	0.23	1.25	1.25	1.25	0.31	0.94	0.88
	C	0.67	0.67	0.58	0.45	0.66	0.63	0.63	0.63	0.72	0.37	0.31
	D	0.15	0.15	0.16	0.13	0.13	0.17	0.17	0.17	0.10	0.15	0.14
	E	0.68	0.68	0.60	0.55	0.61	0.61	0.61	0.61	0.56	0.62	0.68
Δz of Arch at midpoint	A	2.83	2.83	2.64	2.27	2.83	1.38	1.38	1.38	2.30	1.43	1.43
	B	3.32	3.32	3.17	2.88	3.32	2.33	2.33	2.33	2.91	2.38	2.37

	C	3.11	3.11	2.92	2.58	3.10	1.77	1.77	1.77	2.61	1.82	1.81
	D	0.26	0.26	0.53	0.59	0.24	0.59	0.59	0.59	0.78	0.73	0.58
	E	0.46	0.46	0.82	1.23	0.39	0.72	0.72	0.72	1.17	0.61	0.62
Δx of Arch at hanger 6	A	0.99	0.99	0.48	0.14	1.06	0.24	0.24	0.24	0.15	0.31	0.24
	B	1.15	1.15	0.74	0.24	1.20	0.59	0.59	0.59	0.23	0.66	0.58
	C	0.98	0.98	0.50	0.10	1.05	0.28	0.28	0.28	0.10	0.35	0.27
	D	0.20	0.20	0.19	1.53	0.53	0.20	0.20	0.20	1.53	0.59	0.65
	E	4.40	4.40	1.63	4.60	2.06	1.95	1.95	1.95	4.59	1.40	1.00
Δy of Arch at hanger 6	A	0.10	0.10	0.10	0.10	0.10	0.10	0.10	0.10	0.11	0.10	0.11
	B	1.66	1.66	1.59	1.46	1.66	0.92	0.92	0.92	1.63	1.08	1.12
	C	1.83	1.83	1.77	1.66	1.83	1.20	1.20	1.20	1.80	1.34	1.36
	D	0.49	0.49	0.49	0.50	0.50	0.48	0.48	0.48	0.52	0.49	0.49
	E	0.69	0.69	0.65	0.62	0.66	0.66	0.66	0.66	0.62	0.66	0.70
Δz of Arch at hanger 6	A	1.17	1.17	0.61	0.03	1.25	0.30	0.30	0.30	0.03	0.34	0.28
	B	0.38	0.38	0.07	0.58	0.44	0.23	0.23	0.23	0.61	0.21	0.28
	C	0.14	0.14	0.39	0.99	0.22	0.66	0.66	0.66	1.00	0.63	0.70
	D	1.00	1.00	1.39	2.89	1.84	1.37	1.37	1.37	2.95	0.66	2.05
	E	4.87	4.87	1.98	5.24	2.19	2.45	2.45	2.45	5.20	1.98	1.48

Table F.21 Displacement, relative error in the arch

		Relative Error										
		$\frac{ z_m - z_{0L} }{\max(z_m)}$	$\frac{ z_m - z_{1A} }{\max(z_m)}$	$\frac{ z_m - z_{1B} }{\max(z_m)}$	$\frac{ z_m - z_{1C} }{\max(z_m)}$	$\frac{ z_m - z_{1D} }{\max(z_m)}$	$\frac{ z_m - z_{2L} }{\max(z_m)}$	$\frac{ z_m - z_{3L} }{\max(z_m)}$	$\frac{ z_m - z_{4L} }{\max(z_m)}$	$\frac{ z_m - z_{5L} }{\max(z_m)}$	$\frac{ z_m - z_{6L} }{\max(z_m)}$	$\frac{ z_m - z_{7L} }{\max(z_m)}$
Δx of Arch at hanger 1	A	0.3%	0.3%	0.6%	1.6%	0.5%	0.3%	0.3%	0.3%	1.7%	0.1%	0.3%
	B	1.3%	1.3%	0.5%	0.3%	1.4%	0.7%	0.7%	0.7%	0.4%	0.8%	0.6%
	C	1.5%	1.5%	0.6%	0.3%	1.7%	1.0%	1.0%	1.0%	0.4%	1.1%	0.9%
	D	0.4%	0.4%	0.0%	3.3%	1.4%	0.1%	0.1%	0.1%	2.9%	2.4%	1.0%
	E	11.0%	11.0%	3.3%	10.0%	5.1%	4.6%	4.6%	4.6%	10.1%	3.3%	2.3%
Δy of Arch at hanger 1	A	1.8%	1.8%	1.8%	1.8%	1.8%	1.8%	1.8%	1.8%	1.8%	1.8%	1.8%
	B	4.8%	4.8%	4.6%	4.4%	4.8%	2.8%	2.8%	2.8%	4.9%	3.3%	3.4%
	C	4.7%	4.7%	4.5%	4.4%	4.7%	3.0%	3.0%	3.0%	4.8%	3.4%	3.5%
	D	1.6%	1.6%	1.5%	1.6%	1.6%	1.5%	1.5%	1.5%	1.7%	1.6%	1.6%
	E	1.6%	1.6%	1.5%	1.4%	1.5%	1.5%	1.5%	1.5%	1.4%	1.5%	1.6%
Δz of Arch at hanger 1	A	3.4%	3.4%	4.6%	5.9%	3.2%	4.1%	4.1%	4.1%	5.8%	3.9%	4.2%
	B	0.3%	0.3%	0.6%	1.7%	0.5%	0.5%	0.5%	0.5%	1.6%	0.3%	0.5%
	C	0.7%	0.7%	0.4%	1.6%	0.9%	0.0%	0.0%	0.0%	1.6%	0.2%	0.0%
	D	1.2%	1.2%	1.6%	5.3%	3.3%	1.3%	1.3%	1.3%	5.5%	0.5%	3.4%
	E	15.1%	15.1%	1.8%	9.7%	8.3%	4.0%	4.0%	4.0%	9.3%	2.6%	1.3%
Δx of Arch at midpoint	A	0.0%	0.0%	0.9%	2.0%	0.1%	1.0%	1.0%	1.0%	2.0%	0.9%	1.1%
	B	1.5%	1.5%	0.8%	0.0%	1.6%	0.8%	0.8%	0.8%	0.0%	0.9%	0.7%
	C	1.5%	1.5%	0.7%	0.3%	1.6%	0.6%	0.6%	0.6%	0.3%	0.7%	0.5%
	D	1.0%	1.0%	1.5%	4.2%	2.5%	1.5%	1.5%	1.5%	4.2%	0.1%	2.6%
	E	10.6%	10.6%	1.4%	7.1%	5.8%	2.3%	2.3%	2.3%	7.1%	1.2%	0.4%
Δy of Arch at midpoint	A	1.2%	1.2%	1.2%	1.2%	1.2%	1.2%	1.2%	1.2%	1.2%	1.2%	1.2%
	B	0.6%	0.6%	0.3%	0.0%	0.6%	3.1%	3.1%	3.1%	0.8%	2.3%	2.2%
	C	1.6%	1.6%	1.4%	1.1%	1.6%	1.5%	1.5%	1.5%	1.8%	0.9%	0.8%
	D	0.4%	0.4%	0.4%	0.3%	0.3%	0.4%	0.4%	0.4%	0.2%	0.4%	0.3%
	E	1.7%	1.7%	1.5%	1.3%	1.5%	1.5%	1.5%	1.5%	1.4%	1.5%	1.7%
Δz of	A	7.0%	7.0%	6.5%	5.6%	7.0%	3.4%	3.4%	3.4%	5.7%	3.5%	3.5%

Arch at midpoint	B	8.2%	8.2%	7.8%	7.1%	8.2%	5.7%	5.7%	5.7%	7.2%	5.9%	5.8%
	C	7.6%	7.6%	7.2%	6.3%	7.6%	4.4%	4.4%	4.4%	6.4%	4.5%	4.5%
	D	0.6%	0.6%	1.3%	1.5%	0.6%	1.5%	1.5%	1.5%	1.9%	1.8%	1.4%
	E	1.1%	1.1%	2.0%	3.0%	1.0%	1.8%	1.8%	1.8%	2.9%	1.5%	1.5%
Δx of Arch at hanger 6	A	2.4%	2.4%	1.2%	0.4%	2.6%	0.6%	0.6%	0.6%	0.4%	0.8%	0.6%
	B	2.8%	2.8%	1.8%	0.6%	3.0%	1.5%	1.5%	1.5%	0.6%	1.6%	1.4%
	C	2.4%	2.4%	1.2%	0.2%	2.6%	0.7%	0.7%	0.7%	0.2%	0.9%	0.7%
	D	0.5%	0.5%	0.5%	3.8%	1.3%	0.5%	0.5%	0.5%	3.8%	1.5%	1.6%
	E	10.8%	10.8%	4.0%	11.3%	5.1%	4.8%	4.8%	4.8%	11.3%	3.4%	2.5%
Δy of Arch at hanger 6	A	0.2%	0.2%	0.3%	0.3%	0.3%	0.2%	0.2%	0.2%	0.3%	0.2%	0.3%
	B	4.1%	4.1%	3.9%	3.6%	4.1%	2.3%	2.3%	2.3%	4.0%	2.7%	2.7%
	C	4.5%	4.5%	4.4%	4.1%	4.5%	2.9%	2.9%	2.9%	4.4%	3.3%	3.4%
	D	1.2%	1.2%	1.2%	1.2%	1.2%	1.2%	1.2%	1.2%	1.3%	1.2%	1.2%
	E	1.7%	1.7%	1.6%	1.5%	1.6%	1.6%	1.6%	1.6%	1.5%	1.6%	1.7%
Δz of Arch at hanger 6	A	2.9%	2.9%	1.5%	0.1%	3.1%	0.7%	0.7%	0.7%	0.1%	0.8%	0.7%
	B	0.9%	0.9%	0.2%	1.4%	1.1%	0.6%	0.6%	0.6%	1.5%	0.5%	0.7%
	C	0.3%	0.3%	1.0%	2.4%	0.5%	1.6%	1.6%	1.6%	2.5%	1.5%	1.7%
	D	2.5%	2.5%	3.4%	7.1%	4.5%	3.4%	3.4%	3.4%	7.3%	1.6%	5.1%
	E	12.0%	12.0%	4.9%	12.9%	5.4%	6.0%	6.0%	6.0%	12.8%	4.9%	3.7%

Table F.22 Displacement in the carriageway

		Displacement in the Carriageway at points [mm]											
		z_m	z_0	z_{1A}	z_{1B}	z_{1C}	z_{1D}	z_2	z_3	z_4	z_5	z_6	z_7
Δz at point 10	A	0.31	0.53	0.53	0.28	0.20	0.54	0.24	0.24	0.24	0.03	0.13	0.26
	B	-0.84	-2.10	-2.10	-2.12	-2.18	-2.09	-1.99	-1.99	-1.99	-1.70	-1.46	-1.47
	C	-0.58	-1.51	-1.51	-1.61	-1.68	-1.49	-1.51	-1.51	-1.51	-1.28	-1.06	-1.01
	D	19.28	25.81	25.81	22.99	22.47	25.52	22.86	22.86	22.86	24.80	25.71	28.43
	E	-1.12	-0.71	-0.71	-0.51	-1.54	-1.20	-0.42	-0.42	-0.42	-2.41	-0.80	-1.91
Δz at point 20	A	0.34	0.53	0.53	0.28	0.22	0.55	0.23	0.23	0.23	0.05	0.12	0.27
	B	-0.40	0.16	0.16	0.01	-0.04	0.17	0.02	0.02	0.02	0.50	0.61	0.71
	C	0.54	0.41	0.41	0.20	0.14	0.42	0.19	0.19	0.19	0.60	0.69	0.85
	D	19.82	23.74	23.74	21.02	20.46	23.43	20.88	20.88	20.88	22.88	23.86	26.47
	E	-1.14	-0.80	-0.80	-0.50	-1.58	-1.33	-0.40	-0.40	-0.40	-2.50	-0.82	-2.04
Δz at point 30	A	0.33	0.53	0.53	0.28	0.23	0.54	0.24	0.24	0.24	0.06	0.11	0.27
	B	-0.17	0.31	0.31	0.10	0.06	0.32	0.04	0.04	0.04	-0.85	-0.83	-0.77
	C	-0.03	0.54	0.54	0.29	0.24	0.56	0.21	0.21	0.21	-0.53	-0.50	-0.39
	D	19.04	21.67	21.67	19.18	18.61	21.36	19.04	19.04	19.04	20.86	21.84	24.19
	E	-1.19	-0.70	-0.70	-0.50	-1.58	-1.26	-0.41	-0.41	-0.41	-2.32	-0.66	-1.90
Δz at point 11	A	-0.66	-0.16	-0.16	-0.62	-1.15	-0.08	-0.60	-0.60	-0.60	-1.06	-0.45	-0.55
	B	-18.27	-20.81	-20.81	-21.15	-21.56	-20.75	-20.86	-20.86	-20.86	-22.19	-21.43	-21.55
	C	-16.97	-18.79	-18.79	-19.20	-19.68	-18.71	-18.90	-18.90	-18.90	-20.22	-19.38	-19.50
	D	-0.01	-0.75	-0.75	-0.85	-2.32	-1.57	-0.72	-0.72	-0.72	-3.61	-1.34	-3.06
	E	22.89	30.06	30.06	23.31	20.18	27.37	22.55	22.55	22.55	20.78	23.48	24.05
Δz at point 21	A	-0.12	-0.82	-0.82	-1.28	-1.80	-0.73	-1.22	-1.22	-1.22	-1.72	-1.08	-1.17
	B	-5.34	-3.92	-3.92	-4.29	-4.71	-3.86	-4.24	-4.24	-4.24	-4.80	-4.28	-4.37
	C	-5.12	-4.50	-4.50	-4.93	-5.42	-4.42	-4.83	-4.83	-4.83	-5.51	-4.86	-4.96
	D	0.26	-0.51	-0.51	-0.64	-2.13	-1.35	-0.51	-0.51	-0.51	-3.19	-0.88	-2.57
	E	19.12	26.08	26.08	19.29	16.13	23.36	18.50	18.50	18.50	16.61	19.33	19.89
Δz at point 31	A	-0.66	-0.81	-0.81	-1.27	-1.78	-0.72	-1.21	-1.21	-1.21	-1.70	-1.07	-1.16
	B	6.01	5.87	5.87	5.48	5.06	5.93	5.38	5.38	5.38	5.34	5.72	5.64

	C	3.30	3.65	3.65	3.20	2.71	3.73	3.18	3.18	3.18	2.94	3.47	3.38
	D	-0.40	-0.49	-0.49	-0.63	-2.11	-1.33	-0.50	-0.50	-0.50	-3.15	-0.83	-2.52
	E	19.21	26.27	26.27	19.48	16.33	23.55	18.69	18.69	18.69	16.77	19.49	20.05
Δz at point 22	A	6.40	8.30	8.30	7.82	7.21	8.36	7.42	7.42	7.42	7.26	7.52	7.45
	B	-4.66	-0.10	-0.10	-0.47	-0.96	-0.05	-0.75	-0.75	-0.75	-1.03	-0.77	-0.84
	C	-0.98	0.94	0.94	0.50	-0.08	1.01	0.18	0.18	0.18	-0.14	0.17	0.09
	D	2.21	-0.21	-0.21	-0.45	-1.63	-0.84	-0.36	-0.36	-0.36	-2.24	-0.38	-1.56
	E	17.40	21.45	21.45	15.96	13.30	19.38	15.16	15.16	15.16	13.60	15.72	16.16
Δz at point 32	A	7.35	8.30	8.30	7.83	7.22	8.37	7.43	7.43	7.43	7.28	7.53	7.46
	B	15.22	17.99	17.99	17.60	17.10	18.03	17.16	17.16	17.16	17.29	17.39	17.33
	C	14.89	16.26	16.26	15.80	15.22	16.32	15.34	15.34	15.34	15.37	15.54	15.48
	D	0.77	-0.19	-0.19	-0.44	-1.61	-0.82	-0.34	-0.34	-0.34	-2.21	-0.35	-1.52
	E	20.09	21.84	21.84	16.35	13.69	19.78	15.55	15.55	15.55	13.98	16.10	16.54
Δz at point 24	A	23.15	26.11	26.11	25.95	25.62	26.10	24.94	24.94	24.94	25.65	24.99	24.98
	B	4.02	4.65	4.65	4.53	4.28	4.64	3.89	3.89	3.89	4.19	3.83	3.81
	C	8.94	10.66	10.66	10.51	10.21	10.65	9.64	9.64	9.64	10.13	9.59	9.58
	D	2.01	0.57	0.57	0.33	0.33	0.62	0.27	0.27	0.27	0.17	0.14	0.34
	E	-1.17	-1.64	-1.64	-1.72	-1.99	-1.48	-1.65	-1.65	-1.65	-1.93	-1.56	-1.58
Δz at point 34	A	23.27	26.10	26.10	25.94	25.61	26.09	24.93	24.93	24.93	25.64	24.98	24.97
	B	24.79	29.07	29.07	28.94	28.68	29.07	28.14	28.14	28.14	28.84	28.32	28.31
	C	31.00	35.68	35.68	35.53	35.22	35.68	34.52	34.52	34.52	35.35	34.67	34.67
	D	1.43	0.58	0.58	0.34	0.34	0.63	0.28	0.28	0.28	0.19	0.16	0.36
	E	-0.20	-1.41	-1.41	-1.49	-1.76	-1.24	-1.41	-1.41	-1.41	-1.71	-1.33	-1.36

Table F.23 Displacement, absolute error in the carriageway

		Absolute Error [mm]										
		$ z_m - z_0 $	$ z_m - z_{1A} $	$ z_m - z_{1B} $	$ z_m - z_{1C} $	$ z_m - z_{1D} $	$ z_m - z_2 $	$ z_m - z_3 $	$ z_m - z_4 $	$ z_m - z_5 $	$ z_m - z_6 $	$ z_m - z_7 $
Δz at point 10	A	0.22	0.22	0.03	0.11	0.23	0.08	0.08	0.08	0.28	0.18	0.05
	B	1.27	1.27	1.29	1.35	1.26	1.15	1.15	1.15	0.87	0.62	0.63
	C	0.92	0.92	1.02	1.10	0.91	0.93	0.93	0.93	0.70	0.47	0.42
	D	6.53	6.53	3.71	3.19	6.24	3.58	3.58	3.58	5.52	6.43	9.15
	E	0.41	0.41	0.61	0.42	0.08	0.70	0.70	0.70	1.29	0.32	0.79
Δz at point 20	A	0.19	0.19	0.06	0.12	0.21	0.11	0.11	0.11	0.29	0.22	0.07
	B	0.55	0.55	0.41	0.36	0.56	0.42	0.42	0.42	0.90	1.00	1.11
	C	0.13	0.13	0.34	0.40	0.12	0.36	0.36	0.36	0.05	0.15	0.30
	D	3.91	3.91	1.20	0.63	3.60	1.06	1.06	1.06	3.06	4.03	6.65
	E	0.34	0.34	0.64	0.44	0.19	0.74	0.74	0.74	1.36	0.32	0.90
Δz at point 30	A	0.19	0.19	0.05	0.10	0.21	0.10	0.10	0.10	0.27	0.22	0.07
	B	0.48	0.48	0.28	0.23	0.49	0.22	0.22	0.22	0.68	0.65	0.59
	C	0.57	0.57	0.32	0.27	0.59	0.24	0.24	0.24	0.50	0.47	0.36
	D	2.63	2.63	0.14	0.43	2.32	0.00	0.00	0.00	1.82	2.80	5.15
	E	0.48	0.48	0.69	0.39	0.07	0.78	0.78	0.78	1.14	0.53	0.71
Δz at point 11	A	0.50	0.50	0.04	0.49	0.58	0.06	0.06	0.06	0.40	0.21	0.11
	B	2.54	2.54	2.88	3.28	2.48	2.59	2.59	2.59	3.92	3.16	3.27
	C	1.82	1.82	2.23	2.71	1.74	1.93	1.93	1.93	3.25	2.41	2.53
	D	0.73	0.73	0.84	2.31	1.56	0.71	0.71	0.71	3.60	1.33	3.05
	E	7.17	7.17	0.42	2.71	4.47	0.34	0.34	0.34	2.11	0.59	1.16
Δz at point 21	A	0.70	0.70	1.16	1.68	0.61	1.10	1.10	1.10	1.60	0.96	1.06
	B	1.43	1.43	1.05	0.64	1.49	1.11	1.11	1.11	0.54	1.06	0.98
	C	0.62	0.62	0.19	0.30	0.70	0.29	0.29	0.29	0.39	0.27	0.16
	D	0.77	0.77	0.90	2.38	1.61	0.77	0.77	0.77	3.45	1.14	2.82
	E	6.96	6.96	0.17	2.98	4.25	0.62	0.62	0.62	2.50	0.22	0.77
Δz at point 31	A	0.15	0.15	0.61	1.12	0.06	0.55	0.55	0.55	1.04	0.41	0.50
	B	0.15	0.15	0.54	0.96	0.09	0.63	0.63	0.63	0.67	0.30	0.37

	C	0.35	0.35	0.10	0.59	0.43	0.12	0.12	0.12	0.36	0.17	0.08
	D	0.09	0.09	0.23	1.71	0.93	0.10	0.10	0.10	2.75	0.43	2.12
	E	7.07	7.07	0.27	2.88	4.34	0.52	0.52	0.52	2.44	0.28	0.84
Δz at point 22	A	1.90	1.90	1.42	0.81	1.96	1.02	1.02	1.02	0.86	1.12	1.05
	B	4.56	4.56	4.18	3.70	4.60	3.91	3.91	3.91	3.63	3.89	3.82
	C	1.93	1.93	1.48	0.90	1.99	1.16	1.16	1.16	0.85	1.15	1.07
	D	2.42	2.42	2.67	3.84	3.06	2.57	2.57	2.57	4.45	2.59	3.77
	E	4.04	4.04	1.45	4.11	1.98	2.25	2.25	2.25	3.80	1.68	1.24
Δz at point 32	A	0.96	0.96	0.48	0.13	1.02	0.08	0.08	0.08	0.07	0.18	0.11
	B	2.76	2.76	2.37	1.88	2.81	1.94	1.94	1.94	2.06	2.17	2.11
	C	1.37	1.37	0.91	0.33	1.43	0.45	0.45	0.45	0.48	0.65	0.59
	D	0.96	0.96	1.21	2.38	1.59	1.11	1.11	1.11	2.97	1.12	2.29
	E	1.75	1.75	3.73	6.39	0.31	4.53	4.53	4.53	6.11	3.99	3.55
Δz at point 24	A	2.96	2.96	2.80	2.47	2.95	1.79	1.79	1.79	2.50	1.83	1.83
	B	0.63	0.63	0.51	0.26	0.62	0.13	0.13	0.13	0.17	0.20	0.21
	C	1.72	1.72	1.58	1.27	1.72	0.70	0.70	0.70	1.20	0.65	0.64
	D	1.45	1.45	1.68	1.68	1.40	1.74	1.74	1.74	1.84	1.87	1.68
	E	0.48	0.48	0.56	0.83	0.31	0.48	0.48	0.48	0.77	0.39	0.42
Δz at point 34	A	2.83	2.83	2.67	2.34	2.82	1.66	1.66	1.66	2.37	1.70	1.70
	B	4.28	4.28	4.15	3.89	4.27	3.35	3.35	3.35	4.04	3.52	3.52
	C	4.69	4.69	4.53	4.22	4.68	3.52	3.52	3.52	4.35	3.67	3.67
	D	0.85	0.85	1.09	1.09	0.80	1.15	1.15	1.15	1.24	1.27	1.07
	E	1.21	1.21	1.29	1.56	1.04	1.21	1.21	1.21	1.51	1.13	1.16

Table F.24 Displacement, relative error in the carriageway

		Relative Error										
		$\frac{ z_m - z_{0L} }{\max(z_m)}$	$\frac{ z_m - z_{1A} }{\max(z_m)}$	$\frac{ z_m - z_{1B} }{\max(z_m)}$	$\frac{ z_m - z_{1C} }{\max(z_m)}$	$\frac{ z_m - z_{1D} }{\max(z_m)}$	$\frac{ z_m - z_{2L} }{\max(z_m)}$	$\frac{ z_m - z_{3L} }{\max(z_m)}$	$\frac{ z_m - z_{4L} }{\max(z_m)}$	$\frac{ z_m - z_{5L} }{\max(z_m)}$	$\frac{ z_m - z_{6L} }{\max(z_m)}$	$\frac{ z_m - z_{7L} }{\max(z_m)}$
		$\max(z_m)$										
Δz at point 10	A	0.5%	0.5%	0.1%	0.3%	0.6%	0.2%	0.2%	0.2%	0.7%	0.5%	0.1%
	B	3.1%	3.1%	3.2%	3.3%	3.1%	2.8%	2.8%	2.8%	2.1%	1.5%	1.6%
	C	2.3%	2.3%	2.5%	2.7%	2.2%	2.3%	2.3%	2.3%	1.7%	1.2%	1.0%
	D	16.1%	16.1%	9.1%	7.9%	15.4%	8.8%	8.8%	8.8%	13.6%	15.8%	22.5%
	E	1.0%	1.0%	1.5%	1.0%	0.2%	1.7%	1.7%	1.7%	3.2%	0.8%	2.0%
Δz at point 20	A	0.5%	0.5%	0.1%	0.3%	0.5%	0.3%	0.3%	0.3%	0.7%	0.5%	0.2%
	B	1.4%	1.4%	1.0%	0.9%	1.4%	1.0%	1.0%	1.0%	2.2%	2.5%	2.7%
	C	0.3%	0.3%	0.8%	1.0%	0.3%	0.9%	0.9%	0.9%	0.1%	0.4%	0.7%
	D	9.6%	9.6%	2.9%	1.6%	8.9%	2.6%	2.6%	2.6%	7.5%	9.9%	16.4%
	E	0.8%	0.8%	1.6%	1.1%	0.5%	1.8%	1.8%	1.8%	3.3%	0.8%	2.2%
Δz at point 30	A	0.5%	0.5%	0.1%	0.2%	0.5%	0.2%	0.2%	0.2%	0.7%	0.5%	0.2%
	B	1.2%	1.2%	0.7%	0.6%	1.2%	0.5%	0.5%	0.5%	1.7%	1.6%	1.5%
	C	1.4%	1.4%	0.8%	0.7%	1.4%	0.6%	0.6%	0.6%	1.2%	1.2%	0.9%
	D	6.5%	6.5%	0.3%	1.1%	5.7%	0.0%	0.0%	0.0%	4.5%	6.9%	12.7%
	E	1.2%	1.2%	1.7%	1.0%	0.2%	1.9%	1.9%	1.9%	2.8%	1.3%	1.7%
Δz at point 11	A	1.2%	1.2%	0.1%	1.2%	1.4%	0.2%	0.2%	0.2%	1.0%	0.5%	0.3%
	B	6.2%	6.2%	7.1%	8.1%	6.1%	6.4%	6.4%	6.4%	9.6%	7.8%	8.1%
	C	4.5%	4.5%	5.5%	6.7%	4.3%	4.8%	4.8%	4.8%	8.0%	5.9%	6.2%
	D	1.8%	1.8%	2.1%	5.7%	3.8%	1.7%	1.7%	1.7%	8.9%	3.3%	7.5%
	E	17.6%	17.6%	1.0%	6.7%	11.0%	0.8%	0.8%	0.8%	5.2%	1.5%	2.9%
Δz at point 21	A	1.7%	1.7%	2.9%	4.1%	1.5%	2.7%	2.7%	2.7%	3.9%	2.4%	2.6%
	B	3.5%	3.5%	2.6%	1.6%	3.7%	2.7%	2.7%	2.7%	1.3%	2.6%	2.4%
	C	1.5%	1.5%	0.5%	0.7%	1.7%	0.7%	0.7%	0.7%	1.0%	0.7%	0.4%
	D	1.9%	1.9%	2.2%	5.9%	4.0%	1.9%	1.9%	1.9%	8.5%	2.8%	7.0%
	E	17.1%	17.1%	0.4%	7.3%	10.5%	1.5%	1.5%	1.5%	6.2%	0.5%	1.9%
Δz at	A	0.4%	0.4%	1.5%	2.8%	0.2%	1.3%	1.3%	1.3%	2.6%	1.0%	1.2%

point 31	B	0.4%	0.4%	1.3%	2.4%	0.2%	1.6%	1.6%	1.6%	1.7%	0.7%	0.9%
	C	0.9%	0.9%	0.2%	1.5%	1.1%	0.3%	0.3%	0.3%	0.9%	0.4%	0.2%
	D	0.2%	0.2%	0.6%	4.2%	2.3%	0.2%	0.2%	0.2%	6.8%	1.1%	5.2%
	E	17.4%	17.4%	0.7%	7.1%	10.7%	1.3%	1.3%	1.3%	6.0%	0.7%	2.1%
Δz at point 22	A	4.7%	4.7%	3.5%	2.0%	4.8%	2.5%	2.5%	2.5%	2.1%	2.8%	2.6%
	B	11.2%	11.2%	10.3%	9.1%	11.3%	9.6%	9.6%	9.6%	8.9%	9.6%	9.4%
	C	4.7%	4.7%	3.6%	2.2%	4.9%	2.8%	2.8%	2.8%	2.1%	2.8%	2.6%
	D	6.0%	6.0%	6.6%	9.5%	7.5%	6.3%	6.3%	6.3%	11.0%	6.4%	9.3%
	E	9.9%	9.9%	3.6%	10.1%	4.9%	5.5%	5.5%	5.5%	9.4%	4.1%	3.1%
Δz at point 32	A	2.4%	2.4%	1.2%	0.3%	2.5%	0.2%	0.2%	0.2%	0.2%	0.4%	0.3%
	B	6.8%	6.8%	5.8%	4.6%	6.9%	4.8%	4.8%	4.8%	5.1%	5.3%	5.2%
	C	3.4%	3.4%	2.2%	0.8%	3.5%	1.1%	1.1%	1.1%	1.2%	1.6%	1.4%
	D	2.4%	2.4%	3.0%	5.9%	3.9%	2.7%	2.7%	2.7%	7.3%	2.7%	5.6%
	E	4.3%	4.3%	9.2%	15.7%	0.8%	11.2%	11.2%	11.2%	15.0%	9.8%	8.7%
Δz at point 24	A	7.3%	7.3%	6.9%	6.1%	7.3%	4.4%	4.4%	4.4%	6.1%	4.5%	4.5%
	B	1.5%	1.5%	1.3%	0.6%	1.5%	0.3%	0.3%	0.3%	0.4%	0.5%	0.5%
	C	4.2%	4.2%	3.9%	3.1%	4.2%	1.7%	1.7%	1.7%	2.9%	1.6%	1.6%
	D	3.6%	3.6%	4.1%	4.1%	3.4%	4.3%	4.3%	4.3%	4.5%	4.6%	4.1%
	E	1.2%	1.2%	1.4%	2.0%	0.8%	1.2%	1.2%	1.2%	1.9%	1.0%	1.0%
Δz at point 34	A	7.0%	7.0%	6.6%	5.8%	6.9%	4.1%	4.1%	4.1%	5.8%	4.2%	4.2%
	B	10.5%	10.5%	10.2%	9.6%	10.5%	8.2%	8.2%	8.2%	10.0%	8.7%	8.7%
	C	11.5%	11.5%	11.2%	10.4%	11.5%	8.7%	8.7%	8.7%	10.7%	9.0%	9.0%
	D	2.1%	2.1%	2.7%	2.7%	2.0%	2.8%	2.8%	2.8%	3.1%	3.1%	2.6%
	E	3.0%	3.0%	3.2%	3.8%	2.6%	3.0%	3.0%	3.0%	3.7%	2.8%	2.9%

Table F.25 Displacement in the carriageway

		Displacement in the Carriageway at points [mm]											
		z_m	z_0	z_{1A}	z_{1B}	z_{1C}	z_{1D}	z_2	z_3	z_4	z_5	z_6	z_7
Δz at point 13	A	23.13	25.53	25.53	25.22	24.74	25.55	24.29	24.29	24.29	24.78	24.35	24.33
	B	-26.32	-32.03	-32.03	-32.23	-32.59	-32.01	-32.55	-32.55	-32.55	-33.12	-33.04	-33.10
	C	-20.98	-24.33	-24.33	-24.58	-25.02	-24.31	-25.15	-25.15	-25.15	-25.46	-25.55	-25.60
	D	1.65	0.37	0.37	0.10	-0.35	0.17	0.09	0.09	0.09	-0.68	0.00	-0.29
	E	4.39	6.22	6.22	4.10	2.89	5.58	3.84	3.84	3.84	3.06	4.12	4.27
Δz at point 23	A	20.13	23.24	23.24	22.94	22.46	23.26	21.97	21.97	21.97	22.49	22.03	22.01
	B	-0.31	4.74	4.74	4.51	4.13	4.75	3.89	3.89	3.89	4.05	3.84	3.80
	C	10.13	10.37	10.37	10.09	9.64	10.39	9.26	9.26	9.26	9.57	9.22	9.19
	D	2.44	0.44	0.44	0.16	-0.29	0.24	0.15	0.15	0.15	-0.59	0.09	-0.19
	E	3.07	6.34	6.34	4.21	3.00	5.69	3.96	3.96	3.96	3.14	4.21	4.36
Δz at point 33	A	20.79	23.24	23.24	22.94	22.46	23.26	21.97	21.97	21.97	22.50	22.04	22.01
	B	27.57	27.74	27.74	27.49	27.11	27.75	26.72	26.72	26.72	27.27	26.91	26.89
	C	31.32	32.60	32.60	32.30	31.85	32.62	31.34	31.34	31.34	31.99	31.50	31.48
	D	0.27	0.45	0.45	0.17	-0.27	0.25	0.16	0.16	0.16	-0.56	0.11	-0.17
	E	4.65	6.61	6.61	4.48	3.28	5.96	4.23	4.23	4.23	3.40	4.47	4.62
Δz at point 15	A	21.12	22.75	22.75	22.76	22.62	22.72	21.91	21.91	21.91	22.64	21.94	21.96
	B	-27.33	-32.92	-32.92	-32.87	-32.96	-32.94	-33.14	-33.14	-33.14	-33.49	-33.65	-33.67
	C	-23.80	-25.62	-25.62	-25.58	-25.69	-25.65	-26.07	-26.07	-26.07	-26.14	-26.50	-26.51
	D	2.46	0.43	0.43	0.29	0.73	0.72	0.21	0.21	0.21	0.67	-0.04	0.58
	E	-8.39	-8.76	-8.76	-6.79	-6.09	-7.80	-6.44	-6.44	-6.44	-6.08	-6.48	-6.67
Δz at point 25	A	18.56	20.55	20.55	20.56	20.43	20.52	19.69	19.69	19.69	20.44	19.72	19.74
	B	0.88	3.51	3.51	3.53	3.43	3.49	2.97	2.97	2.97	3.34	2.90	2.90
	C	5.93	8.47	8.47	8.49	8.36	8.44	7.74	7.74	7.74	8.29	7.67	7.68
	D	0.88	0.49	0.49	0.35	0.79	0.79	0.26	0.26	0.26	0.74	0.03	0.66
	E	-5.07	-8.66	-8.66	-6.68	-5.98	-7.70	-6.32	-6.32	-6.32	-5.98	-6.38	-6.57
Δz at point 35	A	18.69	20.56	20.56	20.57	20.43	20.53	19.69	19.69	19.69	20.45	19.73	19.74
	B	24.34	26.30	26.30	26.31	26.20	26.28	25.59	25.59	25.59	26.36	25.76	25.77

	C	26.92	30.19	30.19	30.19	30.06	30.16	29.31	29.31	29.31	30.19	29.45	29.47
	D	0.09	0.50	0.50	0.35	0.80	0.80	0.27	0.27	0.27	0.77	0.05	0.68
	E	-8.43	-8.46	-8.46	-6.47	-5.77	-7.49	-6.12	-6.12	-6.12	-5.79	-6.18	-6.38
Δz at point 26	A	1.66	4.00	4.00	4.34	4.64	3.93	4.13	4.13	4.13	4.66	4.14	4.18
	B	-1.09	-2.95	-2.95	-2.66	-2.41	-3.00	-2.81	-2.81	-2.81	-2.49	-2.89	-2.86
	C	-1.04	-2.78	-2.78	-2.44	-2.15	-2.85	-2.60	-2.60	-2.60	-2.23	-2.68	-2.64
	D	-1.15	-0.29	-0.29	-0.16	1.01	0.39	-0.25	-0.25	-0.25	1.11	-0.70	0.53
	E	-12.87	-17.12	-17.12	-11.71	-9.31	-14.90	-11.09	-11.09	-11.09	-9.38	-11.38	-11.84
Δz at point 36	A	3.33	4.01	4.01	4.35	4.66	3.94	4.13	4.13	4.13	4.67	4.15	4.19
	B	12.34	14.50	14.50	14.78	15.02	14.46	14.48	14.48	14.48	15.20	14.65	14.69
	C	9.96	11.87	11.87	12.19	12.47	11.80	11.90	11.90	11.90	12.61	12.03	12.08
	D	-0.24	-0.29	-0.29	-0.16	1.02	0.40	-0.24	-0.24	-0.24	1.12	-0.68	0.54
	E	-13.01	-16.98	-16.98	-11.57	-9.16	-14.76	-10.96	-10.96	-10.96	-9.25	-11.25	-11.71
Δz at point 46	A	3.97	5.04	5.04	5.39	5.69	4.97	5.15	5.15	5.15	5.71	5.18	5.21
	B	40.62	47.51	47.51	47.77	47.99	47.46	47.20	47.20	47.20	48.63	47.82	47.88
	C	33.06	39.40	39.40	39.70	39.98	39.34	39.18	39.18	39.18	40.50	39.70	39.76
	D	-0.70	-0.29	-0.29	-0.16	1.01	0.39	-0.25	-0.25	-0.25	1.12	-0.68	0.54
	E	-12.21	-16.54	-16.54	-11.14	-8.74	-14.32	-10.54	-10.54	-10.54	-8.84	-10.83	-11.30
Δz at point 17	A	-2.40	-3.55	-3.55	-3.00	-2.38	-3.63	-2.85	-2.85	-2.85	-2.34	-2.80	-2.77
	B	-19.50	-22.66	-22.66	-22.18	-21.67	-22.72	-21.82	-21.82	-21.82	-22.30	-22.46	-22.45
	C	-17.53	-21.20	-21.20	-20.64	-20.04	-21.27	-20.26	-20.26	-20.26	-20.59	-20.80	-20.79
	D	-2.37	-1.41	-1.41	-1.01	0.44	-0.59	-1.03	-1.03	-1.03	0.51	-1.65	-0.35
	E	-11.47	-16.59	-16.59	-9.86	-6.69	-13.97	-9.42	-9.42	-9.42	-6.76	-9.76	-10.31
Δz at point 27	A	-3.46	-4.16	-4.16	-3.61	-2.98	-4.24	-3.42	-3.42	-3.42	-2.94	-3.39	-3.35
	B	-5.12	-6.46	-6.46	-6.00	-5.49	-6.52	-5.86	-5.86	-5.86	-5.60	-5.98	-5.94
	C	-6.79	-7.51	-7.51	-6.97	-6.38	-7.59	-6.76	-6.76	-6.76	-6.48	-6.87	-6.83
	D	-1.49	-1.40	-1.40	-1.01	0.46	-0.58	-1.03	-1.03	-1.03	0.54	-1.65	-0.33
	E	-12.29	-16.64	-16.64	-9.86	-6.64	-13.99	-9.41	-9.41	-9.41	-6.71	-9.77	-10.31
Δz at point 37	A	-3.35	-4.15	-4.15	-3.60	-2.97	-4.23	-3.41	-3.41	-3.41	-2.93	-3.38	-3.34
	B	3.44	2.87	2.87	3.31	3.81	2.81	3.32	3.32	3.32	4.09	3.58	3.63

C	0.66	0.27	0.27	0.80	1.39	0.20	0.90	0.90	0.90	1.60	1.10	1.15
D	-2.19	-1.40	-1.40	-1.00	0.47	-0.57	-1.02	-1.02	-1.02	0.55	-1.64	-0.32
E	-12.11	-16.56	-16.56	-9.78	-6.56	-13.92	-9.33	-9.33	-9.33	-6.63	-9.69	-10.24

Table F.26 Displacement, absolute error in the carriageway

		Absolute Error [mm]										
		$ z_m - z_0 $	$ z_m - z_{1A} $	$ z_m - z_{1B} $	$ z_m - z_{1C} $	$ z_m - z_{1D} $	$ z_m - z_2 $	$ z_m - z_3 $	$ z_m - z_4 $	$ z_m - z_5 $	$ z_m - z_6 $	$ z_m - z_7 $
Δz at point 13	A	2.39	2.39	2.09	1.61	2.41	1.16	1.16	1.16	1.64	1.22	1.20
	B	5.71	5.71	5.91	6.27	5.69	6.23	6.23	6.23	6.80	6.72	6.78
	C	3.34	3.34	3.60	4.04	3.33	4.17	4.17	4.17	4.48	4.57	4.62
	D	1.28	1.28	1.55	1.99	1.48	1.56	1.56	1.56	2.32	1.65	1.94
	E	1.84	1.84	0.29	1.50	1.19	0.55	0.55	0.55	1.33	0.26	0.12
Δz at point 23	A	3.11	3.11	2.80	2.32	3.13	1.84	1.84	1.84	2.36	1.90	1.88
	B	5.04	5.04	4.81	4.44	5.06	4.20	4.20	4.20	4.35	4.14	4.11
	C	0.24	0.24	0.04	0.49	0.26	0.87	0.87	0.87	0.56	0.91	0.94
	D	2.00	2.00	2.29	2.73	2.21	2.30	2.30	2.30	3.03	2.36	2.64
	E	3.27	3.27	1.14	0.06	2.63	0.89	0.89	0.89	0.08	1.14	1.29
Δz at point 33	A	2.45	2.45	2.15	1.67	2.47	1.18	1.18	1.18	1.71	1.25	1.22
	B	0.17	0.17	0.08	0.46	0.18	0.85	0.85	0.85	0.30	0.67	0.69
	C	1.28	1.28	0.99	0.53	1.30	0.02	0.02	0.02	0.67	0.19	0.16
	D	0.18	0.18	0.10	0.55	0.02	0.12	0.12	0.12	0.84	0.16	0.44
	E	1.97	1.97	0.16	1.37	1.32	0.41	0.41	0.41	1.24	0.18	0.03
Δz at point 15	A	1.63	1.63	1.63	1.50	1.60	0.79	0.79	0.79	1.51	0.82	0.83
	B	5.59	5.59	5.54	5.63	5.61	5.81	5.81	5.81	6.16	6.32	6.34
	C	1.82	1.82	1.79	1.90	1.85	2.28	2.28	2.28	2.35	2.71	2.72
	D	2.03	2.03	2.16	1.73	1.73	2.25	2.25	2.25	1.79	2.50	1.88
	E	0.36	0.36	1.61	2.30	0.59	1.95	1.95	1.95	2.32	1.91	1.72
Δz at point 25	A	2.00	2.00	2.00	1.87	1.97	1.13	1.13	1.13	1.89	1.16	1.18
	B	2.63	2.63	2.65	2.55	2.61	2.10	2.10	2.10	2.47	2.02	2.02

	C	2.54	2.54	2.55	2.43	2.51	1.80	1.80	1.80	2.35	1.74	1.75
	D	0.39	0.39	0.54	0.10	0.09	0.62	0.62	0.62	0.14	0.85	0.22
	E	3.59	3.59	1.61	0.91	2.62	1.25	1.25	1.25	0.91	1.31	1.50
Δz at point 35	A	1.86	1.86	1.87	1.74	1.83	1.00	1.00	1.00	1.76	1.03	1.05
	B	1.96	1.96	1.96	1.86	1.94	1.25	1.25	1.25	2.01	1.42	1.43
	C	3.28	3.28	3.28	3.15	3.25	2.39	2.39	2.39	3.28	2.53	2.55
	D	0.41	0.41	0.27	0.71	0.71	0.18	0.18	0.18	0.68	0.04	0.59
	E	0.03	0.03	1.95	2.66	0.93	2.31	2.31	2.31	2.64	2.24	2.04
Δz at point 26	A	2.34	2.34	2.68	2.99	2.27	2.47	2.47	2.47	3.00	2.48	2.52
	B	1.86	1.86	1.57	1.32	1.91	1.72	1.72	1.72	1.39	1.80	1.77
	C	1.74	1.74	1.40	1.11	1.80	1.56	1.56	1.56	1.19	1.64	1.60
	D	0.86	0.86	0.99	2.16	1.55	0.91	0.91	0.91	2.26	0.45	1.68
	E	4.25	4.25	1.17	3.57	2.02	1.78	1.78	1.78	3.49	1.49	1.03
Δz at point 36	A	0.68	0.68	1.03	1.33	0.61	0.81	0.81	0.81	1.35	0.83	0.87
	B	2.17	2.17	2.45	2.69	2.12	2.15	2.15	2.15	2.86	2.31	2.35
	C	1.91	1.91	2.23	2.52	1.84	1.94	1.94	1.94	2.65	2.08	2.12
	D	0.04	0.04	0.09	1.26	0.64	0.00	0.00	0.00	1.36	0.44	0.78
	E	3.97	3.97	1.44	3.85	1.75	2.06	2.06	2.06	3.76	1.77	1.30
Δz at point 46	A	1.07	1.07	1.42	1.72	1.01	1.19	1.19	1.19	1.74	1.21	1.25
	B	6.89	6.89	7.15	7.37	6.84	6.58	6.58	6.58	8.01	7.20	7.26
	C	6.34	6.34	6.64	6.91	6.27	6.12	6.12	6.12	7.44	6.63	6.69
	D	0.40	0.40	0.53	1.70	1.09	0.45	0.45	0.45	1.82	0.02	1.24
	E	4.33	4.33	1.07	3.47	2.11	1.67	1.67	1.67	3.38	1.38	0.91
Δz at point 17	A	1.15	1.15	0.60	0.02	1.23	0.45	0.45	0.45	0.06	0.41	0.37
	B	3.17	3.17	2.68	2.17	3.22	2.33	2.33	2.33	2.81	2.96	2.95
	C	3.67	3.67	3.11	2.51	3.74	2.72	2.72	2.72	3.06	3.27	3.26
	D	0.96	0.96	1.35	2.81	1.78	1.34	1.34	1.34	2.87	0.72	2.02
	E	5.12	5.12	1.60	4.78	2.50	2.05	2.05	2.05	4.71	1.71	1.16
Δz at point 27	A	0.70	0.70	0.15	0.48	0.78	0.04	0.04	0.04	0.52	0.07	0.11
	B	1.34	1.34	0.88	0.38	1.40	0.74	0.74	0.74	0.48	0.86	0.82

	C	0.72	0.72	0.19	0.41	0.80	0.03	0.03	0.03	0.31	0.08	0.04
	D	0.09	0.09	0.48	1.96	0.92	0.47	0.47	0.47	2.03	0.16	1.16
	E	4.34	4.34	2.43	5.65	1.70	2.89	2.89	2.89	5.58	2.52	1.98
Δz at point 37	A	0.80	0.80	0.24	0.38	0.88	0.06	0.06	0.06	0.42	0.02	0.02
	B	0.57	0.57	0.13	0.37	0.63	0.12	0.12	0.12	0.64	0.13	0.19
	C	0.39	0.39	0.13	0.73	0.47	0.24	0.24	0.24	0.94	0.44	0.49
	D	0.80	0.80	1.19	2.66	1.62	1.17	1.17	1.17	2.74	0.55	1.87
	E	4.46	4.46	2.33	5.54	1.81	2.78	2.78	2.78	5.48	2.42	1.87

Table F.27 Displacement, relative error in the carriageway

		Relative Error										
		$ z_m - z_{0j} $	$ z_m - z_{1A} $	$ z_m - z_{1B} $	$ z_m - z_{1C} $	$ z_m - z_{1D} $	$ z_m - z_{2j} $	$ z_m - z_{3j} $	$ z_m - z_{4j} $	$ z_m - z_{5j} $	$ z_m - z_{6j} $	$ z_m - z_{7j} $
		$max(z_m)$										
Δz at point 13	A	5.9%	5.9%	5.1%	4.0%	5.9%	2.9%	2.9%	2.9%	4.0%	3.0%	2.9%
	B	14.1%	14.1%	14.6%	15.4%	14.0%	15.3%	15.3%	15.3%	16.7%	16.5%	16.7%
	C	8.2%	8.2%	8.9%	9.9%	8.2%	10.3%	10.3%	10.3%	11.0%	11.2%	11.4%
	D	3.2%	3.2%	3.8%	4.9%	3.7%	3.8%	3.8%	3.8%	5.7%	4.1%	4.8%
	E	4.5%	4.5%	0.7%	3.7%	2.9%	1.3%	1.3%	1.3%	3.3%	0.7%	0.3%
Δz at point 23	A	7.6%	7.6%	6.9%	5.7%	7.7%	4.5%	4.5%	4.5%	5.8%	4.7%	4.6%
	B	12.4%	12.4%	11.8%	10.9%	12.5%	10.3%	10.3%	10.3%	10.7%	10.2%	10.1%
	C	0.6%	0.6%	0.1%	1.2%	0.6%	2.1%	2.1%	2.1%	1.4%	2.2%	2.3%
	D	4.9%	4.9%	5.6%	6.7%	5.4%	5.7%	5.7%	5.7%	7.5%	5.8%	6.5%
	E	8.1%	8.1%	2.8%	0.2%	6.5%	2.2%	2.2%	2.2%	0.2%	2.8%	3.2%
Δz at point 33	A	6.0%	6.0%	5.3%	4.1%	6.1%	2.9%	2.9%	2.9%	4.2%	3.1%	3.0%
	B	0.4%	0.4%	0.2%	1.1%	0.5%	2.1%	2.1%	2.1%	0.7%	1.6%	1.7%
	C	3.2%	3.2%	2.4%	1.3%	3.2%	0.1%	0.1%	0.1%	1.7%	0.5%	0.4%
	D	0.4%	0.4%	0.3%	1.3%	0.1%	0.3%	0.3%	0.3%	2.1%	0.4%	1.1%
	E	4.8%	4.8%	0.4%	3.4%	3.2%	1.0%	1.0%	1.0%	3.1%	0.4%	0.1%
Δz at point 15	A	4.0%	4.0%	4.0%	3.7%	3.9%	1.9%	1.9%	1.9%	3.7%	2.0%	2.1%
	B	13.8%	13.8%	13.6%	13.9%	13.8%	14.3%	14.3%	14.3%	15.2%	15.6%	15.6%
	C	4.5%	4.5%	4.4%	4.7%	4.6%	5.6%	5.6%	5.6%	5.8%	6.7%	6.7%
	D	5.0%	5.0%	5.3%	4.3%	4.3%	5.5%	5.5%	5.5%	4.4%	6.2%	4.6%
	E	0.9%	0.9%	4.0%	5.7%	1.5%	4.8%	4.8%	4.8%	5.7%	4.7%	4.2%
Δz at point 25	A	4.9%	4.9%	4.9%	4.6%	4.8%	2.8%	2.8%	2.8%	4.7%	2.9%	2.9%
	B	6.5%	6.5%	6.5%	6.3%	6.4%	5.2%	5.2%	5.2%	6.1%	5.0%	5.0%
	C	6.2%	6.2%	6.3%	6.0%	6.2%	4.4%	4.4%	4.4%	5.8%	4.3%	4.3%
	D	1.0%	1.0%	1.3%	0.2%	0.2%	1.5%	1.5%	1.5%	0.3%	2.1%	0.5%

	E	8.8%	8.8%	4.0%	2.2%	6.5%	3.1%	3.1%	3.1%	2.2%	3.2%	3.7%
Δz at point 35	A	4.6%	4.6%	4.6%	4.3%	4.5%	2.5%	2.5%	2.5%	4.3%	2.5%	2.6%
	B	4.8%	4.8%	4.8%	4.6%	4.8%	3.1%	3.1%	3.1%	5.0%	3.5%	3.5%
	C	8.1%	8.1%	8.1%	7.7%	8.0%	5.9%	5.9%	5.9%	8.1%	6.2%	6.3%
	D	1.0%	1.0%	0.7%	1.7%	1.7%	0.4%	0.4%	0.4%	1.7%	0.1%	1.5%
	E	0.1%	0.1%	4.8%	6.5%	2.3%	5.7%	5.7%	5.7%	6.5%	5.5%	5.0%
Δz at point 26	A	5.8%	5.8%	6.6%	7.3%	5.6%	6.1%	6.1%	6.1%	7.4%	6.1%	6.2%
	B	4.6%	4.6%	3.9%	3.2%	4.7%	4.2%	4.2%	4.2%	3.4%	4.4%	4.4%
	C	4.3%	4.3%	3.5%	2.7%	4.4%	3.8%	3.8%	3.8%	2.9%	4.0%	3.9%
	D	2.1%	2.1%	2.4%	5.3%	3.8%	2.2%	2.2%	2.2%	5.6%	1.1%	4.1%
	E	10.5%	10.5%	2.9%	8.8%	5.0%	4.4%	4.4%	4.4%	8.6%	3.7%	2.5%
Δz at point 36	A	1.7%	1.7%	2.5%	3.3%	1.5%	2.0%	2.0%	2.0%	3.3%	2.0%	2.1%
	B	5.3%	5.3%	6.0%	6.6%	5.2%	5.3%	5.3%	5.3%	7.0%	5.7%	5.8%
	C	4.7%	4.7%	5.5%	6.2%	4.5%	4.8%	4.8%	4.8%	6.5%	5.1%	5.2%
	D	0.1%	0.1%	0.2%	3.1%	1.6%	0.0%	0.0%	0.0%	3.4%	1.1%	1.9%
	E	9.8%	9.8%	3.6%	9.5%	4.3%	5.1%	5.1%	5.1%	9.3%	4.3%	3.2%
Δz at point 46	A	2.6%	2.6%	3.5%	4.2%	2.5%	2.9%	2.9%	2.9%	4.3%	3.0%	3.1%
	B	17.0%	17.0%	17.6%	18.1%	16.8%	16.2%	16.2%	16.2%	19.7%	17.7%	17.9%
	C	15.6%	15.6%	16.4%	17.0%	15.4%	15.1%	15.1%	15.1%	18.3%	16.3%	16.5%
	D	1.0%	1.0%	1.3%	4.2%	2.7%	1.1%	1.1%	1.1%	4.5%	0.0%	3.0%
	E	10.7%	10.7%	2.6%	8.5%	5.2%	4.1%	4.1%	4.1%	8.3%	3.4%	2.2%
Δz at point 17	A	2.8%	2.8%	1.5%	0.0%	3.0%	1.1%	1.1%	1.1%	0.2%	1.0%	0.9%
	B	7.8%	7.8%	6.6%	5.4%	7.9%	5.7%	5.7%	5.7%	6.9%	7.3%	7.3%
	C	9.0%	9.0%	7.7%	6.2%	9.2%	6.7%	6.7%	6.7%	7.5%	8.1%	8.0%
	D	2.4%	2.4%	3.3%	6.9%	4.4%	3.3%	3.3%	3.3%	7.1%	1.8%	5.0%
	E	12.6%	12.6%	3.9%	11.8%	6.2%	5.0%	5.0%	5.0%	11.6%	4.2%	2.9%
Δz at point 27	A	1.7%	1.7%	0.4%	1.2%	1.9%	0.1%	0.1%	0.1%	1.3%	0.2%	0.3%
	B	3.3%	3.3%	2.2%	0.9%	3.4%	1.8%	1.8%	1.8%	1.2%	2.1%	2.0%
	C	1.8%	1.8%	0.5%	1.0%	2.0%	0.1%	0.1%	0.1%	0.8%	0.2%	0.1%
	D	0.2%	0.2%	1.2%	4.8%	2.3%	1.1%	1.1%	1.1%	5.0%	0.4%	2.9%

	E	10.7%	10.7%	6.0%	13.9%	4.2%	7.1%	7.1%	7.1%	13.7%	6.2%	4.9%
Δz at point 37	A	2.0%	2.0%	0.6%	0.9%	2.2%	0.1%	0.1%	0.1%	1.0%	0.1%	0.0%
	B	1.4%	1.4%	0.3%	0.9%	1.6%	0.3%	0.3%	0.3%	1.6%	0.3%	0.5%
	C	1.0%	1.0%	0.3%	1.8%	1.1%	0.6%	0.6%	0.6%	2.3%	1.1%	1.2%
	D	2.0%	2.0%	2.9%	6.6%	4.0%	2.9%	2.9%	2.9%	6.7%	1.3%	4.6%
	E	11.0%	11.0%	5.7%	13.6%	4.5%	6.8%	6.8%	6.8%	13.5%	5.9%	4.6%

F.4 Hanger loads

Table F.28 Hanger loads

		Hanger load [kN]											
		z_m	z_0	z_{1A}	z_{1B}	z_{1C}	z_{1D}	z_2	z_3	z_4	z_5	z_6	z_7
Hanger 1E	A	95.9	95.6	95.6	96.2	96.6	95.5	87.5	87.5	87.5	101.5	91.9	91.5
	B	259.5	267.5	267.5	268.0	268.4	267.5	263.8	263.8	263.8	281.3	276.3	276.2
	C	216.5	222.8	222.8	223.4	223.8	222.7	216.6	216.6	216.6	234.7	227.1	226.8
	D	-21.5	-23.7	-23.7	-21.5	-20.1	-22.9	-22.4	-22.4	-22.4	-90.4	-99.3	-105.0
	E	288.8	297.8	297.8	302.8	305.8	300.2	310.8	310.8	310.8	328.2	327.5	330.6
Hanger 1W	A	96.7	95.2	95.2	95.7	96.2	95.1	87.1	87.1	87.1	100.9	91.4	91.0
	B	-21.7	-34.6	-34.6	-34.2	-33.8	-34.7	-41.2	-41.2	-41.2	-35.9	-43.7	-43.9
	C	-14.2	-25.9	-25.9	-25.4	-24.9	-26.0	-34.5	-34.5	-34.5	-26.6	-36.7	-37.1
	D	-22.4	-23.5	-23.5	-21.3	-19.9	-22.6	-22.1	-22.1	-22.1	-91.5	-100.3	-106.1
	E	281.8	289.4	289.4	294.3	297.3	291.8	302.3	302.3	302.3	321.2	320.5	323.4

Table F.29 Hanger loads, absolute error

		Absolute Error [kN]										
		$ z_m - z_0 $	$ z_m - z_{1A} $	$ z_m - z_{1B} $	$ z_m - z_{1C} $	$ z_m - z_{1D} $	$ z_m - z_2 $	$ z_m - z_3 $	$ z_m - z_4 $	$ z_m - z_5 $	$ z_m - z_6 $	$ z_m - z_7 $
Hanger 1E	A	0.3	0.3	0.3	0.7	0.4	8.4	8.4	8.4	5.6	4.0	4.4
	B	8.0	8.0	8.5	8.8	7.9	4.3	4.3	4.3	21.7	16.8	16.6
	C	6.3	6.3	6.9	7.3	6.3	0.2	0.2	0.2	18.3	10.7	10.3

	D	2.3	2.3	0.1	1.4	1.4	0.9	0.9	0.9	69.0	77.8	83.6
	E	9.1	9.1	14.0	17.1	11.5	22.0	22.0	22.0	39.4	38.7	41.8
Hanger 1W	A	1.5	1.5	0.9	0.5	1.6	9.6	9.6	9.6	4.2	5.3	5.7
	B	12.9	12.9	12.5	12.1	13.0	19.5	19.5	19.5	14.2	22.0	22.2
	C	11.7	11.7	11.1	10.7	11.8	20.3	20.3	20.3	12.4	22.5	22.9
	D	1.1	1.1	1.1	2.5	0.3	0.2	0.2	0.2	69.2	77.9	83.8
	E	7.7	7.7	12.6	15.6	10.0	20.5	20.5	20.5	39.5	38.7	41.7

Table F.30 Hanger loads, relative error

		Relative Error										
		$\frac{ z_m - z_0 }{\max(z_m)}$	$\frac{ z_m - z_{1A} }{\max(z_m)}$	$\frac{ z_m - z_{1B} }{\max(z_m)}$	$\frac{ z_m - z_{1C} }{\max(z_m)}$	$\frac{ z_m - z_{1D} }{\max(z_m)}$	$\frac{ z_m - z_2 }{\max(z_m)}$	$\frac{ z_m - z_3 }{\max(z_m)}$	$\frac{ z_m - z_4 }{\max(z_m)}$	$\frac{ z_m - z_5 }{\max(z_m)}$	$\frac{ z_m - z_6 }{\max(z_m)}$	$\frac{ z_m - z_7 }{\max(z_m)}$
		$\max(z_m)$	$\max(z_m)$	$\max(z_m)$	$\max(z_m)$	$\max(z_m)$	$\max(z_m)$	$\max(z_m)$	$\max(z_m)$	$\max(z_m)$	$\max(z_m)$	$\max(z_m)$
Hanger 1E	A	0.1%	0.1%	0.1%	0.3%	0.1%	2.9%	2.9%	2.9%	1.9%	1.4%	1.5%
	B	2.8%	2.8%	2.9%	3.1%	2.7%	1.5%	1.5%	1.5%	7.5%	5.8%	5.8%
	C	2.2%	2.2%	2.4%	2.5%	2.2%	0.1%	0.1%	0.1%	6.3%	3.7%	3.6%
	D	0.8%	0.8%	0.0%	0.5%	0.5%	0.3%	0.3%	0.3%	23.9%	27.0%	28.9%
	E	3.1%	3.1%	4.9%	5.9%	4.0%	7.6%	7.6%	7.6%	13.6%	13.4%	14.5%
Hanger 1W	A	0.5%	0.5%	0.3%	0.2%	0.6%	3.3%	3.3%	3.3%	1.5%	1.8%	2.0%
	B	4.5%	4.5%	4.3%	4.2%	4.5%	6.7%	6.7%	6.7%	4.9%	7.6%	7.7%
	C	4.0%	4.0%	3.9%	3.7%	4.1%	7.0%	7.0%	7.0%	4.3%	7.8%	7.9%
	D	0.4%	0.4%	0.4%	0.9%	0.1%	0.1%	0.1%	0.1%	23.9%	27.0%	29.0%
	E	2.7%	2.7%	4.4%	5.4%	3.5%	7.1%	7.1%	7.1%	13.7%	13.4%	14.4%

Appendix G. FE Updating Results for the New Svinesund Bridge

G.1 Model 7 optimized for frequencies

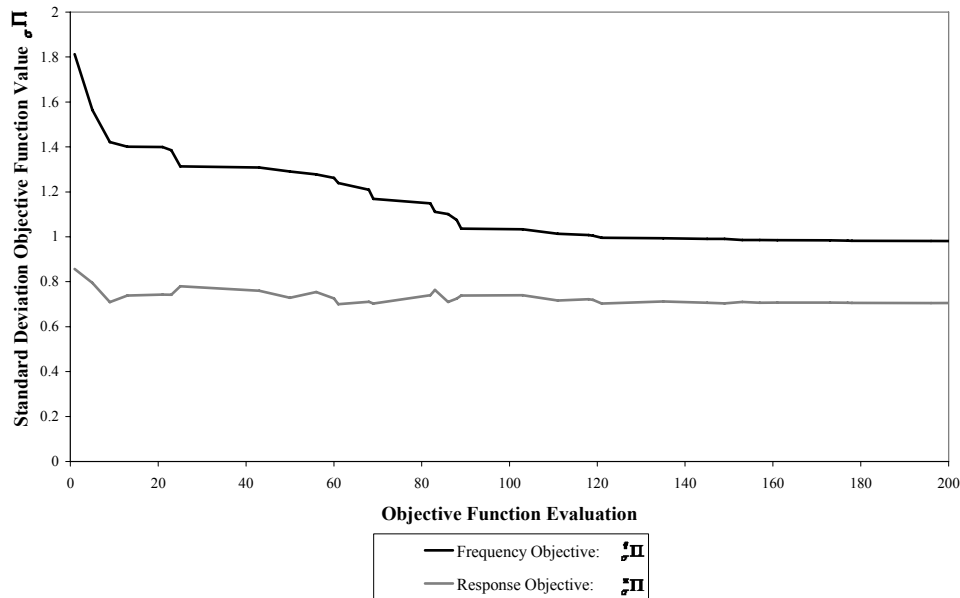


Figure G.1 Convergence of frequency optimization, also showing behaviour of the objective function for the entire response.

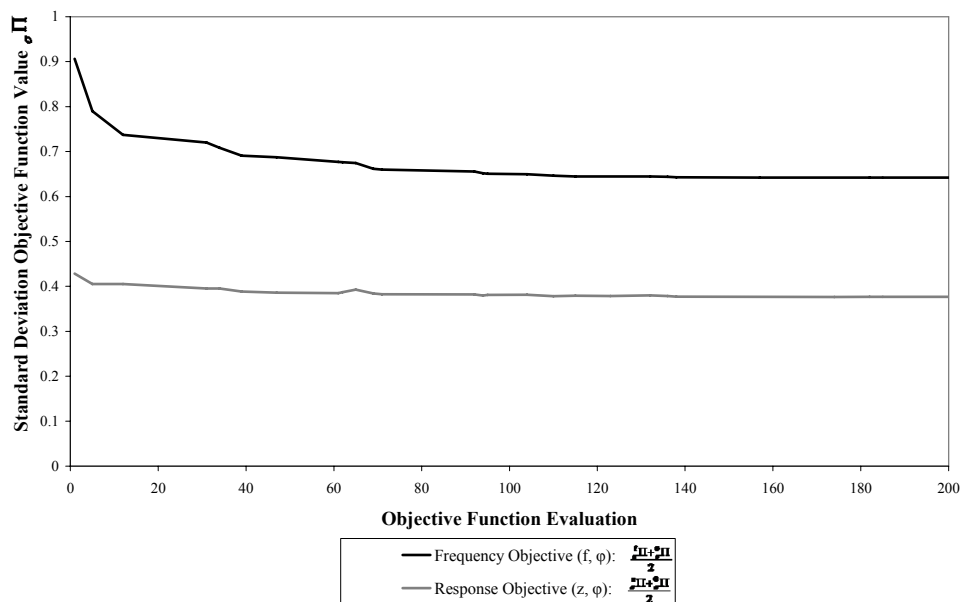


Figure G.2 Convergence of frequency optimization with regularization, also showing behaviour of the regularized objective function for the entire response.

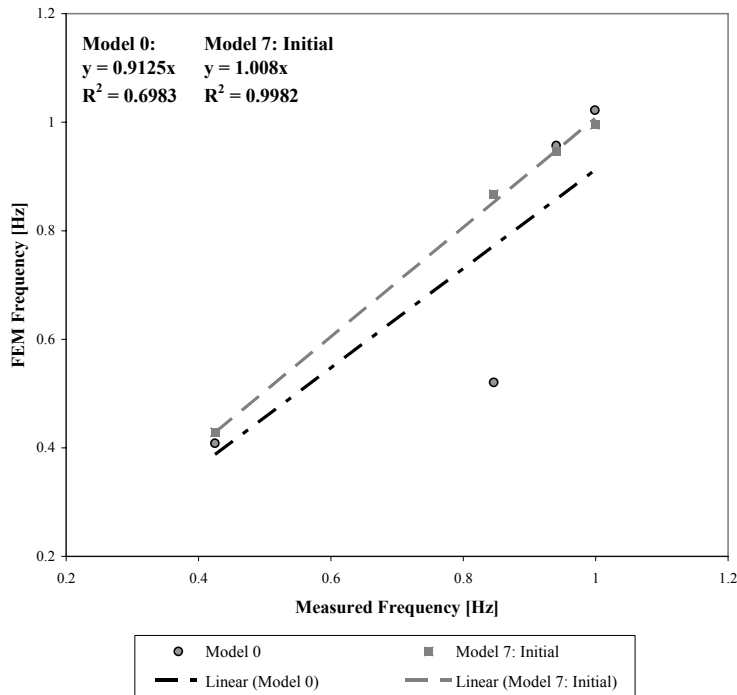


Figure G.3 Eigenfrequencies from Model 0 and Model 7 before optimization compared with measured frequencies.

G.2 Model 7 optimized for strains

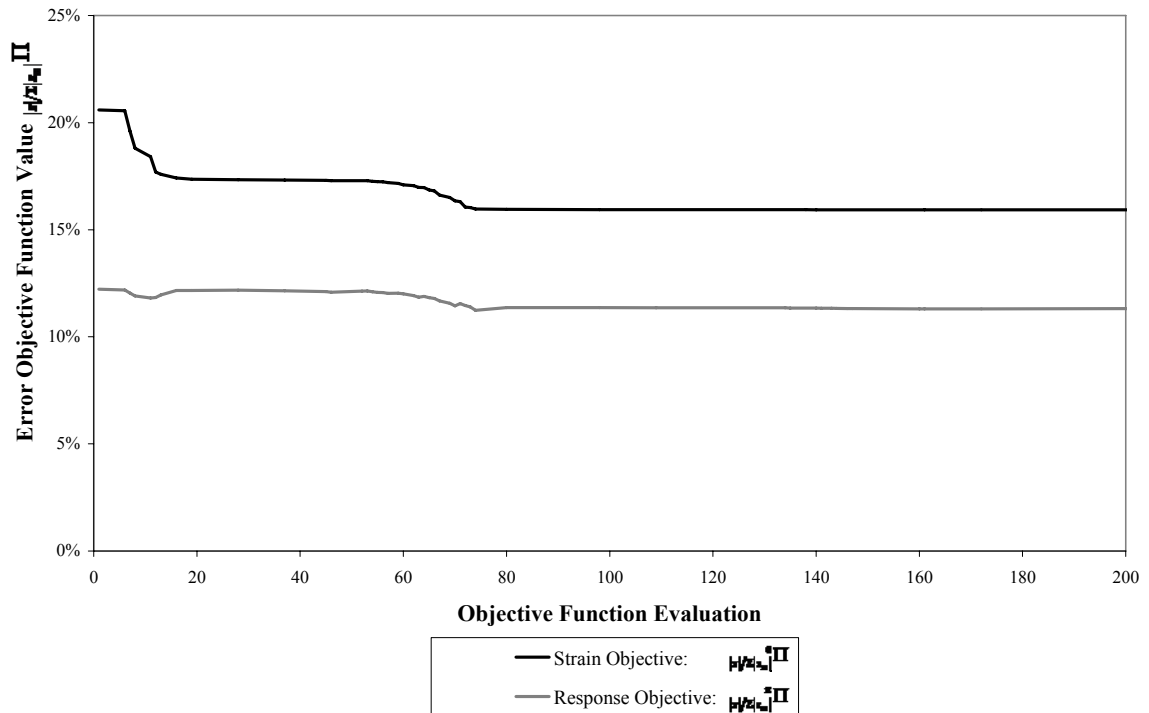


Figure G.4 Convergence of strain optimization, also showing behaviour of the objective function for the entire response.

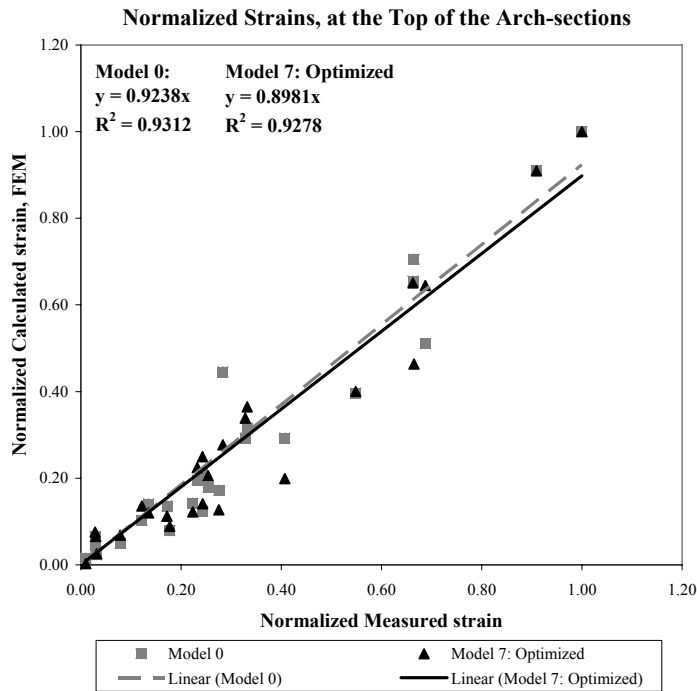


Figure G.5 Normalized strain for strain gauges located in the top of the arch sections from Model 0 and Model 7 after strain optimization compared with measured strains.

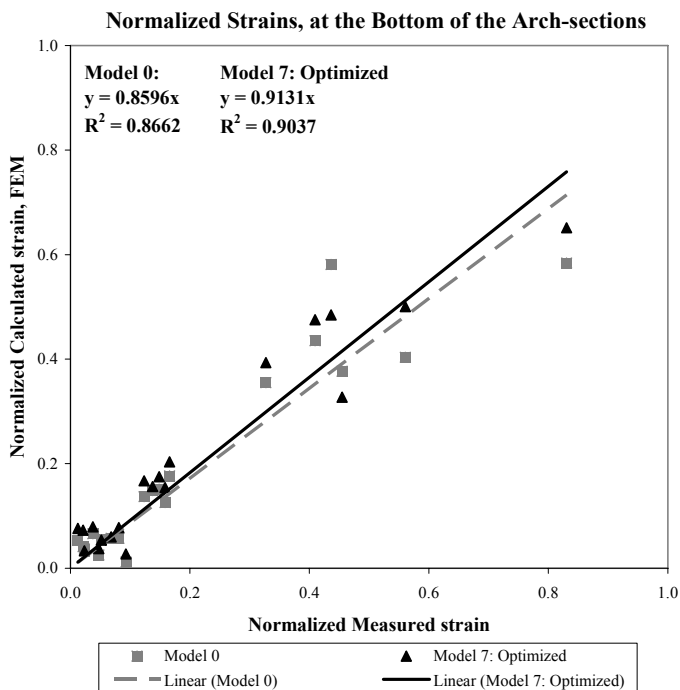


Figure G.6 Normalized strain for strain gauges located in the bottom of the arch sections from Model 0 and Model 7 after strain optimization compared with measured strains.

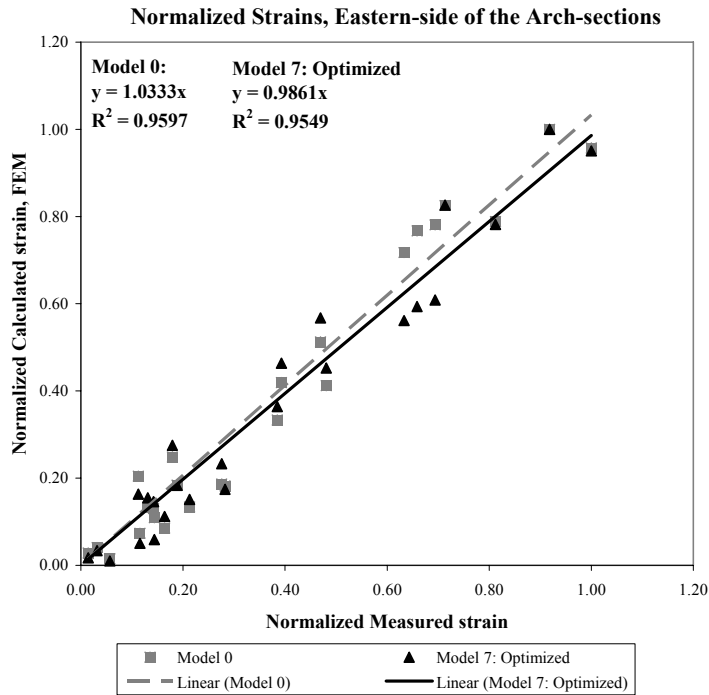


Figure G.7 Normalized strain for strain gauges located in the Eastern side of the arch sections from Model 0 and Model 7 after strain optimization compared with measured strains.

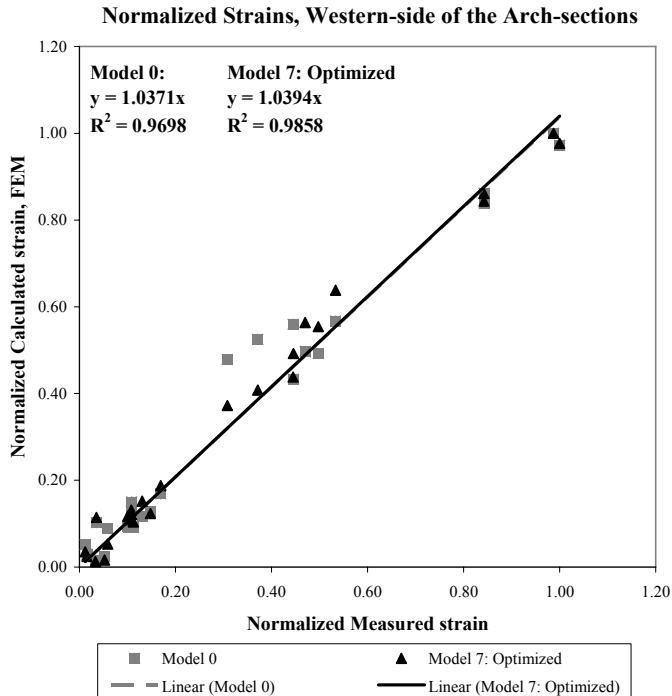


Figure G.8 Normalized strain for strain gauges located in the Western side of the arch sections from Model 0 and Model 7 after strain optimization compared with measured strains.

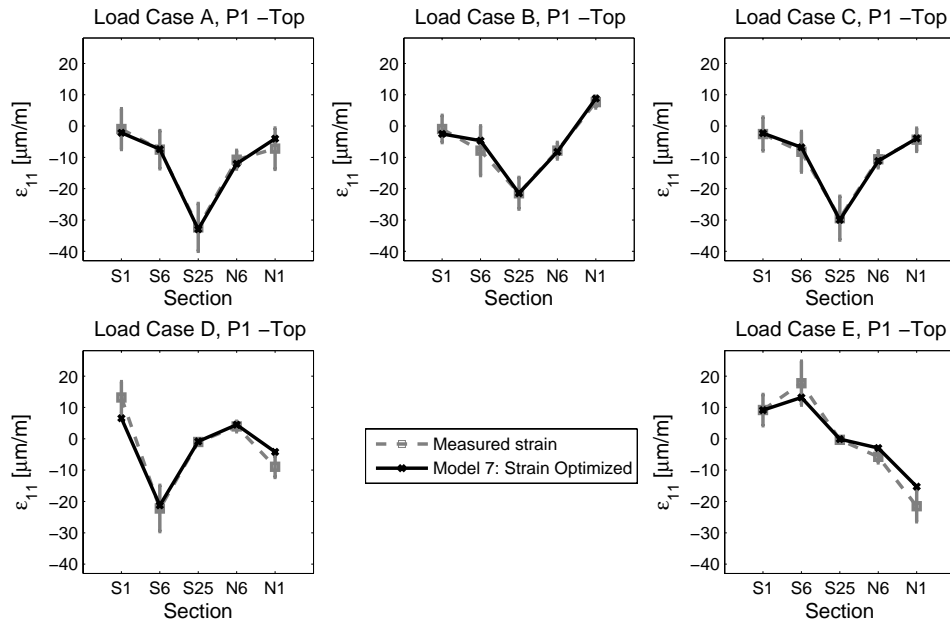


Figure G.9 Measured strain compared with optimized strains from FE model 7 optimized for strains in top sections of arch.

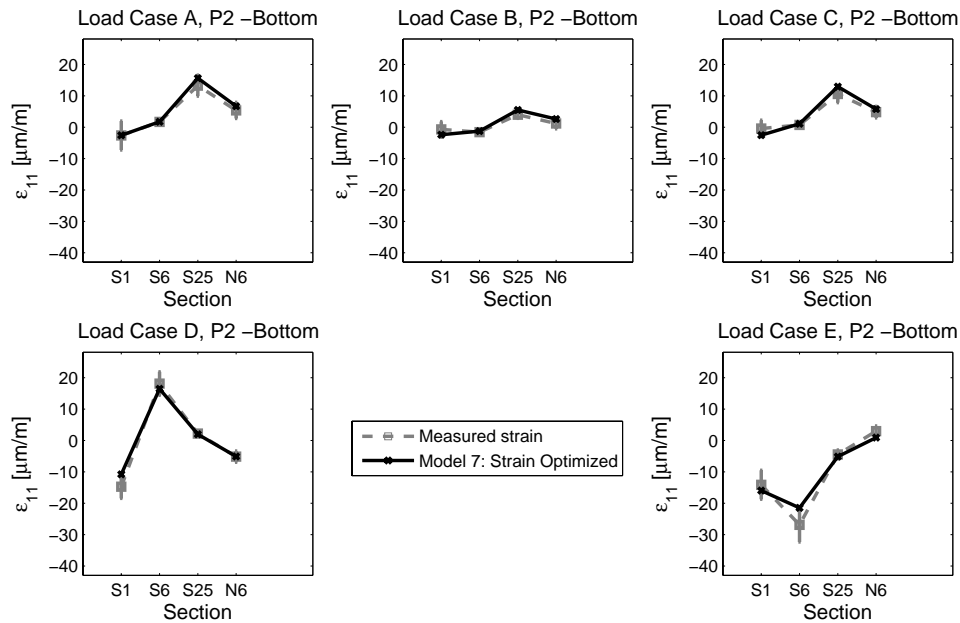


Figure G.10 Measured strain compared with optimized strains from FE model 7 optimized for strains in bottom sections of arch.

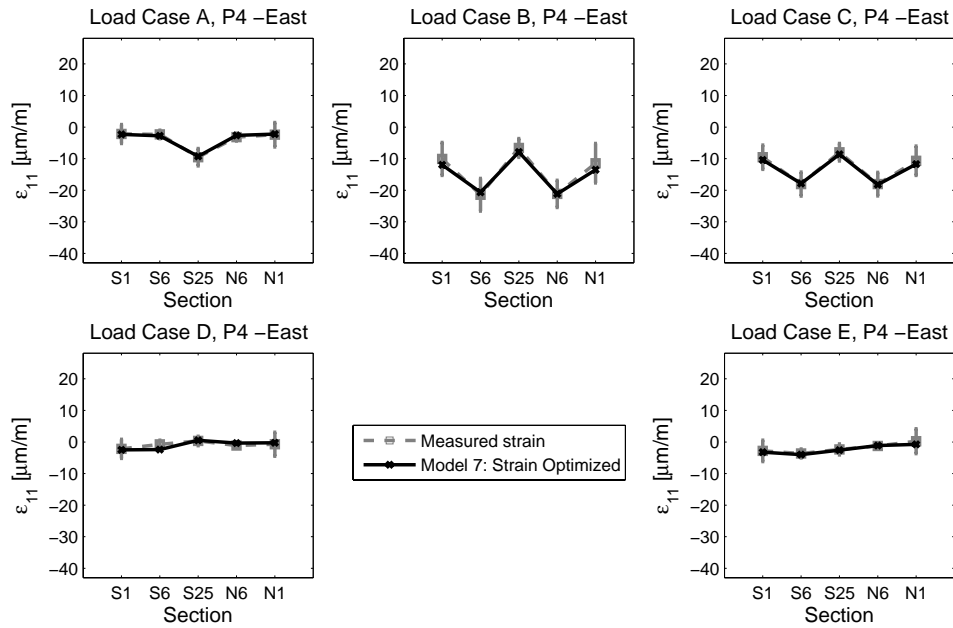


Figure G.11 Measured strain compared with optimized strains from FE model 7 optimized for strains in East sections of arch.

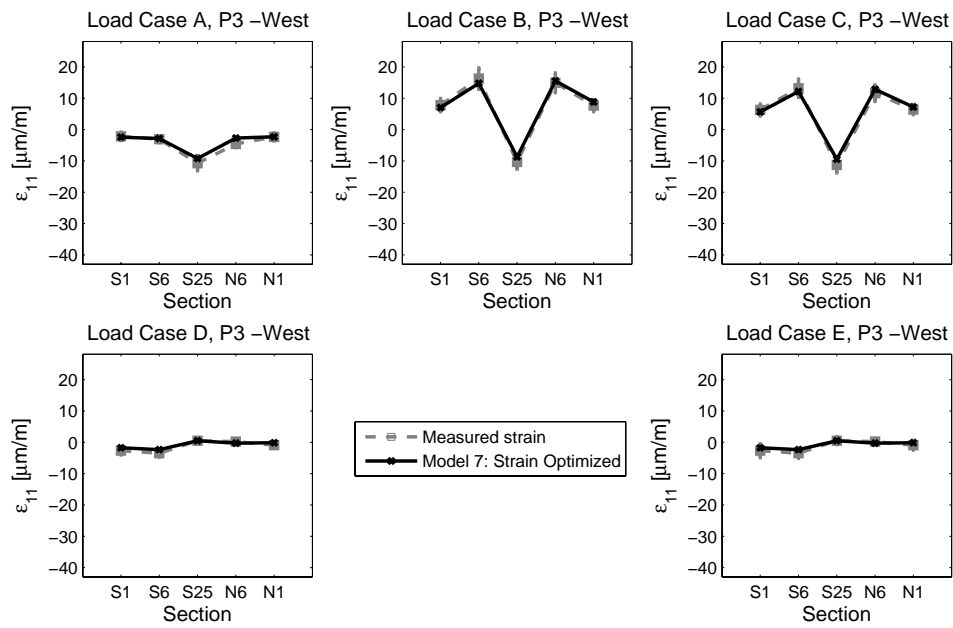


Figure G.12 Measured strain compared with optimized strains from FE model 7 optimized for strains in West sections of arch.

G.3 Model 7 optimized for displacements

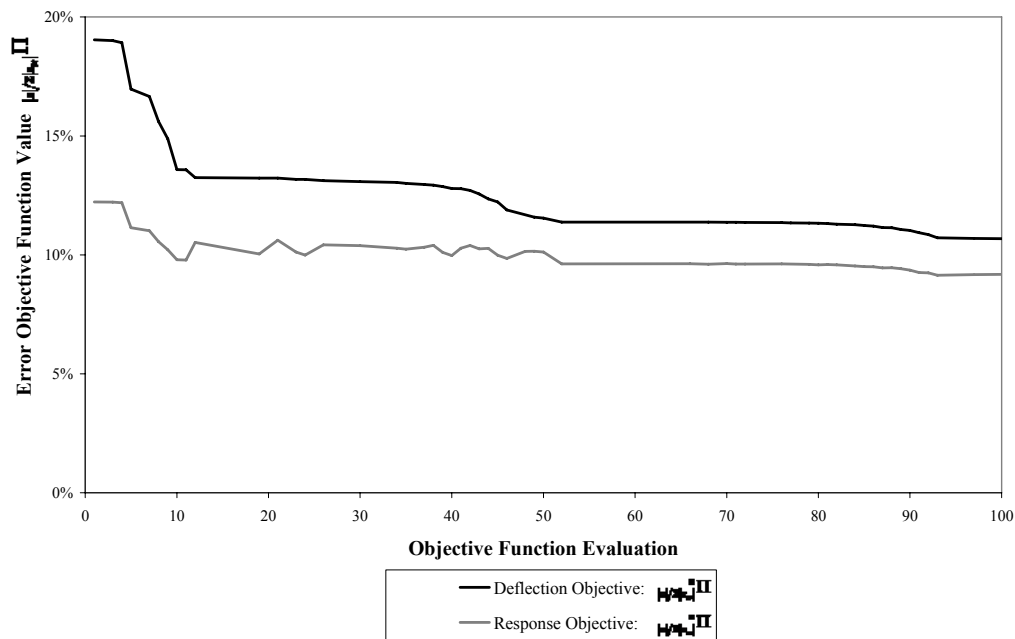


Figure G.13 Convergence of displacement optimization, also showing behaviour of the objective function for the entire response.

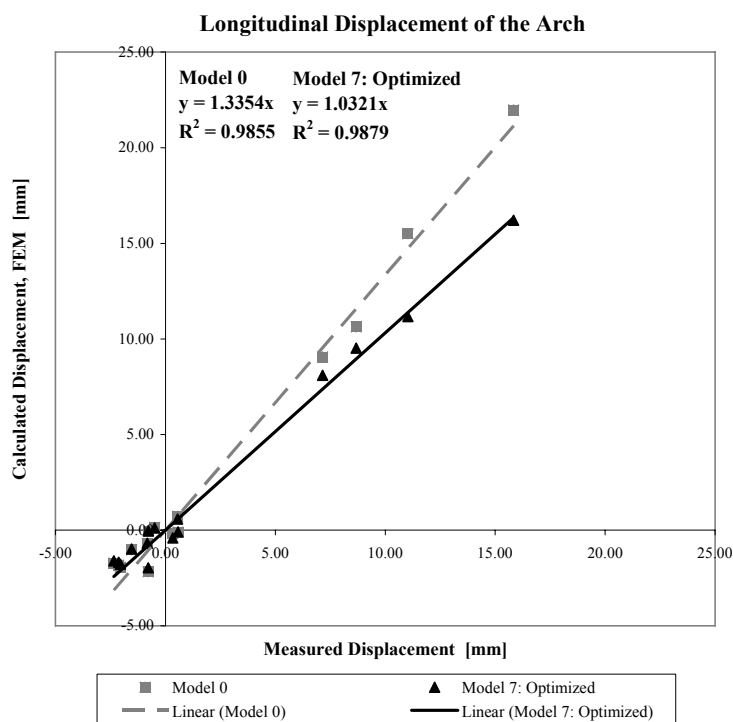


Figure G.14 Normalized longitudinal displacement from Model 0 and Model 7 after displacement optimization compared with measured displacement.

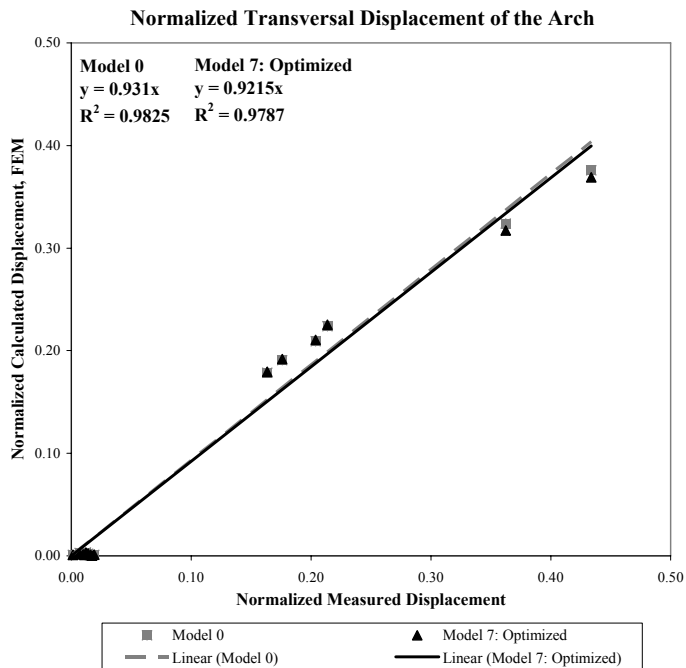


Figure G.15 Normalized transversal displacement of arch from Model 0 and Model 7 after displacement optimization compared with measured displacement.

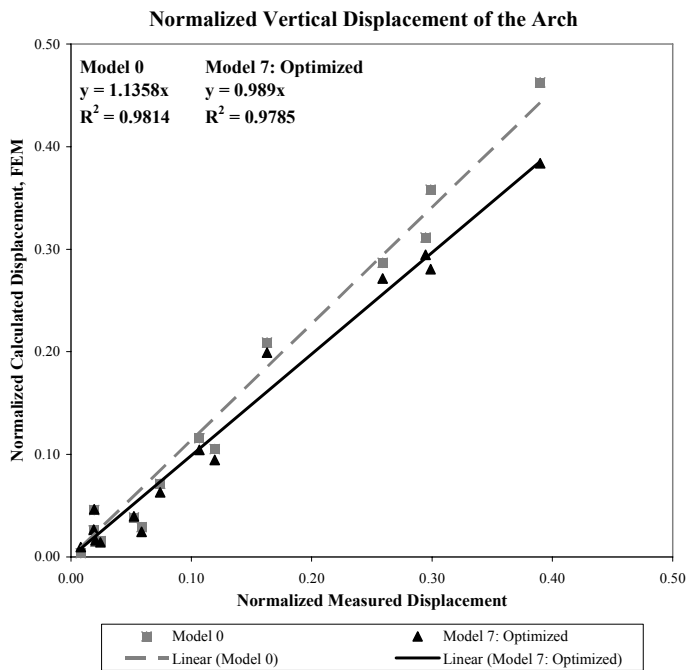


Figure G.16 Normalized vertical displacement of arch from Model 0 and Model 7 after displacement optimization compared with measured displacement.

G.4 Model 7 optimized for hanger loads

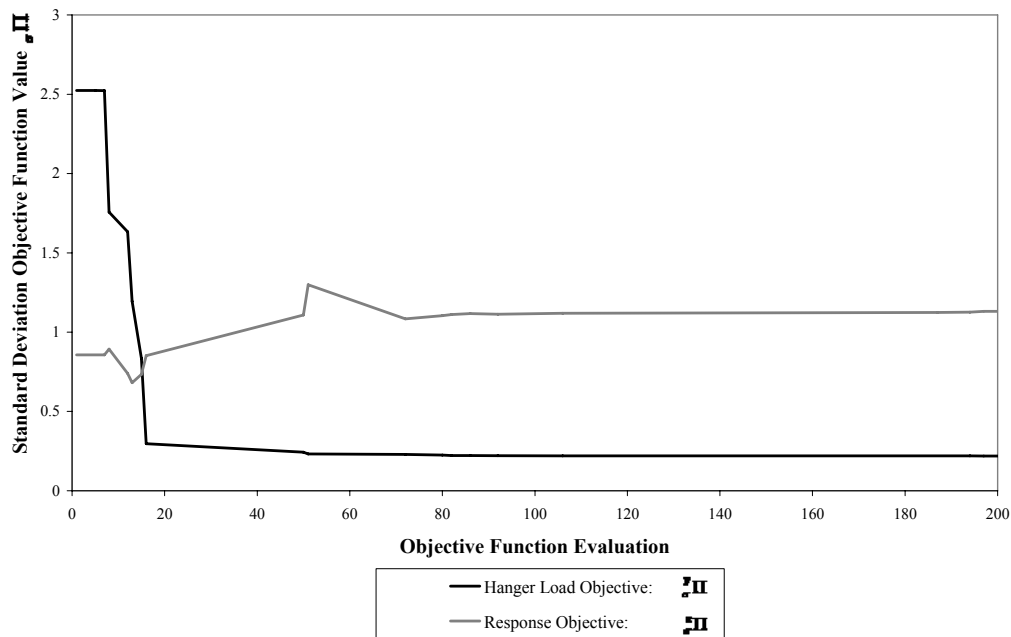


Figure G.17 Convergence of hanger load optimization, also showing reduced accuracy for the entire response.

G.5 Model 7 optimized for entire response

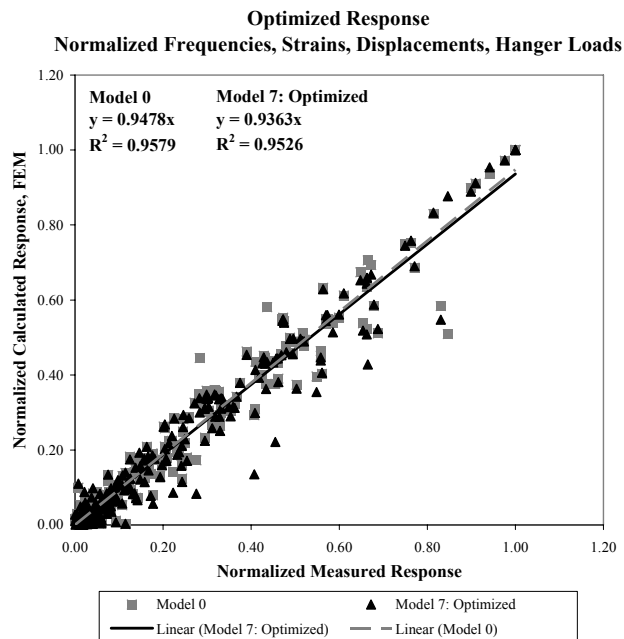


Figure G.18 Normalized response from Model 0 and Model 7 after optimization compared with normalized measured response.

G.6 Model 7 optimized for entire response with regularization

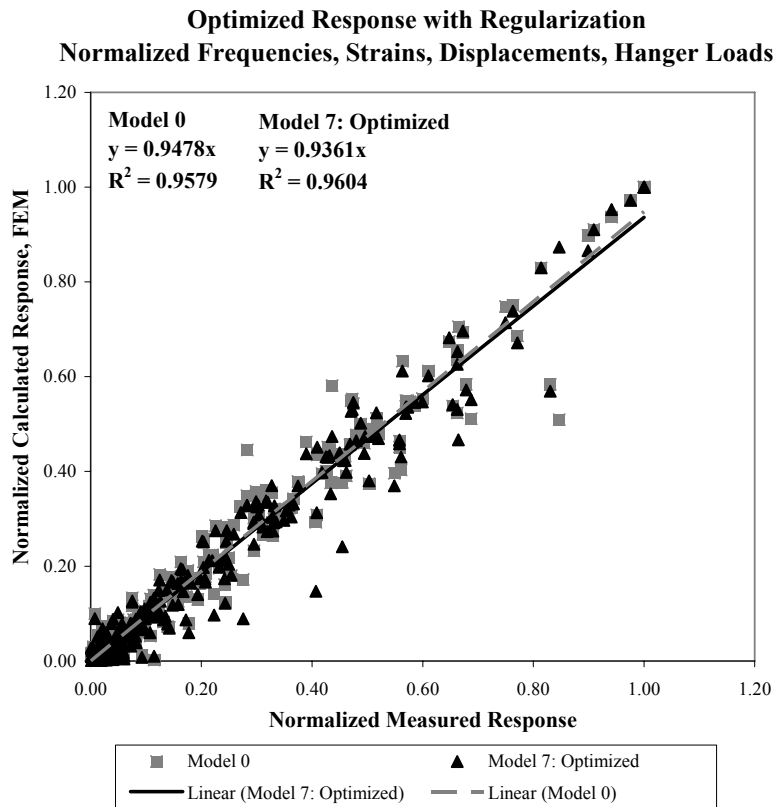


Figure G.19 Normalized response from Model 0 and Model 7 after optimization with regularization compared with normalized measured response.

G.7 FE model updating results summary

Table G.1 Initial normalized updating parameters for manually refined FE model to be used for updating.

	θ	Φ	Model 7: Initial (Refined Manually)
Arch Base Stiffness, E_c	39.8 GPa	ϕ_1	1.062
Arch Crown Stiffness, E_c	44.6 GPa	ϕ_2	1.19
Asphalt mass, M_{asph}	3924 kg	ϕ_3	0.95
	1962 kg		
Asphalt elastic modulus, E_{asph}	210 GPa	ϕ_4	1.6
Abutment bearing static friction, $F_{s,\text{abut}}$	60 kN	ϕ_5	0.2
Pier bearing static friction, $F_{s,\text{pier}}$	16 kN	ϕ_6	0.2
Carriageway longitudinal stiffener area, A_{stiff}	0 m ²	ϕ_7	0
Carriageway steel elastic modulus, E_{steel}	210 GPa	ϕ_8	1

Table G.2 Normalized updating parameters from optimization analyses of FE model 7.

Model 7: Optimized						σ_Φ
$f_\sigma \Pi$	$z/\Sigma z_m ^\epsilon \Pi$	$z/\Sigma z_m ^u \Pi$	$F_\sigma \Pi$	$\frac{z_\sigma \Pi + \Phi_\sigma \Pi}{2}$	$z_\sigma \Pi$	
1.208	0.769	---	1.015	1.062	1.145	0.15
1.010	1.231	---	1.054	1.133	1.032	0.15
0.896	---	---	---	0.965	1.017	1.00
1.596	---	---	---	1.576	1.410	1000
---	0.001	0.001	0.216	0.207	0.204	1000
---	0.556	0.782	0.200	0.204	0.211	1000
0.000	---	---	0.000	0.000	0.000	0.50
0.957	---	1.175	1.105	1.015	1.108	0.10

Table G.3 Mean deviation of response from optimization analyses of FE model 7.

	Model 0	Model 7: Initial	Model 7: Optimized					
			f_{σ}^{Π}	$z/\Sigma z_m ^{\epsilon\Pi}$	$z/\Sigma z_m ^u\Pi$	F_{σ}^{Π}	$\frac{z\Pi + \Phi\Pi}{2}$	z_{σ}^{Π}
$\frac{z\Pi + \Phi\Pi}{2}$	1.84	0.43	0.57	1.40	0.96	0.75	0.37	0.44
z_{σ}^{Π}	3.69	0.86	0.71	2.24	1.34	1.13	0.67	0.54
f_{σ}^{Π}	13.39	1.81	0.98	7.40	4.54	3.76	1.25	1.38
ϵ_{σ}^{Π}	0.20	0.23	0.27	0.18	0.23	0.22	0.23	0.25
u_{σ}^{Π}	0.70	0.59	0.72	0.64	0.35	0.50	0.59	0.48
F_{σ}^{Π}	0.46	0.80	0.84	0.74	0.26	0.06	0.61	0.06

Table G.4 Mean error of response from optimization analyses of FE model 7.

	Model 0	Model 7: Initial	Model 7: Optimized					
			f_{σ}^{Π}	$z/\Sigma z_m ^{\epsilon\Pi}$	$z/\Sigma z_m ^u\Pi$	F_{σ}^{Π}	$\frac{z\Pi + \Phi\Pi}{2}$	z_{σ}^{Π}
$z/\Sigma z_m ^z\Pi$	14.5%	12.2%	13.9%	11.3%	9.2%	9.7%	11.7%	10.0%
$z/\Sigma z_m ^f\Pi$	11.9%	1.1%	0.4%	2.9%	2.8%	1.8%	0.9%	1.0%
$z/\Sigma z_m ^{\epsilon\Pi}$	18.4%	20.6%	23.7%	15.9%	20.7%	19.3%	20.5%	21.9%
$z/\Sigma z_m ^u\Pi$	23.1%	19.0%	22.9%	18.8%	10.7%	17.3%	19.1%	16.4%
$z/\Sigma z_m ^F\Pi$	4.6%	8.2%	8.6%	7.6%	2.4%	0.5%	6.3%	0.6%

Appendix H. Subroutines for FE Model Updating for the New Svinesund Bridge

H.1 MATLAB CODE – zSB

```
function z=zSB(phi)
% z=SBresponce(phi)
% 2007-09-17
% David Johnson and Fredrik Jonsson
% -----
% Purpose:
%           -Delete files made in the previous iteration step
%           -Execute ABAQUS, calculate the new target responses
%           -Execute the post processing program (reads the requested
%           output data from ABAQUS results record)
%           -Read in post processed data in matrices
% Files:
%           file1 ---- SBfreq.dat (data file first ABAQUS run)
%           file2 ---- SBfreq.fre (eigen frequencies first ABAQUS
%           run)
%           file3 ---- SBstatic.dat (data file second ABAQUS run)
%           file4 ---- SBstatic.str (strains second ABAQUS run)
%           file5 ---- SBstatic.dis (displacements second ABAQUS run)
% Input:
%           - The updated material parameters
% Function calls:
%           rmOLDfile --- removes old files so that they don't
%           collaborate in the new iteration step
%           update    --- writes the updated parameters in to the
%           input file for ABAQUS
% Output:
%           - The calculated responses
%=====
%--initialize theta0--
% load theta0
%--initialize filename--
fn1='SBfreq';
fn2='SBstatic';
disp('      << zSB >>')
%--Delete old eigen value files--
rmOLDfile(fn1);

%--update input file for ABAQUS--
SBphi(phi);

%--execute ABAQUS for frequency responce--
unix(['abaqus input=' , fn1, '.inp job=' , fn1]);

%--initialize files---
file1=[fn1, '.dat'];
file2=[fn1, '.fre'];
% --search for ANALYSIS COMPLETE, to know when SBfreq.dat is written--
len=0;
while len <= 0;
    fp1 = fopen(file1, 'r');
    if fp1>=0
        [text, count]=fscanf(fp1, '%c', inf);
        position=findstr(text, 'ANALYSIS COMPLETE');
        len=length(position);
    end
end

%--close file--
fclose(fp1);
disp('      ')
disp('      << ABAQUS RUN COMPLETE >>')
disp('      ')
%
% --execute post processing program.exe--
unix(['abaqus SBfreq']);
%
%--search for EOF (end of file), in order to know when result file is done--
len=0;
while len <= 0;
    fp2=fopen(file2, 'r');
    if fp2 >= 0
        [text, count] = fscanf(fp2, '%c', inf);
        position = findstr(text, 'EOF');
        len = length(position);
    end
end
```

```

% --close the file--
fclose(fp2);

% --EIGEN VALUES--
fp3 = fopen(file2, 'r');           % open Eigen value file
[EIGFREQ, count]=...
    fscanf(fp3, '%e', [1, inf]);   % read in Eigen values to MATLAB [Hz]
EIGFREQ=EIGFREQ';
fclose(fp3);                       % closing the eigenfrequency file
FREQ=[EIGFREQ(1:4)];
%--Delete old static files--
rmOLDfile(fn2);

%--update input file for ABAQUS--
% new function to be written

%--execute ABAQUS for static response--
unix(['abaqus input=' , fn2, '.inp job=' , fn2]);

%--initialize files---
file3=[fn2, '.dat'];
file4=[fn2, '.str'];
file5=[fn2, '.dis'];
file6=[fn2, '.sfo'];

% --search for ANALYSIS COMPLETE, to know when SBstatic.dat is written--
len=0;
while len <= 0;
    fp4 = fopen(file3, 'r');
    if fp4>=0
        [text, count]=fscanf(fp4, '%c', inf);
        position=findstr(text, 'ANALYSIS COMPLETE');
        len=length(position);
    end
end
%--close file--
fclose(fp4);
disp('          ')
disp('          << ABAQUS RUN COMPLETE >>')
disp('          ')

% --execute post processing program.exe--
unix(['abaqus SBstat']);

%--search for EOF (end of file), in order to know when result file is done--
len=0;
while len <= 0;
    fp5=fopen(file6, 'r');
    if fp5 >= 0
        [text, count] = fscanf(fp5, '%c', inf);
        position = findstr(text, 'EOF');
        len = length(position);
    end
end
%--close file--
fclose(fp5);

%--STRAINS--
fp6 = fopen(file4, 'r');           % open strain file
[E11, count] = ...
    fscanf(fp6, '%e', [3, inf]);   % read in strain to MATLAB
fclose(fp6);                       % closing the displacement file
E11=E11';
%--call strain sort--
STR=strainsort(E11);

%--Displacements--
fp7 = fopen(file5, 'r');
[U, count]=...
    fscanf(fp7, '%e', [4, inf]);
fclose(fp7);
U=U';
%--call displacementsort--
DSP=displacementsort(U);
DSP=DSP(:, 2);
%--Hanger loads--
fp8 = fopen(file6, 'r');
[HngF, count]=...
    fscanf(fp8, '%e', [2, inf]);
fclose(fp8);
HngF=HngF';

%-- Call hangersort--
Hfor=hangersort(HngF);
z=[FREQ; STR; DSP; Hfor];

```

H.2 MATLAB CODE – SBphi hat

```

function phi =SBphi hat(phi hat)

% SBphi hat maps uncertain structural parameters of interest to the general
% SBphi to facilitate FE updating of uncertain structural parameters.
%
% phi hat
%   Concrete stiffness updating parameters
%   1   Ec           Global concrete stiffness
%   2   Ecbase      Concrete stiffness increase at arch base
%   3   Eccrown     Concrete stiffness increase at arch crown
%
%   Asphalt updating parameters
%   4   Masph       Global asphalt mass
%   5   Easph       Global asphalt stiffness
%
%   Arch to carriageway connection updating parameters
%   6   Ka-carrS    Arch to carriageway rotational spring (Swedish side)
%   7   Ka-carrN    Arch to carriageway rotational spring (Norwegian side)
%
%   Arch foundation updating parameters
%   8   Ka-fS       Arch foundation rotational stiffness (Swedish side)
%   9   Ka-fN       Arch foundation rotational stiffness (Norwegian side)
%
%   Bearing updating parameters
%   10  KbearS      Non-linear springs at Swedish abutment bearings
%   11  Kbear2      Non-linear springs at Pier 2 bearings
%   12  Kbear3      Non-linear springs at Pier 3 bearings
%   13  Kbear4      Non-linear springs at Pier 4 bearings
%   14  Kbear5      Non-linear springs at Pier 5 bearings
%   15  Kbear8      Non-linear springs at Pier 8 bearings
%   16  KbearN      Non-linear springs at Norwegian abutment bearings
%
%   Carriageway stiffeners updating parameter
%   17  Astiffbeam  Area of the carriageway stiffeners
%   18  Esteel      Elastic modulus of steel

%-----%
%
% Initialize total vector of updating parameters
%
%-----%
%
phi =ones(165, 1);

%-----%
%
% Concrete stiffness updating parameters:
%
%-----%
%
% Global concrete stiffness normalized updating parameter:
phi (1)=phi hat(1);

% Initial stiffness of concrete arch sections
%   Min increase (base): 4.11%
%   Max increase (crown): 16.7%
phi Ecbase=phi hat(2);
phi Eccrown=phi hat(3);
% Quadratic interpolation of arch profile
t=[1 58.5 116]';
X = [ones(size(t)) t t.^2];
% y=[1+0.0411*phi Ecbase 1+0.167*phi Eccrown 1+0.0411*phi Ecbase]';
y=[phi Ecbase phi Eccrown phi Ecbase]';
a = X\y;

% Normalized updating parameters for arch profile
phi Earch=a(1)+a(2)*[1:116]+a(3)*[1:116].^2;
phi (49+[1:116])=phi Earch;

%-----%
%
% Asphalt updating parameters:
%
%-----%
%
% Asphalt layer:
% T=22.72;           % Mean temperature of asphalt during freq measurements
% f = 1;             % Loading frequency [Hz]
% P200 = 24.5;       % Percent Aggregate Passing #200 Sieve
% Pac = 7.8;         % Bitumen Content, Percent by Weight of Mix
% Vv = 0.1;          % Percent Air Voids
dmm=65;             % Depth of asphalt layer
% eta = 0.75;        % Absolute Viscosity at 70deg F [10^6 poise]
% Easph=EASPH(T, f, dmm, P200, Pac, Vv, eta)*1e9;

```

```

% Initial value for asphalt dynamic stiffness: 4899801884 Pa
% Normalized updating parameter for asphalt mass
phi(2)=phi_hat(4);

% Normalized updating parameter for asphalt stiffness
Easph=4899801884*phi_hat(5);

% Asphalt layer dimensions: (dmm) x 10 m
Aasph=(dmm/1000)*10;

%-----%
%
% Arch to carriageway connection updating parameters:
%-----%
%
% Rotational spring at Swedish side updating parameter:
phi(30)=phi_hat(6);
phi(31)=phi_hat(6);

% Rotational spring at Norwegian side updating parameter:
phi(32)=phi_hat(7);
phi(33)=phi_hat(7);

%-----%
%
% Arch foundation updating parameters:
%-----%
%
% Swedish side:
phi(15)=phi_hat(8); % Rotational spring updating parameter

% Norwegian side:
phi(16)=phi_hat(9); % Rotational spring updating parameter

%-----%
%
% Bearing updating parameters:
%-----%
%
% Swedish abutment bearings updating parameter:
phi(34)=phi_hat(10);
phi(35)=phi_hat(10);
phi(36)=phi_hat(10);
phi(37)=phi_hat(10);

% Pier 2 bearings updating parameter:
phi(38)=phi_hat(11);
phi(39)=phi_hat(11);

% Pier 3 bearing updating parameter (1 bearing with motion):
phi(40)=phi_hat(12);

% Pier 4 bearings updating parameter (1 bearing with motion):
phi(41)=phi_hat(13);

% Pier 5 bearings updating parameter:
phi(42)=phi_hat(14);
phi(43)=phi_hat(14);

% Pier 8 bearings updating parameter:
phi(44)=phi_hat(15);
phi(45)=phi_hat(15);

% Norwegian abutment bearings updating parameter:
phi(46)=phi_hat(16);
phi(47)=phi_hat(16);
phi(48)=phi_hat(16);
phi(49)=phi_hat(16);

%-----%
%
% Carriageway stiffeners updating parameter
%-----%
%
% Carriageway sectional parameters at midspan of main span:
Esteel=210E9*phi_hat(18);
phi(4)=phi_hat(18);
% Sectional area of carriageway:
A_A11=1.1e-1;
A_A21=2.2e-1;
A_A51=1.3e-1;
Asteel=A_A11+A_A21+A_A51;

```

```

% Longitudinal bending inertia of carriageway:
I11_A11=3.800E-02;
I11_A21=3.170E-01;
I11_A51=2.310E-01;
I11steel=I11_A11+I11_A21+I11_A51;
% Transversal bending inertia of carriageway:
I22_A11=1.000E-04;
I22_A21=5.500E+00;
I22_A51=1.000E-04;
rA11=5.5;
rA51=5.5;
I22steel=I22_A11+(A_A11*rA11^2)+I22_A21+I22_A51+(A_A51*rA51^2);
% Torsional inertia of carriageway:
J_A11=1.000E-04;
J_A21=1.240E+00;
J_A51=1.000E-04;
Jsteel=J_A11+(A_A11*rA11^2)+J_A21+J_A51+(A_A51*rA51^2);

% Carriageway stiffeners (estimated from structural drawings)
tsteel=0.012; % Steel plate thickness
w=0.200; % Width of stiffening beam
h=0.200; % Height of stiffening beam
Astiffbeam0=(2*h+w)*tsteel; % Area of stiffening beam

% Carriageway stiffening beam area update:
Astiffbeam=Astiffbeam0*phi_hat(17);

Astiff=28*Astiffbeam; % Total area of stiffeners
I11stiff=18*Astiffbeam*1.4^2; % Inertia of top flange stiffeners
I11stiffb=4*Astiffbeam*1.4^2; % Inertia of bottom flange stiffeners
I11stiffw=4*Astiffbeam*0.75^2; % Inertia of web stiffeners
I11stiffsw=4*Astiffbeam*0.5^2; % Inertia of sloped web stiffeners
I11stiff=I11stiff+I11stiffb+I11stiffw+I11stiffsw; % Total I11 inertia
I22stiff=1/12*(Astiff/10)*(10/2)^2; % Approximated transversal inertia
Jstiff=I11stiff+I22stiff; % Torsional inertia

% Longitudinal inertia of asphalt layer:
I11asph=Aasph*(1.5+(dmm/2)*1e-3)^2;

% Transversal inertia of asphalt layer:
I22asph=1/12*(dmm/1000)*5^2;

% Torsional inertia of asphalt layer:
Jasph=I11asph+I22asph;

% Updating parameters:
% Equivalent steel area of carriageway updating parameter:
phi(5)=(Asteel+Astiff)/(Asteel);
Asteel=Asteel+Astiff;

% Equivalent dynamic stiffness of carriageway updating parameter:
Eeq=(Asteel*Esteel+Aasph*Easph)/(Asteel);
phi(10)=Eeq/(210E9);

% Equivalent static longitudinal inertia of carriageway updating parameter:
I11eq=(I11steel*Esteel+I11stiff*Esteel)/(Esteel);
phi(6)=I11eq/I11steel;

% Equivalent dynamic longitudinal inertia of carriageway updating parameter:
I11eq=(I11steel*Esteel+I11stiff*Esteel+I11asph*Easph)/(Esteel);
phi(11)=I11eq/I11steel;

% Equivalent static transversal inertia of carriageway updating parameter:
I22eq=(I22steel*Esteel+I22stiff*Esteel)/(Esteel);
phi(8)=I22eq/I22steel;

% Equivalent dynamic transversal inertia of carriageway updating parameter:
I22eq=(I22steel*Esteel+I22stiff*Esteel+I22asph*Easph)/(Esteel);
phi(13)=I22eq/I22steel;

% Equivalent static torsional inertia of carriageway updating parameter:
Jeq=(Jsteel*Esteel+Jstiff*Esteel)/(Esteel);
phi(9)=Jeq/Jsteel;

% Equivalent dynamic torsional inertia of carriageway updating parameter:
Jeq=(Jsteel*Esteel+Jstiff*Esteel+Jasph*Easph)/(Esteel);
phi(14)=Jeq/Jsteel;

%-----%
%
% Return normalized updating parameter values mapped to total updating
% parameter vector to be written to file using SBphi
%
%-----%

```

H.3 MATLAB CODE – SBphi

function SBphi (phi)

```
% Open file for writing
fid = fopen('SBphi.prn','w');
fprintf(fid,'** Normalized Updating parameters\n**\n*PARAMETER\n**\n');

% Global updating parameters are applied to multiple element sets
fprintf(fid,'**\n** Global Updating Parameters:\n**\n');
fprintf(fid,'** Global Concrete Stiffness Update:\n');
fprintf(fid,['PHI_EC=', num2str(phi(1))]);
fprintf(fid,'\n**\n');
fprintf(fid,'** Global Carriageway Asphalt Mass Update:\n');
fprintf(fid,['PHI_MASPH=', num2str(phi(2))]);
fprintf(fid,'\n**\n');
fprintf(fid,'** Global Steel Carriageway Density Update:\n');
fprintf(fid,['PHI_RHOS=', num2str(phi(3))]);
fprintf(fid,'\n**\n');
fprintf(fid,'** Global Steel Carriageway Static Stiffness Update:\n');
fprintf(fid,['PHI_ES=', num2str(phi(4))]);
fprintf(fid,'\n**\n');
fprintf(fid,'** Global Steel Carriageway Sectional Area Update:\n');
fprintf(fid,['PHI_AS=', num2str(phi(5))]);
fprintf(fid,'\n**\n');
fprintf(fid,'** Global Steel Carriageway Static Bending Inertia (I11) Update:\n');
fprintf(fid,['PHI_I11S=', num2str(phi(6))]);
fprintf(fid,'\n**\n');
fprintf(fid,'** Global Steel Carriageway Static Bending Inertia (I12) Update:\n');
fprintf(fid,['PHI_I12S=', num2str(phi(7))]);
fprintf(fid,'\n**\n');
fprintf(fid,'** Global Steel Carriageway Static Bending Inertia (I22) Update:\n');
fprintf(fid,['PHI_I22S=', num2str(phi(8))]);
fprintf(fid,'\n**\n');
fprintf(fid,'** Global Steel Carriageway Static Torsional Inertia (J) Update:\n');
fprintf(fid,['PHI_JS=', num2str(phi(9))]);
fprintf(fid,'\n**\n');
fprintf(fid,'** Global Steel Carriageway Dynamic Stiffness Update:\n');
fprintf(fid,['PHI_ESD=', num2str(phi(10))]);
fprintf(fid,'\n**\n');
fprintf(fid,'** Global Steel Carriageway Dynamic Bending Inertia (I11) Update:\n');
fprintf(fid,['PHI_I11SD=', num2str(phi(11))]);
fprintf(fid,'\n**\n');
fprintf(fid,'** Global Steel Carriageway Dynamic Bending Inertia (I12) Update:\n');
fprintf(fid,['PHI_I12SD=', num2str(phi(12))]);
fprintf(fid,'\n**\n');
fprintf(fid,'** Global Steel Carriageway Dynamic Bending Inertia (I22) Update:\n');
fprintf(fid,['PHI_I22SD=', num2str(phi(13))]);
fprintf(fid,'\n**\n');
fprintf(fid,'** Global Steel Carriageway Dynamic Torsional Inertia (J) Update:\n');
fprintf(fid,['PHI_JSD=', num2str(phi(14))]);
fprintf(fid,'\n**\n');
fprintf(fid,'** Arch and Pier Foundation Stiffness Update:\n');
fprintf(fid,['PHI_kS3001_5=', num2str(phi(15)), '\n'];
fprintf(fid,['PHI_kS3117_5=', num2str(phi(16)), '\n'];
fprintf(fid,['PHI_kS4201_5=', num2str(phi(17)), '\n'];
fprintf(fid,['PHI_kS4201_4=', num2str(phi(18)), '\n'];
fprintf(fid,['PHI_kS4301_4=', num2str(phi(19)), '\n'];
fprintf(fid,['PHI_kS4301_5=', num2str(phi(20)), '\n'];
fprintf(fid,['PHI_kS4401_1=', num2str(phi(21)), '\n'];
fprintf(fid,['PHI_kS4401_2=', num2str(phi(22)), '\n'];
fprintf(fid,['PHI_kS4401_3=', num2str(phi(23)), '\n'];
fprintf(fid,['PHI_kS4401_4=', num2str(phi(24)), '\n'];
fprintf(fid,['PHI_kS4401_5=', num2str(phi(25)), '\n'];
fprintf(fid,['PHI_kS4401_6=', num2str(phi(26)), '\n'];
fprintf(fid,['PHI_kS4501_4=', num2str(phi(27)), '\n'];
fprintf(fid,['PHI_kS4501_5=', num2str(phi(28)), '\n'];
fprintf(fid,['PHI_kS4801_5=', num2str(phi(29)), '\n'];
fprintf(fid,'**\n');
fprintf(fid,'** Arch to Carriageway Connection Stiffness Update:\n');
fprintf(fid,['PHI_kARCHCARRSW=', num2str(phi(30)), '\n'];
fprintf(fid,['PHI_kARCHCARRSE=', num2str(phi(31)), '\n'];
fprintf(fid,['PHI_kARCHCARRNW=', num2str(phi(32)), '\n'];
fprintf(fid,['PHI_kARCHCARRNE=', num2str(phi(33)), '\n'];
fprintf(fid,'**\n');
fprintf(fid,'** Non Linear Spring Stiffness Update (Abutment/Piers):\n**\n');
fprintf(fid,'**\n');
fprintf(fid,['PHI_ABUTCARRS1=', num2str(phi(34)), '\n'];
fprintf(fid,['PHI_ABUTCARRS2=', num2str(phi(35)), '\n'];
fprintf(fid,['PHI_ABUTCARRS3=', num2str(phi(36)), '\n'];
fprintf(fid,['PHI_ABUTCARRS4=', num2str(phi(37)), '\n'];
fprintf(fid,['PHI_PIERCARRW2=', num2str(phi(38)), '\n'];
fprintf(fid,['PHI_PIERCARRE2=', num2str(phi(39)), '\n'];
fprintf(fid,['PHI_PIERCARRW3=', num2str(phi(40)), '\n'];
fprintf(fid,['PHI_PIERCARRW4=', num2str(phi(41)), '\n'];
fprintf(fid,['PHI_PIERCARRW5=', num2str(phi(42)), '\n'];
```

```

fprintf(fid, [' PHI_P1 ERCARRE5=', num2str(phi (43)), '\n' ]);
fprintf(fid, [' PHI_P1 ERCARRW8=', num2str(phi (44)), '\n' ]);
fprintf(fid, [' PHI_P1 ERCARRE8=', num2str(phi (45)), '\n' ]);
fprintf(fid, [' PHI_ABUTCARRN1=', num2str(phi (46)), '\n' ]);
fprintf(fid, [' PHI_ABUTCARRN2=', num2str(phi (47)), '\n' ]);
fprintf(fid, [' PHI_ABUTCARRN3=', num2str(phi (48)), '\n' ]);
fprintf(fid, [' PHI_ABUTCARRN4=', num2str(phi (49)), '\n**\n' ]);
fprintf(fid, '**\n');
% Local updating parameters applied to individual arch sections
fprintf(fid, '**\n** Local Concrete Arch Stiffness Update:\n**');
for i=1:116
    fprintf(fid, '\n');
    fprintf(fid, [' PHI_EC_A', int2str(i+300), '= ', num2str(phi (i+49))]);
end

fclose(fid);

```

H.4 MATLAB CODE – SBobj

```

function OBJ=SBobj (p, choose, fid)

% Objective function options:
% 'VARIANCEZPHI' (average variance of z) + (average variance of phi)
% 'VARIANCEZ' (average variance of z)
% 'UNCERTZPHI' (average uncertainty of z) +
% (average uncertainty of phi)
% 'UNCERTZ' (average uncertainty of z)
% 'ERRORZPHI' (average error of z) + (average error of phi)
% 'ERRORZ' (average error of z)
% 'STDEVZPHI' (average standard deviation of z) +
% (average standard deviation of phi)
%
% default:
% 'STDEVZ'

% Load measured response and standard deviation
load('zmsi gmaz. mat');

% Initial values of normalized updating parameters:
p0=[1.062;
    1.190;
    0.95;
    1.6;
    0.2;
    0.2;
    0;
    1];

% Standard deviation of input parameters
sigmap=[0.15;
    0.15;
    1.00;
    1000;
    1000;
    1000;
    0.50;
    0.10];

% Control of input parameter range (to use unconstrained minimization)
prange= [ 0.8 2;
    0.8 2;
    0.5 2;
    0 4;
    0.001 4;
    0.001 4;
    -0.5 0.5;
    0.8 1.2];
p_lb=prange(:, 1);
p_ub=prange(:, 2);
p=(p<p_lb). *p_lb+(p>p_ub). *p_ub + ((p>=p_lb)&(p<=p_ub)). *p;

% Response of bridge for given input parameters:
z=zSB(SBphi hat([1 p(1) p(2) p(3) p(4) 500 500 1 1 p(5) p(6) p(6) p(6) p(6) p(6) ...
    p(5) p(7) p(8)]));

% Indices for measurement types:
ixfreq=[1:4];
ixstraln=[5:99];
ixdisp=[100:254];
ixhng=[255:264];

switch choose
case 'VARIANCEZPHI'
%-----%
% Variance:

```

```

% Objective function calculations:
dZxWz=((zm-z).^2)./sigmaz.^2;
dpxWp=((p0-p).^2)./sigmap.^2;

% Contribution of frequency to objective function:
OBJfreq=mean(dZxWz(ixfreq));

% Contribution of strain to objective function:
OBJstrain=mean(dZxWz(ixstrain));

% Contribution of displacement to objective function:
OBJdisplacement=mean(dZxWz(ixdisplacement));

% Contribution of hanger load to objective function:
OBJhanger=mean(dZxWz(ixhanger));

% Contribution of bridge response to objective function:
OBJz=mean([OBJfreq OBJstrain OBJdisplacement OBJhanger]);

% Contribution of input parameters to objective function:
OBJp=mean(dpxWp);

OBJ=mean([OBJz OBJp]);

case 'VARIANCEZ'
%-----%
% Variance:

% Objective function calculations:
dZxWz=((zm-z).^2)./sigmaz.^2;

% Contribution of frequency to objective function:
ixfreq=[1:4];
OBJfreq=mean(dZxWz(ixfreq));

% Contribution of strain to objective function:
ixstrain=[5:99];
OBJstrain=mean(dZxWz(ixstrain));

% Contribution of displacement to objective function:
ixdisplacement=[100:254];
OBJdisplacement=mean(dZxWz(ixdisplacement));

% Contribution of hanger load to objective function:
ixhanger=[255:264];
OBJhanger=mean(dZxWz(ixhanger));

% Contribution of bridge response to objective function:
OBJz=mean([OBJfreq OBJstrain OBJdisplacement OBJhanger]);

OBJ=mean(OBJz);

case 'UNCERTZPHI'
%-----%
% Uncertainty:

% FE Model uncertainty:
sigmazFEM=0.1*max([abs(zm)';abs(z)']');
sigmazuncert=sqrt(sigmaz.^2+sigmazFEM.^2);

% Define uncertainty function:
uncertfun=@(xm,x,sigma)(2*abs(normcdf(xm,x,sigma)-0.5))';

% Uncertainty of response:
Zuncert=uncertfun(zm,z,sigmazuncert);

% Uncertainty of input parameters:
puncert=uncertfun(p0,p,sigmap);
UNCERTp=mean(puncert);

% Mean uncertainty of frequency:
UNCERTfreq=mean(Zuncert(ixfreq));

% Mean uncertainty of frequency:
UNCERTstrain=mean(Zuncert(ixstrain));

% Mean uncertainty of frequency:
UNCERTdisplacement=mean(Zuncert(ixdisplacement));

% Mean uncertainty of frequency:
UNCERThanger=mean(Zuncert(ixhanger));

% Mean uncertainty of response:
UNCERTz=mean([UNCERTfreq UNCERTstrain UNCERTdisplacement UNCERThanger]);

OBJ=mean([UNCERTz UNCERTp]);

```

```

case ' UNCERTZ'
%-----%
% Uncertainty:

% FE Model uncertainty:
si gmazFEM=0.1*max([abs(zm)';abs(z)'])';
si gmazuncert=sqrt(si gmaz.^2+si gmazFEM.^2);

% Define uncertainty function:
uncertfun=@(xm, x, si gma) (2*abs(normcdf(xm, x, si gma)-0.5))';

% Uncertainty of response:
Zuncert=uncertfun(zm, z, si gmazuncert);

% Mean uncertainty of frequency:
UNCERTfreq=mean(Zuncert(i xfreq));

% Mean uncertainty of frequency:
UNCERTstrain=mean(Zuncert(i xstrain));

% Mean uncertainty of frequency:
UNCERTdisplacement=mean(Zuncert(i xdisplacement));

% Mean uncertainty of frequency:
UNCERThang=mean(Zuncert(i xhang));

% Mean uncertainty of response:
OBJ=mean([UNCERTfreq UNCERTstrain UNCERTdisplacement UNCERThang]);

case ' ERRORZPHI '
%-----%
% Error:

% Contribution of frequency to error function:
ERRORfreq=sum(abs(zm(i xfreq)-z(i xfreq)))/sum(abs(zm(i xfreq)));

% Contribution of strain to error function:
ERRORstrain=sum(abs(zm(i xstrain)-z(i xstrain)))/sum(abs(zm(i xstrain)));

% Contribution of displacement to error function:
ERRORdisplacement=sum(abs(zm(i xdisplacement)-z(i xdisplacement)))/sum(abs(zm(i xdisplacement)));

% Contribution of hanger load to error function:
ERRORhang=sum(abs(zm(i xhang)-z(i xhang)))/sum(abs(zm(i xhang)));

% Contribution of bridge response to error function:
ERRORz=mean([ERRORfreq ERRORstrain ERRORdisplacement ERRORhang]);

% Contribution of input parameters to error function:
ERRORp=sum(abs(p0-p))/sum(p0);

OBJ=mean([ERRORz ERRORp]);

case ' ERRORZ'
%-----%
% Error:

% Contribution of frequency to error function:
ERRORfreq=sum(abs(zm(i xfreq)-z(i xfreq)))/sum(abs(zm(i xfreq)));

% Contribution of strain to error function:
ERRORstrain=sum(abs(zm(i xstrain)-z(i xstrain)))/sum(abs(zm(i xstrain)));

% Contribution of displacement to error function:
ERRORdisplacement=sum(abs(zm(i xdisplacement)-z(i xdisplacement)))/sum(abs(zm(i xdisplacement)));

% Contribution of hanger load to error function:
ERRORhang=sum(abs(zm(i xhang)-z(i xhang)))/sum(abs(zm(i xhang)));

% Contribution of bridge response to error function:
ERRORz=mean([ERRORfreq ERRORstrain ERRORdisplacement ERRORhang]);

OBJ=ERRORz;

case ' STDEVZPHI '
%-----%
% Standard Deviation:

% Objective function calculations:
dZxWz=abs((zm-z))./si gmaz;
dpxWp=abs((p0-p))./si gmap;

% Contribution of frequency to objective function:
OBJfreq=mean(dZxWz(i xfreq));

% Contribution of strain to objective function:

```

```

OBJstrai n=mean(dZxWz(i xstrai n));

% Contribution of displacement to objective function:
OBJdi sp=mean(dZxWz(i xdi sp));

% Contribution of hanger load to objective function:
OBJhang=mean(dZxWz(i xhang));

% Contribution of bridge response to objective function:
OBJz=mean([OBJfreq OBJstrai n OBJdi sp OBJhang]);

% Contribution of input parameters to objective function:
OBJp=mean(dpxWp);

OBJ=mean([OBJz OBJp]);

otherwise
%-----%
% Standard Deviation: 'STDEVZ'

% Objective function calculations:
dZxWz=abs((zm-z))./si gmaz;

% Contribution of frequency to objective function:
OBJfreq=mean(dZxWz(i xfreq));

% Contribution of strain to objective function:
OBJstrai n=mean(dZxWz(i xstrai n));

% Contribution of displacement to objective function:
OBJdi sp=mean(dZxWz(i xdi sp));

% Contribution of hanger load to objective function:
OBJhang=mean(dZxWz(i xhang));

% Contribution of bridge response to objective function:
OBJz=mean([OBJfreq OBJstrai n OBJdi sp OBJhang]);

OBJ=OBJz;

end

% Load data from previous iteration:
load(fi d);
[m, n]=si ze(phi _save);
phi _save(:, n+1)=p;
z_save(:, n+1)=z;
OBJ_save(:, n+1)=OBJ;

% Save iteration data:
save(fi d, 'phi _save', 'z_save', 'OBJ_save');

```

H.5 User subroutine – SBfreq

```

SUBROUTINE ABQMAIN
C=====
C This program must be compiled and linked with the command:
C   abaqus make job=SBfreq
C Run the program using the command:
C   abaqus SBfreq
C=====
C PURPOSE:
C
C This program reads results record stored in an ABAQUS results file
C (.fil), save the eigen values and calculates the eigenfrequencies
C and creates an ASCII file for reading the eigenfrequencies to MATLAB
C Input file names <fname.fil>
C
C=====
C
C VARIABLES USED BY THIS PROGRAM
C
C LOUTF ---- FORMAT OF OUTPUT FILE:
C           0 --> Standard ASCII format.
C           1 --> ABAQUS results file ASCII format.
C           2 --> ABAQUS results file binary format.
C JUNIT ---- Unit number of file to be opened (=8 for .fil).
C KEY ---- Current element key identifier.
C JRCD ---- Error check return code
C           .EQ 0 --> No errors
C           .NE 0 --> Errors detected
C FNAME ---- Name of the results file
C ARRAY ---- Real array containing individual components of
C           the output variable.
C EIGEN ---- Eigen values
C FREQ ---- Eigen frequencies [Hz]
C DBFILE --- Read from file (ABAQUS utility routine)
C DBRNU ---- set unit number for a file (ABAQUS utility routine)
C INITPF --- initialize a file (ABAQUS utility routine)
C=====
C
C The use of ABA_PARAM.INC eliminates the need to have different
C versions of the code for single and double precision.
C ABA_PARAM.INC defines an appropriate IMPLICIT REAL statement
C and sets the value of NRCD to 1 or 2, depending on whether
C the machine uses single or double precision.
C=====
C
C The use of ABA_PARAM.INC eliminates the need to have different
C versions of the code for single and double precision.
C ABA_PARAM.INC defines an appropriate IMPLICIT REAL statement
C and sets the value of NRCD to 1 or 2, depending on whether
C the machine uses single or double precision.
C=====
C
C   INCLUDE 'aba_param.inc'
C   CHARACTER*80 FNAME
C   DIMENSION ARRAY(513),JRRAY(2,513),LRUNIT(2,1)
C   EQUIVALENCE (ARRAY(1),JRRAY(1,1))
C   REAL PI
C   PARAMETER (PI = 3.1415926535897932384626434)
C   OPEN(UNIT=105,FILE='SBfreq.fre',STATUS='UNKNOWN')
C   --Define key number, modal file--
C   MOD=1980

```

```

C      --Function name--
      FNAME='SBfreq'
      NRU=1
      LRUNIT(1,1) = 8
      LRUNIT(2,1) = 2
      LOUTF = 0
      CALL INITPF(FNAME,NRU,LRUNIT,LOUTF)
C      --Unit number for ABAQUS.fil (results file)--
      JUNIT = 8
      CALL DBRNU(JUNIT)
C      --Loop an all records in results file--
      DO 100 K1=1,999999
      CALL DBFILE(0,ARRAY,JRCD)
      IF(JRCD.NE.0) GO TO 110
      KEY=JRRAY(1,2)
C      --Find right key for eigen values--
      IF(KEY.EQ.MOD) THEN
C      --save eigen values--
      EIGEN=ARRAY(4)
C      --calculate eigen frequencies [Hz]--
      FREQ=SQRT(EIGEN)/(2*PI)
C      --Write eigen frequencies to the file FNAME.fre--
      WRITE(105,*) FREQ
      END IF
      100 CONTINUE
      110 CONTINUE
C      --Write EOF (end of file)--
      WRITE(105,*) 'EOF'
      CLOSE(UNIT=105)
      STOP
      END

```

H.6 User subroutine – SBstat

```
SUBROUTINE ABQMAIN
C=====
C This program must be compiled and linked with the command:
C   abaqus make job=SBstatic
C Run the program using the command:
C   abaqus SBstatic
C=====
C PURPOSE:
C
C This program reads results file stored in an ABAQUS results (.fil)
C file and creates ASCII files for reading in to MATLAB
C
C Input file names <fname.fil>
C
C=====
C
C VARIABLES USED BY THIS PROGRAM
C
C LOUTF   ----   FORMAT OF OUTPUT FILE:
C           0 --> Standard ASCII format.
C           1 --> ABAQUS results file ASCII format.
C           2 --> ABAQUS result file binary format.
C JRRAY   ----   Integer array containing values read from results
file.
C           Equivalenced to array.
C JUNIT   ----   Unit number of file to be opened.
C KEY     ----   Current element key identifier.
C NOEL    ----   Current element number
C NPT     ----   Integration point number
C JRCD    ----   Error check return code
C           .EQ 0 --> No errors
C           .NE 0 --> Errors detected
C FNAME   ----   Name of the results file
C ARRAY   ----   Real array containing individual components of
C                 the output variable.
C DBFILE  ---    Read from file (ABAQUS utility routine)
C DBRNU   ----   set unit number for a file (ABAQUS utility routine)
C INITPF  ---    initialize a file (ABAQUS utility routine)
C
C=====
C
C The use of ABA_PARAM.INC eliminates the need to have different
C versions of the code for single and double precision.
C ABA_PARAM.INC defines an appropriate IMPLICIT REAL statement
C and sets the value of NRCD to 1 or 2, depending on whether
C the machine uses single or double precision.
C=====
C   INCLUDE 'aba_param.inc'
C
C CHARACTER*80 FNAME
C DIMENSION ARRAY(513),JRRAY(2,513),LRUNIT(2,1)
C EQUIVALENCE (ARRAY(1),JRRAY(1,1))
C OPEN(UNIT=120,FILE='SBstat.str',STATUS='UNKNOWN')
C OPEN(UNIT=130,FILE='SBstat.dis',STATUS='UNKNOWN')
C OPEN(UNIT=140,FILE='SBstat.sfo',STATUS='UNKNOWN')
C --Define key number, strain--
C STR=21
C --Define key number, displacement--
C DIS=101
```

```

C      --Define key number, section forces--
      SEFO=13
C      --Function name--
      FNAME='SBstat'
      NRU=1
      LRUNIT(1,1) = 8
      LRUNIT(2,1) = 2
      LOUTF = 0
      CALL INITPF(FNAME,NRU,LRUNIT,LOUTF)
C      --Unit number for ABAQUS.fil (results file)--
      JUNIT = 8
      CALL DBRNU(JUNIT)
C      --Loop an all records in results file--
      STRESS=0.
      DO 100 K1=1,999999
      CALL DBFILE(0,ARRAY,JRCD)
      IF(JRCD.NE.0)GO TO 110
      KEY=JRRAY(1,2)
      IF(KEY.EQ.1) THEN
      NOEL=JRRAY(1,3)
      JPNT=JRRAY(1,4)
      SECPT=JRRAY(1,5)
C      --Find the right key, strains--
      ELSE IF(KEY.EQ.STR) THEN
      E1=ARRAY(3)
C      --Write strains to the file FNAME.str--
      WRITE(120,*) NOEL,SECPT,E1
C      --Find the right key, displacements--
      ELSE IF (KEY.EQ.DIS) THEN
      NODNR=JRRAY(1,3)
      U1=ARRAY(4)
      U2=ARRAY(5)
      U3=ARRAY(6)
C      --Write displacements to the file FNAME.str--
      WRITE(130,*) NODNR,U1,U2,U3
C      --Find the right key, section forces--
      ELSE IF(KEY.EQ.SEFO) THEN
      SF1=ARRAY(3)
      SF2=ARRAY(4)
      SF3=ARRAY(5)
      WRITE(140,*) NOEL,SF1
      END IF
      100 CONTINUE
      110 CONTINUE
C      --Write EOF (end of file)--
      WRITE(120,*) 'EOF'
      WRITE(130,*) 'EOF'
      WRITE(140,*) 'EOF'
      CLOSE(UNIT=120)
      CLOSE(UNIT=130)
      CLOSE(UNIT=140)
      STOP
      END

```